

Spring 2006

Multicomponent patterning of nanocomposite polymer and nanoparticle films using photolithography and layer-by-layer self-assembly

Javeed Shaikh Mohammed
Louisiana Tech University

Follow this and additional works at: <https://digitalcommons.latech.edu/dissertations>



Part of the [Nanoscience and Nanotechnology Commons](#)

Recommended Citation

Shaikh Mohammed, Javeed, "" (2006). *Dissertation*. 566.
<https://digitalcommons.latech.edu/dissertations/566>

This Dissertation is brought to you for free and open access by the Graduate School at Louisiana Tech Digital Commons. It has been accepted for inclusion in Doctoral Dissertations by an authorized administrator of Louisiana Tech Digital Commons. For more information, please contact digitalcommons@latech.edu.

MULTICOMPONENT PATTERNING OF NANOCOMPOSITE
POLYMER AND NANOPARTICLE FILMS USING
PHOTOLITHOGRAPHY AND LAYER-BY-LAYER SELF-ASSEMBLY

by

Javeed Shaikh Mohammed, M.S.

A Dissertation Presented in Partial Fulfillment
of the Requirement for the Degree
Doctor of Philosophy

COLLEGE OF ENGINEERING AND SCIENCE
LOUISIANA TECH UNIVERSITY

May 2006

UMI Number: 3218992

INFORMATION TO USERS

The quality of this reproduction is dependent upon the quality of the copy submitted. Broken or indistinct print, colored or poor quality illustrations and photographs, print bleed-through, substandard margins, and improper alignment can adversely affect reproduction.

In the unlikely event that the author did not send a complete manuscript and there are missing pages, these will be noted. Also, if unauthorized copyright material had to be removed, a note will indicate the deletion.

UMI[®]

UMI Microform 3218992

Copyright 2006 by ProQuest Information and Learning Company.

All rights reserved. This microform edition is protected against unauthorized copying under Title 17, United States Code.

ProQuest Information and Learning Company
300 North Zeeb Road
P.O. Box 1346
Ann Arbor, MI 48106-1346

LOUISIANA TECH UNIVERSITY

THE GRADUATE SCHOOL

4-13-2006

Date

We hereby recommend that the dissertation prepared under our supervision
by JAVEED SHAIKH MOHAMMED

entitled MULTICOMPONENT PATTERNING OF NANOCOMPOSITE POLYMER AND

NANOPARTICLE FILMS USING PHOTOLITHOGRAPHY AND

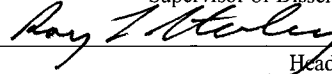
LAYER-BY-LAYER SELF-ASSEMBLY

be accepted in partial fulfillment of the requirements for the Degree of

DOCTOR OF PHILOSOPHY



Supervisor of Dissertation Research



Head of Department

ENGINEERING

Department

Recommendation concurred in:

V. Ural 

C. Luo 

David Mills

P. Srinivasan

Advisory Committee

Approved:

Bala Ramachandran
Director of Graduate Studies

W. J. McConally
Dean of the Graduate School

Alan Haggm
Dean of the College

GS Form 13
(5/03)

ABSTRACT

In this dissertation, the fabrication, characterization, and application examples of 3D multicomponent nanocomposite micropatterns (MNM)s with precise spatial arrangements are described. The ability to produce such small-scale 3D structures with versatility in composition and structure is a new development based on the integration of nanoscale layer-by-layer (LbL) self-assembly and microscale photolithographic patterning, enabling construction of surfaces with microscale patterns that possess nanotopographies. The techniques used here are analogous to surface micromachining, except that the deposition materials are polymers, biological materials, and colloidal nanoparticles used to produce 3D MNMs. A key feature of the resulting 3D MNMs is that the physical and chemical properties of the multilayer nanofilms may be finely tuned using the versatile LbL assembly process, which makes them attractive for many applications requiring polymeric structures with small features.

The work presented here involves development of techniques for the fabrication, characterization, and applications of 3D MNMs, and evaluation of the process parameters involved in the developed techniques. These results clearly demonstrate the feasibility of the polymer 3D MNMs for biotechnological applications; specifically, they have potential as tailored surfaces for direct comparison of cell-material interactions on a single substrate, and for co-culture systems. In reality, the approach described here may enable study of and control over cell-biomaterial and cell-cell interactions in a whole new

fashion. The techniques developed in this work represent a major advancement of nanoscale engineering through the integration of nanoscale LbL self-assembly and microscale photolithographic patterning for constructing 3D MNMs with varying physical and chemical properties in precise spatial arrangements. A major finding of this work, related to the applicability of the developed techniques, is that most of the seemingly harsh processes involved in constructing the 3D MNMs have minimal or no deleterious effects on the biological models used here. The exception is the resist developer (MF319), which due to its highly basic nature, results in disintegration of nanofilms exposed to it directly. Nevertheless, the methods developed here are not limited by the photoresists and resist developers used here; biocompatible photoresists and aqueous base developers could potentially be used.

This work has pursued the development of organic and inorganic nanofilm scaffolds which can eventually be combined to achieve functionality desired for specific applications. It is anticipated that the 3D MNMs developed in this work will provide general platforms for studying biological processes, which will not only impact stem cell research in general but also provide useful information in support of biomedical device development, and tissue engineering. Although the intended purpose for developing 3D MNMs is to produce novel bioactive systems, their applicability is more general and may find use in a broad range of applications including electronics, photonics, optoelectronics, and chemical and biochemical sensors.

APPROVAL FOR SCHOLARLY DISSEMINATION

The author grants to the Prescott Memorial Library of Louisiana Tech University the right to reproduce, by appropriate methods, upon request, any or all portions of this Dissertation. It is understood that "proper request" consists of the agreement, on the part of the requesting party, that said reproduction is for his personal use and that subsequent reproduction will not occur without written approval of the author of this Dissertation. Further, any portions of the Dissertation used in books, papers, and other works must be appropriately referenced to this Dissertation.

Finally, the author of this Dissertation reserves the right to publish freely, in the literature, at any time, any or all portions of this Dissertation.

Author S. Mohammed Jaweed

Date 5/3/2006

DEDICATION

This dissertation is dedicated to my parents, Moula Basha Shaikh and Malin Mohammed, and my brother Jameel Shaik.

TABLE OF CONTENTS

ABSTRACT.....	iii
DEDICATION.....	vi
TABLE OF CONTENTS.....	vii
LIST OF TABLES.....	xii
LIST OF FIGURES	xiii
ACKNOWLEDGMENTS	xix
CHAPTER 1 INTRODUCTION.....	1
1.1 Nanoscale Self-Assembly.....	7
1.1.1 Self-Assembled Monolayers.....	7
1.1.2 Layer-by-Layer Self-assembly.....	9
1.2 Significance of Patterning.....	14
1.3 Patterning of Self-Assembled Films.....	19
1.3.1 Soft Lithography.....	19
1.3.2 Photolithography.....	21
1.3.3 Other Techniques.....	21
1.4 Objectives and Novel Aspects.....	22
1.5 Organization of Chapters.....	23
CHAPTER 2 BACKGROUND.....	25
2.1 Single-Component Patterning.....	26
2.1.1 Monolayer Film Patterning.....	26
2.1.1.1 Microcontact printing.....	26
2.1.1.2 Patterning using microfluidic networks	27
2.1.1.3 Patterning using elastomeric membranes	27
2.1.1.4 Photolithography.....	28
2.1.1.5 Other techniques.....	28
2.1.2 Multilayer Nanocomposite Film Patterning.....	29
2.1.2.1 Photochemical reactions.....	29
2.1.2.2 Chemically templated patterning.....	30
2.1.2.3 Patterning using microfluidic networks	31
2.1.2.4 Microcontact printing.....	31
2.1.2.5 Layer-by-layer-lift-off.....	32

2.1.2.6 Other techniques	32
2.2 Multicomponent Patterning	33
2.2.1 Monolayer Film Patterning	33
2.2.1.1 Printing using multilevel stamps	33
2.2.1.2 Patterning using 2D and 3D microfluidic networks	33
2.2.1.3 Patterning using elastomeric membranes	34
2.2.1.4 Thermo-biolithography	35
2.2.1.5 Photolithography	35
2.2.1.6 Other techniques	35
2.2.2 Multilayer Nanocomposite Film Patterning	36
2.2.2.1 Multilayer transfer printing	36
2.2.2.2 Comparison chips	37
2.2.2.3 Polymer surface micromachining	38
CHAPTER 3 MULTICOMPONENT POLYMER PATTERNING-PART I:	
COMPARISON CHIPS	39
3.1 Introduction	39
3.2 Materials	41
3.2.1 Substrates	41
3.2.2 Chemicals	41
3.2.3 Preparation of Polyelectrolyte and Polypeptide Solutions	42
3.3 Methods	42
3.3.1 Mask Design	42
3.3.2 Fabrication	43
3.3.2.1 Substrate pretreatment	43
3.3.2.2 Photolithography	45
3.3.2.3 Layer-by-layer self-assembly	45
3.3.2.4 Lift-off	46
3.3.3 Characterization	47
3.3.3.1 Quartz crystal microbalance	47
3.3.3.2 Fluorescence microscopy	48
3.3.3.3 Surface profilometry	49
3.3.3.4 Atomic force microscopy	49
3.3.4 Cell Culture	50
3.4 Results and Discussion	50
3.4.1 QCM Measurements	50
3.4.2 Fluorescence Microscopy	53
3.4.3 Surface Profiler Measurements	57
3.4.4 AFM Measurements	59
3.4.5 Cell Culture Results	60
3.5 Conclusions	63
CHAPTER 4 MULTICOMPONENT POLYMER PATTERNING-PART II: POLYMER	
SURFACE MICROMACHINING	65
4.1 Introduction	65
4.2 Materials	68

4.2.1 Substrates	68
4.2.2 Chemicals.....	68
4.2.3 Preparation of Polyelectrolyte and Polypeptide Solutions.....	68
4.3 Methods.....	69
4.3.1 Mask Design	69
4.3.2 Fabrication	69
4.3.2.1 Substrate pretreatment	69
4.3.2.2 Photolithography	70
4.3.2.3 Layer-by-layer self-assembly	70
4.3.2.4 Lift-off	71
4.3.2.5 Multicomponent patterning	71
4.3.3 Characterization	72
4.3.3.1 Fluorescence and phase contrast microscopy.....	72
4.3.3.2 Surface profilometry.....	73
4.3.3.3 Atomic force microscopy	73
4.3.3.4 Ellipsometry	73
4.3.3.5 Scanning electron microscopy.....	74
4.3.3.6 Roughness step testing.....	74
4.3.4 Cell Culture.....	74
4.4 Results and Discussion	76
4.4.1 Two-Component Patterns	78
4.4.1.1 Fluorescence and phase contrast microscopy.....	78
4.4.1.2 Surface profiler measurements	81
4.4.1.3 AFM measurements.....	82
4.4.1.4 Ellipsometer measurements	82
4.4.1.5 SEM measurements	83
4.4.1.6 RST measurements	84
4.4.1.7 Cell culture results.....	84
4.4.2 Two-Component Patterns of Varying Heights: Effect on Cell Adhesion.....	93
4.4.2.1 Phase contrast microscopy.....	94
4.4.2.2 Surface profiler measurements	95
4.4.2.3 AFM measurements.....	96
4.4.2.4 Cell culture results	97
4.4.3 Two-Component Pattern-on-Pattern Systems.....	98
4.4.3.1 Fluorescence and phase contrast microscopy	98
4.4.3.2 AFM measurements.....	100
4.4.4 Four-Component Patterns	101
4.4.4.1 Fluorescence microscopy	101
4.5 Conclusions.....	103
CHAPTER 5 MULTICOMPONENT NANOPARTICLE PATTERNING.....	106
5.1 Introduction.....	106
5.2 Materials	107
5.2.1 Substrates	107
5.2.2 Chemicals.....	107

5.2.3 Preparation of Polyelectrolyte and Nanoparticle Solutions	108
5.3 Methods.....	108
5.3.1 Mask Design	108
5.3.2 Fabrication	108
5.3.2.1 Substrate pretreatment	109
5.3.2.2 Photolithography	110
5.3.2.3 Layer-by-layer self-assembly	110
5.3.2.4 Lift-off	111
5.3.2.5 Multicomponent patterning	111
5.3.3 Characterization	111
5.3.3.1 Bright field microscopy	111
5.3.3.2 Surface profilometry	112
5.3.3.3 Atomic force microscopy	112
5.3.3.4 Ellipsometry.....	112
5.3.3.5 Scanning electron microscopy.....	113
5.4 Results and Discussion	113
5.4.1 Two-Component Patterns	114
5.4.1.1 Bright field microscopy	114
5.4.1.2 Surface profiler measurements	115
5.4.1.3 AFM measurements.....	117
5.4.1.4 SEM measurements	118
5.4.1.5 Ellipsometer measurements.....	119
5.4.2 Two-component Hybrid Patterns	121
5.4.2.1 Bright field microscopy	121
5.4.2.2 Surface profiler measurements	121
5.4.2.3 AFM measurements.....	124
5.4.2.4 SEM measurements	125
5.4.2.5 Ellipsometer measurements.....	126
5.4.3 Four-Component Patterns	128
5.4.3.1 Bright field microscopy	128
5.4.3.2 Surface profiler measurements	130
5.4.3.3 AFM measurements.....	130
5.4.3.4 SEM measurements	133
5.5 Conclusions.....	134

CHAPTER 6 EFFECT OF FABRICATION PROCESS PARAMETERES ON THE CHARACTERISTICS OF NANOFILMS	136
6.1 Introduction.....	136
6.2 Materials	138
6.2.1 Substrates	138
6.2.2 Chemicals.....	138
6.2.3 Preparation of Polyelectrolyte and Enzyme Solutions.....	138
6.3 Methods.....	139
6.3.1 Fabrication	139
6.3.2 Characterization	139
6.3.2.1 Ellipsometry.....	140

6.3.2.2 Fluorescence microscopy	140
6.3.2.3 UV-Vis absorbance spectroscopy	141
6.3.2.4 Attenuated total reflection-FTIR spectroscopy	142
6.3.2.5 Statistical analysis	142
6.4 Results and Discussion	142
6.4.1 Effect of Processes on Nanofilm Thickness	142
6.4.1.1 Effect of acetone on nanofilm thickness	142
6.4.1.2 Effect of resist developer-MF319 on nanofilm thickness	144
6.4.1.3 Effect of heating time at 115 °C on nanofilm thickness	146
6.4.1.4 Effect of photoresist-S1813 on nanofilm thickness	147
6.4.2 Effect of Processes on Fluorescence Intensity of Nanofilms	150
6.4.2.1 Effect of acetone on fluorescence intensity of nanofilms	150
6.4.2.2 Effect of resist developer-MF319 on fluorescence intensity of nanofilms	151
6.4.2.3 Effect of heating time at 115 °C on fluorescence intensity of nanofilms	152
6.4.2.4 Effect of photoresist-S1813 on fluorescence intensity of nanofilms	153
6.4.3 Effect of Processes on Activity of Enzyme Nanofilms	154
6.4.4 Effect of Processes on Chemical Characteristics of Nanofilms	156
6.4.5 Temporal Stability of Nanofilm Thickness	157
6.4.6 Temporal Stability of Fluorescence Intensity of Nanofilms	159
6.5 Conclusions	160
CHAPTER 7 CONCLUSIONS AND FUTURE WORK	162
7.1 Conclusions	162
7.2 Future Work	164
7.2.1 Dynamic Micropatterns of Biodegradable Nanofilms	164
7.2.2 Co-culture Systems for Stem Cell Research	165
REFERENCES	166

LIST OF TABLES

Table 1. Average thicknesses of the different multilayer architectures used in building the five different types of micropattern systems measured using a surface profilometer.....	96
Table 2. Average roughnesses of the surfaces of the different multilayer architectures used in building the five different types of micropattern systems measured using an AFM.	97

LIST OF FIGURES

Figure 1.	Schematic illustration of assorted 3D multilayer nanocomposite microstructures.....	1
Figure 2.	Template used for LBL-LO fabrication process (a), (b) Photolithography, (c) LbL assembly process, (d) LbL processed chips, (e) After lift-off, (f) Top view of the fabricated chip: Green-FITC labeled sPLA ₂ , Red-TRITC labeled BSA/PLL/gelatin.....	44
Figure 3.	Mass deposited as a function of number of layers for the assembly of (a) {PDDA/PSS} ₃ /{PEI/sPLA ₂ } ₅ , {PDDA/PSS} ₃ /{PEI/gelatin} ₅ , {PDDA/PSS} ₃ /{PEI/BSA} ₅ , and {PDDA/PSS} ₃ /{PLL/PSS} ₅ (b) {PDDA/PSS} ₃ /{PEI/(FITC-sPLA ₂)} ₅ , {PDDA/PSS} ₃ /{PEI/(TRITC-gelatin)} ₅ , {PDDA/PSS} ₃ /{(PEI/TRITC-BSA)} ₅ , and {PDDA/PSS} ₃ /{(TRITC-PLL/PSS)} ₅	52
Figure 4.	Demarcation of {PSS/PDDA} ₃ /{(FITC-sPLA ₂)/PEI} ₄ /(FITC-sPLA ₂) and {PSS/PDDA} ₃ /{PSS/(TRITC-PLL)} ₅ 20 μm patterns at 10X (a) overlay of FITC and TRITC cube images, (b) Intensity profile (green: FITC, red: TRITC) of fluorescence intensity along one of the rows in (a), {PSS/PDDA} ₃ /{(FITC-sPLA ₂)/PEI} ₄ /(FITC-sPLA ₂) 20 μm patterns at 40X (c) FITC, (d) TRITC cube, {PSS/PDDA} ₃ /{(TRITC-BSA)/PEI} ₄ /(TRITC-BSA) 20 μm patterns at 40X (e) FITC, (f) TRITC cube.	54
Figure 5.	Sequential FITC-TRITC scanning confocal images and intensity profiles of (a) {PSS/PDDA} ₃ /{(FITC-sPLA ₂)/PEI} ₄ /(FITC-sPLA ₂), (c) {PSS/PDDA} ₃ /{(TRITC-BSA)/PEI} ₄ /(TRITC-BSA) patterns, Intensity profiles (Left: FITC, Right: TRITC) of fluorescence intensity along the lines (b) {PSS/PDDA} ₃ /{(FITC-sPLA ₂)/PEI} ₄ /(FITC-sPLA ₂), (d) {PSS/PDDA} ₃ /{(TRITC-BSA)/PEI} ₄ /(TRITC-BSA).	56
Figure 6.	Average thickness of patterns on each half of the chips of three different combinations of sPLA ₂ with other proteins/polypeptide (n=3).	57
Figure 7.	(a) Average roughness (R _a) and (b) RMS roughness (R _q) of patterns on each half of the chips of three different combinations of sPLA ₂ with other proteins/polypeptide(n=3).....	58
Figure 8.	Average thickness of patterns obtained from 2-D analysis (n=3).....	59

- Figure 9. Specific attachment of neurons to FITC-labeled sPLA₂ nanofilm micropatterns. In all images, green squares are FITC-labeled sPLA₂ nanofilm micropatterns, and cells are at one day *in vitro*. Panels A and B show merged images of phase and FITC-labeled sPLA₂ nanofilm micropatterns. Panel C shows a merged image of cells plated onto TRITC-BSA nanofilms. Original microscope magnification = 100X (panel A), 400X (panel B), and 200x (panel C). Scale bars indicate 160 microns in panel A, 40 microns in panel B, and 80 microns in panel C.....61
- Figure 10. Template used for PSM method (a), (b) Photolithography of pretreated substrate, (c) LbL deposition of component 1, (d) After first lift-off, (e) Second photolithography step, (f) LbL deposition of component 2, (g) After second lift-off, (h) Top view of the chip.....77
- Figure 11. 3D interdigitated multicomponent micropatterns constructed on glass substrates: Images of 20 μm patterns (40X) collected through FITC cube with the second component (a) Offset by 50 μm in vertical and horizontal direction, (b) Offset of 50 μm in vertical direction [Green: {PSS/PDDA}₃/ {sPLA₂/(FITC-PEI)₄/sPLA₂ and Red: {PSS/PDDA}₃/ {PSS/ (TRITC-PLL)₅], (c) Phase contrast image [Dark squares: PLL patterns and Bright squares : sPLA₂ patterns], (d) Cartoon of the cross-section view of patterns.80
- Figure 12. Surface profiler line scan structural data of 3D interdigitated multicomponent nanocomposite micropatterns of PLL and sPLA₂.81
- Figure 13. (a) Scanning electron micrograph of 3D interdigitated multicomponent micropatterns comprised of PLL and sPLA₂, (b) 3D optical profiler surface micrograph of 3D interdigitated multicomponent micropatterns comprised of PLL and sPLA₂.83
- Figure 14. Tiled TRITC fluorescence, phase, FITC fluorescence, and merged phase+TRITC+FITC images (Top to bottom) of primary rat cortical neurons grown on {PSS/PDDA}₃/ {sPLA₂/(FITC-PEI)₄/sPLA₂ patterns (green) next to {PSS/PDDA}₃/ {PSS/(TRITC-PLL)₅ patterns (red). Neurons were plated onto nanofilm substrates at a density of 100,000 cells/ml in 2.7 ml of culture medium in a 35 mm Petri dish. Images were captured after 2 weeks *in vitro*. As is obvious from the location of cells on the surfaces, preferential attachment of neurons to sPLA₂-terminated films was observed.....85

- Figure 15. Merged phase+TRITC images of primary spinal cord neurons grown on $\{\text{PSS/PDDA}\}_3/\{\text{sPLA}_2/(\text{FITC-PEI})\}_4/\text{sPLA}_2$ patterns (uncolored) next to $\{\text{PSS/PDDA}\}_3/\{\text{PSS}/(\text{TRITC-PLL})\}_5$ patterns (red) after 7 DIV: (a) Cells of neuronal morphology (consistent with Figure 14) were captured by the sPLA_2 -terminated nanofilms (FITC fluorescence omitted for clarity), (b) Cells of glial morphology (in contrast to Figure 14) are captured by the PLL-terminated patterns (red)..... 88
- Figure 16. Tiled merged phase+TRITC images of primary brain neurons grown on $\{\text{PSS/PDDA}\}_3/\{\text{sPLA}_2/(\text{FITC-PEI})\}_4/\text{sPLA}_2$ patterns (uncolored) next to $\{\text{PSS/PDDA}\}_3/\{\text{PSS}/(\text{TRITC-PLL})\}_5$ patterns (red) after 40 DIV: Preferential attachment of astrocytes to PLL-terminated patterns (red)..... 89
- Figure 17. Phase (left) and merged phase+TRITC+FITC (right) images of primary rat cortical neurons at 4 DIV grown on $\{\text{PSS/PDDA}\}_3/\{\text{sPLA}_2/(\text{FITC-PEI})\}_4/\text{sPLA}_2$ patterns (green) next to $\{\text{PSS/PDDA}\}_3/\{\text{PSS}/(\text{TRITC-PLL})\}_5$ patterns (red). Neuronal cells attach and form networked cell-cell connections only on the sPLA_2 nanofilm patterns. 90
- Figure 18. Primary cortical neurons at 7 DIV grown on $\{\text{PSS/PDDA}\}_3/\{\text{sPLA}_2/(\text{FITC-PEI})\}_4/\text{sPLA}_2$ patterns (green) next to $\{\text{PSS/PDDA}\}_3/\{\text{PSS}/(\text{TRITC-PLL})\}_5$ patterns (red), loaded with calcium indicator (Fluo-3 AM): (a) Quantitative fluorescence analysis of intracellular calcium dynamics for three neurons (marked), pseudocolor fluorescence+ phase merge image of neurons after 500 μM glutamate stimulus (inset). Calcium concentrations are represented as fluorescence intensity (F) divided by baseline intensity (F_0) values for each individual cell, (b) Neurons specifically adhering to sPLA_2 -terminated nanofilms post-treatment with glutamate. 91
- Figure 19. 3D interdigitated multicomponent micropatterns of varying heights of sPLA_2 and PLL nanofilms: Images of 20 μm patterns (40X) with the second component offset by 50 μm in vertical and horizontal direction: (a)-(c) sPLA_2 micropatterns taller than PLL patterns (type I, II, III), (d) PLL patterns taller than sPLA_2 patterns (type IV), and (e) PLL and sPLA_2 micropatterns of same heights (type V)..... 95
- Figure 20. Two-component pattern-on-pattern systems: Images of 50 μm stripe patterns with multilayer architectures of $\{\text{PSS}/\text{TRITC-PAH}\}/\{\text{PSS}/\text{PDDA}\}_3/\{\text{PSS}/\text{PLL}\}_5$ and $\{\text{PSS}/\text{FITC-PAH}\}/\{\text{PSS}/\text{PDDA}\}_3/\{\text{PSS}/\text{PDL}\}_5$ collected (40X) through (a) TRITC cube, (b) FITC cube, and (c) overlay of images in (a) and (b); (d) phase contrast image of stripe patterns with multilayer architectures of $\{\text{PSS}/\text{PDDA}\}_3/\{\text{PSS}/\text{Cy5-PAH}\}_5$ and $\{\text{PSS}/\text{PDDA}\}_3/\{\text{PSS}/\text{TRITC-PAH}\}_5$ 99

Figure 21. AFM micrograph of two-component pattern-on-pattern system: 50 μm stripe patterns with multilayer architectures of $\{\text{PSS/PDDA}\}_3/\{\text{PSS/Cy5-PAH}\}_5$ and $\{\text{PSS/PDDA}\}_3/\{\text{PSS/TRITC-PAH}\}_5$	100
Figure 22. (a) Sequential Cy5-FITC-TRITC scanning CLSM images and overlay image at 10X, (b) Overlay image at 63X, (c) Digitally zoomed overlay image showing one pattern each for the four-component patterns: Blue- $\{\text{PSS/PDDA}\}_3/\{\text{PSS}/(\text{Cy5-PAH})\}_5$, Light red- $\{\text{PSS/PDDA}\}_3/\{\text{PSS}/(\text{TRITC-PLL})\}_5$, Green- $\{\text{PSS/PDDA}\}_3/\{\text{PSS}/(\text{FITC-PEI})\}_5$, and Bright red: $\{\text{PSS/PDDA}\}_3/\{\text{PSS}/(\text{Texas Red-PAH})\}_5$; (d) Linescan intensity data for image in (c), before processing: Blue long dash-Cy5, Red-TRITC, Maroon dash-dot-Texas Red, Green short dash-FITC.	102
Figure 23. General template used for the PSM method (a) Photolithography of pretreated substrate, (b) LbL deposition of component 1, (c) After first lift-off, (d) Second photolithography step, (e) LbL deposition of component 2, (f) After second lift-off.....	109
Figure 24. Brightfield images of two-component nanocomposite NP-on-NP micropatterns fabricated under (a) Condition I and (b) condition II.	115
Figure 25. Thicknesses data obtained from surface profilometry and AFM measurements for the two-component nanocomposite NP-on-NP micropatterns fabricated under (a) Condition I and (b) Condition II.....	116
Figure 26. AFM micrographs of two-component nanocomposite NP-on-NP micropatterns fabricated under (a) Condition I and (b) Condition II.....	117
Figure 27. Tiled SEM micrographs of two-component nanocomposite NP-on-NP micropatterns fabricated under (a) Condition I and (b) Condition II.....	119
Figure 28. Thicknesses data for the non-patterned nanofilms obtained from ellipsometric measurements and patterned NP-on-NP nanofilms obtained from surface profilometry and AFM measurements.....	120
Figure 29. Brightfield images of two-component hybrid polymer-on-NP micropatterns fabricated under condition I.	122
Figure 30. Thicknesses data obtained from surface profilometry and AFM measurements for the two-component hybrid polymer-on-NP micropatterns fabricated under (a) Condition I and (b) Condition II.....	123
Figure 31. AFM micrographs of two-component hybrid polymer-on-NP micropatterns fabricated under (a) Condition I and (b) Condition II.....	125

Figure 32. Tiled SEM micrographs of two-component hybrid polymer-on-NP micropatterns fabricated under (a) Condition I and (b) Condition II.....	126
Figure 33. Thicknesses data for the non-patterned nanofilms obtained from ellipsometric measurements and patterned polymer-on-NP nanofilms obtained from surface profilometry and AFM measurements.	127
Figure 34. Tiled brightfield images at magnifications of 5X (left) and 50X (right) of four-component interdigitated NP micropatterns fabricated under (a) Condition I and (b) condition II, (c) Cartoon of the cross-sectional view of the patterns.	129
Figure 35. Thicknesses data obtained from surface profilometry and AFM measurements for the four-component interdigitated NP micropatterns fabricated under (a) Condition I and (b) Condition II.....	131
Figure 36. Tiled AFM micrographs of four-component interdigitated NP micropatterns fabricated under (a) Condition I and (b) Condition II.....	132
Figure 37. Tiled SEM micrographs of four-component interdigitated NP micropatterns fabricated under (a) Condition I and (b) Condition II.....	133
Figure 38. Tiled SEM micrographs of four-component interdigitated NP micropatterns fabricated under condition I.	134
Figure 39. Ellipsometric measurements of nanofilm thickness: Effect of acetone on PEMs of (a) PSS/PDDA, (b) PSS/PEI, (c) PSS/PAH, (d) PSS/FITC-PEI, (e) GOx.....	143
Figure 40. Ellipsometric measurements of nanofilm thickness: Effect of resist developer-MF319 on PEMs of (a) PSS/PDDA, (b) PSS/PEI, (c) PSS/PAH, (d) PSS/FITC-PEI, (e) GOx.....	145
Figure 41. Ellipsometric measurements of nanofilm thickness: Effect of heating time at 115 °C on PEMs of (a) PSS/PDDA, (b) PSS/PEI, (c) PSS/PAH, (d) PSS/ FITC-PEI, (e) GOx.....	147
Figure 42. Ellipsometric measurements of nanofilm thickness: Effect of photoresist-S1813 on PEMs of (a) PSS/PDDA, (b) PSS/PEI, (c) PSS/PAH, (d) PSS/FITC-PEI, (e) GOx.....	148
Figure 43. Quantitative measurements of fluorescence intensity of nanofilms: Effect of acetone on PEMs of (a) PSS/FITC-PEI, (b) PSS/FITC-PAH.	150

Figure 44. Quantitative measurements of fluorescence intensity of nanofilms: Effect of resist developer-MF319 on PEMs of (a) PSS/FITC-PEI, (b) PSS/FITC-PAH.	151
Figure 45. Quantitative measurements of fluorescence intensity of nanofilms: Effect of heating time at 115 °C on PEMs of (a) PSS/FITC-PEI, (b) PSS/FITC-PAH.	152
Figure 46. Quantitative measurements of fluorescence intensity of nanofilms: Effect of photoresist-S1813 on PEMs of (a) PSS/FITC-PEI, (b) PSS/FITC-PAH.	153
Figure 47. Quantitative measurements of activity of enzyme embedded in PEM nanofilms: Effect of (a) acetone, (b) resist developer-MF319, (c) heating time at 115 °C, (d) photoresist-S1813 on the activity of GOx.	155
Figure 48. ATR-FTIR spectra of {PSS/PAH} ₅ PEM nanofilms showing the effect of resist developer-MF319 on the characteristic bands of interest (indicated by the arrows).....	157
Figure 49. Ellipsometric measurements of nanofilm thickness: Temporal stability of (a) PSS/PDDA, (b) PSS/PEI, (c) PSS/PAH, (d) PSS/FITC-PEI, and (e) GOx PEMs in DI water.....	158
Figure 50. Quantitative measurements of fluorescence intensity of nanofilms: Temporal stability of (a) PSS/FITC-PEI and (b) PSS/FITC-PAH PEMs in DI water.....	160

ACKNOWLEDGMENTS

I would like to express my sincere gratitude to my advisor Dr. Michael J. McShane for his tireless dedication to his students and for his excellent guidance and mentorship. I would like to thank Dr. Mark A. DeCoster for fruitful collaborations, and for the cell culture work. I would also gratefully acknowledge the expert technical assistance of Bron Daniel. Dr. Mengyan Li, Drexel University, is acknowledged for her initial work in developing the liftoff procedure for nanofilm patterning. Dr. Huiguang Zhu and Erich Stein are thanked for assistance with confocal imaging. Rajendra Aithal and Aaron Mack are thanked for assistance with infrared spectroscopy. I would like to appreciate the time and support of my advisory committee members, Dr. Yuri M. Lvov, Dr. David K. Mills, Dr. Sidney Sit, and Dr. Cheng Luo. I would like to acknowledge Mr. Philip Coane, Dr. Alfred Gunasekaran, Dr. Xu, Mr. Scott Williams, Mr. Donald Tatum, Ms. Deborah Wood, Mr. Ji Fang, and Mr. John McDonald for their assistance in metrology, and for arranging special facilities needs and access. I appreciate the continuous support from past and current BIOMINDS lab members. I would like to acknowledge financial support from the College of Engineering & Science, National Science Foundation (Grant No. 0092001), and National Institutes of Health (Grant No. P20RR016816). Finally, I would like to thank my parents Moula Basha Shaikh and Malin Mohammed, whose persistent support has put me at this position in life.

CHAPTER 1

INTRODUCTION

Nanotechnology is an evolving field encompassing and impacting every walk of life. It allows the manipulation and control of matter at the nanometer level (roughly 1 to 100 nanometers), where unique bio-physicochemical phenomena enable novel applications¹ and therefore are believed to have broader impacts on several different fields including medicine, biology, photonics, electronics, analytical chemistry, etc. This work is focused on developing platform techniques through the integration of “bottom-up” nanoscale self-assembly approaches with “top-down” microscale lithography approaches for the fabrication of assorted three-dimensional multilayer nanocomposite microstructures as shown in Figure 1.

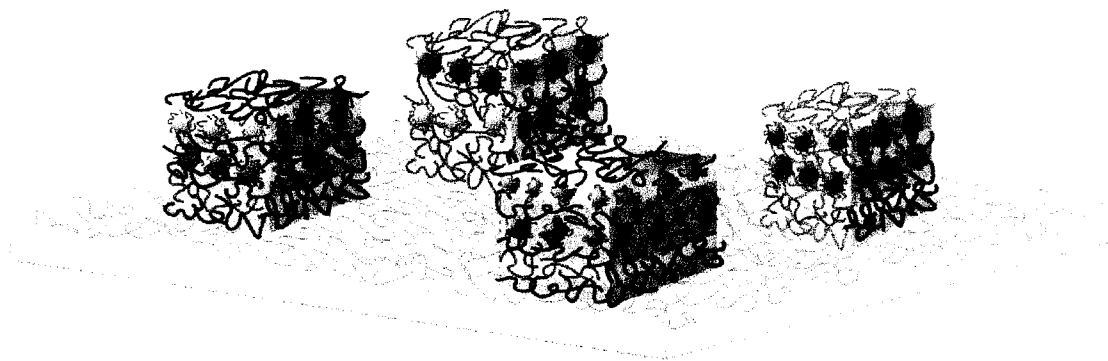


Figure 1. Schematic illustration of assorted 3D multilayer nanocomposite microstructures.

Such nanocomposite microstructures could be used for applications in a variety of fields such as biology, sensors, electronics, chemical microsystems, etc. Discoveries in the areas of cell-biomaterial and cell-cell interactions are highly significant² due to the great insight they can provide into fundamental cell biology³ and their potential value for medicine and biotechnology. It is generally understood that the ability to engineer and control cellular behavior is highly dependent on presentation of physical and chemical cues.²⁻⁴ Therefore, development of complex functional biointerfaces, where the positioning of and interaction between cells of different types can be precisely controlled, requires placement of biomaterials with differing functionality in specific configurations on the same substrate.³ The biological, biotech, or medical applications of any emerging technology are highly intriguing and useful for the well being of the human beings; therefore, the applications presented for the techniques developed in this research work are related to the definition, characterization, and understanding of spatial cell microenvironment.

The cell microenvironment, comprising physical and chemical cues, greatly influences cell behavior. Extracellular matrix (ECM) molecules provide the physicochemical cues that influence cell growth and tissue development *in vivo*.⁴ Cells respond to and help maintain a complex ECM with specific chemical properties and nanoscale and microscale features. This “dynamic reciprocity” between cells and ECM is well known and is considered critical to tissue engineering and development of artificial organs. The development of a complex multicellular organ requires precise control over cell migration, proliferation, and survival that in turn requires integration of long-range signals like growth factors⁵ with short-range cues that define physical location of cells.⁶

Similarly, the ability to engineer and control the physicochemical cues *in vitro* is critical for a better understanding of fundamental cell biology.^{3,7} Parameters such as hydrophobicity, surface charge, molecular and elemental composition, and roughness are known to affect protein adsorption and, consequently, cell-matrix interactions.⁸

Recent reports have provided significant evidence that substrate roughness strongly influences the behavior of adherent cells. For example, osteoblasts have been shown to attach and proliferate on smooth surfaces (tissue culture plastic, tissue culture glass, and titanium), but exhibit relatively low expression of differentiation markers; in contrast, opposite behavior osteoblasts cultured on microrough Ti surfaces ($R_a = 4\text{--}7\mu\text{m}$), and the hydroxyapatite production from cells on microtextured surfaces was more typical of natural bone. Furthermore, the osteoblasts exhibited enhanced responses to 1,25-dihydroxy vitamin D3 or β -estradiol when grown on roughened substrates, and increased production of TGF- β_1 that promote osteogenesis.⁹

Mechanical forces have long been known to play a critical role in cellular interactions with the extracellular matrix, particularly for adherent cells (mesenchymal cells).¹⁰⁻¹⁴ However, an appreciation of substrate stiffness as a significant factor in modulating cell behavior has only recently developed.¹⁵ A prime example of how cells sense their mechanical as well as molecular microenvironment can be found in the interaction of myocytes with surface of varied elasticity,¹⁶ where it has been shown that fusion into myotubes occurs independent of substrate flexibility, whereas myosin/actin striations emerge later only on gels with stiffness typical of normal muscle (passive Young's modulus, E , ~ 12 kPa). On glass and much softer or stiffer gels, including gels emulating stiff, dystrophic muscle, cells do not striate. It was further noted that myotubes

grown on top of a more compliant, earlier-seeded layer of glass-attached myotubes will striate, whereas the bottom cells will only assemble stress fibers and vinculin-rich adhesions. Similarly, myofibroblast differentiation (α -SMA content) induced by TGF- β_1 is dependent on the resistance of the substrate to deformation, leading to the conclusion that the generation of intracellular tension is a central determinant of contractile cytoskeletal gene expression.¹⁷ In a very recent study, when various types of differentiated cells were cultured on fibronectin- or collagen-coated as surfaces with stiffness ranging from 2 to 55,000 Pa, fibroblasts and endothelial cells exhibited a marked change in spread area and appearance of actin stress fibers above a stiffness of 3,000 Pa; neutrophils, in contrast, showed no dependence on substrate stiffness.¹⁸ Interestingly, these surface-dependent behaviors disappeared when fibroblasts or endothelial cells made cell-cell contact in denser cultures. These results support the concept that mechanical factors influence different cell types in fundamentally different ways, and can trigger specific changes similar to those stimulated by soluble ligands.

Since stem cells are precursors to “anchorage-dependent” cells, it is logical to expect that substrate stiffness will also directly influence stem cell behavior, especially in the expression of markers associated with anchorage-dependent cells. Only a single example was found where this concept had been explored.¹⁹ Also, experiments have demonstrated differentiation of stem cells within supports that provide desired biomechanical properties for tissue engineering.²⁰⁻²⁴ All these findings prove the importance of having an optimal mechanical environment to support specific cell behaviors, and it is believed that precise arrangement of specific chemical and mechanical cues will enable production of bioactive systems.^{2,7,8,25,26}

Tremendous interest in cell-based therapeutic systems has led to an ever-growing need for tools to investigate the intricate details of cell-substrate²⁷ and cell-cell interactions. Especially with the advent of stem cell research, there has been a surge in efforts to understand biochemical pathways of proliferation, migration, and differentiation under different physical and chemical conditions. Stem cells have the potential for self-renewal, have an uncommitted phenotype, and can differentiate into multiple lineages.²⁸ However, one of the major challenges facing stem cell use is the lack of knowledge of how chemical, spatial and temporal cues within the *in vivo* microenvironment direct their differentiation. During tissue development, the character and composition of the ECM not only play a significant role in cell adhesion and migration, but also direct cellular differentiation through molecular signaling by mitogens and morphogens in the local microenvironment. Therefore, an ultimate goal is to define the factors (spatial organization, specific two- or three-dimensional configurations, instructional biofactors, mechanical forces) that influence the type, timing and extent of cell fate decisions. Hence, there is an immediate demand for developing platforms with precise control over the presentation of physical and chemical cues to the cells, in space and time.

Such a goal requires the ability to control and analyze physical and chemical properties at the molecular (nano) to supra-cell (hundreds of microns) level, and do so over wide areas (few millimeters to many centimeters). To attack these complex problems, a number of enabling technologies exist to provide exquisite control over the arrangement of physicochemical cues. Self-assembly methods, such as self-assembled monolayers (SAMs) and layer-by-layer (LbL) self-assembly provide precise nanoscale-

control over the fabrication of pre-designed heterogeneous structures, with tunable structural properties and compositions, and lithographic patterning techniques have been applied for lateral nanofilm definition. However, the systems developed thus far are primitive and limited in applicability toward cell-based studies. For example, a progressive decrease in the size of micropatterns containing ECM caused human and bovine capillary endothelial cells to switch from growth to apoptosis, suggesting “geometric control over cell life and death.”²⁹ Furthermore, application of this knowledge to engineer complex systems has been demonstrated: a conduit of a porous biodegradable poly(D,L-lactic acid) tubular support structure with a micropatterned inner lumen, pre-seeded with Schwann cells, provided a combination of physical, chemical and biological guidance cues for regenerating axons at the cellular level.³⁰

Through these limited examples, the power of micro/nanoscale manipulation of cells and biomolecules to study basic processes and build functional biological systems is clear; however, it is just beginning to be realized, and critical gaps remain in understanding of the translation of surface properties into cellular behavior. It has been difficult to recreate pseudo-ECM *in vitro*, largely due to limitations in construction of appropriate culture scaffolds. In view of the recent developments in cell biology and the recognized need for improved biointerfaces, the primary emphasis of this research work aims at exploring the integration of nanoscale multilayer self-assembly with photolithographic patterning toward creation of three-dimensional nanocomposite systems. The patterns will have microscale dimensions to match the scale of cells; however, the surface variations in chemistry and topography provided by the self-assembly will be nanoscale to approximate the natural cellular microenvironment.

The ultimate goal of this research work is to use the techniques developed to construct biomimetic nanofilm surfaces, with designed properties, which will define the spatial microenvironment of different cell types. It is anticipated that the successful development of the biomimetic systems will provide a general platform for studying biological processes, which will impact stem cell research, biomedical devices, and tissue engineering.

1.1 Nanoscale Self-Assembly

Nanoscale self-assembly refers to the deposition of an organized layer of thickness in nanometer to micron range onto a substrate with precise control and/or ordering. Self-assembly methods, such as SAMs and LbL self-assembly provide precise nanoscale-control over the fabrication of high resolution pre-designed heterogeneous structures, with tunable composition and properties. SAM and LbL self-assembly techniques have been widely used, either separately or in integrated approaches, for cell-related studies. Both techniques have unique features which allow tuning of the physicochemical environment of cells in a defined spatial fashion. These approaches may be combined with micro/nanofabrication processes to produce three-dimensional nanocomposite systems with specific chemical, electrical, mechanical, and biological functionality.

1.1.1 Self-Assembled Monolayers

Self-assembled monolayers, studied first by Nuzzo and Allara in 1983,³¹ are homogeneous, highly ordered, and can be easily formed on appropriate substrates by dipping them into solutions of desired composition.³² Being ultrathin (~1-5 nm) as well as optically transparent and electrically conductive, they are compatible with

spectroscopic and electrochemical studies.³³ The packing density and chain lengths can be varied to tune the monolayer properties.³⁴ A major advantage with SAMs is that their end groups can be different functional groups or molecules that may be incorporated either before or after the monolayer deposition.^{35,36} Thus, the end groups may be functionalized to be either cell-adhesive or cell-repellent, reactive for later modification, or have features required for integration with the assembly process (e.g., certain charge or hydrophilicity). With these capabilities to tailor surface physical and chemical properties, SAMs have been broadly used for cell-related studies.^{37,38} Whitesides³⁹ and others^{40,41} have studied a wide range of SAMs⁴² and also demonstrated that, using simple lithographic techniques, they are highly amenable to patterning.^{32,43}

Self-assembled monolayers provide flexibility in materials, for example different chain lengths and functional groups, and possibilities for changing the molecular properties of the monolayer, before or after deposition. For example, SAMs have been modified in low densities,⁴⁴ and ligands have been patterned on SAMs, demonstrating potential for fabricating gradients or for immobilizing multiple ligands.⁴⁵ Gradient surfaces of immobilized biomaterials are useful tools to understand the cellular response to concentration changes.⁴⁶ In the case of mixed SAMs used to generate different functional group densities, the degree of conformational rearrangements of adsorbed proteins depends upon the density of the surface hydrophobic groups and the concentration of protein in the solution.^{41,47}

Generally, SAMs have been employed to develop a static surface for desired interfacial properties.⁴⁸⁻⁵⁰ However, recently Mrksich et al. have demonstrated the fabrication of dynamic substrates based on electroactive SAMs.⁵¹⁻⁵³ SAMs adsorbed to

gold surfaces have been used in conjunction with electrical signals to elicit temporal variations, releasing attached groups through an electrical potential applied to the metal.⁵⁴⁻⁵⁷ Furthermore, dynamic behavior of a more complex system involving release of one ligand followed by the immobilization of a second ligand was demonstrated using a SAM incorporated with an *o*-silyl hydroquinone moiety.⁵⁸ The advantage of these electrically activated systems is that the triggers are essentially noninvasive and the effects are well controlled, but a limitation is that they provide only a single type of temporal variation. To mimic the more complex dynamics of the ECM, multiple time-varying signals are required, and their actions must be orchestrated.

1.1.2 Layer-by-Layer Self-Assembly

Layer-by-layer self-assembly, introduced to practice by Decher in 1991,^{59,60} is a versatile method based primarily on the alternating deposition of charged polymers from dilute aqueous solutions onto surfaces of any size, shape, or material.⁶¹ The electrostatically-adsorbed molecules are used to produce nanoscale films with highly tunable architectures and properties, including film thickness (typically 2-10 nm per layer), uniformity, composition, conformation, roughness, porosity, and molecular structure. LbL assembly may also be based on interactions other than electrostatic, such as van der Waals,⁶² hydrogen bonding,⁶³ biomolecular recognition,⁶⁴ and others. The LbL method allows incorporation of functionalized macromolecules, enzymes, DNA, colloids, nanoparticles, and proteins in the film architecture embedded at different depths, thereby realizing complex nanoarchitectures with specific biomimetic properties.^{8,25,61,65-73}

A broad body of knowledge has been generated on the properties of polyelectrolyte multilayers (PEMs) in general, yet infinite possibilities exist for

combinations of materials to realize films of desired thickness (with nanometer resolution), chemical, physical, mechanical, and optical properties.⁷⁴⁻⁷⁸ The LbL self-assembly method allows deposition of nanofilms with features similar to SAMs, with an additional capability of more easily varying the composition of a multilayer film in the direction normal to the substrate. A second key difference from SAMs is the amorphous structure and interpenetration of neighboring layers. In addition, while the LbL process adds the flexibility in composition and ease of construction, molecular arrangements and gradients are harder to control. In the case of LbL multilayer nanofilms, the parameters that may be varied to control the nanofilm architecture include the molecules assembled, number of layers, assembly pH,^{79,80} concentration, charge density,⁸¹⁻⁸⁵ and ionic strength.⁸⁶⁻⁹⁰

With these versatile capabilities, the LbL technique is now being applied to study cellular interactions with different materials and structures.^{8,25,65,67,91-93} In addition, recent studies have employed bioactive molecules, such as hormones, embedded in multilayers.^{67,94} For example, it was reported that cells interact with proteins embedded in multilayer films through the local degradation of the film and the extension of cellular membrane up to the protein layer.⁷³ Retinal cells cultured on micropatterned polyelectrolyte multilayer lines were observed to be more elongated than cells cultured on polystyrene.⁹⁵ The cell adhesion and morphology⁹¹ depended upon the underlying material properties. Depending upon the film composition and assembly conditions (pH), films exhibited variability in resistance to fibroblast adhesion.^{25,61} Highly crosslinked films attracted cells, whereas weakly ionically crosslinked multilayers, which swell substantially in physiological conditions to present hydrated surfaces, resisted fibroblast

attachment. It was found that by manipulating the molecular architecture of the thin films, it is possible to cause even a single multilayer combination to be either cell adhesive or cell resistant.

Multilayer films have been shown to exhibit thickness-dependent stiffness when deposited on solid substrates, and the effective modulus was found to increase tenfold after crosslinking.⁹⁶ For poly(L-lysine)/hyaluronan multilayers, measured moduli range from ~40-90 kPa up to ~800 kPa for native and crosslinked films, respectively. Much higher moduli have been reported for PAH/PSS nanofilms, ranging from 100s of MPa in the hydrated state to GPa when dried.⁹⁷ Polycations have also been modified with silanes⁹⁸ that condense and form a sol-gel-like material with increased stiffness relative to the unmodified polymers. These capabilities are crucial for mimicking *in vivo* microenvironment because it is expected that the nanofilm mechanical properties are key factors in determining cellular response. In a recent report, mouse embryonic stem cells were seeded onto polystyrene coated with multilayer assemblies containing various cell-adhesive proteins and synthetic polycations using the layer-by-layer technique.¹⁹ Interestingly, no significant differences were observed in the growth of stem cells in the presence (non-differentiated) and absence (differentiated) of leukemia inhibitory factor in complete serum-containing media, presumably due to the modification of the surfaces due to protein adsorbing from the media. However, when seeded in serum-free media, crosslinked (stiffer) polycation surfaces promoted and hindered the growth of non-differentiated cells and differentiated cells, respectively. In a very recent report, it has been shown that the adhesion and spreading of chondrosarcoma cells depends on the stiffness of poly(L-lysine)/hyaluronan multilayers.⁹⁹

Layer-by-layer self-assembly has also been explored for developing responsive systems¹⁰⁰ with control over temporal release properties. The permeability properties of PEMs can be dynamically varied using, for example, changes in solvent, pH, and salt concentration. Microcapsules with PEM walls were found to be 'closed' at pH 8 and higher but permeable to macromolecules at pH lower than 6, with the states being completely reversible.¹⁰¹ Furthermore, PEMs of poly(ethyleneimine) and poly(acrylic acid) showed reversible switching for controlled uptake and release of the proteins lysozyme and human serum albumin attached to their surface, mediated through changing the ambient pH.¹⁰² It has also been shown that small molecules absorbed within hydrogen-bonded and electrostatically-assembled multilayers can be released from films by application of an external stimulus (pH change).¹⁰³

Some key demonstrations involving biodegradable systems are also worth further discussion. A multilayered assembly of plasmid DNA and a synthetic degradable polyamine was constructed for transfection applications, and the construct gradually eroded upon incubation in phosphate buffered saline at 37 °C, leading to sustained release of functional plasmid DNA under physiological conditions.^{104,105} It has also been shown that multilayer assemblies of weak polyacids and strongly dissociated polycations decompose rapidly in aqueous NaCl solutions (>0.6 M).¹⁰⁶ In multilayer constructs comprising degradable polycations and non-degradable polyanions, it was observed that the structures eroded gradually under physiological conditions and that they were suitable for the incorporation and subsequent release of functional polyanions such as DNA.¹⁰⁷ These findings point to the potential for tremendous control over release by designing nanocomposite structures with tailored degradation rates. It is also noteworthy that cells

can modify surfaces through local secretion of adhesive proteins and degradative enzymes, or may indirectly degrade the surfaces through local mechanical stress or pH variations, adding another level of complexity to the system.¹⁰⁸

Advanced materials comprising nanocomposite multilayer assemblies of polymers and nanoparticles have been demonstrated using a variety of metal, semiconductor, and dielectric materials.¹⁰⁹⁻¹¹² Ordered nanostructured films with desired periodicity have been created to tune mechanical, magnetic, electrical, optical, and optoelectronic properties.^{109,112} LbL self-assembly has been widely used in conjunction with different kinds of nanoparticles to form either flat surfaces or spherical templates.¹¹³⁻¹¹⁸ Densely packed, conformable sheets of rigid crystals form in the adsorption process when alternated with flexible polyion “glue.”¹¹⁰ Growth of nanoparticle-polyelectrolyte multilayers may occur in both normal (vertical) and in-plane (lateral) directions, depending upon assembly conditions and particle properties.¹¹¹ Patterning of nanofilms containing nanoparticles has also been demonstrated, and it has been shown that roughness of patterns can be controlled by colloidal inclusions.¹¹⁹⁻¹²⁵ LbL assembly of nanoparticles has also been employed for the modification of various surfaces for improved attachment of cells.¹²⁶ TiO₂ thin films were shown to be an optimal surface that promoted faster attachment and spreading of cells compared with other kinds of nanoparticle thin films.¹²⁷ This apparent preference of stem cells for rougher surfaces, given otherwise identical composition, may be due to the increased surface area available for the cells to interact with the material.¹²⁸

These reports, along with others, indicate the significance of multilayer nanofilms for biological applications based on a few limited morphological and functional

observations, but great detail is missing regarding the specific interactions between cells and nanoassembled materials, particularly regarding the influence of nanoscale composition and physical arrangement of the surfaces.

1.2 Significance of Patterning

It is clear from the discussion in previous sections that cells interact with an environment—natural, artificial, or hybrid—through a combination of chemical and physical cues, and respond by changing morphology, orientation, motility, or various activation/deactivation processes, including apoptosis. Because of the exquisite control over these critical features at the micro/nanoscale, the topographical control of cells using micro/nanopatterned surfaces has been of increasing interest. Patterning offers potential for control and manipulation of two fundamental external signals, the cell-substrate and cell-cell interactions.^{25,61,108,129-134} A number of methods have been developed to generate chemical patterns and physical structures with specific interest in studying cell-material interactions at the micro/nanoscale. Anisotropic cell culture surfaces patterned with amino- and alkylsilanes have been shown to guide cell distribution and provide an approach to study important processes involved in tissue engineering, such as cell attachment, locomotion, and programmed cell death.^{29,135-138}

While excellent progress has been made in understanding the differential effect of microstructural and chemical cues on cell adhesion and orientation,¹³⁹ little progress has been made in patterning methods that have been applied to control cell adhesion, in general,²⁹ and in attempts to define on-chip neural networks.¹⁴⁰ This is especially important for neurons because of the intrinsic potential of one neuron to influence, or be influenced by, many other neurons. Thus, neurons form networks *in vivo* and *in vitro*, but

until recently, the ordering or “patterning” of neurons *in vitro* has not been utilized to study their cell biology. Patterning of surface chemistry has been used to study materials that are conducive to long-term neural cell compliance in cultures.¹³⁸ Early work on patterning of neurons used selective removal of cell-adhesive self-assembled monolayers.^{135,136,138} A photoresist-based technique for patterning of covalently bound silanes on glassy substrates was developed to control growth of primary hippocampal neurons in low-density culture with microscale resolution.¹⁴¹ A technique for micropatterning of cells based on the use of oxygen plasma through an elastomeric stencil as a patterning tool was recently reported.¹⁴²

Nevertheless, tissue engineering requires patterning of multiple cells types on different areas of a substrate in order to build defined architecture into multifunctional tissues. The controlled attachment of desired cell populations using specific cell-signaling molecules or adhesion ligands in precisely engineered geometries will enable production of truly bioactive systems with a broad spectrum of applications.^{2,7,25} The capability to capture and maintain a permissive environment for multiple cell types is particularly important for cases where co-culture is desired, such as patterned neuronal networks, where incorporation of neuron-supporting glial cells are required,¹⁴³ and hepatocyte cultures, where the presence of fibroblasts is critical for preserving characteristics of native liver tissue.¹⁴⁴ While randomly-oriented co-cultures of multiple cell types have been used to better mimic *in vivo* systems, the type and degree of cell–cell interactions in such systems are not typically controllable at a desirable level. Therefore, recent efforts have targeted development of approaches to obtain cell cultures employing adhesive

patterns to enhance microenvironmental control through spatial localization of multiple cell types relative to each other.^{143,145,146}

Co-culture of different cell types is a useful tool to study cell-cell interactions *in vitro*.¹⁴⁷⁻¹⁴⁹ Co-culture methods, such as the Transmembrane[®] system, permit culture of multiple cell types but only approximate *in vivo* spatial relationships; micropatterned co-cultures are better tools compared with random co-cultures due to the precise arrangement of interacting cells.¹⁵⁰ For example, co-cultivation of hepatocytes and nonparenchymal cells has been used to preserve and modulate the hepatocyte phenotype.¹⁵¹ In a microfabricated co-culture system of 3T3-J2 fibroblasts and primary hepatocytes, it was observed that the hepatocyte albumin increased in the presence of fibroblasts; the albumin increase depended upon the microscale distance between the cell patterns.¹⁵² Another major step towards this understanding is the application to stem cells, which demonstrate plasticity depending on their environment.¹⁵³⁻¹⁵⁷ It is clear from above examples that studies of cell-cell communication and engineering of functional tissues are two areas that benefit from co-culture of multiple cell types, particularly stem cells in the presence of differentiated “partner” cells. A better understanding of cell-cell interactions is essential in embryogenesis, in adult physiology and pathophysiology of many disease processes.¹⁴⁴

Stem cells are of interest in fundamental biology because of their unique ability to express many phenotypes downstream of applied selection pressures and their robust nature, though it is clear that stem cell behavior is influenced by extremely complex, nonlinear interactions among many factors. It is believed that research on stem cell differentiation will clear up mysteries related to development and maturation of

individual organisms as well as interspecies relationships. Furthermore, these pluripotent precursor cells hold great potential in medicine, particularly as the central components of strategies for replacing diseased or damaged tissue. Due to the implications of stem cells in answering fundamental questions as well as their potential use in critical medical applications, a tremendous recent effort has been mounted at understanding fundamental *in vitro* and *in vivo* properties of stem cells, especially the effects of media conditions and soluble factors. An ATCC (American Type Culture Collection) multipotent mouse bone marrow stromal precursor cell (BMSC) line, is currently under investigation as a promising source for cell therapeutics and regenerative medicine strategies. This heterogeneous cell population can differentiate along multiple mesenchymal lineages to produce functional cell types, including osteoblasts, chondrocytes and adipocytes, in the presence of the appropriate stimulus and environment.¹⁵⁸ Stem cells of neural origin CRL-9392 (ATCC) can be induced to differentiate into astrocyte-type morphology by treating with transforming growth factor β (TGF- β) or by serum. Cells from a second ATCC neural line, CE3, intensely express green fluorescent protein (GFP) under conditions favorable to neuronal differentiation, enabling microscopic tracking of cells in cultures. As a complement, the ATCC G-Olig2 cell line also expresses GFP, but demonstrates oligodendrocyte (glial) cell properties.¹⁵⁹

While it is clear that environmental chemicals are powerful signals for stem cell differentiation, it is also becoming obvious that stem cells respond to a set of conditions that is much more complicated. Specifically, a strong influence of cell-cell contact, extracellular materials and structural factors has recently been demonstrated. Very recent reports have provided insight to the diverse response of stem cells to different matrix

properties and mechanical forces. For example, astrocyte stem cells grown in monolayer culture have been found to be restricted to the astroglial lineage, whereas the same cells cultured in suspension culture express neuron-specific markers.¹⁶⁰ Environmental conditions such as gravity, shear force, cell-substrate adhesion and cell-cell contact are suspected to play important roles in determining cell fate. However, the picture is clearly more complex than that because stem cells grown in monolayers on different polymeric supports, and exposed to otherwise identical conditions, exhibit very different proliferation, differentiation, and survival behaviors.¹⁶¹ Thus, an apparent underlying influence of surface properties goes beyond stem cell adhesion for anchoring; there appears to be a strong connection between cell-material interactions and phenotypic expression.

Many recent, disconnected reports have described stem cell characteristics for cultures with varying media and substrate conditions. These studies have shown clear potential for control over stem cell fate via environmental cues, though the input-output relationships are extremely complex. Unfortunately, despite strong capabilities in materials synthesis and surface engineering, and the tremendous potential for these to be applied to developing optimal environments for cell culture and tissue engineering, the picture in terms of specific substrate influences on stem cell behavior as of now is very fuzzy; no systematic work has been undertaken to fully elucidate the relationship between surface properties and stem cell fate. Furthermore, while capabilities for precise surface patterning have expanded rapidly over the past few years, these have not been exploited to investigate the spatial dependence of communications between stem cells and differentiated cells.

Spatial arrangements of anchorage-dependent cells could create a high level of complexity in co-cultures and could be used as a tool for analyzing stem cell behavior under various physicochemical conditions.¹⁶² A combination of dynamic physical and chemical cues could be intelligently used for permissive environments designed to elicit specific cell behavior, and potentially be used for selective differentiation of stem cells.¹⁶³ Recently, patterned co-cultures of hepatocytes and embryonic stem cells with fibroblasts were demonstrated using micropatterned LbL nanofilms comprising hyaluronic acid and poly-L-lysine.¹⁶⁴ Despite these advances, there is still a need for fundamental understanding of the response of stem cells to spatially-varied physical and chemical cues. These biomimetic systems with co-cultures would be suitable platforms for studying stem cell differentiation.

1.3 Patterning of Self-Assembled Films

Soft lithography and photolithography are the most commonly used techniques for the micropatterning of self-assembled nanofilms. Dip-pen nanolithography (DPN) is the most commonly used technique for the patterning of nanoscale features of self-assembled nanofilms. However, other less commonly used patterning techniques exist and are generally used for specialized applications.

1.3.1 Soft Lithography

Several soft lithography techniques have been used in conjunction with SAMs and LbL self-assembly.^{131,165,166} Soft lithography uses a transparent elastomeric poly(dimethylsiloxane) (PDMS) stamp/mold to transfer a monolayer of the desired material (inorganic, organic, or living materials) onto the surface of the substrate. Several different versions based on soft lithography have recently been developed. Some of the

most important techniques are microcontact printing (μ CP),¹⁶⁷⁻¹⁷² replica molding (REM), microtransfer molding (μ TM), micromolding in capillaries (MIMIC), solvent-assisted micromolding (SAMIM), 3D micromolding in capillaries (3D MIMIC),³² patterning using microfluidic networks (μ FN), elastomeric membranes,¹⁷³⁻¹⁷⁷ chemically templated surfaces,^{165,166,178} multilayer transfer printing (MTP).^{179,180}

Although these soft lithography techniques have advantages that include rapid prototyping, relatively inexpensive, inherent biocompatibility, and the ability to pattern on non-planar substrates, the efficiency of pattern transfer is not repeatable because it depends on several factors such as quality of the patterns on the mold/stamp, hydrophobicity of the mold/stamp and material being molded/stamped, and others that are not completely repeatable. Furthermore, the alignment of multiple material (e.g., proteins) patterns cannot be easily done using these methods. The 3D microfluidic systems used for such applications are highly complex. The chemically patterned templates have constraints on the choice of materials and stringent deposition conditions. While these methods are fast and inexpensive to use, they do not provide much versatility, particularly if more complex patterns are desired; moving from two materials to three presents a significant challenge in the processing because it is difficult to properly align the masks to existing patterns for subsequent steps. Also, the MTP process needs a fine balance of forces between the bottom-most layer of the multilayer films and the PDMS stamp (that would become the top-most layer after the multilayer films are transfer printed), which must be optimized for different materials.

1.3.2 Photolithography

Conventional photolithography has been extensively refined for advanced applications in integrated circuit (IC) technology and microelectromechanical systems (MEMS); even in the case of all the soft lithography techniques the stamp/mold is obtained through conventional lithography processes. It has also been successfully applied to patterning of self-assembled nanofilms.¹⁸¹⁻¹⁸⁵ Recently, research is being conducted on biocompatible photolithographic processes¹⁸¹ that utilize chemically amplified photoresists and dilute aqueous base developers.¹⁸⁶⁻¹⁹⁰ However, these studies have been thus far restricted to patterning monolayers of biomolecules. Photolithography combined with LbL self-assembly technique provides a powerful tool for fabricating surfaces with well-defined structures of differing functionality next to each other.¹¹⁹ The “LbL-LO” technique has recently been developed to combine photolithography and LbL processes with a single lift-off (LO) step to pattern multilayer nanofilms of biomolecules,¹⁹¹ and has been extended to production of multiprotein patterns.¹⁹²

In general, the advantages of using conventional lithography over soft lithography are ease in fabrication process, precise alignment, undistorted patterns, and unconstrained choice of materials.

1.3.3 Other Techniques

Techniques such as inkjet-based robotic printing,^{193,194} electron-beam lithography,¹⁹⁵ electrochemical patterning,¹⁹⁶ have also been used to pattern self-assembled nanofilms. DPN is another widely used technique to direct-write molecules using an atomic force microscope tip.¹⁹⁷⁻²⁰¹ DPN offers significant flexibility in

producing patterns of aligned multiple types of biomaterials,^{202,203} with features in the nanometer range.²⁰⁴

1.4 Objectives and Novel Aspects

From previous sections, it is clear that studies involving engineering of nanoscale self-assembled films for cell-related studies have three general limitations: (1) they have been limited to the use of surface chemistry to control cell-material interactions; (2) they have employed only binary (two-component) chemical signals; and (3) lack of versatility and low resolution in topographical control. In view of these limitations and the need for better scaffolding for multiple cell types, this research work represents an advancement of nanoscale engineering through the integration of nanoscale LbL self-assembly and photolithographic patterning to develop techniques for constructing 3D multilayer nanocomposite microstructures. This work describes the fabrication and characterization of these microstructures towards better understanding of spatial cell microenvironment. These microstructures could provide the appropriate physical-chemical properties, involving adhesive moieties that will selectively capture cells, non-toxicity, stability, and appropriate stiffness to support the cells of interest and the patterns could be oriented properly relative to one another.

The major contributions of this work to the field of nanoscale engineering are the development of platform techniques for constructing two-component microstructures of multilayer nanocomposite polymer films on each half of a substrate, development of platform techniques for constructing multicomponent microstructures of multilayer nanocomposite polymer and colloid films on a single substrate, and illustrations of applications of these techniques to cell-related studies. This is the first demonstration of

physically segregated multicomponent microstructures of multilayer nanocomposite films using combinations of photolithography and LbL techniques.

The implications of this research work extend beyond the application studied here. This work was pursued towards the development of organic and inorganic nanofilm scaffolds, which can eventually be combined to achieve functionality desired for specific applications. The results point to the potential for tailoring surfaces for specific interactions and inducing desired behavior of cells, and improved systems for investigating cell-cell communication and capabilities for spatial microenvironmental control providing scaffolding for multiple cell types. It is anticipated that the systems developed in this work will provide a general platform for studying biological processes, which will not only impact stem cell research in general, but also provide useful information in support of biomedical device development, and tissue engineering. The developed techniques could also find several applications in electronics, photonics, or chemical microsystems.

1.5 Organization of Chapters

The content of this dissertation has been organized by chapter in such a way that the presentation of the material is in the most organized, clear manner possible. Furthermore, several of the chapters are, of themselves, manuscripts that will be submitted for publication or are already published. Chapter 2 is a review of the literature and in-depth discussion of patterning techniques used for single-component and multicomponent patterning of monolayer as well as multilayer nanofilms. Chapters 3, 4 describe the definition, characterization, and biological applications of multicomponent nanocomposite polymer patterns. Chapter 5 describes the definition and characterization

of multicomponent nanocomposite nanoparticle patterns. Chapter 6 describes the effects of fabrication processes, used to create the multicomponent micropatterns, on the physicochemical characteristics of the polymer nanofilms. Finally, Chapter 7 presents the overall conclusion of the work and outlines the future work.

CHAPTER 2

BACKGROUND

Most of the techniques reported until now for the patterning of self-assembled nanofilms have demonstrated patterning of single-component films. Most of these patterning techniques have been used for the deposition of monolayer nanofilms, with few recent examples used in conjunction with multilayer nanocomposite films. Only a handful of examples of patterning techniques have been reported for multicomponent patterning of adjacent nanofilm patterns on a single substrate, but these fail to adequately address the need for deposition of 3D multilayer nanocomposite microstructures, with precise alignment. For example, multilevel stamps,⁴⁰ 2D and 3D microfluidic networks,^{205,206,133} photolithography,¹⁸² thermo-biolithography,²⁰⁷ and photochemical reactions²⁰⁸⁻²¹¹ combined with lithography. These approaches may potentially be adapted to pattern multilayer films; however, each has its own advantages and disadvantages. This chapter presents the existing techniques for patterning self-assembled nanofilms, clearly discussing their limitations with respect to construction of 3D multilayer nanocomposite microstructures. The patterning techniques have been categorized into two major types, single-component and multicomponent patterning; and each type has been further sub-categorized into two types, monolayer film and multilayer nanocomposite patterning.

2.1 Single-Component Patterning

It is noteworthy that most of the patterning techniques applied to cell-related studies are used to construct a nanofilm region that interacts with cells onto a cytophobic background or patterned surfaces are backfilled by a cytophobic background material. So technically, if the background material is accounted for, all such techniques would be categorized under two-component patterning. However, to clearly distinguish these patterning techniques that construct one type of nanofilm pattern surrounded by a background from the techniques that construct more than one types of nanofilm patterns adjacent to each other on a single substrate, the former techniques have been categorized under single-component patterning techniques and the latter techniques as multicomponent patterning techniques.

2.1.1 Monolayer Film Patterning

2.1.1.1 Microcontact printing

Microcontact printing^{3,12,32,212-217} is the simplest and the most commonly used soft lithography based patterning techniques; often used for biological applications such as patterning proteins and cells. It has also been used for patterning nanospheres²¹⁸ and nanoparticles.¹²⁵ A PDMS stamp, with one of its surfaces containing the relief patterns, is used to transfer nanofilm inks onto substrates by contact. On contact, the nanofilms take their shape from the relief patterns present on the stamp.

Like any other soft lithography techniques, μ CP has advantages that include rapid prototyping, relatively inexpensive, inherent biocompatibility, and the ability to pattern on non-planar substrates. However, the efficiency of pattern transfer is not repeatable since it depends on several factors such as quality of the patterns on the mold/stamp,

hydrophobicity of the mold/stamp and material being molded/stamped, and others that are not completely repeatable. While these methods are fast and inexpensive to use, they do not provide much versatility, particularly if more complex patterns are desired; Moving from two materials to three presents a significant challenge in the processing, because it is difficult to properly align the masks to existing patterns for subsequent steps.

2.1.1.2 Patterning using microfluidic networks

Two-dimensional microfluidic networks made of PDMS have been used to pattern nanofilms of different materials.^{176,219} This technique is also referred to as MIMIC.^{32,220} The PDMS mold containing the microchannel relief patterns is placed in contact with the substrate to form the 2D microfluidic channels. The solution of material to be deposited is then placed at one end of the channel network and allowed to fill into the channels through capillary action, and finally the stamp is removed to obtain patterned nanofilm surfaces.

However, the 2D nature of the channels limits the pattern to continuous film structures rather than physically segregated and interdigitated film structures. The patterning is significantly dependent on the wettability of the microfluidic channels. Moreover, due to the elastomeric nature of PDMS, large-area patterning with the 2D microfluidics is problematic.

2.1.1.3 Patterning using elastomeric membranes

In this technique, an elastomeric membrane²²¹ prepared from PDMS is used as a dry resist or masking layer for dry or wet¹⁷⁵ lift-off to deposit a wide variety of materials. The elastomeric membrane is prepared by pouring PDMS onto a patterned surface, which

conforms to the relief patterns on the surface, and finally releasing a free-standing membrane structure. The membranes are placed onto the substrate, material of interest is evaporated, electroplated, or adsorbed, and finally the membrane is peeled off to obtain the patterned regions.

The main advantage of this technique is its biocompatibility; because it does not use any chemicals to define the patterns, it could even be used to pattern cells.^{175,222} However, the drawbacks of this technique are that the features on the membrane should be simple, solid, and discrete. Distortion of the membranes results in less reliable patterns. The membrane should be continuous, self-supporting, and mechanically stable.

2.1.1.4 Photolithography

Conventional photolithography has widely been used for patterning applications in IC technology and MEMS, and successfully applied for self-assembled nanofilm patterning. Different materials have been used as photoresists and developers to pattern biomolecule nanofilms^{181,182,223} as well as nanoparticles.²²⁴ In general, the photoresist layer is patterned using UV photolithography, and the nanofilm is assembled onto the patterned resist surface, and finally the resist is removed using lift-off process. Biocompatible photolithography utilizing chemically amplified photoresists and dilute aqueous base developers has also been reported.¹⁸⁷⁻¹⁹⁰ All these methods based on photolithography could potentially be used for patterning multilayer nanocomposite nanofilms, as demonstrated in this research work.

2.1.1.5 Other techniques

Several more examples of techniques used for the patterning of self-assembled nanofilms can be found; for example, charged latex spheres of poly(methylmethacrylate)

(PMMA) were electrodeposited into electroconductive grooves fabricated using laser holographic patterning on indium tin oxide (ITO) surfaces.²²⁵ Here, the confinement of the colloidal particles depends on the electrostatic interactions between the particles and the surface as well as electrohydrodynamic and capillary forces. In another example, silicon dioxide substrates modified with 3-aminopropyltrimethoxysilane (APTMS) were used to pattern Au/Ag bimetallic core/shell structures using photolithography and rapid microwave heating processes.²²⁶ Galvanic displacement of nanoparticles combined with photolithography, microcontact printing, and dip-pen lithography was also recently demonstrated.²²⁷ Direct e-beam patterning^{228,229} and X-ray lithography²³⁰ of nanoparticles has also been demonstrated. DPN) is another widely used technique to direct-write molecules using an atomic force microscope tip.^{197,199-201,231} Electron beam (e-beam) lithography of PMMA²³² or chemically amplified resists²³³ and lift-off has also been used to generate patterns of gold nanoparticles. Ink-jet printing has also been used to pattern nanoparticles on different substrates using inks comprised of monodispersed nanoparticles.^{234,235} Femtosecond lasers were used to create polymer/metal-oxide-nanoparticle patterns using two-photon polymerization.²³⁶

2.1.2 Multilayer Nanocomposite Film Patterning

2.1.2.1 Photochemical reactions

In recent work, a photogenerated polyelectrolyte bilayer from an aqueous-processible photoresist is used for protein patterning.^{237,238} This approach uses a UV-sensitive water-developable biotinylated photoresist layer that transforms into a polyelectrolyte layer during development and forms an *in situ* polyelectrolyte bilayer with a preexisting cationic polyelectrolyte layer. Using the dependence of the stability of

polyelectrolyte films in aqueous buffers on the pH and streptavidin-biotin-mediated coupling, two-component protein-patterns are obtained, with a patterned region of one protein surrounded by a background protein region. This method could potentially be applied to create multicomponent patterns by using multiple lithography steps. However, this method disallows deposition of multilayers of different biomaterials.

2.1.2.2 Chemically templated patterning

Two-component multilayer films, with one set amidst another in background, have been patterned using chemically templated complimentary surfaces obtained by μ CP. Chemically patterned surfaces have been used to construct polymer-on-polymer¹⁶⁵ structures and side-by-side¹⁶⁶ structures of polymers and colloidal¹⁷⁸ particles. In the polymer-on-polymer stamping approach, a polyelectrolyte multilayer surface serves as the substrate for the direct stamping of functional polymers to obtain complementary functional groups, followed by the use of resulting pattern as a template for further deposition of materials on the surface.²³⁹ In the side-by-side stamping approach, chemically patterned surfaces with alternating carboxylic acid (COOH) and ethylene glycol (EG) functional groups obtained by μ CP are used as templates for directing two different sets of multilayer film; one multilayer set each to one of the complimentary functional groups on the same surface. This approach uses electrostatic and hydrogen bonding interactions to obtain the chemically patterned surfaces.

These processes require a balance between the use of interactions that could prevent deposition (steric and hydration forces or electrostatic repulsion) and those that could encourage it; therefore, the materials that can be employed are limited. Furthermore, micropatterning of more than two components is a challenging task because

the technique is based on the presence of two different, complementary functional groups on the substrate.

2.1.2.3 Patterning using microfluidic networks

Two-dimensional microfluidic networks have elegantly used for the fabrication of multilayer nanocomposite films^{177,240} by combining a spinning step to the MIMIC technique. The PDMS mold is placed in contact with the substrate to form the 2D microfluidic channels. The solution of the material (dissolved in an appropriate solvent such as DMF or ethanol) to be deposited is then placed at one end of the channel network and allowed to fill into the channels by capillary pressure. The excess solution is removed by spinning the substrate-PDMS combined structure. This process is repeated to deposit multilayer nanofilms, and finally the PDMS stamp removed to obtain the patterned multilayer structures.

However, the 2D nature of the channels limits the patterning to parallel, continuous multilayer film structures rather than physically segregated and interdigitated multilayer film structures. Also, the patterning depends significantly on the solvent used for the multilayer deposition, which in turn controls the wettability of the microfluidic channels.

2.1.2.4 Microcontact printing

In a recent report, μ CP has been combined with spinning method to construct 3D multilayer nanocomposite nanofilm structures.²⁴¹ The multilayer structures are initially formed on a patterned PDMS stamp using spin-assembly and then directly transferred onto the substrate using μ CP. Unlike the chemically templated technique which depends on chemical contrast, this technique is based on the topographical contrast between the

pattern region and its background allowing the patterning of amphiphilic molecules such as proteins. Although not demonstrated, this technique could potentially be used for multicomponent patterning. However, as with all stamping approaches, a precise mechanical positioning system is required to obtain aligned multicomponent patterns.

2.1.2.5 Layer-by-layer-lift-off

It appears that photolithography combined with LbL assembly overcomes many of the shortcomings of previously discussed methods for multilayer film patterning.¹¹⁹ The LbL-LO approach^{191,242} combines the lithography and LbL techniques with a single lift-off step for the patterning of multilayer nanofilms. This method is similar to the photolithography approach, in which a photoresist layer is patterned on a substrate. However, instead of depositing a monolayer of a material on the patterned resist surface, multilayers are deposited using the LbL self-assembly technique. The final step is to remove the unwanted resist using lift-off process. LbL-LO has been used to pattern nanosensors²⁴³ and multilayer films of nanoparticles of single type¹²² or multiple types (with one set amidst another in background).^{123,244} The advantages of this method are ease in fabrication process, potential for well-controlled alignment for the registration of multicomponent patterns, unconstrained choice of materials, and variable film architecture.

2.1.2.6 Other techniques

A few other examples have demonstrated fabrication of multilayer structures of self-assembled nanofilms; for example, interference lithography combined with spin-coating was used to physically constrict multilayers of nanoparticles.¹²⁴ However, the nanoparticle patterns are unstable and easily removed through ultrasonic treatment. In

another example, self-assembled silica nanoparticle patterns were fabricated on substrates patterned with octadecyltrichlorosilane (OTS) SAM based on the shrinkage of nanoparticles caused due to the dissolution of methanol (solvent in which nanoparticles were dissolved) into hexane.²⁴⁵ Also, patterned OTS substrates were used to physical entrap colloidal particles in patterned forms.²⁴⁶ Some of the above discussed techniques have been modified to accommodate multicomponent patterning of self-assembled nanofilms, and is presented in the next section.

2.2 Multicomponent Patterning

2.2.1 Monolayer Film Patterning

2.2.1.1 Printing using multilevel stamps

In a multilevel stamp approach,⁴⁰ the 2D spatial information of different photomasks is encoded onto a single elastomeric stamp by mapping each photomask onto distinct heights on the surface of the stamp to fabricate aligned multicomponent micropatterns of inorganic, organic, or living materials. Stepwise sequential contact of the topographies through manually applied pressure along with soft lithography techniques is used for patterning, providing inherent alignment of patterns and eliminating the repeated use of multiple masks. Although, this technique provides aligned multicomponent patterns, it is not possible to obtain multilayer multicomponent patterns. Moreover, it is restricted to patterning of small areas.

2.2.1.2 Patterning using 2D and 3D microfluidic networks

Microfluidic networks offer the capability to pattern biological molecules as well as live cells, and have also been used for multicomponent patterning.²⁰⁵ In this technique

the PDMS stamp containing the microfluidic channel network is placed on the substrate and the solutions of multiple materials are introduced, one type of solution at the end of an individual channel of the channel network, and the solutions are allowed to fill into the channels using the capillary action. The stamp is finally removed to obtain multicomponent patterns. The major constraints on the μ FNs are that they must be sufficiently hydrophilic to promote filling of the channels through capillary action and the contact between the substrate and μ FN should be sufficient to seal the channels.²⁰⁶ Also, the 2D nature of the channels limits the patterning to continuous multicomponent structures rather than physically segregated and interdigitated multicomponent structures.

This limitation is overcome by using complex 3D- μ FNs¹³³ to pattern discontinuous patterns of multiple types of biomaterials and cells. They require two levels of fabrication and one step of registration. However, the complexity in the fabrication of the 3D- μ FN approach is a major factor limiting its use. Nevertheless, due to the elastomeric nature of PDMS, large-area patterning is not feasible with all these techniques.

2.2.1.3 Patterning using elastomeric membranes

Elastomeric membranes made out of PDMS have also been used to deposit patterns of multiple materials.²⁴⁷ Two elastomeric membranes are used to achieve this goal, with the first membrane fixed onto the substrate and the second membrane is aligned with the first membrane to deposit different materials in different regions. However, these membranes are limited to simple, solid, discrete patterns. Moreover, unlike conventional photolithography, this technique is limited to patterning of small areas.

2.2.1.4 Thermo-biolithography

Thermo-biolithography technique²⁰⁷ has been used to fabricate multicomponent patterns. It is a simple and biofriendly method in which a reactive layer of polysaccharide chitosan is used for film deposition. The patterning technique is based on thermally responsive gelatin gel deposited on top of the chitosan layer as a thermoresist and a heated stamp for pattern transfer. However, thermo-biolithography suffers from low resolution of patterns and difficulty in alignment of multiple stamps during pattern transfer.

2.2.1.5 Photolithography

Biocompatible photolithography using chemically amplified photoresists and dilute aqueous base developers has been applied to patterning monolayers of multiple types of biomolecules.¹⁸⁶ To our knowledge, methods based on biocompatible photolithography have only been demonstrated for, but are not limited to, patterning monolayers of multiple types of biomolecules.

2.2.1.6 Other techniques

Few more examples can be found for techniques developed for constructing patterns of multiple biomaterials; for example, photochemical reactions combined with step-repeat photolithography have been used to fabricate multiple protein patterns.²⁰⁸⁻²¹¹ The deposition of proteins is based on the avidin-biotin chemistry, whereas the patterning process is based on the photochemical properties of biotin. In another example, aligned patterns of photosensitive alkanethiolate SAMs were fabricated on gold substrates using light at different wavelengths.²⁴⁸ A single step of photolithography is performed using a photosensitive alkanethiolate SAM and a mask that acts as area-selective filter for light at

two different wavelengths. The alkanethiolate SAM is photosensitive to the light at those two wavelengths of light. However, this method requires an alkanethiol that contains a photoprotecting group and also the fabrication of the mask with required wavelength filtering properties, which could be limiting factors in terms of material choice and number of the components to be patterned. Also, an amino-functionalized substrate in combination with a photoprocessable nitroveratryloxycarbonyl (NVOC) masking layer has been used for fabrication of multiple patterns of nanocrystals.²⁴⁹ Thermally evaporated octadecylamine (ODA) surfaces were sequentially exposed to different carboxylic acid derivatized nanoparticle solutions to create multiple patterns of nanoparticles.²⁵⁰ Recently, pulsed electrodeposition combined with photolithography was used to pattern multicomponent nanoparticle arrays that were later used for nanotube growth.²⁵¹ Further, μ CP has recently been extended to construct pattern-on-pattern fashion stamping of nanoparticles.¹²⁵ For features in the nanometer range,²⁰⁴ DPN offers significant flexibility in producing patterns of aligned multiple types of biomaterials.^{202,203}

2.2.2 Multilayer Nanocomposite Film Patterning

2.2.2.1 Multilayer transfer printing

Multilayer transfer printing, another soft lithography based technique, is a recent development for fabricating multicomponent multilayer patterns.¹⁷⁹ In this method, polyelectrolyte multilayers formed on the surface of a PDMS stamp are directly transferred onto a surface with a charge opposite to that of the topmost layer of the multilayer film printed. Despite the promise this technique brings for versatile micropatterning of nanocomposite films, two significant issues appear to limit the

approach: First, as with all stamping approaches, a precise mechanical positioning system is required to obtain aligned multicomponent patterns. This limitation has recently been resolved by implementing an alignment system in the MTP process, though the misalignment is directly proportional to the size of the stamp used, with a misalignment of 50 μm (18% deviation) for a $2.8 \times 3.3 \text{ cm}^2$ stamp.¹⁸⁰ Second, the MTP process needs a fine balance of forces between the bottom-most layer of the multilayer films and the PDMS stamp (that would become the topmost layer after the multilayer films are transfer printed), which must be optimized for different materials.

2.2.2.2 Comparison chips

The “comparison chips” approach is an extension of the LbL-LO technique, which combines the lithography and LbL techniques with a single lift-off step for the patterning of multilayer surfaces. Using this approach two-component multilayer patterns are constructed, with one component (protein/polypeptide) on each half of a single substrate.¹⁹² Similar to the LbL-LO approach, the photoresist layer is patterned using photolithography. Using the LbL technique, the desired film architectures, different on each side of the chip, are obtained within the patterned regions, and the two-component are finally obtained using a single lift-off step. This approach has the same advantages as the LbL-LO approach, except that two-components can be constructed with this one. The details of this technique are elaborated in Chapter 3 of this dissertation. The limitation of this technique to pattern two spatially separate components is overcome by the polymer surface micromachining approach.

2.2.2.3 Polymer surface micromachining

In the polymer surface micromachining (PSM)²⁵² approach, complex 3D multilayers in aligned interdigitated micropatterns are constructed with a combination of lithography and LbL methods. The first nanofilm pattern is constructed using photolithography, followed by LbL multilayer assembly and lift-off, and the process is repeated with optical alignment to obtain complex structures on the same substrate. Thus, the method is analogous to surface micromachining, except that the deposition materials are polymers and biological materials used to produce multilayer nanocomposite structures. The versatility of this technique has been elaborately discussed in Chapters 4 and 5 of this dissertation.

CHAPTER 3

MULTICOMPONENT POLYMER

PATTERNING-PART I:

COMPARISON CHIPS

Most of the content of this chapter has been published as a full paper: Shaikh Mohammed, J.; DeCoster, M. A.; McShane, M. J., Micropatterning of nanoengineered surfaces to study neuronal cell attachment in vitro. *Biomacromolecules* **2004**, 5, (5), 1745-1755.

3.1 Introduction

Methods for producing protein patterns with defined spatial arrangement and micro- and nanoscale features are important for studying cellular-level interactions, including basic cell-cell communications, cell signaling, and mechanisms of drug action. Toward this end, a straightforward, versatile procedure for fabricating micropatterns of bioactive nanofilm coatings as multifunctional biological testbeds is demonstrated in this chapter. The method, based on a combination of photolithography and LbL, allows for precise construction of nanocomposite films of potentially complex architecture, and patterning of these films on substrates using a modified lift-off procedure. As a first step in evaluating nanostructures made with this process, “comparison chips,” comprising two coexisting regions of square patterns with relevant proteins/polypeptides on a single

substrate, were fabricated with poly(diallyldimethylammonium chloride) (PDDA) as a cell-repellent background. In previous work done by our group,¹⁹¹ multilayered patterns of one type of protein (gelatin) were fabricated over a polyelectrolyte (PDDA) thin film layer. The gelatin patterns were cytophilic to smooth muscle cells (SMCs), whereas the PDDA layer was cytophobic. It was observed that the properties of the underlying material and bulk substrate affect the cell behavior. It was also observed that the dimensions of the patterns affected the cell adhesion, alignment, and proliferation. In this chapter, a simple method (based on the LbL-LO technique) for fabricating multiprotein patterns, with one type of protein on each half of a single substrate has been presented. Using neuronal cells as a model biological system, comparison chips were produced with secreted phospholipase A₂ (sPLA₂), a known membrane-active enzyme for neurons, for direct comparison with gelatin, poly-L-lysine (PLL), or bovine serum albumin (BSA).

The present study focuses on the engineered substrates for neuronal cells, since the *in vitro* assembly of neuronal cells is a useful tool not only in basic neuroscience research but also impacts applied research such as drug development and neuroprosthetic design. Secreted phospholipase A₂, a low molecular weight transcellular enzyme, has been shown to be involved in digestive and inflammatory response mechanisms, and is known to have potent deleterious effects on neurons of the central nervous system.²⁵³⁻²⁵⁵ Since sPLA₂-binding proteins and receptors have been identified in muscle and brain cells, the enzymatic and signaling function of sPLA₂s are believed to have cell surface targets.²⁵⁶⁻²⁵⁸

Using the current method, comparison chips have been fabricated to determine the potential of sPLA₂ as a neuronal binding target. The assembly properties of these

molecules were studied, and a method for the precise spatial arrangement of these molecules into micropatterned nanofilm patches was developed. Quartz crystal microbalance (QCM) measurements were made to determine the required adsorption times for the proteins/polypeptide. Using basic photolithography, the desired patterns were obtained on the chips and using the LbL technique the desired film architectures were obtained within the patterned regions. The comparison chips were characterized using fluorescence microscopy, surface profilometry, and atomic force microscopy techniques, and ultimately used in preliminary cell culture experiments to assess cell-material interactions.

Preliminary cell culture studies show that neurons respond and bind specifically to the sPLA₂ enzyme embedded in the polyelectrolyte thin films and present as the outermost layer. These findings point to the potential for this method to be applied in developing test substrates for a broad array of studies aimed at identifying important biological structure-function relationships.

3.2 Materials

3.2.1 Substrates

Microscope cover glasses ($9 \times 22 \text{ mm}^2$, Electron Microscopy Sciences) were used as substrates for film patterning. These rectangular shaped substrates were chosen to facilitate the LbL assembly process using small reaction vessels.

3.2.2 Chemicals

Nano-Strip™ was purchased from CYANTEK Corporation. Poly(diallyldimethylammonium chloride) (Mw ~100k-200 kDa), poly(sodium 4-styrenesulfonate) (PSS) (Mw ~1 MDa), poly(ethyleneimine) (PEI) (Mw ~750 kDa), poly-

L-lysine hydrobromide (Mw ~25,700 Da), gelatin B (Mw ~50k-100 kDa), BSA (Mw ~66,430 Da), and fluorescein isothiocyanate (FITC) were purchased from Sigma-Aldrich. Secreted phospholipase A₂ (Type III, from bee venom) (Mw ~14 kDa) was purchased from Cayman Chemical. Tetramethylrhodamine-5-(and-6)-isothiocyanate (TRITC) was ordered from Molecular Probes. Positive photoresist, PR1813, and positive resist developer, MF-319, were ordered from Shipley. All chemicals of commercial origin were used as received.

3.2.3 Preparation of Polyelectrolyte and Polypeptide Solutions

Solutions with concentrations of 2 mg mL⁻¹ PDDA and PSS in 0.5 M KCl and a solution of 2 mg mL⁻¹ PEI were prepared for use in self-assembly. Proteins/polypeptides were labeled with FITC or TRITC using standard procedures²⁵⁹ to allow observation of the patterns on the substrates. All proteins and PLL were labeled with TRITC to allow discrimination except sPLA₂, which was tagged with FITC. Proteins were separated from unreacted dye with a desalting column (PD-10, Amersham Pharmacia Biotech AB). PLL was precipitated from dye solution by adding acetone to the mixture, centrifugation, and resuspension in solution. Labeling ratios were determined by UV-Vis absorbance spectroscopy.

3.3 Methods

3.3.1 Mask Design

Since the aim of this work was to test the adhesion of cells on the nanofilm micropatterns, the mask used for defining the patterns on the “comparison chips”

contained array of isolated squares. The 20 μm square patterns were separated from each other by a distance of 80 μm , in horizontal as well as vertical directions.

3.3.2 Fabrication

Substrates were patterned with three different combinations of materials (sPLA₂/gelatin, sPLA₂/PLL, and sPLA₂/BSA), each on one set. That is, each slide was patterned with sPLA₂ in one region and another material in a neighboring region. The cartoon in Figure 2 depicts the fabrication flow used in this chapter (LbL-LO method).

3.3.2.1 Substrate pretreatment

The substrates were first incubated in Nano-Strip™ at 70 °C for 1 hr, rinsed in DI water, and dried using N₂. This step was used to remove any organic material and also create a uniform negative charge on the substrates. A precursor layer of PDDA was then deposited on the negatively-charged substrates by incubating in PDDA for 20 min, rinsing in DI water, and finally drying in N₂. The choice of PDDA was based on previous studies, wherein this material was shown to be cell-repellent for smooth muscle cells, and preliminary screening studies where similar results were observed when tested with neuronal cells.¹⁹¹ However, it is noted here that, in principle, any cytophobic background material available could be used in this approach, as long as it can still provide the necessary charge or functional surface for future film assemblies (or could be activated to produce such).

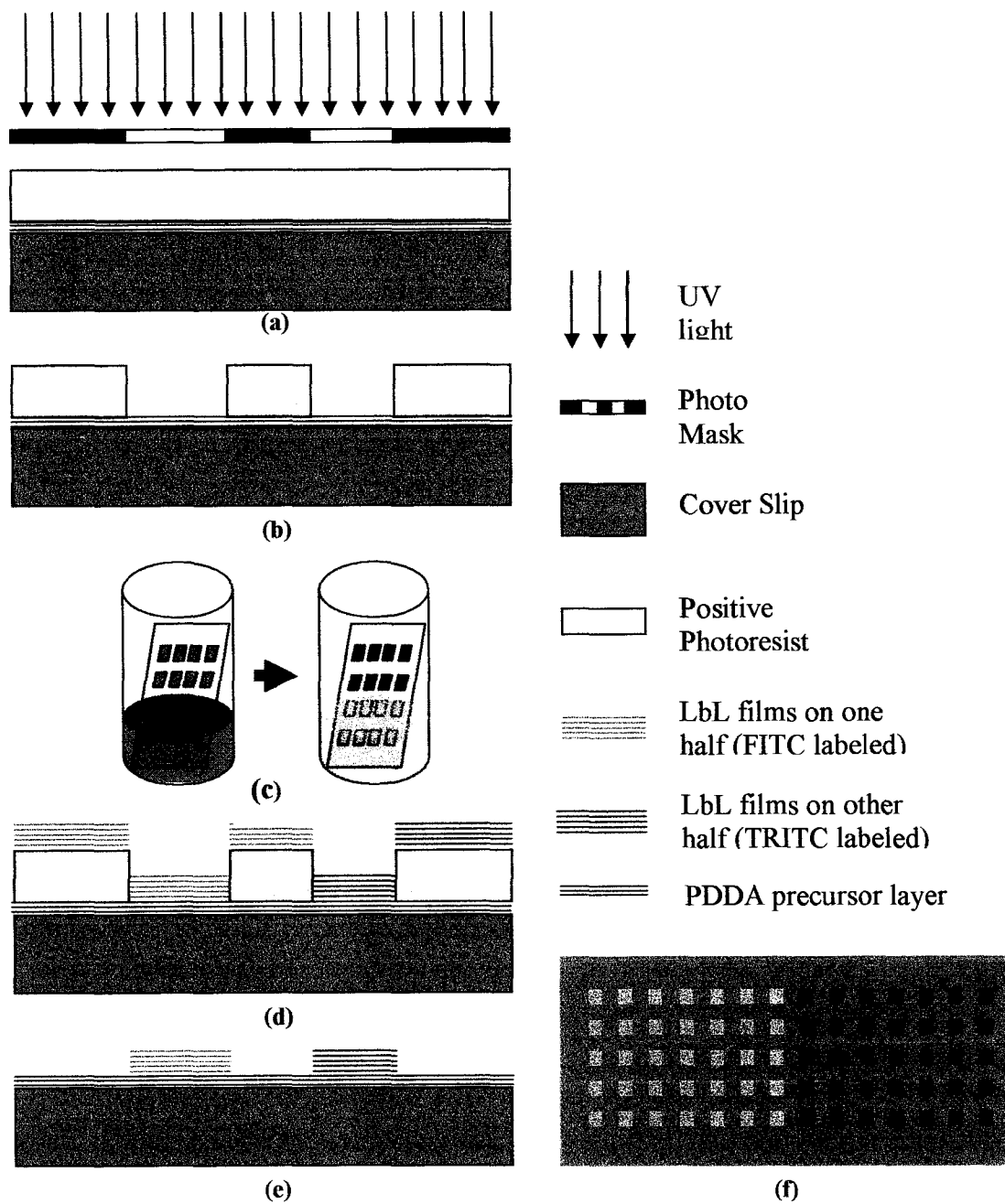


Figure 2. Template used for LBL-LO fabrication process (a), (b) Photolithography, (c) LbL assembly process, (d) LbL processed chips, (e) After lift-off, (f) Top view of the fabricated chip: Green-FITC labeled sPLA₂, Red-TRITC labeled BSA/PLL/gelatin.

3.3.2.2 Photolithography

The PDDA-coated substrates were attached onto plain microscope slides using photoresist, and heated at 165 °C for 5 min to hard bake the photoresist. The microscope cover glasses used as substrates were very thin and fragile; these cover slips were found unsuitable to be spun directly on the available spinner with high probability of breakage. Hence, for all of the work described here, the glasses were first attached to a plain microscope slide to provide underlying mechanical strength to withstand spinning and stresses imposed in further lithography processes.

After the slips were attached to microscope slides, positive photoresist was then spun on the PDDA-coated substrates (1,000 rpm-100 r s⁻¹-10 sec, 3,000 rpm-500 r s⁻¹-50 sec), soft baked at 115 °C for 3 min, and photo-patterned using ultraviolet radiation (365/405 nm, 7 mW cm⁻²) for 18 sec. Finally, the patterns were developed for 1 min, and the substrates were rinsed in DI water and dried using N₂.

3.3.2.3 Layer-by-layer self-assembly

The patterned substrates were then modified using layer-by-layer (LbL) self-assembly processing. The LbL thin-film configuration deposited initially on the patterned substrates was {PSS/PDDA}₃, which denotes deposition of three consecutive bilayers of PSS/PDDA by alternating negatively-charged PSS and positively-charged PDDA layers. This procedure provided precursor layers for the LbL assembly of biopolymers. This is an important step to attain a uniformly charged layer. It was also seen in our earlier studies that these underlying layers also affect the cellular response.¹⁹¹ The substrates were immersed in the PSS or PDDA solutions for 10 min. After each layering step, the substrates were rinsed in DI water and dried in N₂.

A thin-film configuration of $\{(FITC-sPLA_2)/PEI\}_4/(FITC-sPLA_2)$ was then deposited on half of each of the patterned substrates with pre-existing $\{PSS/PDDA\}_3$ nanofilms. Four bilayers of $(FITC-sPLA_2)/PEI$ were deposited by alternate exposure of substrates to negatively-charged $FITC-sPLA_2$ and positively-charged PEI solutions followed by a fifth layer of $FITC-sPLA_2$. For this assembly process, 1 mL of solution was placed in a 1cm cuvette such that when a chip was placed in them only one half was immersed. The substrates were immersed in $FITC-sPLA_2$ and PEI for 50 min and 10 min, respectively, for optimum adsorption (minimum time required for the resaturation of polyion adsorption that results in the charge reversal; measured through QCM experiments). After each layering step, the substrates were rinsed in DI water and dried in N_2 . A thin-film configuration of $\{(TRITC-BSA)/PEI\}_4/(TRITC-BSA)$, $\{(TRITC-gelatin)/PEI\}_4/(TRITC-gelatin)$, or $\{PSS/(TRITC-PLL)\}_5$ was obtained on the other half portions of each of the three different sets of patterned substrates with pre-existing $\{PSS/PDDA\}_3$ nanofilms. The assembly for these followed identical procedures to $sPLA_2$ assembly, excepting that the other half of the substrate was exposed to the assembly solutions. For these cases, $TRITC-BSA$ and $TRITC-gelatin$ adsorption times were 30 and 20 min, respectively. For $TRITC-PLL$ (positive charge), PSS was used as the polyanion, and adsorption times were 20 and 10 min for $TRITC-PLL$ and PSS , respectively.

3.3.2.4 Lift-off

Lift-off was performed by sonicating the substrates in acetone for 5-10 min. During the lift-off process, the photoresist was removed along with the nanofilms on top of the photoresist, and the cover glasses detached from the microscope glass. The critical parameters at this step were the sonication strength and sonicating time. If either of these

parameters are higher than the optimum value (measured earlier through experimentation), then the nanofilm patterns become distorted.¹⁹¹ It is noteworthy that the use of acetone might be expected to cause substantial degradation of biological function. However, previous observations and the results shown below suggest that the features of the molecules responsible for cell binding are retained through the process. Thus, two coexisting regions of square patterns with top coatings of relevant proteins/polypeptide (sPLA₂ with gelatin, PLL, or BSA) on a single substrate were fabricated with PDDA as a cell repellent background.

3.3.3 Characterization

A QCM system (USI) was used to establish assembly conditions for each material before substrate fabrication. After fabrication of the chips, a fluorescence microscope (Nikon, Model-Eclipse TS100) and confocal fluorescence microscope (Leica, Model-TCS SP2) were used to image and characterize the fabricated substrates. A surface profiler (KLA-Tencor, Model-Alpha-Step IQ) was used to analyze the surface topography (line scans) of the patterns and an AFM (Quesant, Model-Q-Scope250) was used to analyze the finer physical features (area scans) of the patterns on the fabricated substrates.

3.3.3.1 Quartz crystal microbalance

QCM crystals (AT-cut, 9 MHz) with silver electrodes were used in this study. The QCM studies were performed before the fabrication of the chips in order to determine the required adsorption times for sPLA₂, PLL, gelatin, and BSA. In all the cases, measurements were performed on both unlabeled as well as labeled protein/polypeptide. The following configurations were used for the measurements:

{PDDA/PSS}₃/ {PEI/sPLA₂}₅, {PDDA/PSS}₃/ {PLL/PSS}₅, {PDDA/PSS}₃/ {PEI/gelatin}₅, {PDDA/PSS}₃/ {PEI/BSA}₅, {PDDA/PSS}₃/ {PEI/(FITC-sPLA₂)}₅, {PDDA/PSS}₃/ {(TRITC-PLL)/PSS}₅, {PDDA/PSS}₃/ {PEI/(TRITC-gelatin)}₅, and {PDDA/PSS}₃/ {PEI/(TRITC-BSA)}₅. Silver electrodes were cleaned with cleaning solution (39% ethanol, 1% KOH, 60% H₂O) for 15 min, followed by rinsing with deionized water and drying by flushing with N₂ gas. Initially, the resonant frequency of the cleaned QCM crystal was measured and then the frequency shift by material adsorption onto the QCM crystal was monitored three times after each step. The amount of material deposited onto the multilayers and bare substrates was calculated using the relation between frequency shift and mass, as derived from the Sauerbrey equation²⁶⁰: Δm (ng) = - 0.87 × Δf (Hz). Thus, a 1 Hz decrease of frequency corresponds to a 0.87 ng increase in mass and the thickness of a film may be estimated from the mass. The adsorbed film thickness at both faces of the electrodes (*t*) may be predicted from the density of the protein/polyion film (~ 1.3 g cm⁻³) and the real film area: $t(\text{nm}) = -(0.016 \pm 0.02) \times \Delta f(\text{Hz})$.^{261, 262}

3.3.3.2 Fluorescence microscopy

After the fabrication of the chips, fluorescence microscopy was used for imaging the resulting structures. On each half portion of the fabricated chips, there are patterns with either FITC-labeled material (sPLA₂) or TRITC-labeled materials (gelatin, BSA, or PLL). Therefore, the imaging was performed to demonstrate successful multi-protein patterning and to assess the uniformity and spatial registration of the multiple protein patterns. Images were taken sequentially using a FITC cube followed by a TRITC cube at every particular position on a chip. The exposure times when the 10X and 40X objectives

were used were 8 and 4 s, respectively. A digital zoom setting of F3.5 was used throughout the imaging process.

Confocal microscopy was also used to perform sequential FITC and TRITC excitation of the fabricated substrates. These measurements also verified discrete patterns of multiple proteins/polypeptide on the chips, and further provide quantitative data on the size and fluorescence intensity of the imaged patterns. Leica confocal software (LCS Lite) was used to analyze the images. Line profiles of the fluorescence intensity were obtained across the patterns.

3.3.3.3 Surface profilometry

Surface profiler measurements were made for quick assessment of the topography of the LbL assembly for different protein patterns. The surface profiler was used to collect line scan structural data of the patterns. The vertical dimensions of the patterns, average roughness (R_a), and root mean square (RMS) (R_q) roughness data were obtained directly from the line scan measurements.

3.3.3.4 Atomic force microscopy

AFM measurements were made to further verify the faithfulness of the pattern transfer using the current fabrication process. AFM was used in tapping mode with silicon cantilevers to collect area scan data from the patterns. The lateral and vertical dimensions of the patterns were obtained from these measurements. Several scans over a region of the surface were performed to verify that the tip did not induce observable modifications of the sample. The parameters used for the measurements were a scan area of $40 \times 40 \mu\text{m}^2$, scanning rate between 1.5-2 Hz, and a resolution of 600 lines.

3.3.4 Cell Culture

All the cell culture work was done in Dr. Mark A. DeCoster's laboratory at LSUHSC, New Orleans. Preliminary cell culture experiments were performed with the fabricated comparison chips to assess the specificity of cell attachment to sPLA₂ over other materials. Primary cultures of cortical neurons were prepared as previously described²⁵³ from embryonic day 15 rat embryos and grown on the fabricated chips in 37 °C, 5% CO₂ incubators. For this work, we have restricted the cell growth area to the surface area of the squares. In reference 253 (as is typical for most cell culture), the entire plating surface was coated with attachment factors.

3.4 Results and Discussion

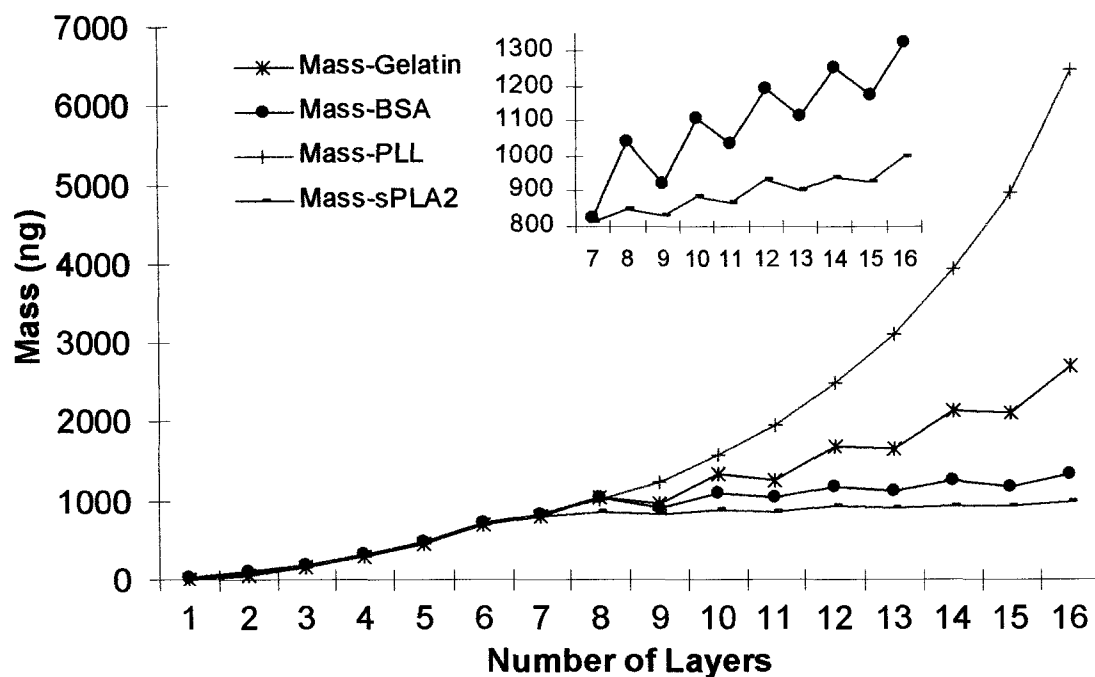
3.4.1 QCM Measurements

The plots of mass versus adsorption cycle during the assembly of unlabeled and labeled proteins/polypeptide are shown in Figure 3(a) and Figure 3(b), respectively. It is obvious from these plots that the measurements are similar up to the sixth layer, due to the identical precursor coatings of three bilayers of PDDA/PSS used in each case. The molecular weights of PSS and PDDA used here are ~1 MDa and ~100-200 kDa respectively, which are higher than that of the other materials used, and these strong polyelectrolytes are both highly charged and partially coiled at the pH and ionic strength used, resulting in large steps in adsorbed mass; thus, a decrease in the slope of the growth curve is observed for additional layers comprising proteins and polypeptides. Of particular interest is the molecular weight of sPLA₂ which, in the form used here was ~14 kDa; this difference in molecular size and weaker charge account for the smaller increase in mass for sPLA₂, which is small in comparison to other materials. In other words, it can be

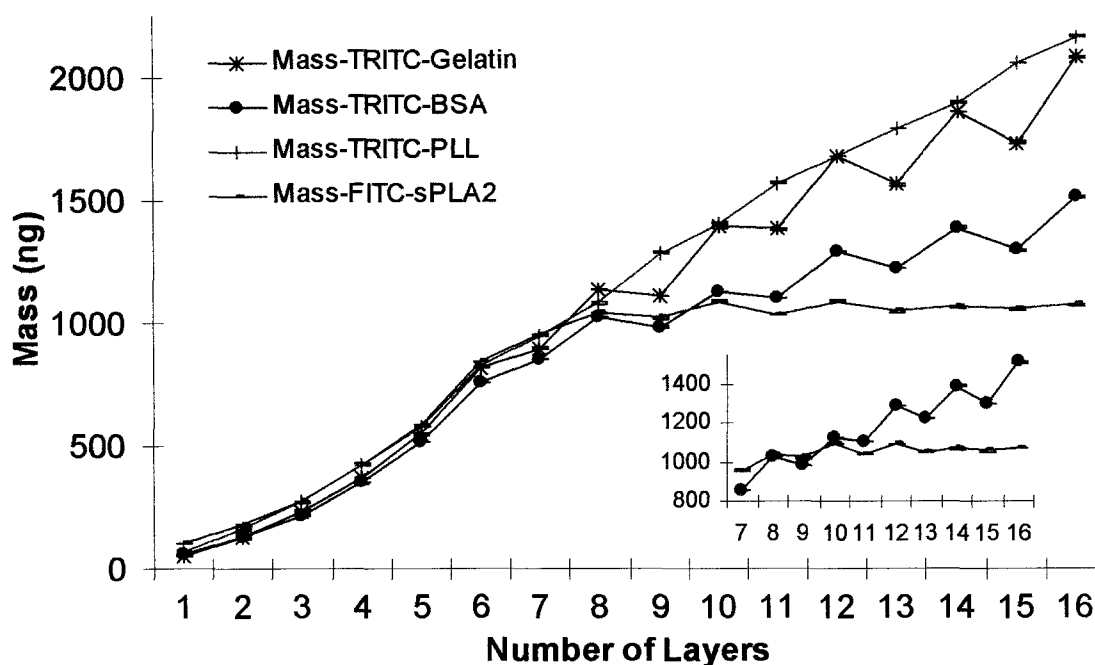
stated that there was steady increase in mass during the deposition of the base bilayers of PDDA/PSS; further, there was also a steady increase in mass, though much smaller in magnitude, during the deposition of the protein (or polypeptide)/polyelectrolyte bilayers.

It is clear that labeling of proteins/polypeptides affects the local and net charge on the molecules. Additionally, labeling may also change the molecular conformation, which occurs as a result of the occupation of amine residues and the presence of an additional group on the macromolecule. The difference in profiles (the quantity rate of adsorption) between the unlabeled and labeled is expected to be mainly dependent upon the difference in the charge.

The QCM results prove that the proteins/polypeptide were alternately layered onto the QCM crystal. At the first adsorption step for the proteins/polypeptide, the QCM measurements were made at intervals of 10 min until saturation in the reading was attained. The optimum adsorption times were measured to be 50 min for sPLA₂, 20 min for gelatin and PLL, and 30 min for BSA.



(a)



(b)

Figure 3. Mass deposited as a function of number of layers for the assembly of (a) $\{\text{PDDA/PSS}\}_3/\{\text{PEI/sPLA}_2\}_5$, $\{\text{PDDA/PSS}\}_3/\{\text{PEI/gelatin}\}_5$, $\{\text{PDDA/PSS}\}_3/\{\text{PEI/BSA}\}_5$, and $\{\text{PDDA/PSS}\}_3/\{\text{PLL/PSS}\}_5$ (b) $\{\text{PDDA/PSS}\}_3/\{\text{PEI/(FITC-sPLA}_2)\}_5$, $\{\text{PDDA/PSS}\}_3/\{\text{PEI/(TRITC-gelatin)}\}_5$, $\{\text{PDDA/PSS}\}_3/\{\text{PEI/(TRITC-BSA)}\}_5$, and $\{\text{PDDA/PSS}\}_3/\{\text{TRITC-PLL/PSS}\}_5$.

3.4.2 Fluorescence Microscopy

Several images were taken on the fabricated chips to confirm that the fabrication was successful. Figure 4 contains images that show a clear demarcation of 20 μm square patterns of $\{\text{PSS/PDDA}\}_3/\{(\text{FITC-sPLA}_2)/\text{PEI}\}_4/(\text{FITC-sPLA}_2)$ and $\{\text{PSS/PDDA}\}_3/\{\text{PSS}/(\text{TRITC-PLL})\}_5$ at a magnification of 10X. Figure 4(a) is an overlay of images collected using FITC and TRITC cubes and Figure 4(b) is the intensity profile (green: FITC, red: TRITC) of fluorescence intensity along one of the rows in Figure 4(a). The presence of green profile on the right half along with the red profile on Figure 4(b) is due to the fact that the available FITC cube contained a long-pass filter in the emission channel, which resulted in some directly excited TRITC-labeled nanofilm patches to appear in the FITC image; this is an artifact of the measurement and not a problem with the fabrication process. Figure 4(c)-(d) are images of the 20 μm square patterns of $\{\text{PSS/PDDA}\}_3/\{(\text{FITC-sPLA}_2)/\text{PEI}\}_4/(\text{FITC-sPLA}_2)$ collected through a FITC and a TRITC cube, respectively, at a magnification of 40X. It is evident from these images that there is only FITC-sPLA₂, and no TRITC-labeled materials in these patterns. Figure 4(e)-(f) are images of the 20 μm square patterns of $\{\text{PSS/PDDA}\}_3/\{(\text{TRITC-BSA})/\text{PEI}\}_4/(\text{TRITC-BSA})$ collected through a FITC and a TRITC cube, respectively, at a magnification of 40X.

It is evident from these images that there is only TRITC-BSA, and no FITC-sPLA₂ in these patterns. Similar observations were made during the imaging of patterns with TRITC labeled PLL and gelatin. These results indicate that the current fabrication method has been successfully used to fabricate comparison chips with selective patterning of different proteins/polypeptide on the same substrate.

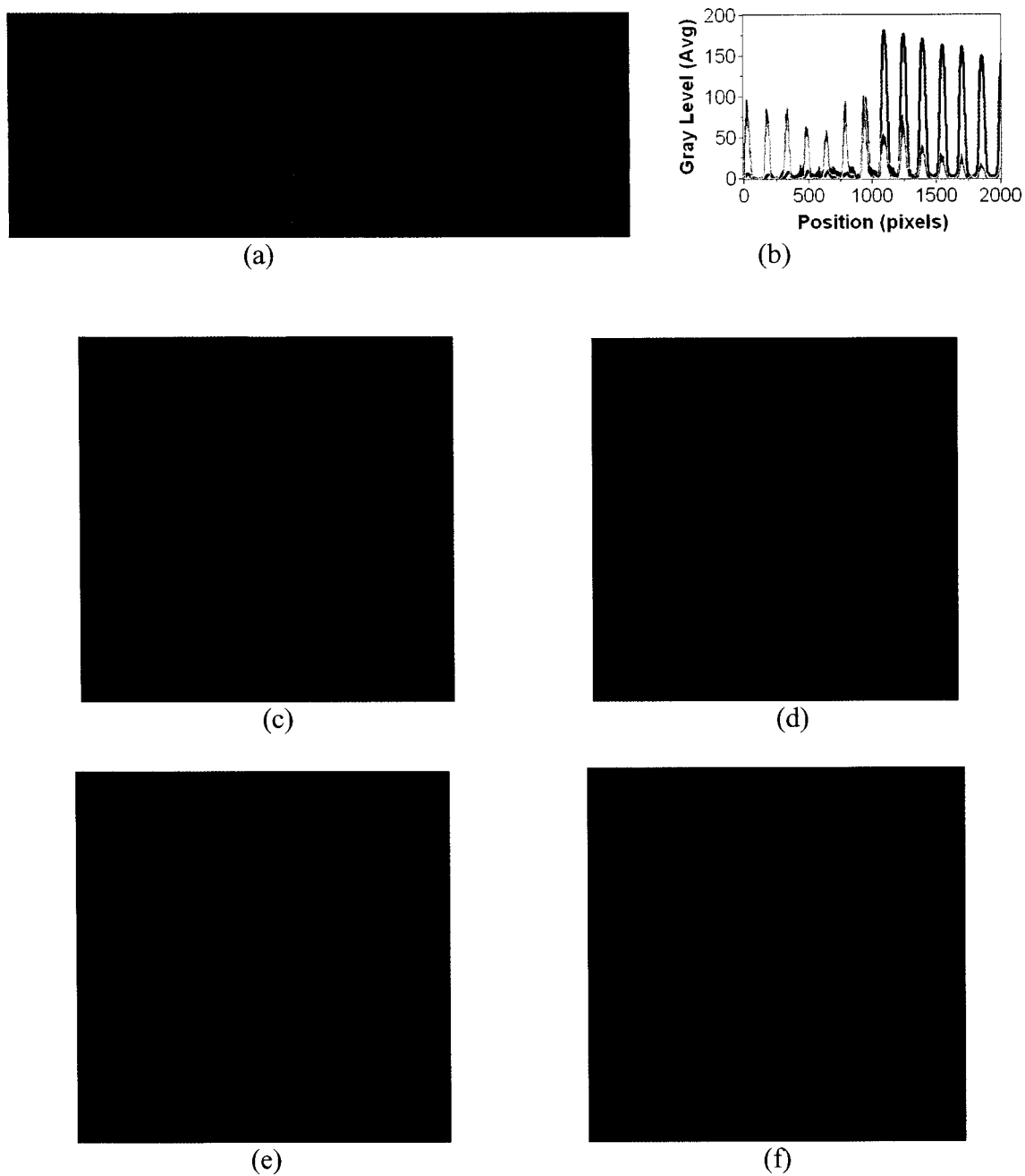


Figure 4. Demarcation of $\{\text{PSS/PDDA}\}_3/\{(\text{FITC-sPLA}_2)/\text{PEI}\}_4/(\text{FITC-sPLA}_2)$ and $\{\text{PSS/PDDA}\}_3/\{\text{PSS}/(\text{TRITC-PLL})\}_5$ 20 μm patterns at 10X (a) overlay of FITC and TRITC cube images, (b) Intensity profile (green: FITC, red: TRITC) of fluorescence intensity along one of the rows in (a), $\{\text{PSS/PDDA}\}_3/\{(\text{FITC-sPLA}_2)/\text{PEI}\}_4/(\text{FITC-sPLA}_2)$ 20 μm patterns at 40X (c) FITC, (d) TRITC cube, $\{\text{PSS/PDDA}\}_3/\{(\text{TRITC-BSA})/\text{PEI}\}_4/(\text{TRITC-BSA})$ 20 μm patterns at 40X (e) FITC, (f) TRITC cube.

Figure 5(a) is the sequential FITC-TRITC scanning confocal image of $\{\text{PSS/PDDA}\}_3/\{(\text{FITC-sPLA}_2)/\text{PEI}\}_4/(\text{FITC-sPLA}_2)$ patterns. Figure 5(b) is the line profile (Left: FITC, Right: TRITC) of fluorescence intensity along the lines drawn in Figure 5(a). Figure 5(c) is the sequential FITC-TRITC scanning confocal image of $\{\text{PSS/PDDA}\}_3/\{(\text{TRITC-BSA})/\text{PEI}\}_4/(\text{TRITC-BSA})$ patterns. Figure 5(d) is the line profile (Left: FITC, Right: TRITC) of fluorescence intensity along the lines drawn in Figure 5(c). These images (Figure 5(a), (c)) again prove that there are discrete patterns of either FITC labeled material or TRITC labeled materials in the patterns. From Figure 5(b) it may be observed that the FITC intensity is ~ 30 counts, and the TRITC intensity is ~ 5 counts. The TRITC signal is ~ 6 times smaller than the FITC intensity is at the same level as the FITC background, and it does not show any spatial pattern. From Figure 5(d) it may be seen that the FITC intensity is ~ 1 counts and TRITC intensity is ~ 35 counts, which is 35 times more compared with the FITC intensity. Therefore, the line profiles shown in Figure 5(b) and 5(d) further support the selective patterning of different proteins/polypeptide on the same substrate.

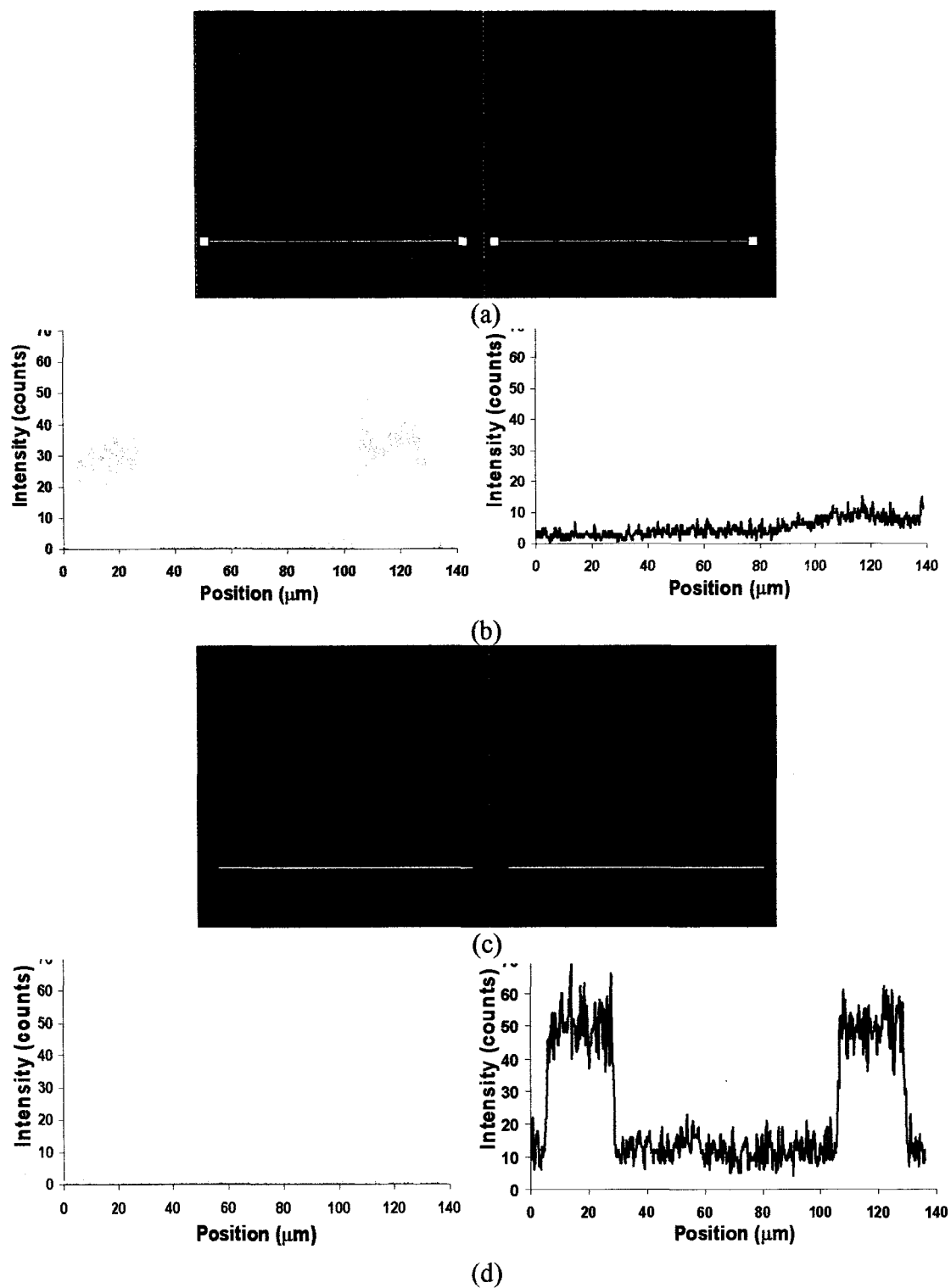


Figure 5. Sequential FITC-TRITC scanning confocal images and intensity profiles of (a) $\{\text{PSS/PDDA}\}_3/\{(\text{FITC-sPLA}_2)/\text{PEI}\}_4/(\text{FITC-sPLA}_2)$, (c) $\{\text{PSS/PDDA}\}_3/\{(\text{TRITC-BSA})/\text{PEI}\}_4/(\text{TRITC-BSA})$ patterns, Intensity profiles (Left: FITC, Right: TRITC) of fluorescence intensity along the lines (b) $\{\text{PSS/PDDA}\}_3/\{(\text{FITC-sPLA}_2)/\text{PEI}\}_4/(\text{FITC-sPLA}_2)$, (d) $\{\text{PSS/PDDA}\}_3/\{(\text{TRITC-BSA})/\text{PEI}\}_4/(\text{TRITC-BSA})$.

3.4.3 Surface Profiler Measurements

Surface profiler scans were performed at three different positions on each half of the fabricated chips of the three different combinations of proteins/polypeptide. Using the software options, the step height, average roughness (R_a), and RMS roughness (R_q) of the patterns in all the scans were determined, and the averages of the three measurements per pattern were calculated. Figure 6 and Figure 7(a)-(b) are bar graphs of average thickness, average roughness (R_a), and RMS roughness (R_q) of the patterns on each half of the chips of the three different combinations of proteins/polypeptide. It can be observed that the average roughness is ~ 5 times smaller than the average thicknesses of the corresponding patterns indicating that a greater number of polyelectrolyte-protein bilayers need to be deposited to attain smoother surfaces.

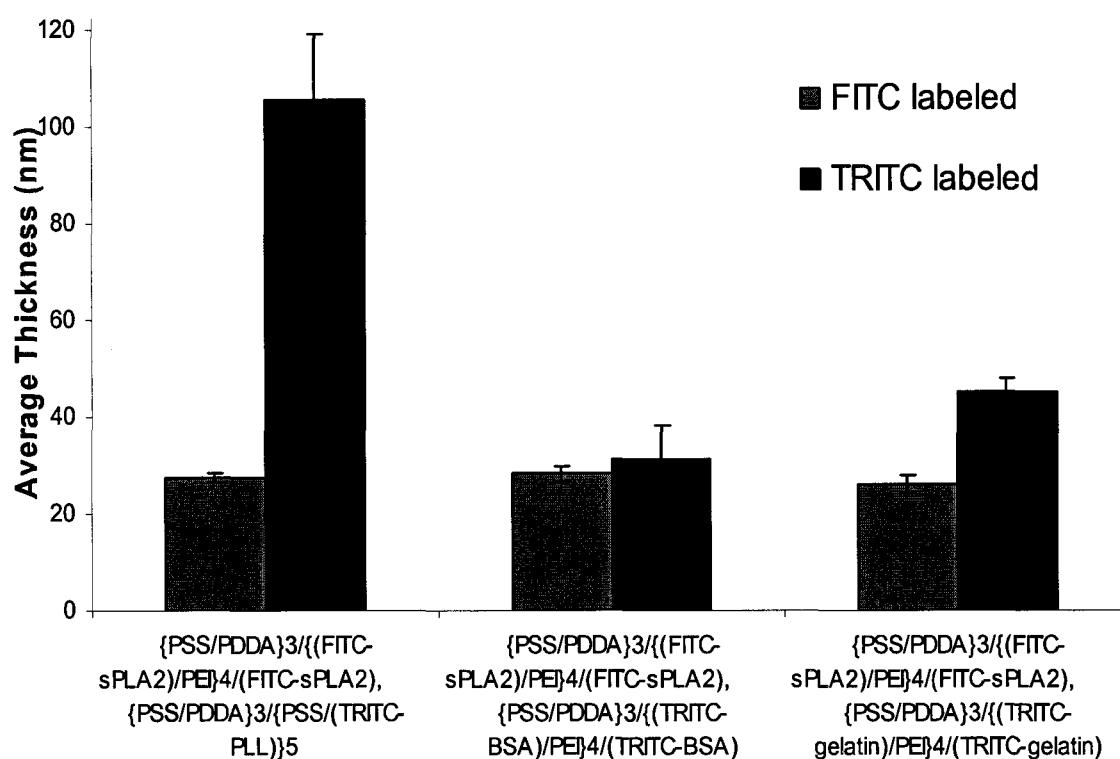
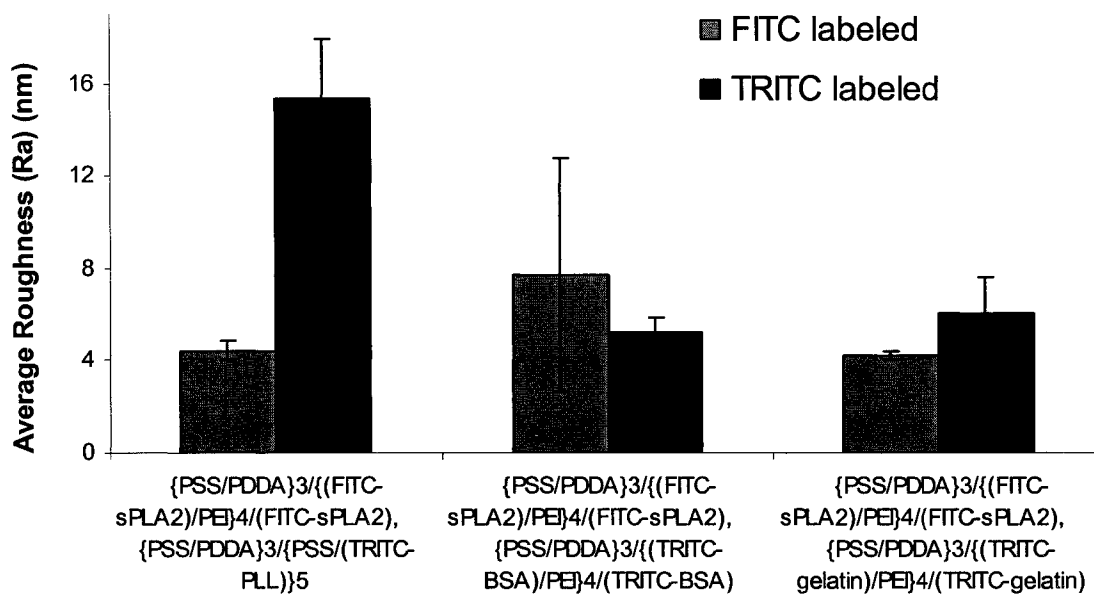
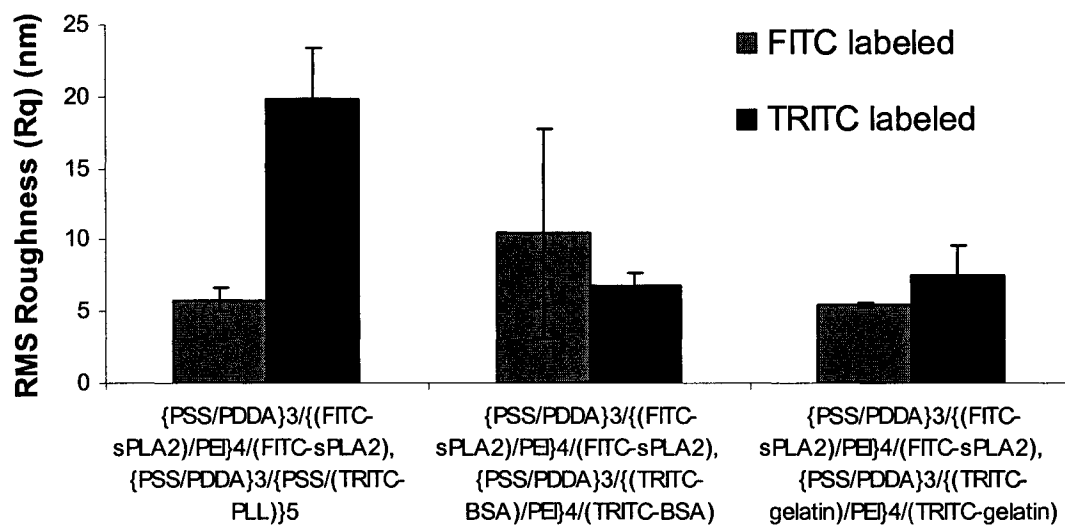


Figure 6. Average thickness of patterns on each half of the chips of three different combinations of sPLA₂ with other proteins/polypeptide ($n=3$).



(a)



(b)

Figure 7. (a) Average roughness (R_a) and (b) RMS roughness (R_q) of patterns on each half of the chips of three different combinations of sPLA₂ with other proteins/polypeptide ($n=3$).

3.4.4 AFM Measurements

AFM scans were performed at three different positions on each half of the fabricated chips of the three different combinations of proteins/polypeptide. Using the 2D analysis option in the software, the step heights of the patterns in all the scans were determined and the averages calculated ($n=3$). Figure 8 is the bar graph of average thickness of the patterns on the chips of the three different combinations of proteins/polypeptide. From Figure 6 and Figure 8, it can be observed that the average thicknesses of the patterns of three different proteins/polypeptide measured through the surface profiler are almost equal to those measured through the AFM.

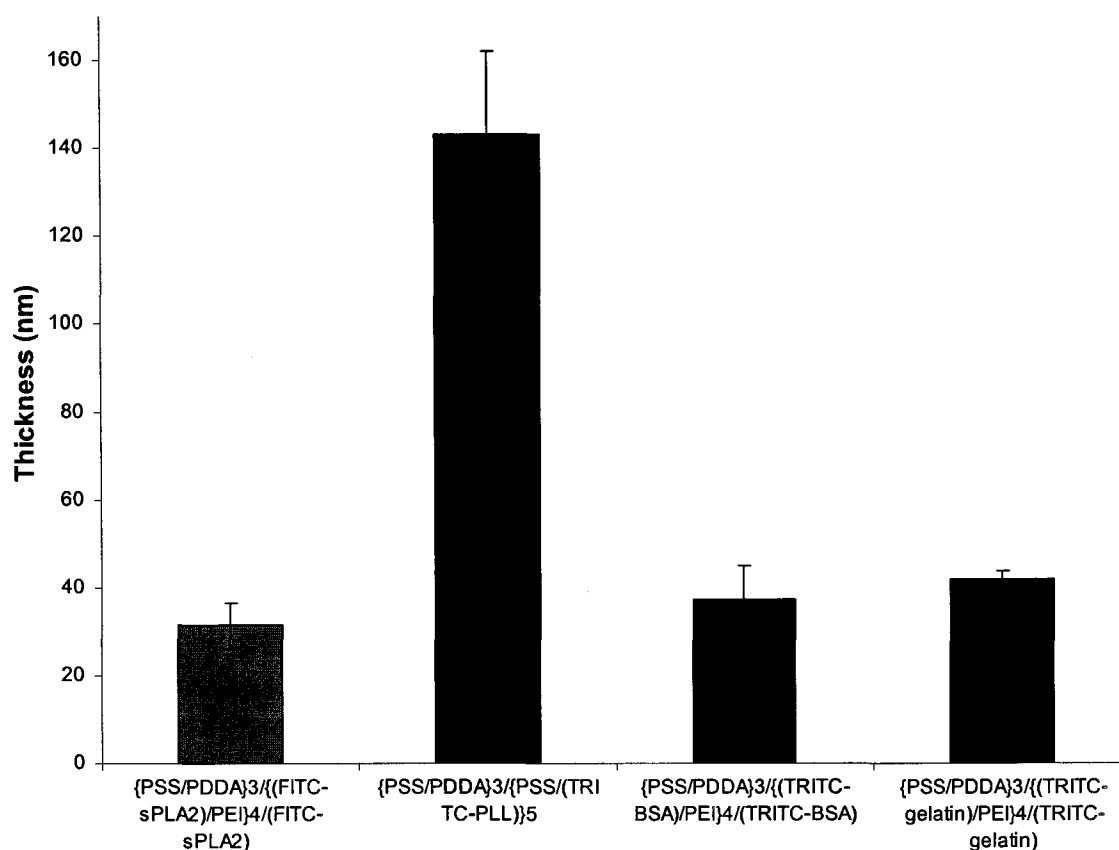


Figure 8. Average thickness of patterns obtained from 2D analysis ($n=3$).

It is notable that it might be useful to have either smooth or rough surfaces for different applications such as fine tuning of cell attachment and possibly differentiation. For example, Boyan et al. have recently demonstrated that osteoblasts differentiate more effectively when grown on “microrough,” as compared with smooth plating surfaces.⁹ More directly related to work with multilayer nanofilms, Rubner’s group reported on tuning cytophilicity/phobicity by assembling and using polyelectrolyte assemblies with identical architecture, but assembled under different conditions.²⁵ Here we have looked at neuronal cell attachment, but more research on substrate roughness may also indicate what topographies neurons prefer for differentiation.

3.4.5 Cell Culture Results

Figure 9 shows the neurons on FITC-sPLA₂ square patterns after one day culture *in vitro*. Figure 9(a) was taken with a monochrome camera, at 100X magnification and Figure 9(b) with a color camera, at 400X magnification. It can be observed that the cells attach specifically to the square patterns. The cells shown in Figure 9 are alive. The viability of these cells was examined up to four days *in vitro* on these substrates, and at this time, uptake of propidium iodide into some non-viable cells was observed. From Figure 9(a), and our cumulative results, it was found that approximately 70% of the sPLA₂ squares are occupied by neurons and 5-10% of the PLL squares exhibited neuronal adhesion. Similar results to PLL were observed for BSA, Figure 9(c), and gelatin nanofilms when compared directly on-chip with sPLA₂; that is, little specific attachment of neuronal cells was observed at one day *in vitro* on non-sPLA₂ squares. Furthermore, few non-attached cells were observed on sPLA₂ regions, Figure 9(a), while cells not attached to BSA squares were readily observed, as shown in Figure 9(c).

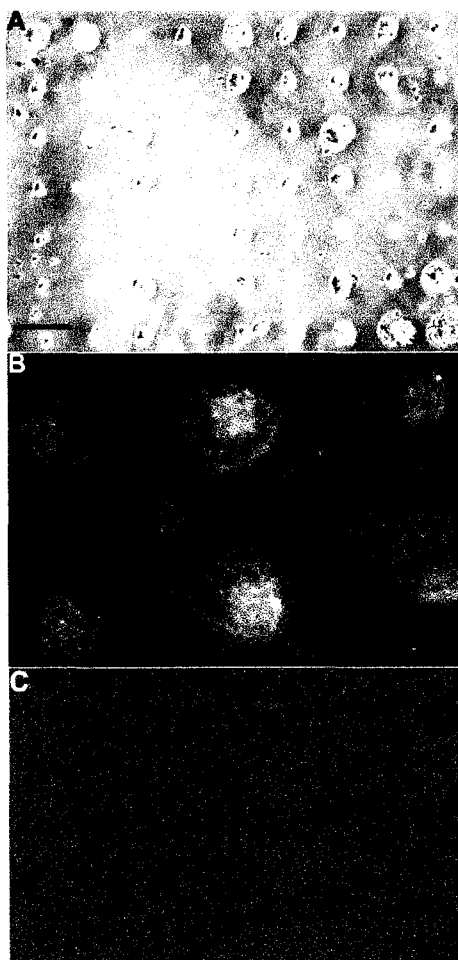


Figure 9. Specific attachment of neurons to FITC-labeled sPLA₂ nanofilm micropatterns. In all images, green squares are FITC-labeled sPLA₂ nanofilm micropatterns, and cells are at one day *in vitro*. Panels A and B show merged images of phase and FITC-labeled sPLA₂ nanofilm micropatterns. Panel C shows a merged image of cells plated onto TRITC-BSA nanofilms. Original microscope magnification = 100X (panel A), 400X (panel B), and 200x (panel C). Scale bars indicate 160 microns in panel A, 40 microns in panel B, and 80 microns in panel C.

The reason for the cell attachment beyond the square patterns, as shown in Figure 9(b), is that after cell dissociation, brain-derived cells in culture tend to re-associate and clump. It is therefore hypothesized that due to high binding affinity of cells to the nanofilm patterns, cells crowd onto the patterned surface and thus appear to go beyond the patterned boundaries. This hypothesis could be tested by diluting out the cell plating density, which we are currently defining in ongoing studies.

These results reveal the quality of the protein deposition and indicate a high degree of selectivity for the targeted neuronal cell interactions. We believe that this is the first demonstration of micropatterning sPLA₂ as a specific cell-attractive material. These results indicate that it is possible to immobilize sPLA₂ with high spatial resolution, and that there is no deleterious effect of lithographic solvents like acetone on the binding properties of the sPLA₂ protein. For the research work described here, layer-by-layer nanofilms were applied to surface areas of approximately 50% of a 9 × 22 mm² cover glass (see methods). Thus, approximately 4 × 10 mm² area was covered by the nanofilm process, with high efficiency. If alignment of the patterns is of no concern, then there is no limit on the surface area using this technique. But if the alignment is indeed a concern, then the patterning technique has the same area coverage limitations as conventional lithography techniques used in semiconductor applications.

The fabrication of comparison chips with two coexisting regions of square patterns with physiological proteins/polypeptide (sPLA₂ and gelatin/PLL/BSA) on a single substrate with PDDA as a cell repellent background on the entire substrate was successful. It is clear that the process described here is limited in the number of proteins that can be patterned on a single chip due to the dipping procedure. Thus, the comparison chips fabricated with the current description would have only two different proteins, or perhaps a few more if a creative dipping procedure or some form of protective overlayer was employed. This research work is a milestone towards more advanced procedures involving multi-step lithography, which will be described in Chapter 4. The fabrication results show that the current method can be used as a platform for the fabrication of comparison chips with other multiple proteins that can be used for simultaneous testing

of cellular (neuronal or others) response to the proteins used. In situations where there is a need to compare the cellular response to different proteins, these comparison chips with multiple proteins on a single substrate help to cancel out any differences in the procedures followed during cell-culture. All the metrology results indicate that the LbL-LO technique is well suited for the current application. It gives great control on the architecture of the patterns. This technique could be further improved in terms of biocompatibility by incorporating the chemically amplified photoresists soluble in dilute aqueous base developers.¹⁸⁶⁻¹⁹⁰ The cell-culture results using the fabricated comparison chips were successfully used to determine the potential of sPLA₂ protein as a neuronal binding target for cell patterning.

3.5 Conclusions

A simple method for the fabrication of bioactive coatings of multiple protein patterns on a single substrate has been demonstrated, based on the LbL-LO technique (combined term for photolithography and LbL assembly technique followed by photoresist-liftoff). Using standard polyelectrolytes in combination with sPLA₂, gelatin, and BSA were used for proteins, PLL for polypeptide, and neuronal cells as a biological test model system. The protein and polypeptide materials were alternately assembled with the polyelectrolytes, and discrete patterns of fluorescent-labeled materials were observed. A clear demarcation of FITC labeled and TRITC labeled proteins/polypeptides was achieved, proving that multi-protein patterns can be deposited on the same substrate with excellent spatial registration. The average roughness of the patterns were found to be approximately five times smaller than the average thickness. Using this simple fabrication method, comparison chips were successfully fabricated and a preliminary

study of neuronal cell interaction of four different materials (sPLA₂, PLL, gelatin, BSA) was performed. The cell culture results on these comparison chips prove that sPLA₂ has the potential as a neuronal binding target. This technique offers the potential for production of a wide array of biological test systems, including comparison chips with different materials, different size and shapes of the micropatterns, and utility with different cell models. This research work has demonstrated the fabrication of two-component “comparison chips” with one component (protein/polypeptide) on each half of a single substrate. However, this limited capability must be further extended to a multi-step procedure enabling deposition of adjacent, overlapping, and/or interdigitated patterns. The description of how this goal was achieved has been presented in the next chapter.

CHAPTER 4

**MULTICOMPONENT POLYMER
PATTERNING-PART II: POLYMER
SURFACE MICROMACHINING**

Most of the content of this chapter has been published as a full paper: Shaikh Mohammed, J.; DeCoster, M. A.; McShane, M. J., Fabrication of Interdigitated Micropatterns of Self-Assembled Polymer Nanofilms Containing Cell-Adhesive Materials. *Langmuir* **2006**, *22*, (6), 2738-2746.

4.1 Introduction

It is clear from previous chapters that micropatterns of different biomaterials with micro- and nanoscale features and defined spatial arrangement on a single substrate are useful tools for studying cellular-level interactions. With the goal of constructing cell-adhesive patterns with precisely tailored physicochemical properties, including stiffness, existing techniques present severe limitations. Use of multilayer nanofilms for creating appropriate scaffolds is desirable, and a straightforward technique to construct multilayer nanofilm scaffolds with few restrictions on materials and excellent alignment of subsequent patterns is needed. It appears that combining photolithography with LbL assembly can overcome many of the shortcomings of current methods for multilayer film

patterning.^{119,191} In the previous chapter two-component “comparison chips”¹⁹² with one component on each half of a single substrate were presented. However, this limited capability must be further extended to a multi-step procedure enabling deposition of adjacent, overlapping, and/or interdigitated patterns.

This chapter describes a simple yet versatile and precise patterning technique which provides the capability to engineer complex 3D nanocomposite multilayers in aligned interdigitated micropatterns on a single substrate (as illustrated in Figure 1). The technique, termed PSM, involves a combination of lithography and LbL methods and has the primary advantage of well-controlled alignment for registration of subsequent patterns of multilayer films. Therefore, complex functional biointerfaces providing different chemical and physical cues may be easily constructed, offering the realization of a wide range of systems requiring precise arrangements of physicochemical features, and could be used for a wide range of related biological applications, including biological testbeds for basic biological studies, multicellular communication and organizational studies, biosensors, drug screening, and tissue engineering. The basic approach may also be applied to constructing complex patterns of self-assembled materials into, for example, polymeric electronic devices, optical systems, or other systems in which nanocomposite materials are required, and the approach can potentially be combined with more standard surface micromachining techniques to further extend the range of applications.

In the PSM method, the first nanofilm pattern is constructed using lithography, followed by LbL multilayer assembly and lift-off, and the process is repeated with optical alignment to obtain adjacent, overlapping, and/or interdigitated patterns on the same

substrate. Thus, the method is analogous to surface micromachining, except that the deposition materials are polymers and biological materials used to produce multilayer nanocomposite structures. A key feature of the multilayers is the capability to tune properties such as stiffness by appropriate selection of materials, deposition conditions, and post-deposition treatments. Two- and four-component systems on glass coverslips are presented to demonstrate the versatility of the approach to construct precisely-defined, homogeneous nanofilm patterns. In addition, an example of a complex system used as a testbed for *in vitro* cell adhesion and growth is provided: micropatterns of poly(sodium 4-styrenesulfonate)/poly-L-lysine hydrobromide (PSS/PLL) and secreted phospholipase A₂/poly(ethyleneimine) (PEI/sPLA₂) multilayers. The interdigitated square nanofilm array patterns were obtained on a single coverslip with PDDA as a cell-repellent background. Cell culture experiments show that cortical neurons respond and bind specifically to the sPLA₂ micropatterns in competition with PLL micropatterns. Preliminary results for neuronal network formation, potential for co-culture systems, and neuronal cell-adhesion response to micropatterns of varying heights using the two-component systems of sPLA₂ and PLL, and pattern-on-pattern two-component systems of PLL and PDL have also been demonstrated. The fabrication and the initial biological results on the nanofilm micropatterns support the usefulness of the technique for use in studies aimed at elucidating important biological structure-function relationships, but the applicability of the fabrication method is much broader and may impact electronics, photonics, and chemical microsystems.

4.2 Materials

4.2.1 Substrates

Microscope cover glasses ($24 \times 60 \text{ mm}^2$) used as substrates for the nanofilm patterning were purchased from VWR International.

4.2.2 Chemicals

Nano-StripTM was purchased from CYANTEK Corporation. Poly(diallyldimethylammonium chloride) (Mw ~100-200 kDa), poly(sodium 4-styrenesulfonate) (Mw ~1 MDa), poly(ethyleneimine) (Mw ~750 kDa), poly-L-lysine hydrobromide (Mw ~25,700 Da and ~84 kDa), poly-D-lysine hydrobromide (PDL) (Mw ~125,100 Da), poly(allylamine hydrochloride) (PAH) (Mw ~70 kDa), and fluorescein isothiocyanate were purchased from Sigma-Aldrich. Secreted phospholipase A₂ (Type III, from bee venom) (Mw ~14 kDa) was purchased from Cayman Chemical. Tetramethylrhodamine-5-(and-6)-isothiocyanate and Texas Red-X, succinimidyl ester (MW ~816.94 Da) were ordered from Molecular Probes. CyTM5-bis-NHS ester was ordered from Amersham Biosciences. Positive photoresist, S1813, and positive resist developer, MF-319, were obtained from Shipley. All chemicals of commercial origin were used as received.

4.2.3 Preparation of Polyelectrolyte and Polypeptide Solutions

Solutions of PDDA, PAH, and PSS with concentration of 2 mg mL^{-1} with 0.5 M KCl and a solution of 2 mg mL^{-1} PEI were prepared in DI H₂O for use in self-assembly. PLL, PAH, and PEI were labeled with TRITC, (Texas Red, Cy5, FITC, and TRITC), and FITC, respectively, using standard procedures.²⁵⁹ PLL, PAH, and PEI were separated from dye solution by precipitation with acetone, centrifugation, and resuspension in

aqueous solution. Solutions for deposition were prepared as $167 \mu\text{g mL}^{-1}$ in DI water for TRITC-PLL, $400 \mu\text{g mL}^{-1}$ in 0.1M sodium bicarbonate at pH 9.0 for sPLA₂, and $125 \mu\text{g mL}^{-1}$ in DI water for PLL and PDL.

4.3 Methods

4.3.1 Mask Design

Because the aim of this work was to test the adhesion of cells and potential for network formation on the nanofilm micropatterns, the mask used for defining the patterns for this work contained arrays of isolated as well as connected squares. The mask contained five different square regions. All the regions contained $20 \mu\text{m}$ square patterns separated from each other by a distance of $80 \mu\text{m}$, in horizontal as well as vertical directions. One of the regions contained only square patterns. The other three regions contained squares connected by $5 \mu\text{m}$ stripe patterns, with the center of the stripe patterns offset from the edge of the squares by a distance of $10 \mu\text{m}$, $13.75 \mu\text{m}$, and $17.5 \mu\text{m}$. Another region contained squares connected by $5 \mu\text{m}$ stripe patterns (offset of $10 \mu\text{m}$) in both vertical and horizontal directions. For the pattern-on-pattern two-component systems, the mask used for pattern transfer contained $50 \mu\text{m}$ wide stripe patterns separated by $50 \mu\text{m}$.

4.3.2 Fabrication

4.3.2.1 Substrate pretreatment

Substrates were incubated in Nano-Strip™ at $70 \text{ }^\circ\text{C}$ for 1 hr to remove organic contaminants and create a uniform negative charge on the substrates, then they were rinsed in DI water and dried using N_2 . A set of alignment marks were deposited on the substrates using standard lithography, sputtering 10 nm of Au-Pd, and lift-off processes.

This was the major modification made to the existing LbL-LO technique to accommodate the alignment of patterns of different materials. A precursor layer of PDDA was then deposited on the negatively-charged substrates by incubating in PDDA for 20 min, rinsing in DI water, and finally drying in N₂. The choice of PDDA as a precursor layer was based on previous observations, where PDDA had proven to be a cell-repellent material for smooth muscle cells,^{191,263} and preliminary screening studies, where similar results were observed when tested with neuronal cells.¹⁹² However, any other cytophobic material, providing the required charge, could in principle replace PDDA or, alternatively, the background surface could be backfilled with a neutral cytophobic material (e.g., PEG) after the completion of all the patterning steps.

4.3.2.2 Photolithography

Photoresist S1813 was spun on the substrates (1,000 rpm -100 r s⁻¹ - 10 s, 3,000 rpm - 500 r s⁻¹ - 50 s), soft baked at 115 °C for 1 min, and photo-patterned using UV radiation (365/405 nm, 7 mW cm⁻²) for 15 s. Patterns were developed for 20 s, then substrates were rinsed in DI water and dried using N₂.

4.3.2.3 Layer-by-layer self-assembly

For all the LbL assembly processes, a basement multilayer of {PSS/PDDA}₃ was deposited on the patterned substrates through immersion in the PSS or PDDA solutions for 10 min, rinsing in DI water, and finally drying in N₂. This precursor multilayer deposition of strong polyelectrolytes is an important step to attain a uniformly charged surface for subsequently deposited layers. The process of rinsing in DI water and drying with N₂ was repeated after each deposition step throughout the LbL assembly process

because it was found to help to obtain undistorted multilayer patterns in the final development stage.

After the first round of photoresist development and the LbL assembly of precursor layers, a nanofilm architecture of $\{\text{sPLA}_2/(\text{FITC-PEI})\}_4/\text{sPLA}_2$ was deposited on top of the patterned substrates with pre-existing $\{\text{PSS/PDDA}\}_3$ films. This step was accomplished through deposition of four bilayers of $\text{sPLA}_2/(\text{FITC-PEI})$ by alternate exposure of substrates to negatively-charged sPLA_2 and positively-charged FITC-PEI solutions, followed by a fifth and final layer of sPLA_2 . The optimum adsorption times (minimum time required for the resaturation of polyion adsorption that results in the charge reversal) were previously determined through QCM experiments to be 20 min for TRITC-PLL and 50 min for sPLA_2 .¹⁹² Hence, the substrates were immersed in sPLA_2 and FITC-PEI for 50 min and 10 min, respectively.

4.3.2.4 Lift-off

The lift-off process was performed by sonicating the substrates in acetone for 3-5 min to obtain the first set of patterns. The sonicator was filled with acetone and the substrates immersed directly into the acetone.

4.3.2.5 Multicomponent patterning

A second lithography step was performed on the substrates, this time with a set of patterns aligned with the first set of patterns using previously patterned alignment marks, and a multilayer architecture of $\{\text{PSS}/(\text{TRITC-PLL})\}_5$ was deposited in a procedure similar to that used for $\{\text{sPLA}_2/(\text{FITC-PEI})\}_4/\text{sPLA}_2$. Here, PSS was used as the polyanion, and adsorption times were 10 and 20 min for PSS and TRITC-PLL, respectively.

For the two-component systems of sPLA₂ and PLL with micropatterns of varying heights, similar procedure was followed. The number of precursor layers and PLL multilayers deposited were altered to obtain micropatterns of varying heights. For the pattern-on-pattern two-component systems, a similar procedure was followed. Nanofilms with architectures {PSS/TRITC-PAH} and {PSS/FITC-PAH} were deposited before depositing the precursor layers, followed by the deposition of PLL and PDL multilayers, respectively. The assembly time used for PDL was 20 min. For the four-component systems, a similar procedure was followed. The adsorption time was 10 min for Cy5-PAH, TRITC-PAH, FITC-PAH, and Texas Red-PAH.

4.3.3 Characterization

4.3.3.1 Fluorescence and phase contrast microscopy

Fluorescence microscopy was used for imaging the resulting multicomponent micropatterns to demonstrate successful multicomponent patterning and to assess the uniformity and spatial registration using an epifluorescence microscope (Nikon, Model-Eclipse TS100) equipped with a Nikon COOLPIX995 digital Camera. The exposure time used with the 40X objective was 2 s for the FITC cube and 0.25 s for the TRITC cube. Digital zoom settings of F3.0 were used for the imaging process. Images were taken sequentially using a FITC cube followed by a TRITC cube. The FITC cube contained a long-pass emission filter. Confocal laser scanning microscopy (CLSM) (Leica, Model-TCS SP2) was also used to perform sequential FITC-TRITC imaging and Cy5-FITC-TRITC imaging of the two- and four-component substrates, respectively, at optical magnifications of 10X and 63X. For the two-component systems of varying heights, the exposure time used was 0.5 s for the brightfield mode.

4.3.3.2 Surface profilometry

Surface profilometry was used for assessment of the topographical differences of the multicomponent micropatterns. The surface profiler (KLA-Tencor, Model-Alpha-Step IQ) was used to collect line scan structural data of the patterns on three different substrates. The vertical dimensions of the patterns were obtained directly from the line scan measurements. Final height values were based on an average of three measurements. The scan parameters used were as follows: stylus force of 20 mg, scan length of 200 μm , scan speed of 20 $\mu\text{m s}^{-1}$, and sampling rate of 50 Hz.

4.3.3.3 Atomic force microscopy

AFM measurements were made to further analyze the finer physical features of the patterns on the fabricated substrates. The AFM (Quesant, Model-Q-Scope250) was used in tapping mode with silicon cantilevers to collect area scan data from the patterns. The lateral and vertical dimensions of the patterns were obtained from these measurements. Several scans over a region of the surface were performed to verify that the tip did not induce observable modifications of the sample. The parameters used for the measurements were: scan area $40 \times 40 \mu\text{m}^2$ for thickness measurements and $10 \times 10 \mu\text{m}^2$ for roughness measurements, scanning rate between 1.5-3 Hz, and a resolution of 300 or 600 lines. The average roughness data was obtained directly from the area scan measurements.

4.3.3.4 Ellipsometry

A spectroscopic ellipsometer (SENTECH, Model-SE 850) was also used to measure the thickness of PSS/PDDA multilayers. The measurements were performed at

an incidence angle of 70° and the 250-850 nm spectral range was used. A refractive index of $n_0=1.5$ was assumed for thickness calculations using the SPECTRARAY software.

4.3.3.5 Scanning electron microscopy

Scanning electron microscopy (SEM) was performed to demonstrate the alignment and differences in heights of the multicomponent micropatterns over a large area on the substrate. A scanning electron microscope (AMRAY, Model-1830) was used to obtain grayscale micrographs of the multicomponent patterns. Before performing the electron microscopy, the substrates were sputter coated with 1 nm of Au-Pd to avoid the charging of the substrates. An acceleration potential of 4 KV was used at different magnifications for the microscopy.

4.3.3.6 Roughness step testing

Alignment and differences in heights of the multicomponent micropatterns over a large area on the substrate was confirmed by optical profilometry. A white-light interferometric optical profiler (Veeco Metrology Group, Model-WYKO NT1000) was used to obtain color-coded surface images of the micropatterns. Before performing the optical profilometry, the substrates were sputter coated with 1 nm of Au-Pd to obtain reflective surface. The vertical-Scanning Interferometry (VSI) measurement option with magnifications of 20X and 50X was used here.

4.3.4 Cell Culture

As a specific example of how this method may be applied to biological studies, primary cultures of cortical neurons were used as a model biological system to compare the results with those obtained using side-by-side “comparison chips.”¹⁹² While poly-L-lysine is well known and widely used as a neuronal cell adhesion material, we have

recently observed preferential attachment of neurons to secreted phospholipase A₂ (sPLA₂), which is a low molecular weight transcellular enzyme that has been shown to be involved in digestive and inflammatory response mechanisms, and is known to have potent deleterious effects on neurons of the central nervous system.^{254,255} Since sPLA₂-binding proteins and receptors have been identified in muscle and brain cells, the enzymatic and signaling functions of sPLA₂s are believed to have cell surface targets, so these observations are not stunning.²⁵⁶⁻²⁵⁸ However, the initial experiments showing that primary cortical neurons preferentially bind to sPLA₂ when presented with both sPLA₂- and PLL-terminated nanofilm patterns were performed with the two patterns on different halves of the same chip; therefore, the question of whether spatial separation plays a key role in this attachment behavior has been raised.¹⁹²

The multicomponent patterning method described here provides the ability to spatially orient the two sets of micropatterns containing PLL and sPLA₂ in different arrangements. Therefore, to compare the results from the current technique with the results obtained through comparison chips,¹⁹² interdigitated two-component nanofilm patterns of PLL and sPLA₂ were constructed. For these experiments, primary cultures of cortical neurons were prepared as previously described²⁵³ from embryonic day 15 rat embryos and grown on the patterned substrates in 37 °C, 5% CO₂ incubators. Cortical neurons grown on the multicomponent micropatterns were imaged using a Nikon inverted microscope and a Roper Scientific CoolSnap HQ camera with Metamorph software (Universal Imaging). For the two-component systems of sPLA₂ and PLL with micropatterns of varying heights, similar procedure was followed. All the cell culture work was done in Dr. Mark A. DeCoster's laboratory at LSUHSC, New Orleans.

4.4 Results and Discussion

The cartoon in Figure 10 depicts the fabrication process flow used in this work. The first step in the fabrication was the treatment of the substrates with Nano-Strip™ followed by the deposition of the PDDA precursor layer. The next step was the patterning of substrates using S1813. The patterned substrates were then modified using LbL self-assembly with the desired multilayer configuration. Lift-off was performed on the substrates to obtain the first set of multilayer patterns.

This procedure was repeated to obtain the second set of multilayer patterns, and could be repeated as necessary to deposit additional nanofilm patterns on the same substrate. This method is analogous to surface micromachining, except that the deposition materials are polymers and biological materials that are used to produce multilayer nanocomposite structures.

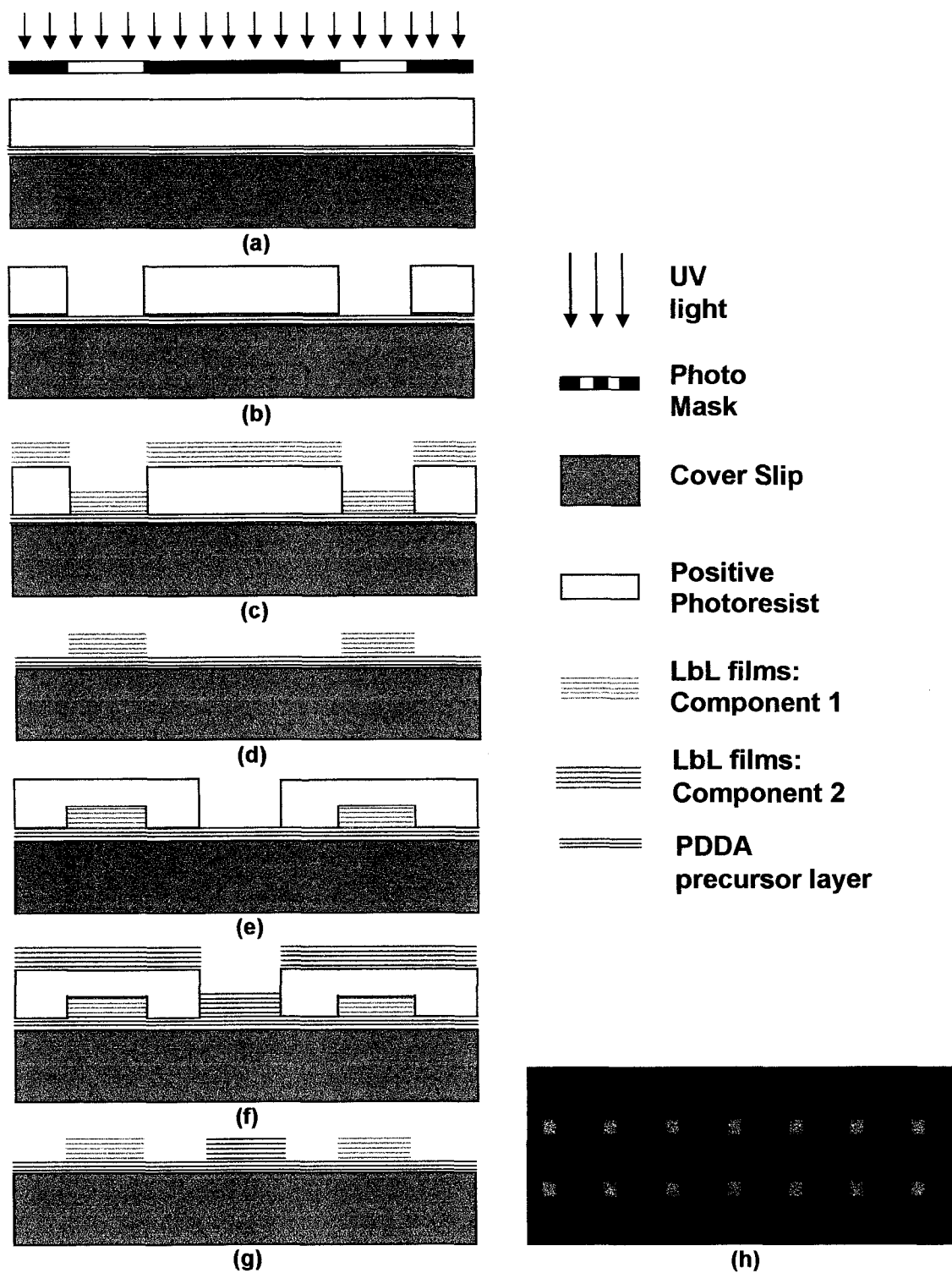


Figure 10. Template used for PSM method (a), (b) Photolithography of pretreated substrate, (c) LbL deposition of component 1, (d) After first lift-off, (e) Second photolithography step, (f) LbL deposition of component 2, (g) After second lift-off, (h) Top view of the chip.

4.4.1 Two-Component Patterns

4.4.1.1 Fluorescence and phase contrast microscopy

Figure 11 contains fluorescence and phase contrast images of the micropatterns fabricated using the PSM method. Figure 11(a) is an image of 20 μm interdigitated square patterns with an offset of 50 μm in both vertical and horizontal direction. The green patterns are multilayer heterostructures with a configuration of $\{\text{PSS/PDDA}\}_3/\{\text{sPLA}_2/(\text{FITC-PEI})\}_4/\text{sPLA}_2$, whereas the red patterns have an architecture of $\{\text{PSS/PDDA}\}_3/\{\text{PSS}/(\text{TRITC-PLL})\}_5$. Figure 11(b) is an image of similar interdigitated patterns, with an offset of 50 μm in the vertical direction only. Figure 11(c) is a phase contrast image of nanocomposite sPLA₂ and PLL patterns. The dark squares are nanocomposite PLL patterns, whereas the bright squares are nanocomposite sPLA₂ patterns. These images prove that the current patterning technique provides the capability of registering micropatterns in the desired configuration, with high precision and accuracy. The average misregistry, M ,²⁶⁴ between the patterns of the two components, was found to be 0.79 μm . For an offset length of 50 μm , this misregistry relates to an error of 1.58%. This error increases for smaller lengths. However, most of the times very small lengths are not required for biological studies related to cells. Figure 11(d) is an illustration representing the cross-sectional side view of the patterns. It is noteworthy that when the total number of layers for the different components is nearly the same, the height difference is substantial.¹⁹² The thickness of $\{\text{PSS/PDDA}\}_3$, measured using an ellipsometer, was found to be 18.2 ± 0.09 nm. The thicknesses of PSS/PLL and PEI/sPLA₂ multilayers were estimated by subtracting the thickness of three bilayers of

PSS/PDDA from the total height values measured through surface profilometry as noted below.

In Figures 11(a)-(b), the fluorescence intensities of the nanocomposite patterns are uniform within a pattern, indicating that the biomaterials were deposited uniformly. In Figure 11(c), it can be seen that the micropatterns have clear, sharp, and defined edges that are faithful reproductions of the photomask. There were no obvious traces of residual photoresist or multilayer nanofilms on the PDDA background regions. Furthermore, these images indicate that using the current method, complex heterostructures of multiple components may be easily obtained with simplicity and high fidelity (edge resolution of the patterns is $<1 \mu\text{m}$) to spatially orient the nanocomposite polymer film micropatterns with precise alignment. However, it is also obvious that the corners of the squares, which are supposed to be sharp, are slightly rounded, but the purpose of this paper was to demonstrate the current technique, not to optimize it. Better edge resolution and sharp corners can certainly be achieved by optimizing the process parameters. We have found that these characteristics depend upon the material (molecular weight, size of molecule) being deposited photoresist thickness used, and the number of multilayers deposited, as well as the solution conditions (pH, ionic strength) affecting the multilayer formation.

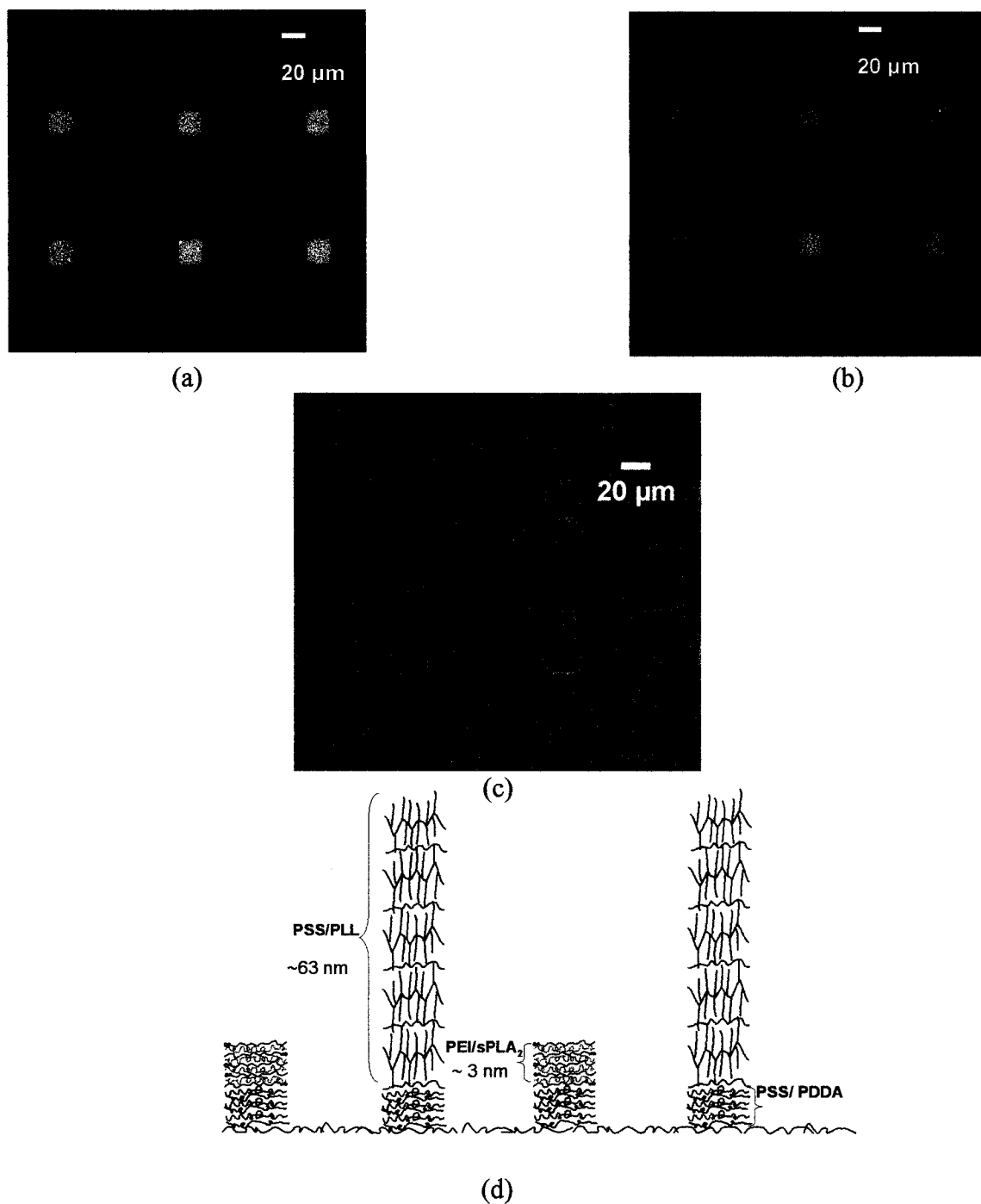


Figure 11. 3D interdigitated multicomponent micropatterns constructed on glass substrates: Images of 20 μm patterns (40X) collected through FITC cube with the second component (a) Offset by 50 μm in vertical and horizontal direction, (b) Offset of 50 μm in vertical direction [Green: $\{\text{PSS/PDDA}\}_3/\{\text{sPLA}_2/(\text{FITC-PEI})\}_4/\text{sPLA}_2$ and Red: $\{\text{PSS/PDDA}\}_3/\{\text{PSS}/(\text{TRITC-PLL})\}_5$], (c) Phase contrast image [Dark squares: PLL patterns and Bright squares : sPLA₂ patterns], (d) Cartoon of the cross-section view of patterns.

4.4.1.2 Surface profiler measurements

Figure 12 contains line scan structural data of interdigitated nanocomposite square micropatterns of sPLA₂ and PLL, with multilayer configuration of {PSS/PDDA}₃/sPLA₂/(FITC-PEI)₄/sPLA₂ and {PSS/PDDA}₃/PSS/(TRITC-PLL)₅, respectively. The height difference, as depicted schematically in Figure 11(d), can clearly be seen from the profile; based on an average of three measurements, the nanocomposite PLL patterns were 81.53 ± 1.31 nm thick, whereas the sPLA₂ patterns were 21.33 ± 0.71 nm thick.

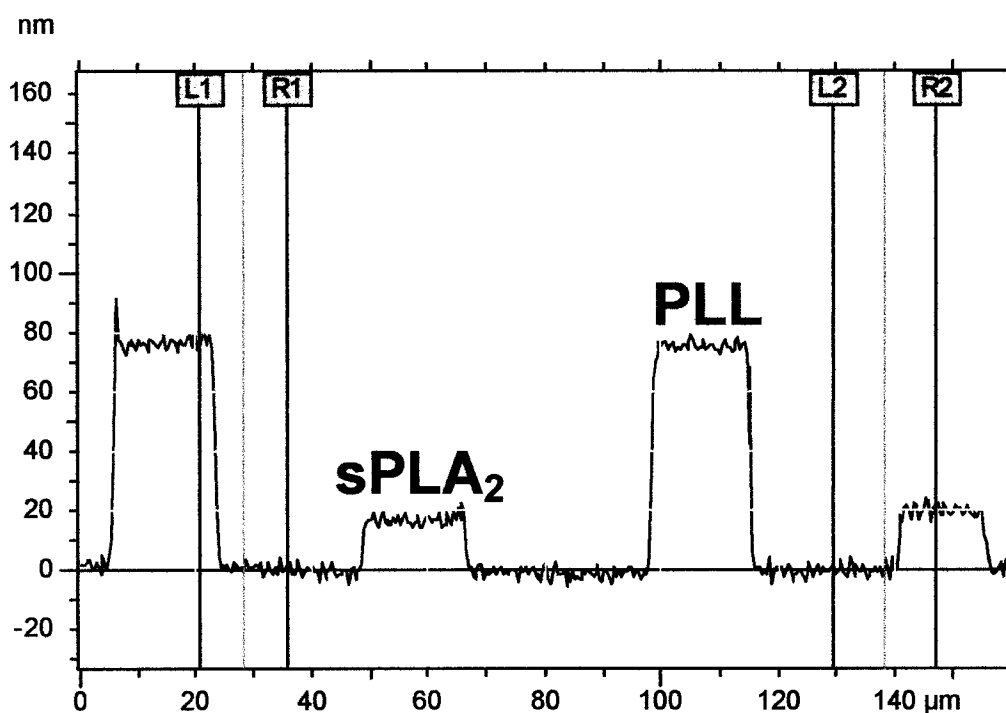


Figure 12. Surface profiler line scan structural data of 3D interdigitated multicomponent nanocomposite micropatterns of PLL and sPLA₂.

This line scan profile demonstrates the ability of the current technique to fabricate complex 3D multilayers in aligned interdigitated micropatterns. The standard deviations

indicate that the heights of the nanocomposite patterns across different substrates are very uniform (~1.6% and ~3% variations for PLL and sPLA₂ patterns, respectively). The inherent ability of the technique to accommodate different surface chemistries and finely tune the topographies will be useful in presenting varying physical and chemical cues to influence cell growth.^{265,266}

4.4.1.3 AFM measurements

The difference in heights of the sPLA₂ and PLL patterns is in agreement with the previously published results from QCM, surface profiler, and AFM measurements.¹⁹² The shorter heights of sPLA₂ patterns compared with PLL patterns of similar multilayer architecture can be attributed to the molecular size and weaker net charge of sPLA₂. However, if scaffolds mimicking complex 3D *in vivo* conditions more closely are to be realized, the heights of the patterns could be easily adjusted during the multilayer LbL assembly process by depositing more or fewer layers as necessary.

4.4.1.4 Ellipsometer measurements

Silicon wafers were used as substrates for the ellipsometric measurements. The ellipsometric measurements were made at three different positions on the substrates after the deposition of each new layer, followed by the estimation of the average thickness (using the SPECTRARAY software) of the newly deposited layer depending on the estimated thickness of the previously deposited layers. Finally, the average thickness of {PSS/PDDA}₃ based on three different samples was found to be 18.2 ± 0.09 nm. The standard deviation indicates very low variation in the average thickness (~0.49%) of the multilayers between different substrates.

4.4.1.5 SEM measurements

Figure 13 contains a scanning electron micrograph and an optical profiler image of the surface of 3D interdigitated multicomponent nanocomposite micropatterns of PLL and sPLA₂, with multilayer configuration of {PSS/PDDA}₃/sPLA₂ and {PSS/PDDA}₃/sPLA₂/(FITC-PEI)₄/sPLA₂, respectively. The grayscale micrograph in Figure 13(a) demonstrates an obvious contrast between the nanocomposite micropatterns of PLL and sPLA₂; nanocomposite PLL patterns appear to be darker than the sPLA₂ patterns due to the difference in height of the patterns. The electron micrograph illustrates the uniformity of the nanocomposite patterns, within a pattern region as well as over a larger area on the substrate. It can also be seen that there are no residual materials left on the PDDA background from the lithography, LbL assembly, and lift-off processes. The tilt in the electron micrograph enhances the misregistry between the two micropatterns.

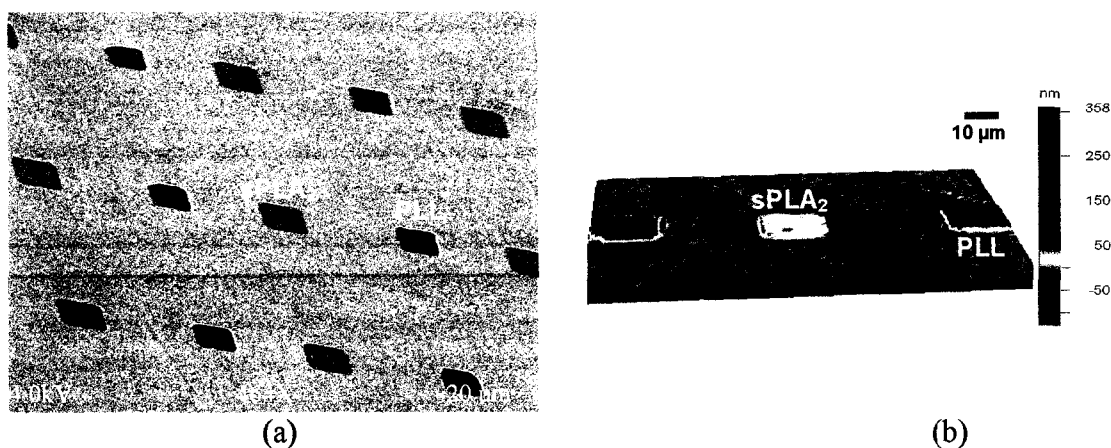


Figure 13. (a) Scanning electron micrograph of 3D interdigitated multicomponent micropatterns comprised of PLL and sPLA₂, (b) 3D optical profiler surface micrograph of 3D interdigitated multicomponent micropatterns comprised of PLL and sPLA₂.

4.4.1.6 RST measurements

The color-coded 3D image in Figure 13(b) illustrates the difference in height of the two components; with the nanocomposite PLL patterns in red color (>50 nm) and the sPLA₂ patterns in green color (0-25 nm range), indicating that the PLL patterns are at least two times taller than the sPLA₂ patterns. The difference in heights of the sPLA₂ and PLL patterns (as shown in Figures 12 and 13) is in agreement with the previously described results (Chapter 3) from QCM, surface profiler, and AFM measurements. The shorter heights of sPLA₂ patterns compared with PLL patterns of similar multilayer architecture can be attributed to the molecular size and weaker net charge of sPLA₂. However, if scaffolds mimicking complex 3D *in vivo* conditions more closely are to be realized, the heights of the patterns could be easily adjusted during the multilayer LbL assembly process by depositing more or less number of multilayer films of organic or inorganic biomaterials.

4.4.1.7 Cell culture results

Initial tests on the applicability of these multicomponent heterostructures to biological studies, performed through preliminary cell culture experiments, resulted in interesting observations. Figure 14 contains the TRITC, phase, FITC, and merged TRITC+FITC+phase images of 3D interdigitated multicomponent nanocomposite micropatterns of PLL and sPLA₂, with multilayer configuration of {PSS/PDDA}₃/{PSS/(TRITC-PLL)}₅ (red) and {PSS/PDDA}₃/{sPLA₂/(FITC-PEI)}₄/sPLA₂ (green), respectively, acquired at an original microscope magnification of 400X.

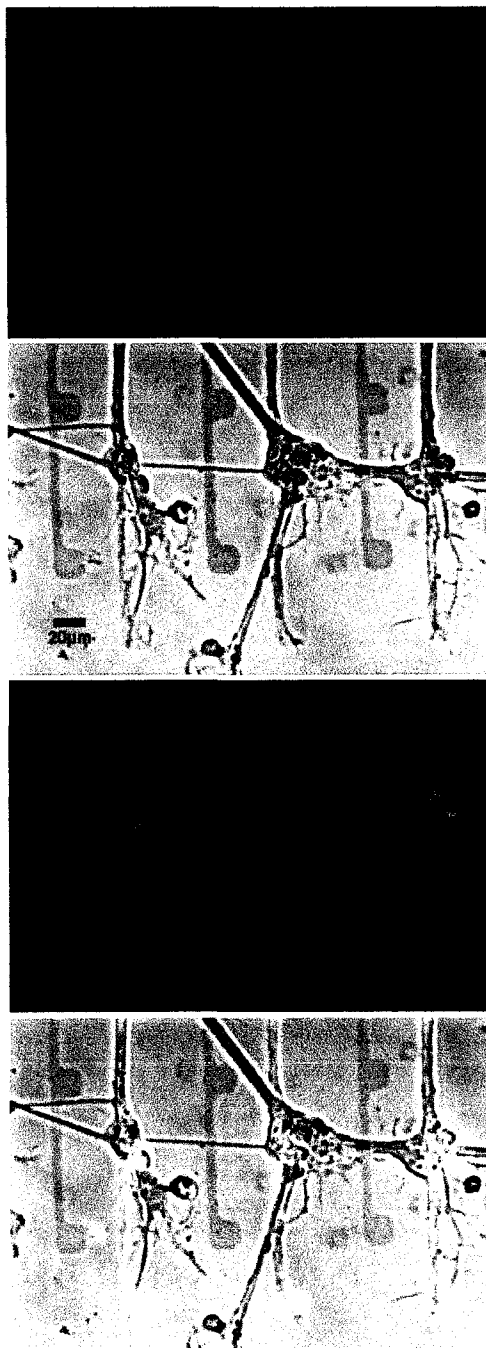


Figure 14. Tiled TRITC fluorescence, phase, FITC fluorescence, and merged phase+TRITC+FITC images (Top to bottom) of primary rat cortical neurons grown on $\{\text{PSS/PDDA}\}_3/\{\text{sPLA}_2/(\text{FITC-PEI})\}_4/\text{sPLA}_2$ patterns (green) next to $\{\text{PSS/PDDA}\}_3/\{\text{PSS}/(\text{TRITC-PLL})\}_5$ patterns (red). Neurons were plated onto nanofilm substrates at a density of 100,000 cells/ml in 2.7 ml of culture medium in a 35 mm Petri dish. Images were captured after 2 weeks *in vitro*. As is obvious from the location of cells on the surfaces, preferential attachment of neurons to sPLA₂-terminated films was observed.

The patterns are $20 \times 20 \mu\text{m}^2$ squares separated by $80 \mu\text{m}$, connected by $5 \mu\text{m}$ wide lines, with the two material patterns offset by $50 \mu\text{m}$ and $40 \mu\text{m}$ in the vertical and horizontal directions, respectively. The area shown is at the end of a line of patterns; thus the FITC patterns extend $50 \mu\text{m}$ beyond the TRITC patterns. The “halo” appearing adjacent to the fluorescent patterns in the merged image is due to the imaging procedure, and not a result of diffusion of the fluorescent molecules away from the patterns. According to observations, the patterns are stable in aqueous solution and cell culture media for at least 5 weeks, with no apparent loss of fluorescence intensity, which agrees with other reports on the stability of multilayer nanofilms.^{61,267,268}

For observations performed up to two weeks *in vitro*, it was found that neurons preferentially bound to $\{\text{PSS/PDDA}\}_3/\{\text{sPLA}_2/(\text{FITC-PEI})_4\}/\text{sPLA}_2$ patterns compared with $\{\text{PSS/PDDA}\}_3/\{\text{PSS}/(\text{TRITC-PLL})\}_5$ patterns. In addition, large and fine neuronal processes were observed, following preferential localization of cells on the FITC patterns. There is no binding of neurons to the nanocomposite PLL patterns, although the large processes do not appear to see the 80 nm tall PLL micropatterns as an obstacle from interacting with neurons binding on other sPLA_2 micropatterns. Also, from these images it is obvious that PDDA proves to act well as a cytophobic material. It is noteworthy that for the data presented here, the sPLA_2 patterns were deposited first, followed by the deposition of the PLL patterns; identical behavior was observed in experiments where the order of deposition was reversed.

In earlier studies, it was shown that when neurons were cultured on substrates with only PLL patterns, they attached to the patterns and were confined to the patterns;²⁶⁹ however, our results suggest that the neurons preferred sPLA_2 patterns over the PLL

patterns. These results agree with and support the cell adhesion behavior observed with the half sPLA₂/half PLL comparison chips,¹⁹² but now any possibility of preferential attachment due to position on the surface has been removed, since squares composed of different biomaterials are adjacent to each other and interdigitated. Thus, the primary neurons used for these investigations appear to select sPLA₂ over PLL as the substrate of choice.

The exact reason behind the observed result of preferential binding of neuron cells to sPLA₂ is not obvious, though several possibilities exist. One explanation could be that sPLA₂ composite nanofilm patterns are thinner in the z-axis than the PLL patterns (~20 vs. ~80 nm), as shown schematically in Figure 11(d) and Figure 12. Additional investigation of the contribution of surface topographical cues towards the specific binding of neuron cells to sPLA₂ is currently underway, and preliminary findings (Section 4.4.2) indeed suggest a dependence of the binding behavior upon the nanoscale film thickness.²⁷⁰ Whether the observations are truly height-dependent, or are also influenced by substrate stiffness of the substrate,¹⁵ which also varies with film height,^{96, 97} is another question to be answered in future work. Regardless of the true nature of the interactions and details of the factors involved, the cell culture results indicate that the current technique could find immediate application in constructing precise co-culture systems by specifically capturing multiple cell types with defined spatial arrangement for better understanding of cell-cell interactions.^{143,144,150-152} The following discussion presents preliminary cell culture results from two-component systems of PLL and sPLA₂.

Additional proof for the applicability of this technique to construct co-culture systems is provided by the preliminary cell culture results on the primary spinal cord

neuronal cell cultures grown for seven days *in vitro* (DIV) on substrates similar to those discussed above with respect to Figure 14. Figure 15 contains the merged TRITC+phase images of 3D interdigitated multicomponent nanocomposite micropatterns of PLL and sPLA₂, with multilayer configuration of {PSS/PDDA}₃/{PSS/(TRITC-PLL)}₅ (red) and {PSS/PDDA}₃/{sPLA₂/(FITC-PEI)}₄/sPLA₂ (uncolored), respectively, acquired at an original microscope magnification of 200X. The patterns are 20 × 20 μm² squares separated by 80 μm, connected by 5 μm wide lines, with the two material patterns offset by 25 μm (Figure 15(a)) and 20 μm (Figure 15(b)) in the horizontal directions. After 7 DIV, it was found that the neurons selectively adhere to sPLA₂-terminated patterns (Figure 15(a)), while glial cells attach to TRITC-PLL patterns (Figure 15(b)).

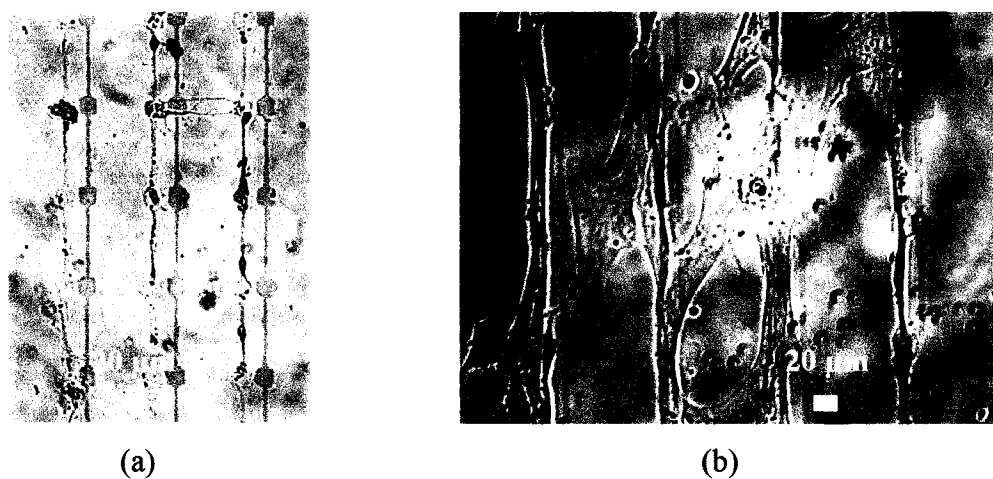


Figure 15. Merged phase+TRITC images of primary spinal cord neurons grown on {PSS/PDDA}₃/{sPLA₂/(FITC-PEI)}₄/sPLA₂ patterns (uncolored) next to {PSS/PDDA}₃/{PSS/(TRITC-PLL)}₅ patterns (red) after 7 DIV: (a) Cells of neuronal morphology (consistent with Figure 14) were captured by the sPLA₂-terminated nanofilms (FITC fluorescence omitted for clarity), (b) Cells of glial morphology (in contrast to Figure 14) are captured by the PLL-terminated patterns (red).

More interesting findings were observed in preliminary cell culture results on the primary brain neuronal cell cultures grown for 40 DIV on substrates similar to those discussed above with respect to Figures 14 and 15. Figure 16 contains the merged TRITC+phase images of 3D interdigitated multicomponent nanocomposite micropatterns of PLL and sPLA₂, with multilayer configuration of {PSS/PDDA}₃/{PSS/(TRITC-PLL)}₅ (red) and {PSS/PDDA}₃/{sPLA₂/(FITC-PEI)}₄/sPLA₂ (uncolored), respectively, acquired at an original microscope magnification of 400X. The patterns are 20 × 20 μm² squares separated by 80 μm, with the two material patterns offset by 30 μm in the horizontal or vertical directions. After 40 DIV, it was observed that astrocytes show preferential attachment to TRITC-PLL patterns (red) as shown in Figure 16.

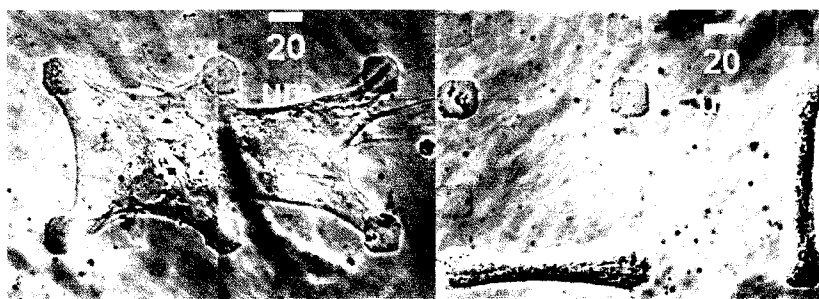


Figure 16. Tiled merged phase+TRITC images of primary brain neurons grown on {PSS/PDDA}₃/{sPLA₂/(FITC-PEI)}₄/sPLA₂ patterns (uncolored) next to {PSS/PDDA}₃/{PSS/(TRITC-PLL)}₅ patterns (red) after 40 DIV: Preferential attachment of astrocytes to PLL-terminated patterns (red).

The results shown in Figures 14 through Figure 16 indicate that the current technique could find immediate application in constructing precise co-culture systems through specifically capturing multiple cell types with defined spatial arrangements.

Recently, the cell culture conditions for optimizing the formation of neuronal processes and cell-cell networking subsequent to specific and selective adhesion of

neurons to nanofilm micropatterns have been determined. Figure 17 contains the phase and merged phase+FITC+TRITC images of 3D interdigitated multicomponent nanocomposite micropatterns of PLL and sPLA₂, with multilayer configuration of {PSS/PDDA}₃/{PSS/(TRITC-PLL)}₅ (red) and {PSS/PDDA}₃/{sPLA₂/(FITC-PEI)}₄/sPLA₂ (green), respectively, acquired at an original microscope magnification of 200X. The patterns are 20 × 20 μm² squares separated by 80 μm, with the two material patterns offset by 50 μm in the horizontal and vertical directions. As shown in Figure 17, decreasing the cell plating density and switching cells to a defined (NeuroBasal) medium promotes culture of networked cell-cell connections by 4 DIV. These results for the primary cortical neurons are similar to those shown in Figure 14, where neuronal cells attach and grow only on the sPLA₂ nanofilm patterns, even though both materials individually support neuronal adhesion when used separately.

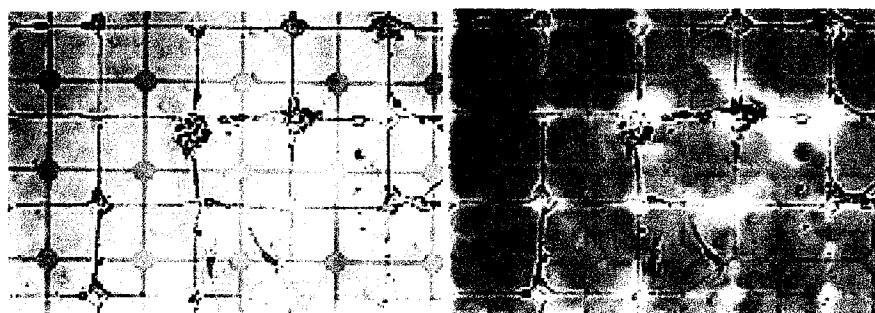


Figure 17. Phase (left) and merged phase+TRITC+FITC (right) images of primary rat cortical neurons at 4 DIV grown on {PSS/PDDA}₃/{sPLA₂/(FITC-PEI)}₄/sPLA₂ patterns (green) next to {PSS/PDDA}₃/{PSS/(TRITC-PLL)}₅ patterns (red). Neuronal cells attach and form networked cell-cell connections only on the sPLA₂ nanofilm patterns.

Calcium imaging of primary cortical neurons immobilized on the nanofilm patterns of PLL and sPLA₂ after treatment with glutamate confirmed specific neuronal associations with the sPLA₂-terminated patterns, and not PLL-terminated patterns. Figure

18 contains merged pseudocolor fluorescence+phase (inset in Figure 18(a)), merged phase+FITC+TRITC (left side images in Figure 18(b)), and merged FITC+TRITC (right side images in Figure 18(b)) images of 3D interdigitated multicomponent nanocomposite micropatterns of PLL and sPLA₂, with multilayer configuration of {PSS/PDDA}₃/{PSS/(TRITC-PLL)}₅ and {PSS/PDDA}₃/{sPLA₂/ (FITC-PEI)}₄/sPLA₂, and a plot of the quantitative fluorescence analysis of intracellular calcium dynamics for three different neurons at 7 DIV (Figure 18(a)) grown on these micropatterns.

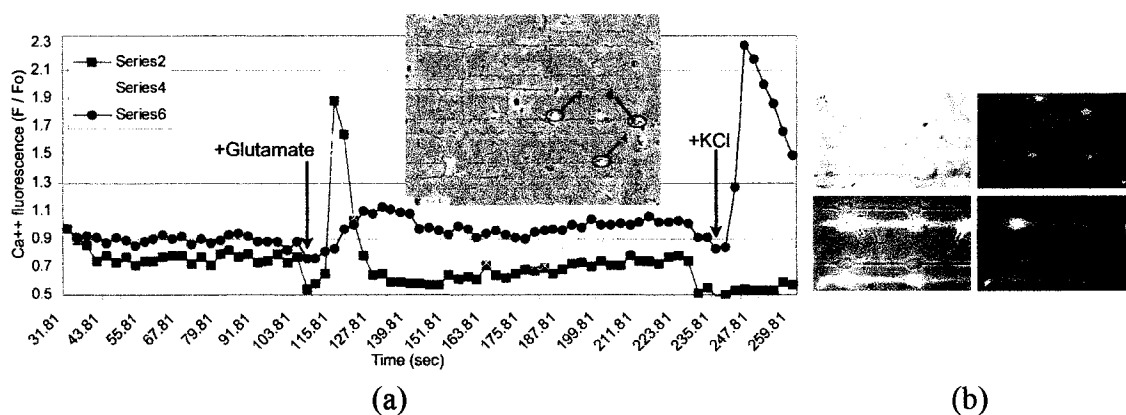


Figure 18. Primary cortical neurons at 7 DIV grown on {PSS/PDDA}₃/{sPLA₂/(FITC-PEI)}₄/sPLA₂ patterns (green) next to {PSS/PDDA}₃/{PSS/(TRITC-PLL)}₅ patterns (red), loaded with calcium indicator (Fluo-3 AM): (a) Quantitative fluorescence analysis of intracellular calcium dynamics for three neurons (marked), pseudocolor fluorescence+phase merge image of neurons after 500 μM glutamate stimulus (inset). Calcium concentrations are represented as fluorescence intensity (F) divided by baseline intensity (F₀) values for each individual cell, (b) Neurons specifically adhering to sPLA₂-terminated nanofilms post-treatment with glutamate.

As shown in Figure 18(a), the patterned neurons respond to excitatory stimuli such as glutamate, as expressed by the increase in intracellular calcium. Image analysis of cells after treatment with glutamate confirmed specific neuronal associations with the sPLA₂ patterns, and not the TRITC-PLL patterns. Figure 18(b) illustrates the neurons

after the glutamate treatment. Blebs (swollen points), a hallmark of ionic influx, and an early indicator of glutamate injury to the cells, can be seen here. Neurons appear green due to the bright fluorescence of the calcium indicator (large calcium influx after glutamate addition).

From the above observations, it can be deduced that this patterning technique may be successfully applied to the fabrication of 3D multilayer multicomponent micropatterns and may aid in studying biological or biochemical pathways. It is noteworthy that the use of acetone might be expected to cause substantial degradation of biological function for patterned molecules. However, previous observations and the current results suggest that the features of the molecules that are responsible for cell binding (e.g., those with specific interaction with cell membrane molecules) are retained through the process, at least for sPLA₂ and PLL used here and also for fibronectin and gelatin.²⁶³ Furthermore, nanofilms of glucose oxidase, for which activity assays are sensitive and straightforward, did not exhibit significant loss of activity when exposed to acetone. Thus, the nanofilm supports appear to provide a degree of anchoring and conformational stability sufficient to protect these molecules from major damage, though it is not immediately clear how general this is and what classes or sizes of molecules will exhibit similar behavior. It is also worthwhile to note that, if adhesion ligands or other molecules of interest do prove sensitive to the solvent exposure, the PSM method described here could be modified to work with these more delicate materials by implementing biocompatible photoresists and developers in the lithography processes.^{189,190,237,238}

As discussed earlier in this section, one explanation for the specific binding behavior of the neuron cells to sPLA₂ is the nanoscale film thickness of the composite

nanofilm patterns, where the sPLA₂ composite nanofilm patterns were thinner in the z-axis than the PLL patterns, as shown schematically in Figure 11(d) and Figure 12. The following section presents the studies performed to investigate the contribution of surface topographical cues towards the specific binding of neuron cells to sPLA₂.

4.4.2 Two-Component Patterns of Varying Heights: Effect on Cell Adhesion

Five different types of micropattern systems that could be placed under three different categories were fabricated using the PSM method to evaluate the dependence of nanofilm thickness on neuronal adhesion. The three categories were sPLA₂ micropatterns taller than PLL patterns, PLL patterns taller than sPLA₂ patterns, and PLL and sPLA₂ micropatterns of same heights. In the category with sPLA₂ patterns taller than PLL patterns, three different types of micropatterns were constructed. Type I system contained 3D interdigitated multicomponent nanocomposite micropatterns of PLL and sPLA₂, with multilayer configuration of {PSS/PDDA}₈/sPLA₂/FITC-PEI₄/sPLA₂ (~125 nm) and {PSS/PDDA}₃/PSS/PLL₅ (~68 nm). Type II system contained micropatterns with multilayer configuration of {PSS/PDDA}₈/sPLA₂/FITC-PEI₄/sPLA₂ (~125 nm) and {PSS/PDDA}₂/PSS/PLL₁ (~16 nm). Type III system contained micropatterns with multilayer configuration of {PSS/PDDA}₃/sPLA₂/FITC-PEI₄/sPLA₂ (~25 nm) and {PSS/PDDA}₂/PSS/PLL₁ (~16 nm). Type IV system under the category with PLL micropatterns taller than sPLA₂ patterns contained micropatterns with multilayer configurations of {PSS/PDDA}₃/sPLA₂/FITC-PEI₄/sPLA₂ (~25 nm) and {PSS/PDDA}₃/PSS/PLL₅ (~68 nm). Type V system under the category with PLL and sPLA₂ patterns of same heights contained micropatterns with multilayer configurations of

$\{\text{PSS/PDDA}\}_3/\{\text{sPLA}_2/\text{FITC-PEI}\}_4/\text{sPLA}_2$ (~ 25 nm) and $\{\text{PSS/PDDA}\}_3/\{\text{PSS/PLL}\}_1$ (~ 28 nm). In order to be able to compare the cell response to these micropattern systems to those tested in previous section, at least one of the material on the different types of micropattern systems fabricated had a multilayer architecture used in the micropatterns used in previous section.

4.4.2.1 Phase contrast microscopy

Figure 19 contains phase contrast images of the 3D interdigitated two-component multicomponent nanocomposite micropatterns with varying heights of sPLA₂ and PLL nanofilms. Figures 19(a), 19(b), and 19(c) are images of 20 μm interdigitated square patterns with an offset of 50 μm in both vertical and horizontal direction, corresponding to micropattern systems of type I, type II, and type III, respectively. In Figure 19(a) and 19(b), the sPLA₂ patterns were estimated to be 125 nm thick and the PLL patterns were estimated to be ~ 68 nm and ~ 16 nm, respectively. This difference in heights of the patterns of the two materials can be clearly seen by the contrast of the thicker nanofilms patterns that appear darker in comparison to the thinner nanofilms patterns that appear brighter. Figure 19(d) is an image of similarly interdigitated patterns corresponding to the micropattern system of type IV. Here again it can be seen that there is a clear contrast between the ~ 68 nm tall PLL patterns that appear darker in comparison to the ~ 25 nm sPLA₂ patterns that appear brighter. Figure 19(e) is an image of similarly interdigitated patterns corresponding to the micropattern system of type V. In this type, the PLL and sPLA₂ patterns approximately of the same heights (~ 25 nm) appear to have same contrast. These images prove that the current patterning technique provides the capability of constructing 3D interdigitated multicomponent nanocomposite micropatterns with

desired multilayer architectures, thereby controlling the 3D topographical surfaces on *in vitro* cell culture substrates.

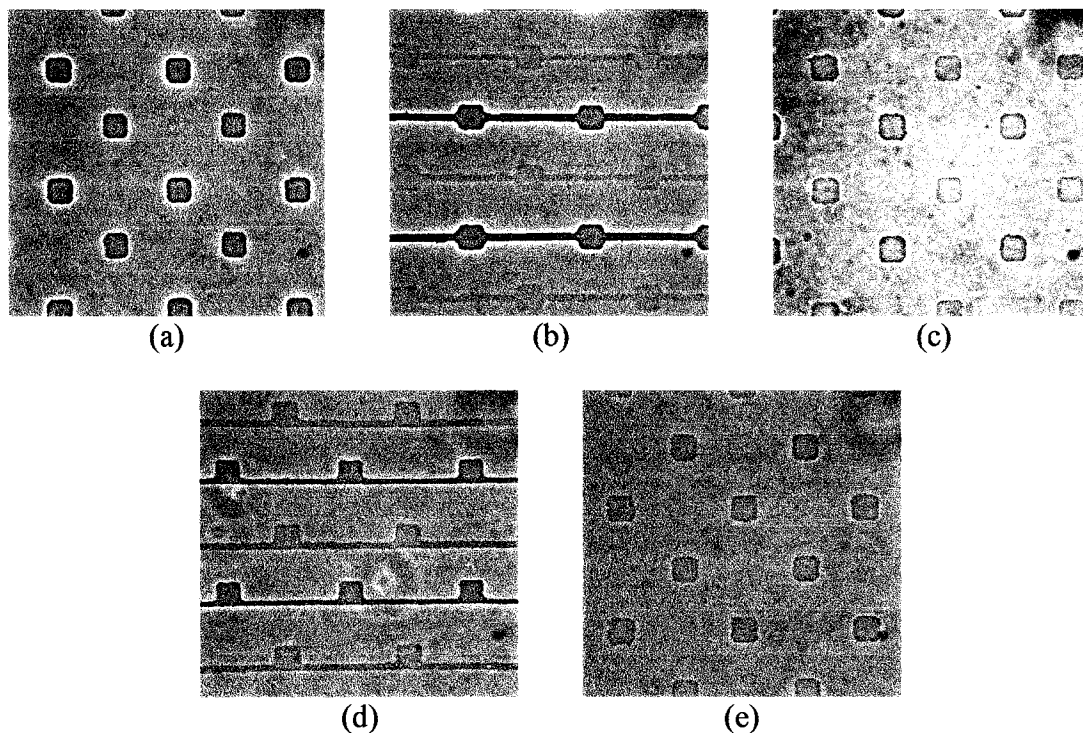


Figure 19. 3D interdigitated multicomponent micropatterns of varying heights of sPLA₂ and PLL nanofilms: Images of 20 μm patterns (40X) with the second component offset by 50 μm in vertical and horizontal direction: (a)-(c) sPLA₂ micropatterns taller than PLL patterns (type I, II, III), (d) PLL patterns taller than sPLA₂ patterns (type IV), and (e) PLL and sPLA₂ micropatterns of same heights (type V).

4.4.2.2 Surface profiler measurements

The average thicknesses of the different multilayer architectures used to build the five different types of micropattern systems, measured using a surface profilometer, are shown in Table 1. The measured thicknesses of the different architectures closely match the expected thicknesses for each of type of the micropattern system. Since these average thickness values were calculated based on different substrates, the standard deviations

indicate that the variability of thicknesses ($\sim 2.8\%$, $\sim 4.5\%$, $\sim 4.3\%$, $\sim 11\%$, and $\sim 8.4\%$ from top to bottom in the table, respectively) from substrate to substrate is very low. The profilometry results indicate the successful precision engineering of the 3D interdigitated multicomponent micropatterns of varying heights of sPLA₂ and PLL nanofilms using the PSM method.

Table 1. Average thicknesses of the different multilayer architectures used in building the five different types of micropattern systems measured using a surface profilometer.

Multilayer Architecture	Average Thickness (nm)
{PSS/PDDA} ₈ / {sPLA ₂ /FITC-PEI} ₄ sPLA ₂	123.75 ± 3.45
{PSS/PDDA} ₃ / {sPLA ₂ /FITC-PEI} ₄ sPLA ₂	22.92 ± 1.02
{PSS/PDDA} ₃ / {PSS/PLL} ₅	70.83 ± 3.03
{PSS/PDDA} ₃ / {PSS/PLL} ₁	25.0 ± 2.74
{PSS/PDDA} ₂ / {PSS/PLL} ₁	12.08 ± 1.02

4.4.2.3 AFM measurements

The average roughnesses of the surfaces of the different multilayer architectures used to build the five different types of micropattern systems, measured using an atomic force microscope, are shown in Table 2. The roughness values indicate that the thicker PLL and sPLA₂ multilayer architectures are smoother than their thinner counter-parts. Also, the standard deviations indicate that the variability of roughness ($\sim 36.5\%$, $\sim 37.3\%$, $\sim 11.1\%$, $\sim 24.1\%$, and $\sim 37.9\%$ from top to bottom in the table, respectively) for thicker PLL and sPLA₂ multilayer architectures is lower compared with their thinner counter-parts. The AFM results indicate the roughness of the nanofilm surfaces could also be finely tuned using the PSM method.

Table 2. Average roughnesses of the surfaces of the different multilayer architectures used in building the five different types of micropattern systems measured using an AFM.

Multilayer Architecture	Average Roughness (nm)
{PSS/PDDA} ₈ / {sPLA ₂ /FITC-PEI} ₄ sPLA ₂	8.30 ± 3.03
{PSS/PDDA} ₃ / {sPLA ₂ /FITC-PEI} ₄ sPLA ₂	8.66 ± 3.23
{PSS/PDDA} ₃ / {PSS/PLL} ₅	5.05 ± 0.56
{PSS/PDDA} ₃ / {PSS/PLL} ₁	7.51 ± 1.81
{PSS/PDDA} ₂ / {PSS/PLL} ₁	10.49 ± 3.97

4.4.2.4 Cell culture results

In the case of the type IV micropattern systems [PLL (~70.83 nm) taller than sPLA₂ (~22.92 nm)], preferential attachment of neurons to sPLA₂-terminated nanofilm patterns was observed, with no attachment on PLL. Neurons formed long processes, primarily on and parallel to the 5 μm stripe patterns. Staining for the neuronal marker MAP-2 showed absolute preference for sPLA₂, with MAP-2 positive staining along the sPLA₂ stripe patterns.

In contrast, for the type I micropattern systems [sPLA₂ (~123.75 nm) taller than PLL (~70.83 nm)], cell patterning was observed on both sPLA₂ and PLL-terminated nanofilm patterns; processes were connecting laterally as well as parallel to (and on) the stripes. Staining for the neuronal marker microtubule-associated protein-2 (MAP-2) showed that cells still appear to prefer the sPLA₂, but send out many fine processes (MAP-2 positive). These preliminary cell culture findings indeed suggest a dependence of the binding behavior on the nanoscale film thickness. The inherent ability of the PSM method to accommodate different surface chemistries and finely tune the topographies will be highly useful in presenting varying physical and chemical cues to influence cell

growth. Whether the observations are truly height-dependent, or are also influenced by the substrate stiffness of the substrate, which also varies with film height, is another question to be answered in future.

From the preceding sections, it is clear that PSM method can potentially be used to tune the surface chemical and topographical cues. The following sections present more complex examples of microstructures constructed using PSM method.

4.4.3 Two-Component Pattern-on-Pattern Systems

The PSM method was also applied to construct two-component pattern-on-pattern micropattern systems. These systems could be used to create additional complexity in the 3D interdigitated multicomponent nanocomposite micropatterns.

4.4.3.1 Fluorescence and phase contrast microscopy

Figure 20 contains TRITC, FITC, and merged FITC+TRITC fluorescence, and phase contrast images of pattern-on-pattern systems constructed using PSM method. Figure 20(a) is an image of horizontally oriented stripe patterns with a multilayer architecture of $\{\text{PSS/TRITC-PAH}\}/\{\text{PSS/PDDA}\}_3/\{\text{PSS/PLL}\}_5$ collected through a TRITC cube. Figure 20(b) is an image of vertically oriented stripe patterns with a multilayer architecture of $\{\text{PSS/FITC-PAH}\}/\{\text{PSS/PDDA}\}_3/\{\text{PSS/PDL}\}_5$ collected through a FITC cube. The image in Figure 20(c) is an overlay of images in Figure 20(a) and (b), clearly depicting the FITC-labeled stripe patterned perpendicularly on top of TRITC-labeled stripe patterns. Figure 20(d) is a phase contrast image of pattern-on-pattern system with stripe micropatterns of multilayer architectures $\{\text{PSS/PDDA}\}_3/\{\text{PSS/Cy5-PAH}\}_5$ patterned perpendicularly on top of stripe micropatterns

of multilayer architectures $\{\text{PSS/PDDA}\}_3/\{\text{PSS/TRITC-PAH}\}_5$. The stripe micropatterns are $50\ \mu\text{m}$ wide and separated by a distance of $50\ \mu\text{m}$. These images prove that the current patterning technique provides the capability to create micropatterns in the desired spatial configurations.

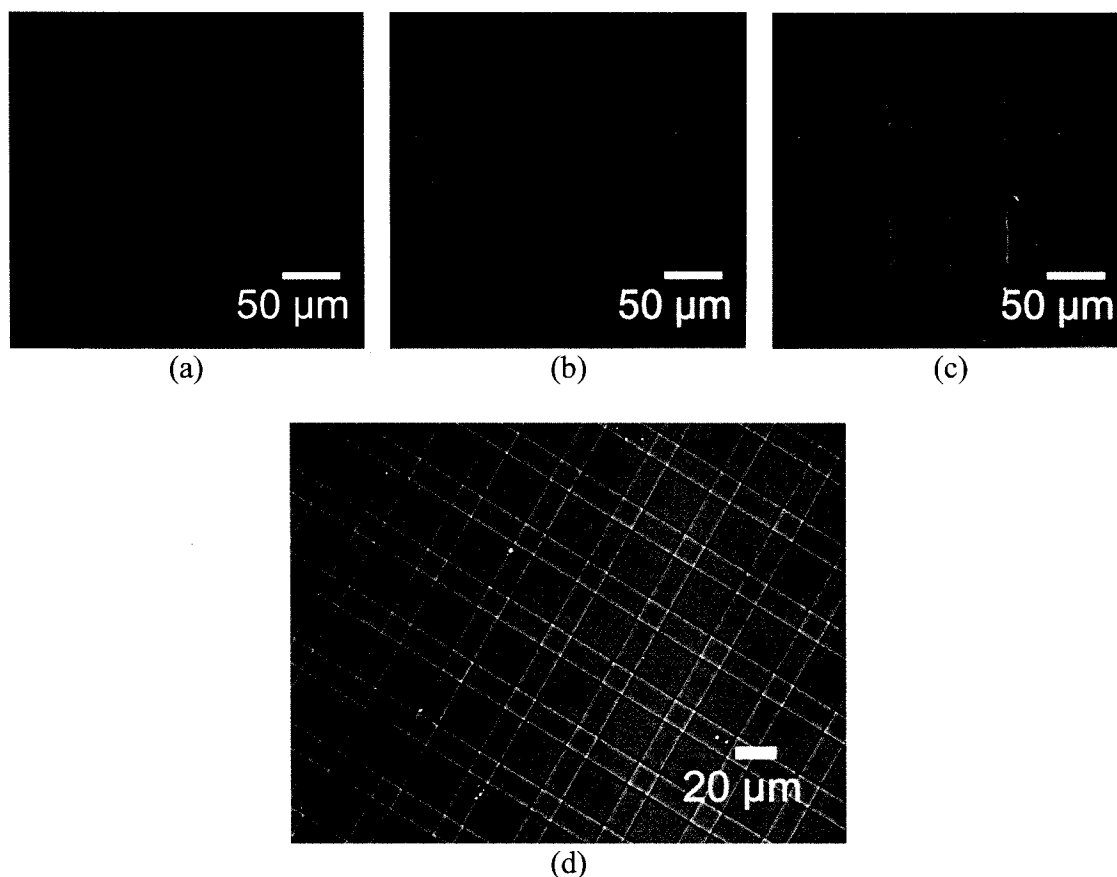


Figure 20. Two-component pattern-on-pattern systems: Images of $50\ \mu\text{m}$ stripe patterns with multilayer architectures of $\{\text{PSS/TRITC-PAH}\}/\{\text{PSS/PDDA}\}_3/\{\text{PSS/PLL}\}_5$ and $\{\text{PSS/FITC-PAH}\}/\{\text{PSS/PDDA}\}_3/\{\text{PSS/PDL}\}_5$ collected (40X) through (a) TRITC cube, (b) FITC cube, and (c) overlay of images in (a) and (b); (d) phase contrast image of stripe patterns with multilayer architectures of $\{\text{PSS/PDDA}\}_3/\{\text{PSS/Cy5-PAH}\}_5$ and $\{\text{PSS/PDDA}\}_3/\{\text{PSS/TRITC-PAH}\}_5$.

4.4.3.2 AFM measurements

Figure 21 contains an AFM micrograph of a two-component pattern-on-pattern system. The micrograph shows the region of intersection of the stripe micropatterns of multilayer architectures $\{\text{PSS/PDDA}\}_3/\{\text{PSS/Cy5-PAH}\}_5$ patterned perpendicularly on top of stripe micropatterns of multilayer architectures $\{\text{PSS/PDDA}\}_3/\{\text{PSS/TRITC-PAH}\}_5$. The stripe micropatterns are $50\ \mu\text{m}$ wide. The average thickness of the stripe patterns is $24.9 \pm 1.45\ \text{nm}$ ($\sim 5.82\%$ variation). The average thickness of the intersection region of the stripe patterns is $39.23 \pm 1.41\ \text{nm}$ (3.6% variation). The thickness of the intersection regions is expected to be double the thickness of the individual stripe patterns, which is $\sim 50\ \text{nm}$. It appears that there is loss of nanofilms in the intersection regions that might have been caused due to the fabrication process. Nevertheless, the above results for the pattern-on-pattern systems prove that the PSM method provides the capability to create complex 3D micropatterns in the desired spatial configurations. More complex microstructures are presented in the following section.

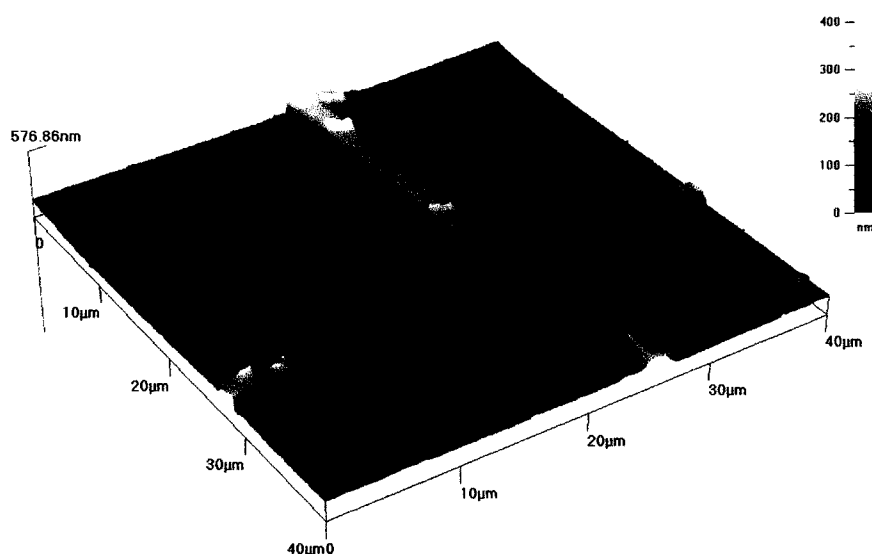


Figure 21. AFM micrograph of two-component pattern-on-pattern system: $50\ \mu\text{m}$ stripe patterns with multilayer architectures of $\{\text{PSS/PDDA}\}_3/\{\text{PSS/Cy5-PAH}\}_5$ and $\{\text{PSS/PDDA}\}_3/\{\text{PSS/TRITC-PAH}\}_5$.

4.4.4 Four-Component Patterns

To demonstrate the ability of the PSM method to fabricate more complex systems, patterns of four different components were fabricated on the same substrate.

4.4.4.1 Fluorescence microscopy

Micropatterns of the four different components had a multilayer configuration of $\{\text{PSS/PDDA}\}_3/\{\text{PSS}/(\text{Cy5-PAH})\}_5$ (blue squares), $\{\text{PSS/PDDA}\}_3/\{\text{PSS}/(\text{TRITC-PLL})\}_5$ (light red squares), $\{\text{PSS/PDDA}\}_3/\{\text{PSS}/(\text{FITC-PEI})\}_5$ (green squares), and $\{\text{PSS/PDDA}\}_3/\{\text{PSS}/(\text{Texas Red-PAH})\}_5$ (bright red squares). Figure 22 contains the sequential Cy5-FITC-TRITC (TRITC=wide emission bandwidth, allowing simultaneous Texas Red and TRITC imaging) scanning confocal images obtained using a CLSM. Figure 22(a) contains the individual sequential scanning images for Cy5, FITC, and TRITC, along with the overlay image, imaged at an optical magnification of 10X. Figure 22(b) contains the overlay image of similarly imaged sequential scanning images at an optical magnification of 63X. Figure 22(c) contains the overlay image of digitally zoomed sequential scanning images. Finally, Figure 22(d) is a graph of average intensities for lines across the square patterns, which gives an indication of the homogeneity of the fluorescence.

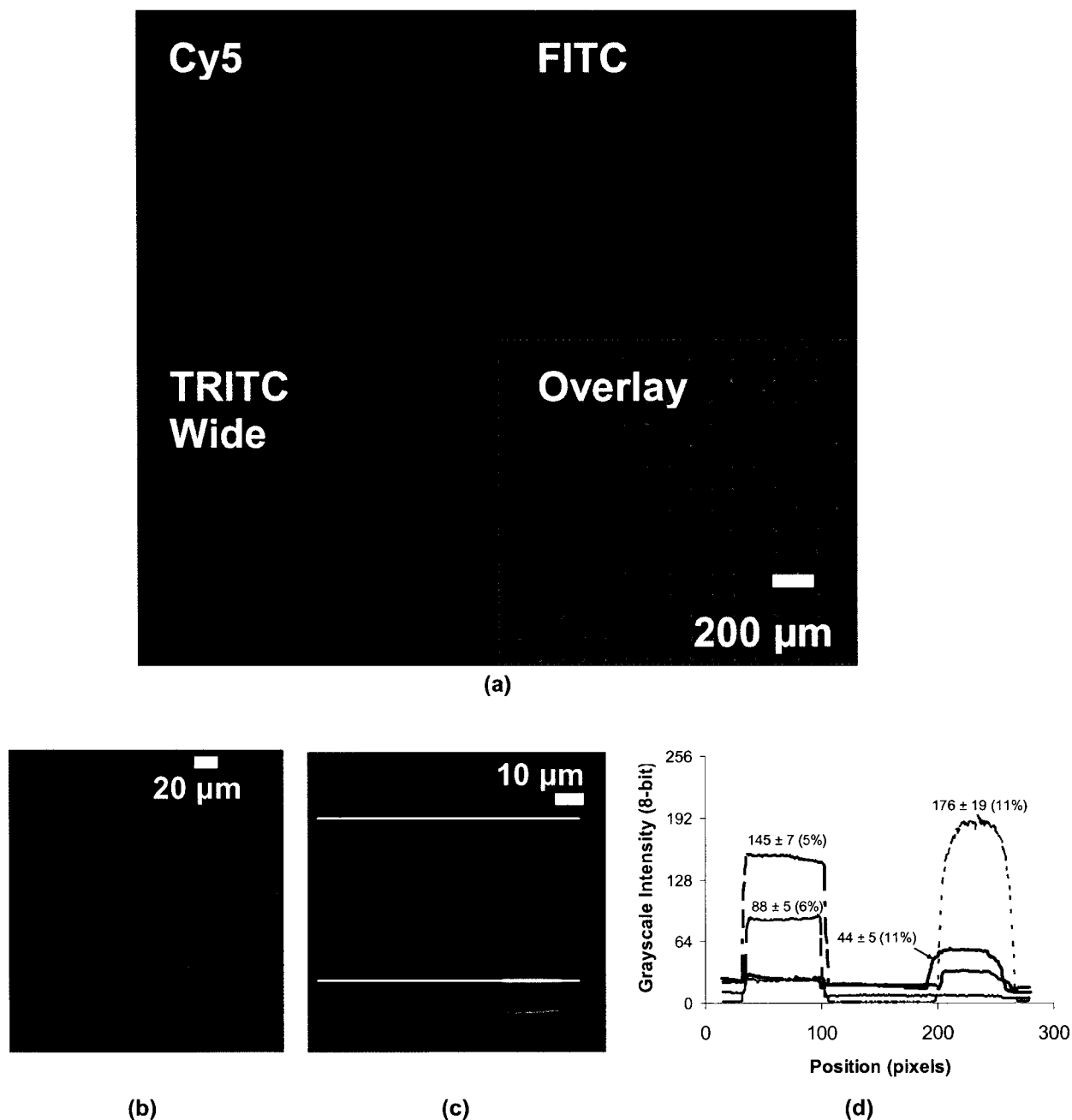


Figure 22. (a) Sequential Cy5-FITC-TRITC scanning CLSM images and overlay image at 10X, (b) Overlay image at 63X, (c) Digitally zoomed overlay image showing one pattern each for the four-component patterns: Blue- $\{PSS/PDDA\}_3/\{PSS/(Cy5-PAH)\}_5$, Light red- $\{PSS/PDDA\}_3/\{PSS/(TRITC-PLL)\}_5$, Green- $\{PSS/PDDA\}_3/\{PSS/(FITC-PEI)\}_5$, and Bright red: $\{PSS/PDDA\}_3/\{PSS/(Texas Red-PAH)\}_5$; (d) Linescan intensity data for image in (c), before processing: Blue long dash-Cy5, Red-TRITC, Maroon dash-dot-Texas Red, Green short dash-FITC.

These images clearly illustrate the aligned micropatterns of four different components. The fluorescence intensities of the nanocomposite patterns are uniform within a pattern as well as over a large area on the substrate, indicating that the biomaterials were deposited uniformly. The fluorescence homogeneity was quantified by calculating average and standard deviation of intensity for 50×50 pixel square regions within the square patterns before image processing, and was found to be ~5% for the brighter Cy5 and Texas Red patterns and ~11% for the TRITC and FITC patterns.

From Figure 22(a), it can be seen that the four components are well aligned over a large area, and there is no obvious cross-contamination of fluorescence, indicating that even though the current technique involves repetition of lithography, LbL assembly, and lift-off processes, the different biomaterials are confined to the patterned regions in which they are deposited. Overall, these images prove the ability of the PSM method to fabricate aligned multilayer multicomponent patterns.

4.5 Conclusions

A simple yet versatile and precise patterning technique to fabricate 3D multilayer multicomponent heterostructures of bioactive coatings on a single substrate has been demonstrated. This method is analogous to surface micromachining, except that the deposition materials are polymers and biological materials that are used to produce multilayer nanocomposite structures. The fabrication results, metrology results, and the initial results from the biological studies on the multicomponent micropatterns prove the success and usefulness of the method. The ability to obtain multicomponent heterostructures with great precision and simplicity overcomes some of the constraints of existing techniques, and the process can be easily integrated into existing automated

systems used for lithography and LbL assembly. The metrology results indicate that nanocomposite micropatterns with varying physical and chemical cues could be easily integrated into scaffolds using the current technique.

The cell-culture results indicate that the lithographic processes undertaken during this technique have minimal or no deleterious effects on the biological model being tested. The metrology and cell-culture results for the two-component nanocomposite micropatterns and the fabrication results for the four-component nanocomposite micropatterns together prove the importance of the immediate applicability of the current technique towards studying cell-biomaterial interactions in a whole new fashion. The current technique could play an important role in stem cell research, as a tool to understand biochemical pathways of proliferation, migration, and differentiation under different physicochemical conditions, since stem cells demonstrate plasticity dependent on their environment.¹⁵³⁻¹⁵⁷ Also, defined spatial arrangements of anchorage-dependent cells could create a high level of complexity in co-cultures and could be used as a tool for analyzing stem cell behavior under various bio-physicochemical conditions.^{146,162,164} Time-varying signals could also be easily presented to the cells by integrating biodegradable materials into the multilayer assembly process,¹⁰⁴⁻¹⁰⁷ thereby dynamically influencing the cell behavior.

Although the intended purpose for developing 3D multilayer multicomponent micropatterns is to produce novel bioactive systems, their applicability is more general and may find use in a broad range of applications including electronics, photonics, optoelectronics, and chemical and biochemical sensors. The description of how the PSM

method was extended to deposition of adjacent, overlapping, and/or interdigitated patterns of colloidal nanoparticles has been presented in the next chapter.

CHAPTER 5

MULTICOMPONENT NANOPARTICLE PATTERNING: COLLOIDAL SURFACE MICROMACHINING

5.1 Introduction

It is clear from previous chapters that PSM is a versatile method to construct micropatterns of different biomaterials with precise micro- and nanoscale features and defined spatial arrangement on a single. In Chapters 3 and 4, 3D multilayer multicomponent micropatterns of biologically relevant polymers in various spatial configurations were presented, and used as cell culture scaffolds, demonstrating interesting biological phenomena that could be controlled using precise nanoscale engineering. Recent reports have used non-biological nanomaterials to study their interactions with cells.^{127,128,271-274} These non-biological nanomaterials, such as nanoparticles or nanotubes, could potentially be used to incorporate additional complexity and ability to tune the physical properties into the 3D multilayer multicomponent micropatterns, as depicted in Figure 1. This chapter describes how the PSM method was extended to the deposition of adjacent, overlapping, and/or interdigitated patterns of colloidal nanoparticles; the technique termed as Colloidal Surface Micromachining (CSM).

The CSM method used in this chapter is analogous to surface micromachining, except that the deposition materials are polymers and colloidal nanoparticles that are used to produce multilayer nanocomposite structures. Two- and four-component systems on silicon substrates are presented to demonstrate the versatility of the approach to construct precisely-defined, homogeneous nanofilm patterns whose nanotopographies depend on the size of the colloids employed.

The nanoparticle micropatterns were characterized using brightfield microscopy and scanning electron microscopy to assess the spatial registration of the multiple components, surface profilometry and atomic force microscopy to obtain height information for the patterns, and ellipsometry to obtain thickness information for non-patterned multilayer nanofilms. The metrology results indicate that nanocomposite micropatterns with varying physical and chemical cues could be easily integrated into scaffolds using the current technique.

5.2 Materials

5.2.1 Substrates

Silicon wafers (<100>) purchased from Silicon Inc., were used as the substrates.

5.2.2 Chemicals

Nano-StripTM was purchased from CYANTEK Corporation. Silica nanoparticles (SiO₂ NP) of diameter 11-14 nm (pH 9.6, 20.4 wt%), 20 nm (pH 9.2, 47.6 wt%), 45 nm (pH 9.6, 10 wt%), and 78 nm (pH 9.6, 40.4 wt%) were purchased from SNOWTEX, Nissan Chemical Industries, Ltd. Poly(diallyldimethylammonium chloride) (Mw ~100-200 kDa), poly(sodium 4-styrenesulfonate) (Mw ~1 MDa), and poly(ethyleneimine) (Mw ~750 kDa) were purchased from Sigma-Aldrich. Positive photoresist, S1813, and positive

resist developer, MF-319, were obtained from Shipley. All chemicals of commercial origin were used as received.

5.2.3 Preparation of Polyelectrolyte and Nanoparticle Solutions

Solutions of PDDA, PAH, and PSS with concentration of 2 mg mL^{-1} with 0.5 M KCl and a solution of 2 mg mL^{-1} PEI were prepared in DI H_2O for use in self-assembly. Solutions of the different SiO_2 NPs were prepared by diluting 1 mL of the original colloidal solution in 50 mL of DI H_2O .

5.3 Methods

5.3.1 Mask Design

For the two-component micropattern systems, one of the masks used for pattern transfer contained $50 \text{ }\mu\text{m}$ wide stripe patterns separated by $50 \text{ }\mu\text{m}$, while the other mask contained $20 \text{ }\mu\text{m}$ square patterns separated from each other by a distance of $80 \text{ }\mu\text{m}$, in horizontal as well as vertical directions. For the four-component systems, the mask used for the four-component polymer patterns in Chapter 4 was used for the pattern transfer.

5.3.2 Fabrication

The cartoon in Figure 23 depicts the general fabrication process flow used in this work. The first step in the fabrication was the treatment of the substrates with NanoStrip™ followed by the deposition of the PDDA precursor layer. The next step was the patterning of substrates using S1813. The patterned substrates were then modified using LbL self-assembly with the desired multilayer configuration. Lift-off was performed on the substrates to obtain the first set of multilayer patterns. This procedure was repeated to

obtain the second set of multilayer patterns, and could be repeated as necessary to deposit additional nanofilm patterns on the same substrate.

5.3.2.1 Substrate pretreatment

Substrates were incubated in Nano-Strip™ at 70 °C for 1 hr to remove organic contaminants and create a uniform negative charge on the substrates, then they were rinsed in DI water and dried using N₂. A set of alignment marks were deposited on the substrates using standard lithography, metal sputtering (10nm Au-Pd), and lift-off processes. A precursor layer of PDDA or PEI was then deposited on the negatively-charged substrates by incubating in PDDA for 20 min, rinsing in DI water, and finally drying in nitrogen.

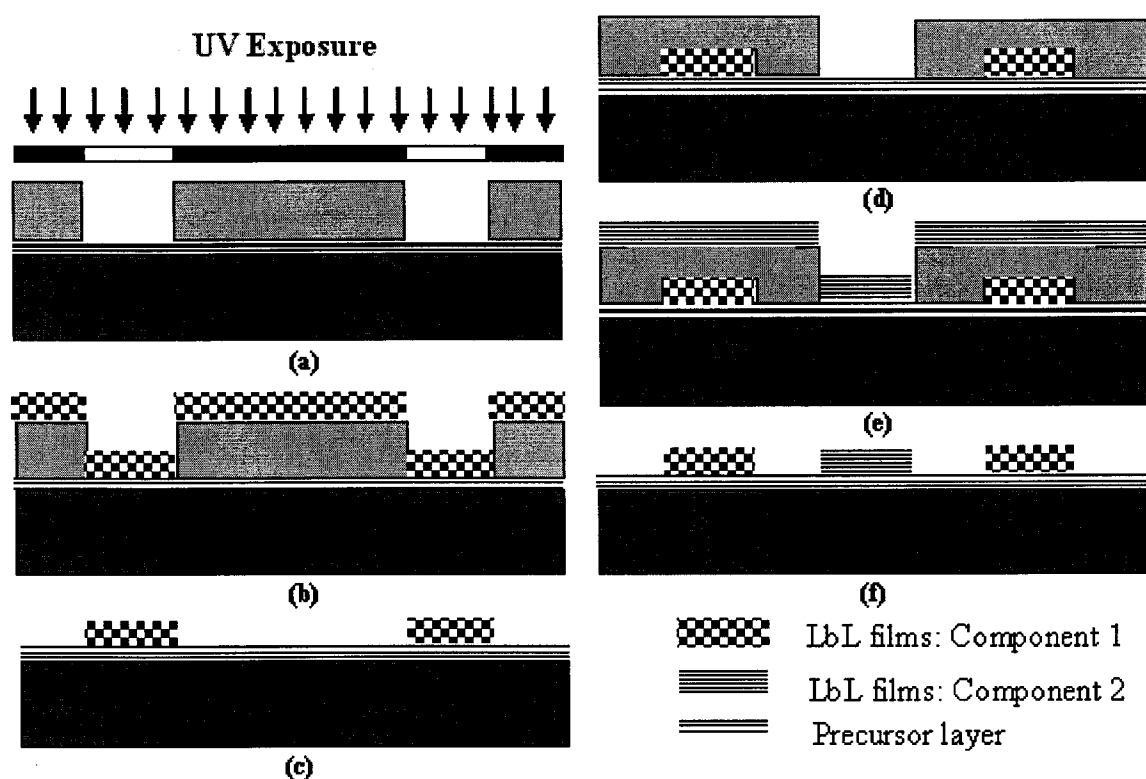


Figure 23. General template used for the CSM method (a) Photolithography of pretreated substrate, (b) LbL deposition of component 1, (c) After first lift-off, (d) Second photolithography step, (e) LbL deposition of component 2, (f) After second lift-off.

5.3.2.2 Photolithography

Photoresist S1813 was spun on the substrates (1,000 rpm - 100 r s^{-1} - 10 s, 3,000 rpm or 2,000 rpm - 500 r s^{-1} - 50 s), soft baked at $115 \text{ }^\circ\text{C}$ for 1 min, and photo-patterned using UV radiation (365/405 nm, 7 mW cm^{-2}) for 15 s. Patterns were developed for 20 s, substrates rinsed in DI water, and dried using N_2 .

5.3.2.3 Layer-by-layer self-assembly

For all the LbL assembly processes, a basement multilayer configuration of $\{\text{PSS/PDDA}\}_3$ was deposited on the patterned substrates through immersion in the PSS or PDDA solutions for 10 min, rinsing in DI water, and finally drying in N_2 or a spinner (1,000 rpm). This precursor multilayer deposition is an important step to attain a uniformly charged surface for subsequently deposited layers.²⁷⁵ The process of rinsing in DI water and drying in N_2 was repeated after each deposition step throughout the LbL assembly process, since it was found to help to obtain undistorted multilayer patterns in the final development stage.

After the first set of lithography processes and the LbL assembly of precursor layers, a nanofilm architecture of $\{\text{SiO}_2 \text{ NP/PDDA}\}_5$ was deposited on top of the patterned substrates with pre-existing $\{\text{PSS/PDDA}\}_3$ films. This step was accomplished through deposition of five bilayers of $\text{SiO}_2 \text{ NP/PDDA}$ by alternate exposure of substrates to negatively-charged $\text{SiO}_2 \text{ NPs}$ and positively-charged PDDA solutions. The substrates were immersed in $\text{SiO}_2 \text{ NP}$ and PDDA for 10 min, rinsed in DI water, and finally dried in N_2 or using a spinner (500 rpm - 50 r s^{-1} - 10 s, 1,000 rpm - 50 r s^{-1} - 30 s).

5.3.2.4 Lift-off

The lift-off process was performed by sonicating the substrates in acetone for 1-2 min to obtain the first set of patterns. The sonicator was filled with acetone and the substrates immersed directly into the acetone. As expected, due to the high level of porosity in the nanoparticle nanofilms, the sonication time for the nanoparticle patterns is less than that required for the polymer micropatterns presented in Chapter 4.

5.3.2.5 Multicomponent patterning

A second lithography process was performed on the substrates, this time with a set of patterns aligned with the first set of patterns using previously patterned alignment marks, and a multilayer configuration of $\{\text{SiO}_2 \text{ NP/PDDA}\}_5$ (for two-component and four-component patterns using a different size of SiO_2 NPs) or $\{\text{PSS/PDDA}\}_5$ (two-component hybrid patterns) was deposited in a procedure similar to that used earlier. For two-component patterns, the square patterns were offset by a distance of 15 μm from the long edge of the stripe patterns. For the four-component patterns, the square patterns were offset from each other by a distance of 30 μm .

5.3.3 Characterization

5.3.3.1 Brightfield microscopy

Brightfield microscopy was used for imaging the resulting multicomponent nanoparticle micropatterns to demonstrate successful multicomponent patterning and to assess the uniformity and spatial registration using an optical microscope (Olympus Vanox AHMT3) equipped with a UNIQ Vision Inc. CCD camera (UC-930CL). The microscopy was performed at different magnifications to assess the spatial registration over a large area as well as to capture the details on individual micropatterns.

5.3.3.2 Surface profilometry

Surface profilometry was used for assessment of the topographical differences of the multicomponent micropatterns. The surface profiler (KLA-Tencor, Model-Alpha-Step IQ) was used to collect line scan structural data of the patterns on three different substrates. The vertical dimensions of the patterns were obtained directly from the line scan measurements. Final height values were based on an average of three measurements. The scan parameters used were as follows: stylus force of 20 mg, scan length of 200 μm , scan speed of 20 $\mu\text{m s}^{-1}$, and sampling rate of 50 Hz.

5.3.3.3 Atomic force microscopy

AFM measurements were made to further verify the faithfulness of the pattern transfer using the current fabrication process and to analyze the finer physical features of the patterns. The AFM (Quesant, Model-Q-Scope250) was used in tapping mode with silicon cantilevers to collect area scan data from the patterns. The lateral and vertical dimensions of the patterns were obtained from these measurements. The parameters used for the measurements were: scan area $40 \times 40 \mu\text{m}^2$ for thickness measurements and $10 \times 10 \mu\text{m}^2$ for roughness measurements, scanning rate of 3 Hz, and a resolution of 600 lines. The average roughness data was obtained directly from the area scan measurements.

5.3.3.4 Ellipsometry

A spectroscopic ellipsometer (SENTECH, Model-SE 850) was used to measure the thicknesses of non-patterned PSS/PDDA and SiO_2 NP/PDDA multilayers on silicon wafers. The measurements were performed at an incidence angle of 70° and the 250-850 nm spectral range was used. A refractive index of $n_0=1.5$ for a Cauchy layer type was assumed for thickness calculations using the SPECTRARAY software for the PSS,

PDDA, and PEI nanofilms. For the SiO₂ NP nanofilms, a refractive index of $n_0=1.456$ for a Cauchy layer type was assumed. The ellipsometric measurements were made at three different positions on the substrates after the deposition of each new layer, followed by the estimation of the average thickness of the newly deposited layer depending on the estimated thickness of the previously deposited layers.

5.3.3.5 Scanning electron microscopy

Scanning electron microscopy was performed to demonstrate the alignment and differences in heights of the multicomponent micropatterns over a large area on the substrate. A scanning electron microscope (AMRAY, Model-1830) was used to obtain grayscale micrographs of the multicomponent patterns. An acceleration potential of 5-20 KV was used at different magnifications. Before performing the microscopy, the substrates were sputter-coated with 1 nm of Au-Pd to avoid charging of the substrates during microscopy.

5.4 Results and Discussion

For each of the following sub-sections, the results for the fabrication of nanoparticle micropatterns using two different fabrication conditions have been presented. Condition I constitutes deposition of PDDA as the initial precursor layer on the substrate, spin-coating of the photoresist at 2,000 rpm, use of {PSS/PDDA}₅ as precursor layers during the LbL assembly, and use of N₂ drying during the deposition of nanoparticle nanofilms. Condition II constitutes deposition of PEI as the initial precursor layer on the substrate, spin-coating of the photoresist at 3,000 rpm, use of {PSS/PDDA}₃ as precursor layers during the LbL assembly, and use of spin drying during the deposition of nanoparticle nanofilms. The choice of PDDA as the initial precursor layer was based

on previous studies presented in Chapters 3 and 4, whereas the choice of PEI was based on previous work by Cui et al.¹²² The choice of 3,000 rpm for resist spinning was based on previous studies presented in Chapters 3 and 4, whereas the choice of 2,000 rpm was made in order to test the effect of resist thickness on pattern quality; reduced spinning speed results in increased resist thickness. Similarly, multilayer architectures of $\{\text{PSS/PDDA}\}_3$ was chosen as precursor layers during the LbL assembly based on previous studies presented in Chapters 3 and 4, and $\{\text{PSS/PDDA}\}_5$ was chosen to test the effect of precursor layers on the pattern quality. However, there was no specific reason for choosing these particular combinations for the two test conditions.

5.4.1 Two-Component Patterns

5.4.1.1 Brightfield microscopy

Figure 24 contains brightfield images of two-component nanocomposite nanoparticle-on-nanoparticle (NP-on-NP) micropatterns acquired at a magnification of 50X. The stripe patterns are 50 μm wide and the square patterns have sides of 20 μm . Figure 24(a) is an image of NP-on-NP patterns fabricated under Condition I. The stripe patterns have a multilayer architecture of $\{\text{PSS/PDDA}\}_5/\{45 \text{ nm SiO}_2 \text{ NP/PDDA}\}_5$ and the square patterns patterned on top of the stripe patterns have an architecture of $\{\text{PSS/PDDA}\}_5/\{11\text{-}14 \text{ nm SiO}_2 \text{ NP/PDDA}\}_5$. Figure 24(b) is an image of NP-on-NP patterns fabricated under Condition II. The stripe patterns have a multilayer architecture of $\{\text{PSS/PDDA}\}_3/\{11\text{-}14 \text{ nm SiO}_2 \text{ NP/PDDA}\}_5$ and the square patterns patterned on top of the stripe patterns have an architecture of $\{\text{PSS/PDDA}\}_3/\{45 \text{ nm SiO}_2 \text{ NP/PDDA}\}_5$. From Figure 24(a) it is clear that when nanofilms of small size NPs are deposited on nanofilms of large size NPs, the roughness of the latter nanofilms propagates into the

former nanofilms. Also, it appears from Figure 24(b) that Condition II results in better line-edge definition of the stripe patterns. The reason for this better edge definition could be the initial precursor layer, smaller size of the nanoparticles, the spin drying, number of precursor layers, or a combination of any of these.

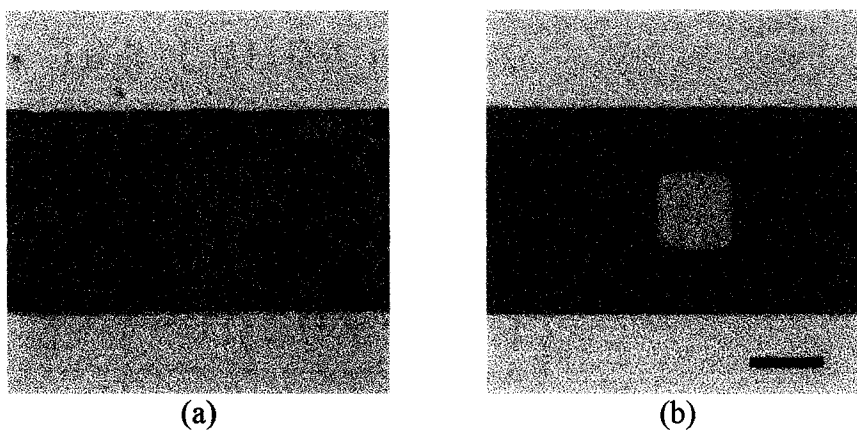
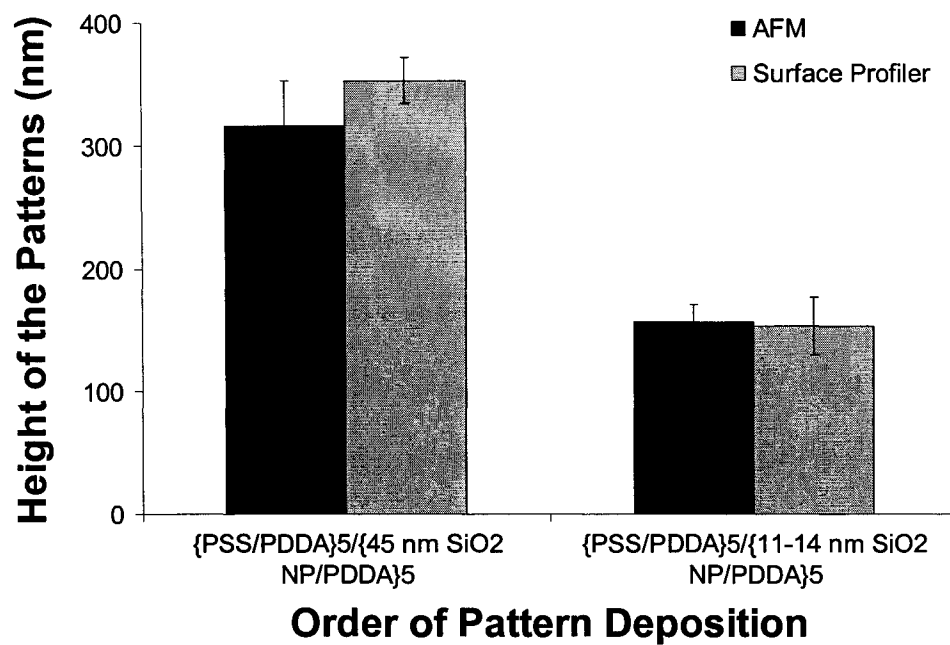


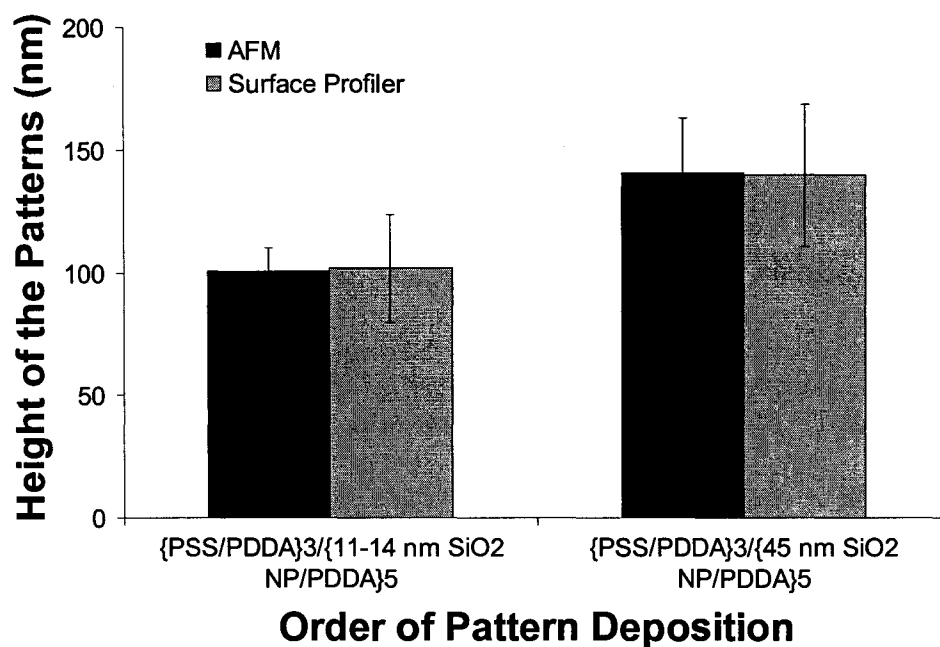
Figure 24. Brightfield images of two-component nanocomposite NP-on-NP micropatterns fabricated under (a) Condition I and (b) Condition II. Scale bar indicates 20 microns.

5.4.1.2 Surface profiler measurements

Figure 25 contains the thickness data measured using surface profilometry for the two-component nanocomposite NP-on-NP micropatterns fabricated under Conditions I [Figure 25(a)] and II [Figure 25(b)]. From Figure 25(a), it can be seen that the thickness of the 45 nm SiO₂ NP nanofilms is ~325 nm. However, in Figure 25(b) the thickness of the same nanofilms is ~140 nm, less than 50% of the thickness in Figure 25(a). This is partly due to the difference in the precursor layers. However, the difference in thickness is still significant even after accounting for the number of precursor layers.



(a)



(b)

Figure 25. Thicknesses data obtained from surface profilometry and AFM measurements for the two-component nanocomposite NP-on-NP micropatterns fabricated under (a) Condition I and (b) Condition II.

This decrease in thickness could be mainly attributed to the fact that under Condition II the nanofilms of large size NPs are deposited on nanofilms of small size NPs, hence do not result in physically stable microstructures and disintegrate during the sonication step performed for the lift-off process.

5.4.1.3 AFM measurements

Figure 25 contains the thickness data measured using atomic force microscopy for the stripe and square micropatterns fabricated under Conditions I [Figure 25(a)] and II [Figure 25(b)]. The thickness data obtained using AFM measurements confirm the observations made from the profilometry measurements. Figure 26 contains AFM micrographs of the two-component nanocomposite NP-on-NP micropatterns under Condition I [Figure 26(a)] and Condition II [Figure 26(b)].

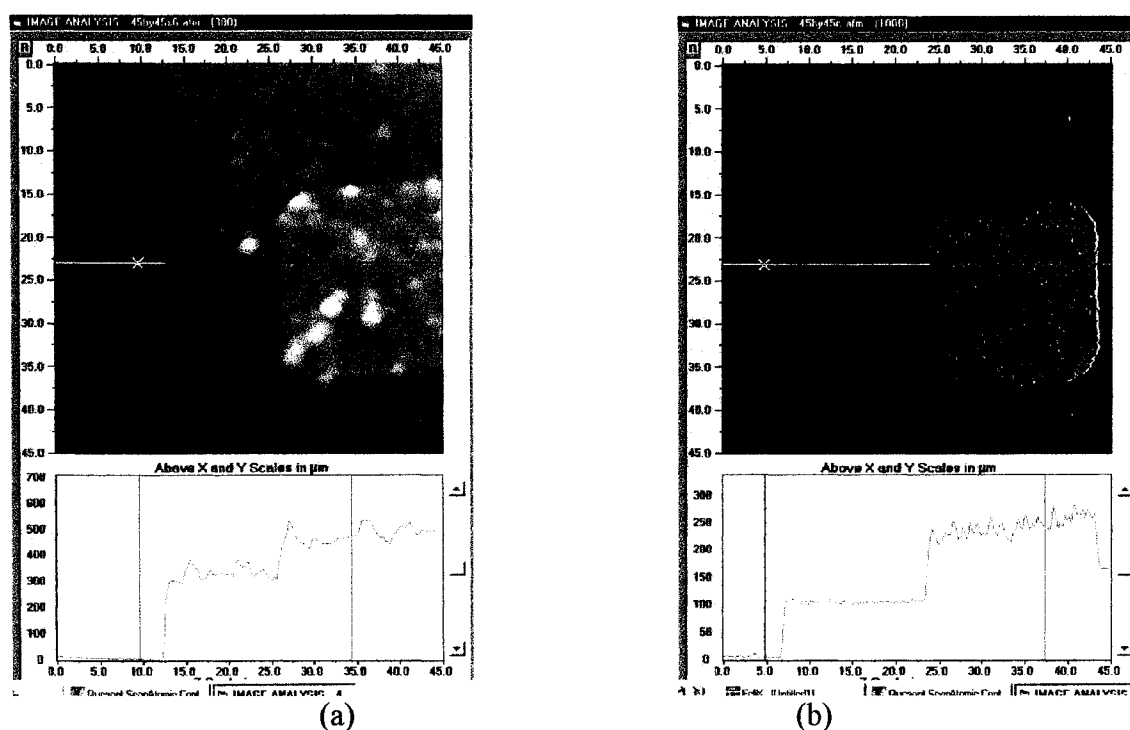


Figure 26. AFM micrographs of two-component nanocomposite NP-on-NP micropatterns fabricated under (a) Condition I and (b) Condition II.

AFM measurements confirmed that the micropatterns had the expected lateral dimensions. From the cross-sectional line data in Figure 26(a) it is evident that the roughness of the 45 nm NP nanofilms has propagated into the 11-14 nm NP nanofilms. It appears that Condition I results in low edge resolution for the 45 nm NP stripe patterns [Figure 26(a)], whereas with similar NP nanofilms Condition II results in better edge resolution for the square patterns [Figure 26(b)]. Also, from the cross-sectional line data in Figure 26(b), it appears that Condition II results in uniform nanofilms.

5.4.1.4 SEM measurements

Figure 27 contains tiled SEM micrographs of the two-component nanocomposite NP-on-NP micropatterns under Condition I [Figure 27(a)] and Condition II [Figure 27(b)]. The images to the right are electron micrographs taken on zoomed regions of the left-hand side images. These zoomed images present the surface details of the NP micropatterns more clearly. The images in Figure 27(a) confirm the observations made in previous measurement techniques that the roughness of the large size NP nanofilms propagates into the small size NP nanofilms.

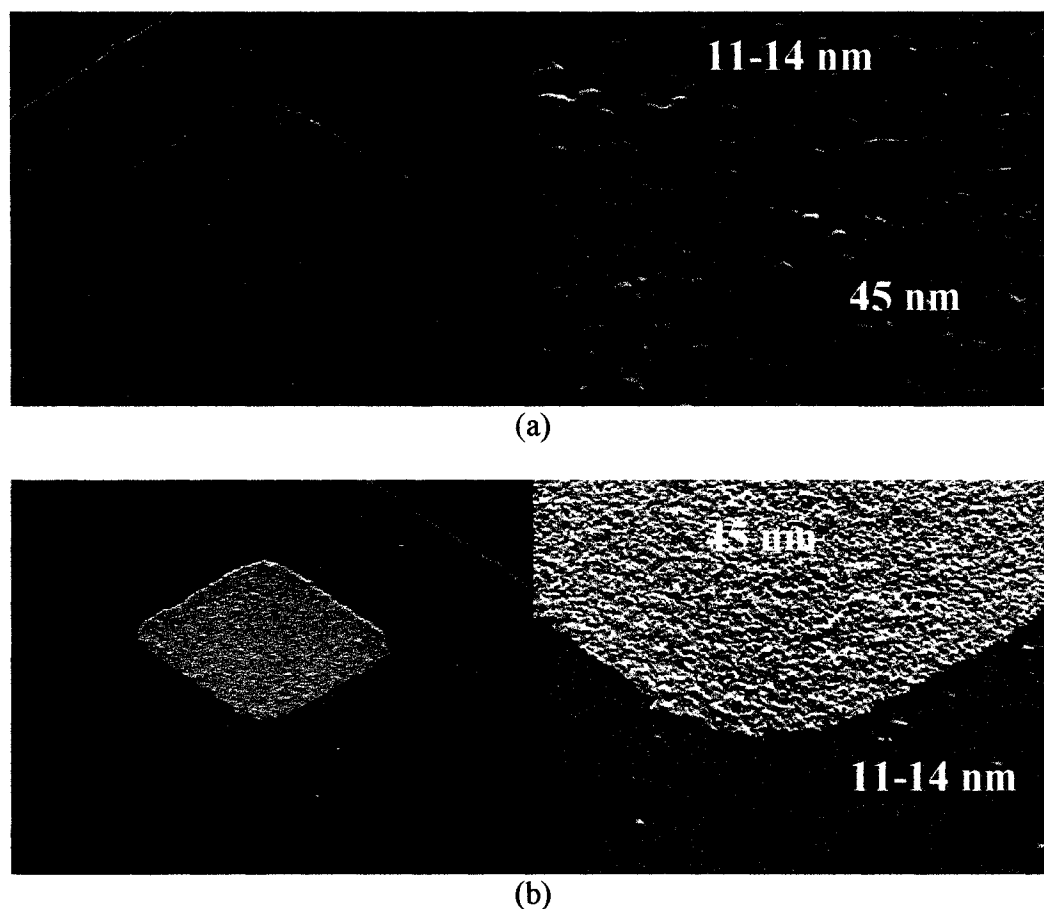


Figure 27. Tiled SEM micrographs of two-component nanocomposite NP-on-NP micropatterns fabricated under (a) Condition I and (b) Condition II.

5.4.1.5 Ellipsometer measurements

It was seen from surface profiler and AFM measurements that the thickness of large size NP nanofilms was less than expected (~ 275 nm), for the multilayer architecture of $\{\text{PSS/PDDA}\}_3/\{\text{45 nm SiO}_2 \text{ NP/PDDA}\}_5$, when deposited on small size NP nanofilms compared to when deposited directly onto a substrate. Therefore, ellipsometric measurements of non-patterned nanofilms with similar multilayer configurations were made, with measurements taken after the deposition of each layer. Figure 28 contains the thickness data for the nanofilms obtained from the ellipsometric measurements.

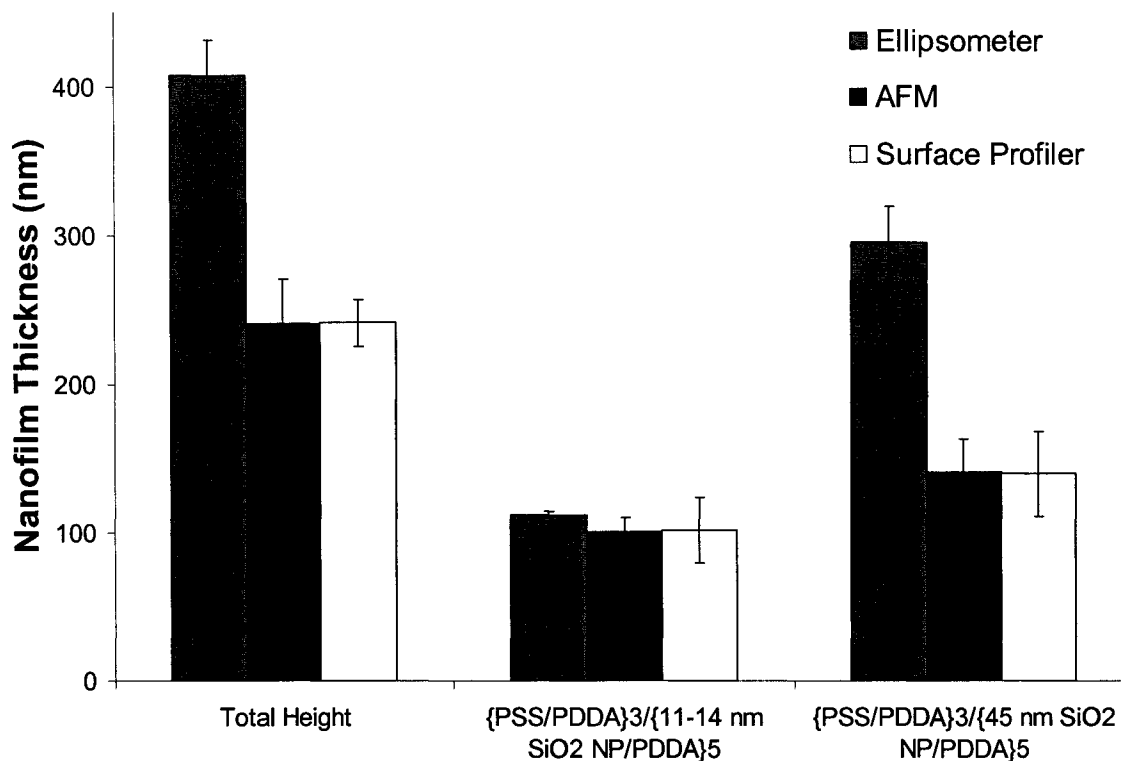


Figure 28. Thicknesses data for the non-patterned nanofilms obtained from ellipsometric measurements and patterned NP-on-NP nanofilms obtained from surface profilometry and AFM measurements.

For comparison purposes, the thickness data have been presented separately for the non-patterned 11-14 nm and 45 nm NP nanofilms as well as for the total nanocomposite film along with the data obtained for the patterned NP nanofilms from profilometry and AFM microscopy. It is clear from the plot that the thickness of the non-patterned 45 nm NP nanofilms is close to the thickness of the patterned 45 nm NP nanofilms as seen in Figure 25(a). However, when the 45 nm NP nanofilm patterns are deposited on top of 11-14 nm NP nanofilms, the thickness of the former nanofilms is lower. It is noteworthy that during the LbL assembly of the 45 nm NP nanofilms, gross examination of the surface indicated that the nanofilm surface was not uniform throughout the substrate. This observation was confirmed during the ellipsometric

measurements across the substrate, also evident from the low standard deviation for the thickness value of the 11-14 nm NP nanofilms compared with that of the 45 nm NP nanofilms. The ellipsometer data indicate that the deposition of nanofilms of large size NPs on nanofilms of small size NPs results in physically unstable nanofilms that could disintegrate during the sonication step performed for the lift-off process resulting in reduced thicknesses. In this section, two-component patterns of nanoparticles constructed using the CSM method were presented. Using the CSM and PSM methods, two-component hybrid patterns of nanoparticle and polymer patterns can also be constructed, as detailed in the next section.

5.4.2 Two-Component Hybrid Patterns

5.4.2.1 Brightfield microscopy

Figure 29 contains a brightfield image of two-component hybrid polymer-on-nanoparticle (polymer-on-NP) micropatterns (Condition I) acquired at a magnification of 50X. The stripe patterns are 50 μm wide and the square patterns have sides of 20 μm . The stripe patterns have a multilayer architecture of $\{\text{PSS/PDDA}\}_5/\{11\text{-}14 \text{ nm SiO}_2 \text{ NP/PDDA}\}_5$ and the square patterns patterned on top of the stripe patterns have an architecture of $\{\text{PSS/PDDA}\}_3/\{\text{PSS/PDDA}\}_5$. The polymer multilayers could easily be replaced with multilayers of proteins, enzymes, or other biologically relevant molecules to create complex 3D multilayer multicomponent micropatterns for use in cell culture.

5.4.2.2 Surface profiler measurements

Figure 30 contains the thickness data measured using surface profilometry for the two-component hybrid polymer-on-NP micropatterns. Figure 30(a) contains the thickness data for polymer-on-NP patterns fabricated under Condition I. The stripe and square

patterns (patterned on top of the stripe patterns) have a multilayer architecture of $\{\text{PSS/PDDA}\}_5/\{11\text{-}14 \text{ nm SiO}_2 \text{ NP/PDDA}\}_5$ and $\{\text{PSS/PDDA}\}_3/\{\text{PSS/PDDA}\}_5$, respectively. Figure 30(b) contains the thickness data for polymer-on-NP patterns fabricated under Condition II. The stripe and square patterns (patterned on top of the stripe patterns) have a multilayer architecture of $\{\text{PSS/PDDA}\}_3/\{11\text{-}14 \text{ nm SiO}_2 \text{ NP/PDDA}\}_5$ and $\{\text{PSS/PDDA}\}_3/\{\text{PSS/PDDA}\}_5$, respectively.

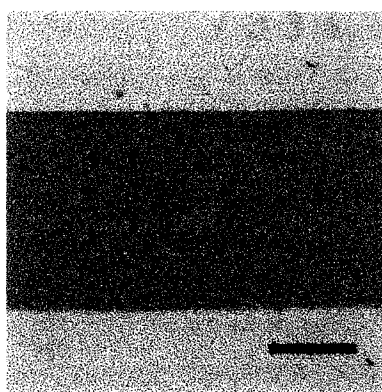
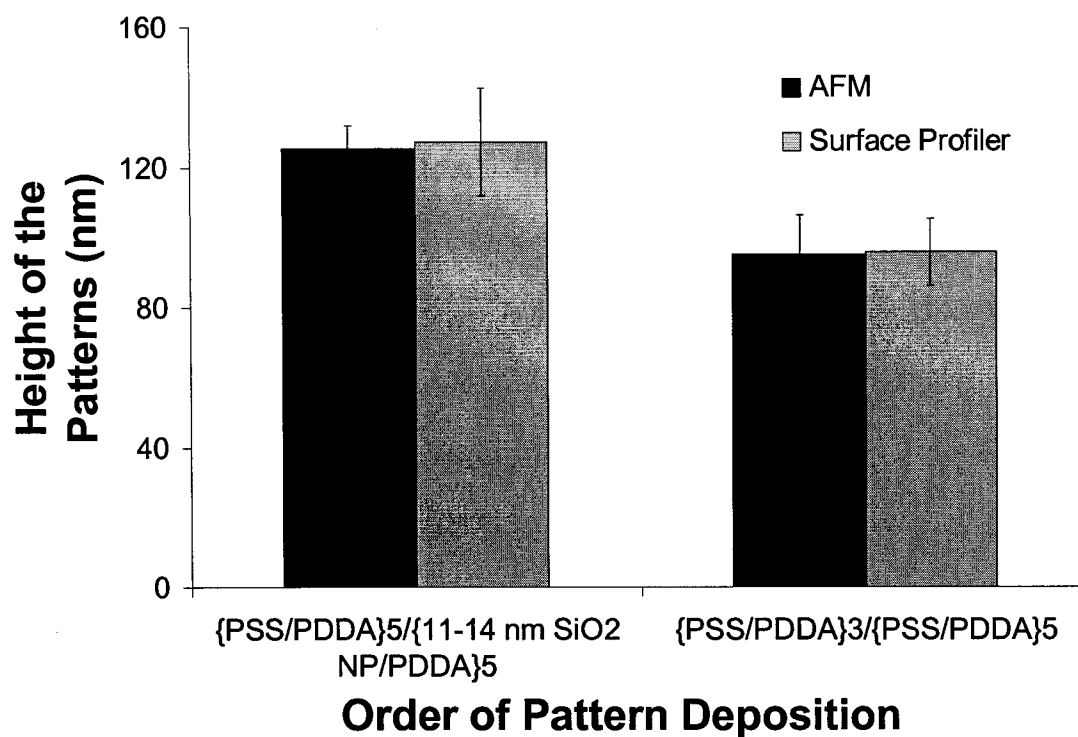
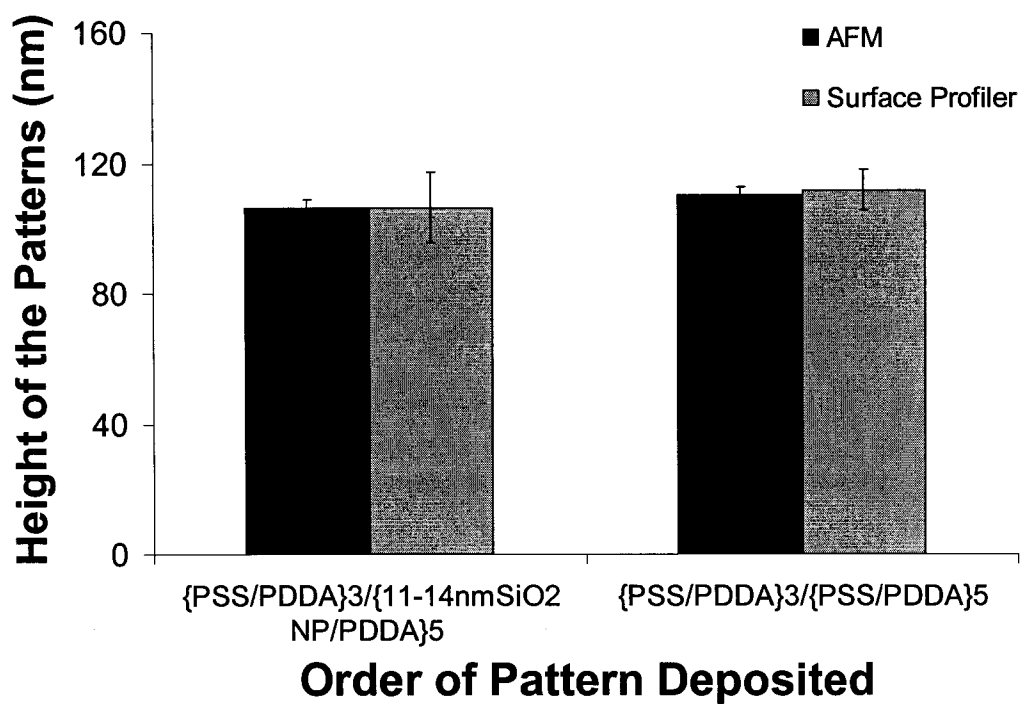


Figure 29. Brightfield images of two-component hybrid polymer-on-NP micropatterns fabricated under Condition I. Scale bar indicates 20 microns.

From Figures 30(a) and 30(b), it can be seen that the thickness of the polymer nanofilms is ~ 95 nm, more than the expected value for eight bilayers of PSS/PDDA (~ 80 nm). One of the reasons for this increased thickness of the polymer nanofilms could be that they were deposited on top of highly porous NP nanofilm surfaces. Also, the thickness of the polymer nanofilms in Figure 30(b) is more compared to those in Figure 30(a). This increased thickness of polymer nanofilms could be attributed to the rougher surfaces of the $\{\text{PSS/PDDA}\}_3/\{11\text{-}14 \text{ nm SiO}_2 \text{ NP/PDDA}\}_5$ compared to $\{\text{PSS/PDDA}\}_5/\{11\text{-}14 \text{ nm SiO}_2 \text{ NP/PDDA}\}_5$ nanofilms.



(a)



(b)

Figure 30. Thicknesses data obtained from surface profilometry and AFM measurements for the two-component hybrid polymer-on-NP micropatterns fabricated under (a) Condition I and (b) Condition II.

5.4.2.3 AFM measurements

Figure 30 contains the thickness data measured using atomic force microscopy for the stripe and square micropatterns fabricated under Conditions I [Figure 30(a)] and II [Figure 30(b)]. The thickness data obtained using AFM measurements are in agreement with the observations made from the profilometry measurements. Figure 31 contains AFM micrographs of the two-component hybrid polymer-on-NP micropatterns under Condition I [Figure 31(a)] and Condition II [Figure 31(b)]. AFM measurements confirmed that the micropatterns had the expected lateral dimensions. From the cross-sectional line data in Figure 31(b), it can be seen that the edge of the stripe patterns has a horn-like feature. Usually, polyelectrolyte solutions with low salt concentrations result in this horn-like feature at the edges of the micropatterns when spin LbL self-assembly²⁷⁶⁻²⁸² is used.²⁴² Because this is not the case in these studies, these features indicate that the lift-off process was not completely done. The roughness of the polymer and NP nanofilm surfaces of patterns constructed under Condition I was found to be 5.13 ± 0.25 nm and 8.44 ± 1.39 nm, respectively, whereas the roughness of the polymer and NP nanofilm surfaces of patterns constructed under Condition II was found to be 9.47 ± 0.98 nm and 9.76 ± 0.79 nm, respectively. These roughness data indicate that the thickness of polymer nanofilms deposited on NP nanofilms is higher when compared with those deposited on smoother surfaces due to the higher surface roughness of the NP nanofilms, and that the thickness as well as roughness of the polymer nanofilms increases with increase in surface roughness of the underlying surface.

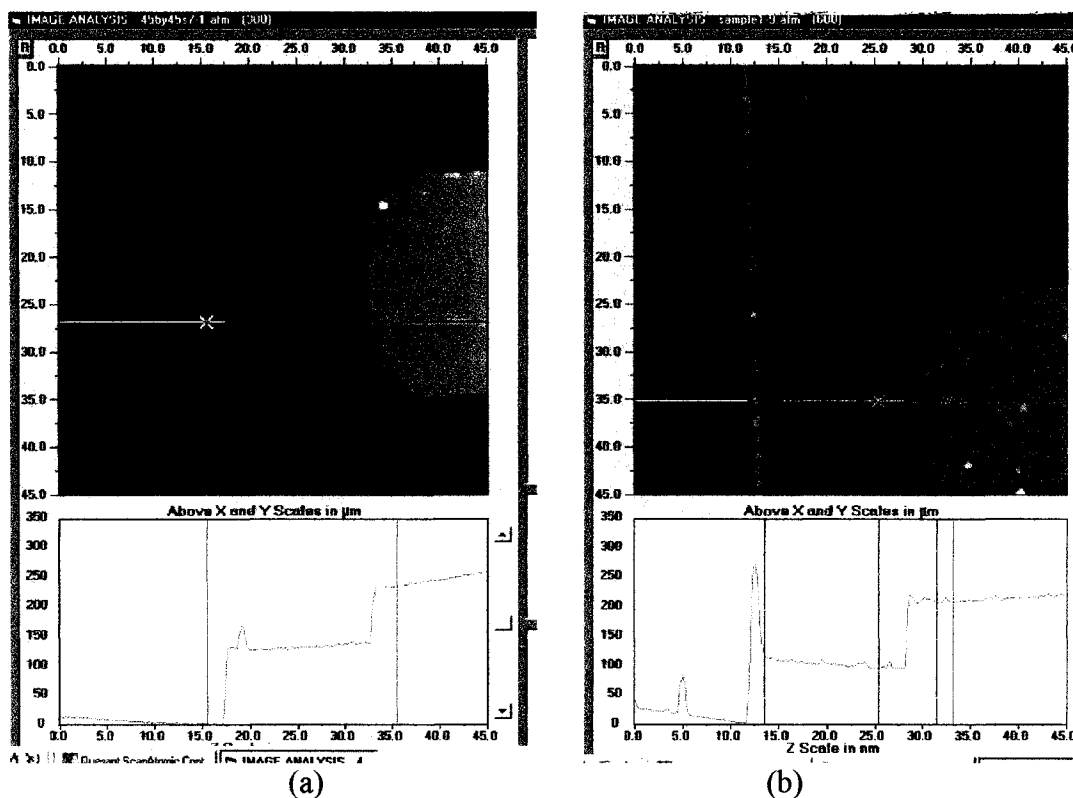


Figure 31. AFM micrographs of two-component hybrid polymer-on-NP micropatterns fabricated under (a) Condition I and (b) Condition II.

5.4.2.4 SEM measurements

Figure 32 contains tiled SEM micrographs of the two-component hybrid polymer-on-NP micropatterns under Condition I [Figure 32(a)] and Condition II [Figure 32(b)]. The images to the right are electron micrographs taken on zoomed regions of the left-hand side images. The edge resolution for the polymer patterns in Figure 32(a) appears to be better than that for those in Figure 32(b). Also, from Figure 32(b) the horn-like features at the edges of the stripe patterns can be clearly seen. This feature is missing in portions of the edge (right hand side of the pattern) indicating that it was due to incomplete lift-off process and not due to lower salt concentration solutions.

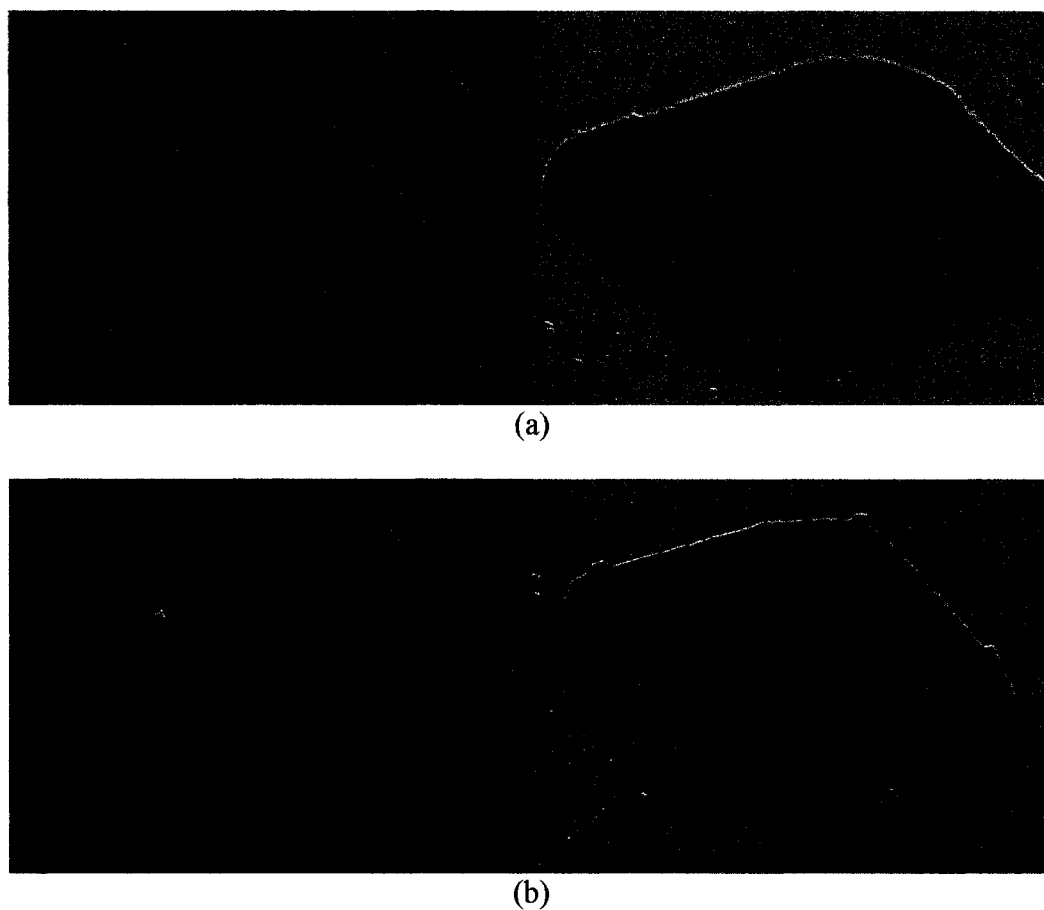


Figure 32. Tiled SEM micrographs of two-component hybrid polymer-on-NP micropatterns fabricated under (a) Condition I and (b) Condition II.

5.4.2.5 Ellipsometer measurements

From the thickness data for the hybrid polymer-on-NP patterns obtained from surface profilometry and AFM measurements it was observed that the thickness of the polymer patterns was more than expected when deposited on NP nanofilms as compared to when deposited directly onto a substrate. Therefore, ellipsometric measurements of non-patterned nanofilms with similar multilayer configurations were made, with measurements taken after the deposition of each layer. Figure 33 contains the thickness data for the nanofilms obtained from the ellipsometric measurements

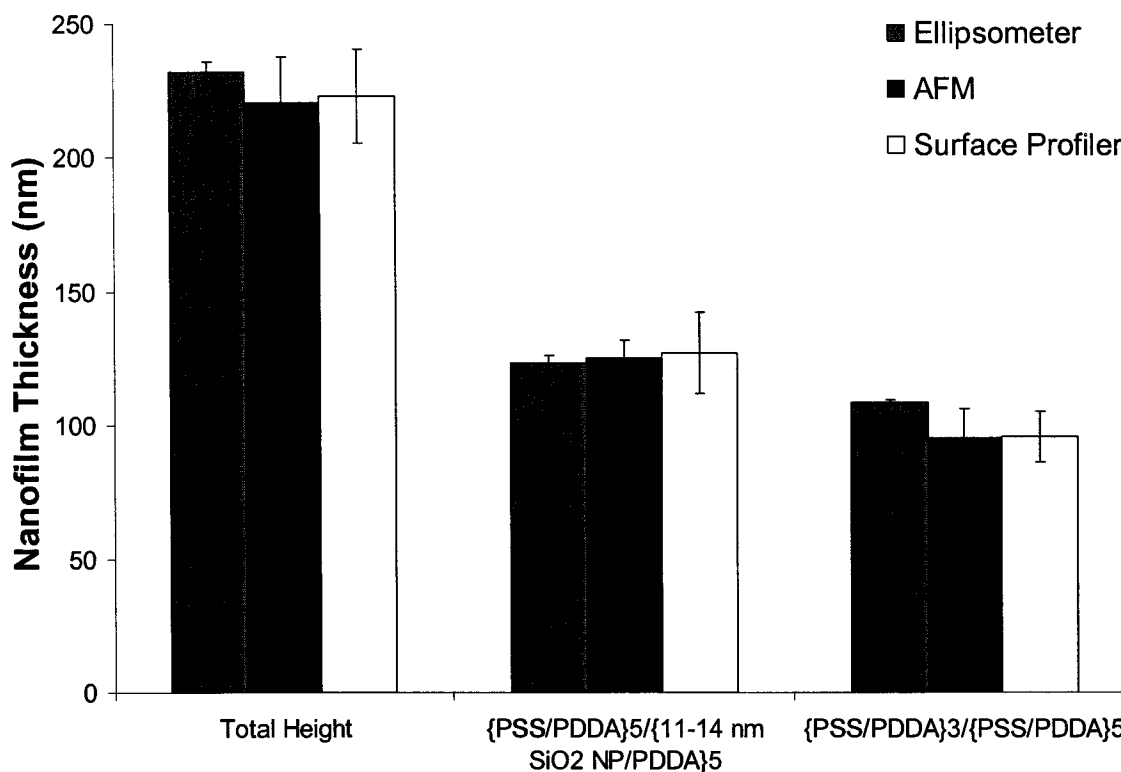


Figure 33. Thicknesses data for the non-patterned nanofilms obtained from ellipsometric measurements and patterned polymer-on-NP nanofilms obtained from surface profilometry and AFM measurements.

For comparison purposes, the thickness data have been presented separately for the non-patterned 11-14 nm and polymer nanofilms as well as for the total nanocomposite film along with the data obtained for the patterned NP nanofilms from profilometry and AFM microscopy. Surprisingly, the ellipsometric measurements are in good agreement with the profilometry and AFM measurements indicating that the polymer nanofilms deposited on NP nanofilms are indeed thicker than those deposited directly onto a substrate. During the ellipsometric measurements, it was observed that the thickness of three bilayers of PSS/PDDA is 18.2 ± 0.09 nm when deposited directly onto a substrate and 29.04 ± 0.79 nm when deposited on top of NP nanofilms.

The ellipsometry data confirm the observations made in profilometry and AFM measurements.

From the preceding sections, it is clear that nanomaterials, such as colloidal nanoparticles, and polymers could be easily integrated to form two-component 3D microstructures using the CSM and PSM methods. The following section presents more complex nanoparticle microstructures constructed using CSM method.

5.4.3 Four-Component Patterns

5.4.3.1 Brightfield microscopy

Figure 34 contains tiled brightfield images of four-component interdigitated NP micropatterns acquired at magnifications of 5X (left) and 50X (right). The square patterns have sides of 20 μm . Figure 34(a) is an image of interdigitated NP patterns fabricated under Condition I. The square patterns have a general multilayer architecture of $\{\text{PSS/PDDA}\}_5/\{\text{SiO}_2 \text{ NP/PDDA}\}_5$. The deposition order for the multilayer patterns of different NP sizes was from largest size NPs to smallest size NPs (78 nm, 45 nm, 20 nm, 11-14 nm). Figure 34(b) is an image of interdigitated NP patterns fabricated under Condition II. The square patterns have a general multilayer architecture of $\{\text{PSS/PDDA}\}_3/\{\text{SiO}_2 \text{ NP /PDDA}\}_5$. The deposition order for the multilayer patterns of different NP sizes was from smallest size NPs to largest size NPs (11-14 nm, 20 nm, 45 nm, 78 nm). Figure 34(c) is an illustration representing the cross-sectional side view of the patterns. From Figures 34(a) and 34(b) it is clear that the CSM method provides the ability to obtain precisely aligned 3D multilayer micropatterns of NP nanofilms.

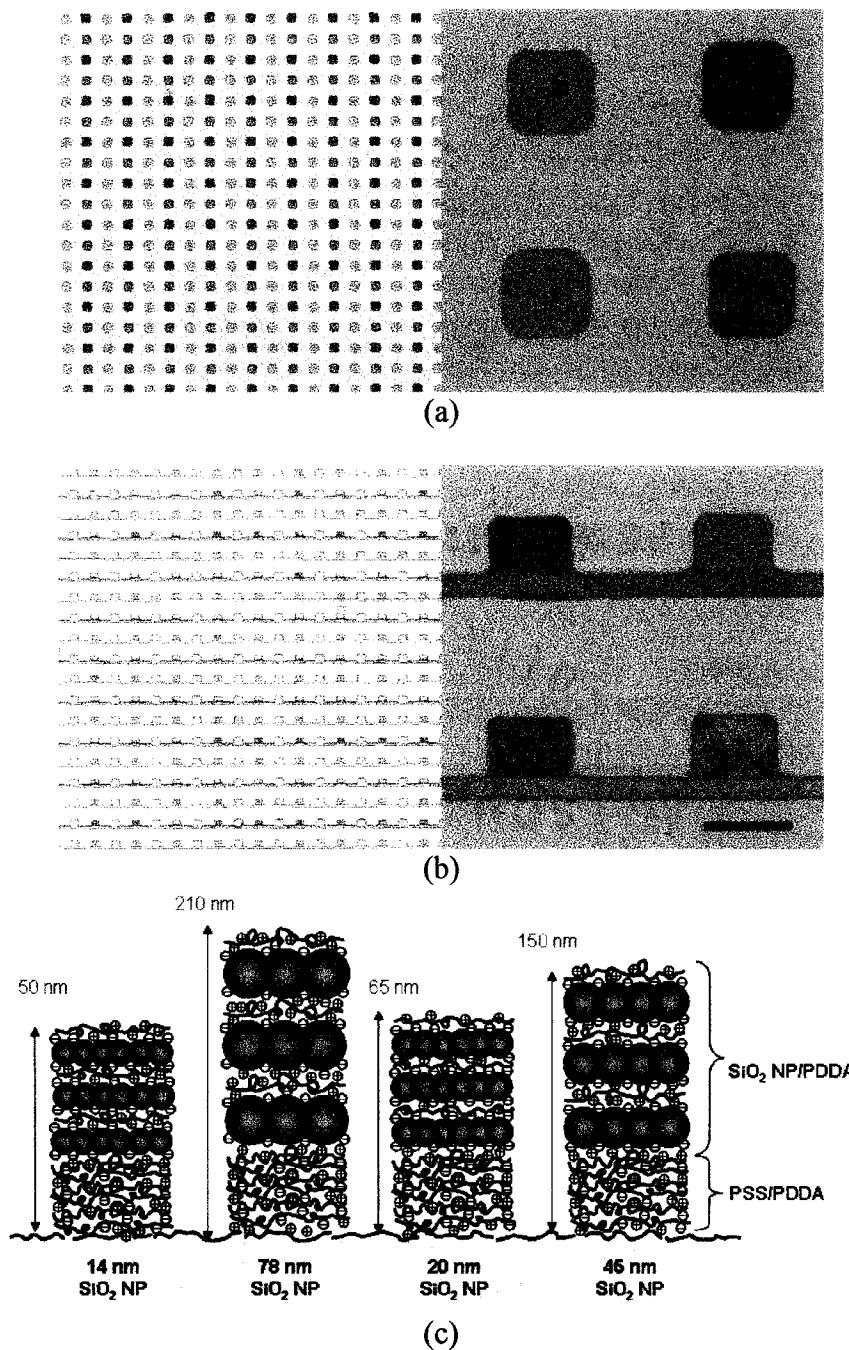


Figure 34. Tiled brightfield images at magnifications of 5X (left) and 50X (right) of four-component interdigitated NP micropatterns fabricated under (a) Condition I and (b) Condition II, (c) Cartoon of the cross-sectional view of the patterns. Scale bar indicates 20 microns.

The average misregistry, M ,²⁶⁴ between the patterns of the two components, was found to be $\sim 0.8 \mu\text{m}$. For an offset length of $50 \mu\text{m}$, this misregistry relates to an error of

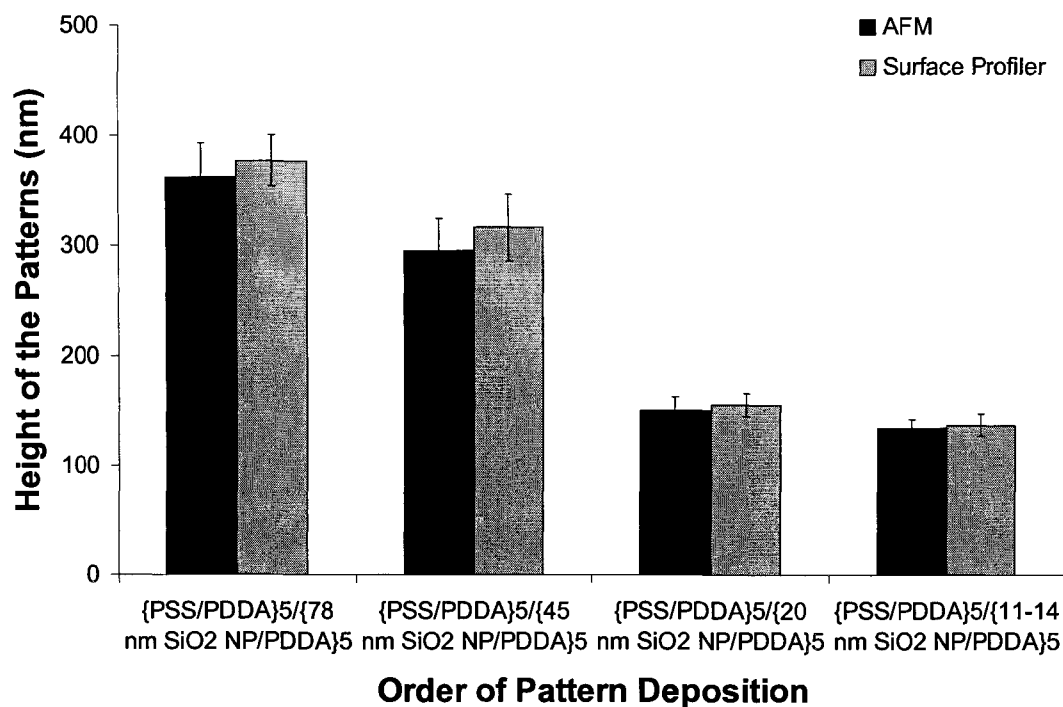
~1.6% for a 4-inch wafer. Hence, it can be concluded that the CSM method provides much better alignment compared to the recently demonstrated MTP method, with a misalignment of 50 μm (18% deviation) for a $2.8 \times 3.3 \text{ cm}^2$ stamp.¹⁸⁰

5.4.3.2 Surface profiler measurements

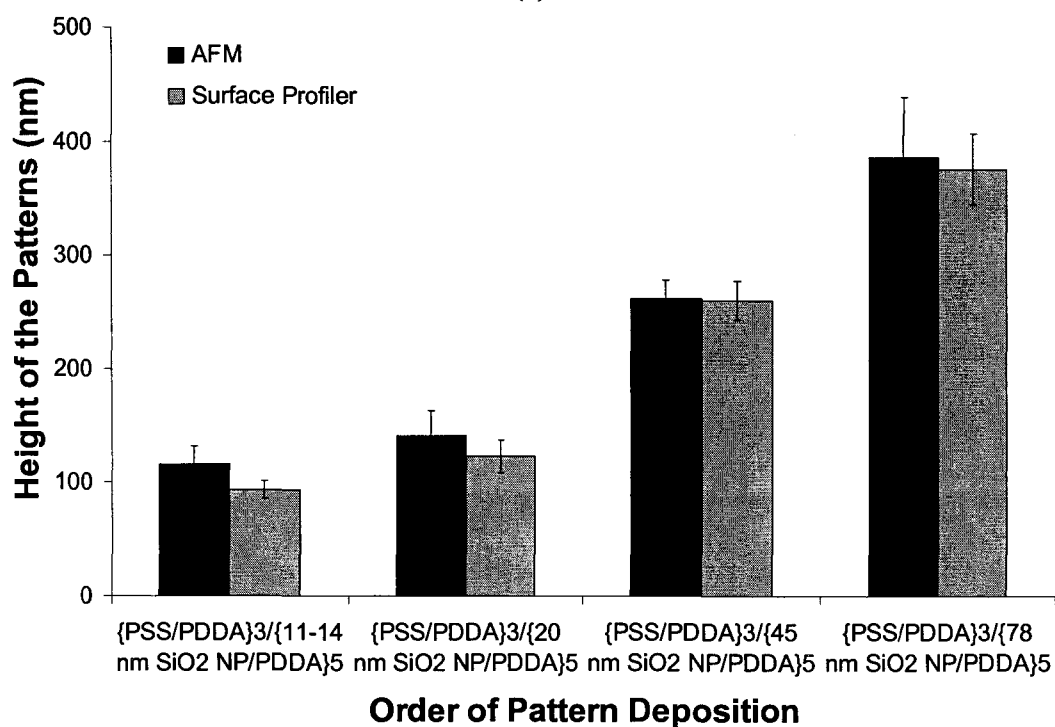
Figure 35 contains the thickness data measured using surface profilometry for the four-component NP micropatterns fabricated under Conditions I [Figure 35(a)] and II [Figure 35(b)]. From Figures 35(a) and 35(b), it can be seen that when NP nanofilms are deposited directly onto a substrate, the order of deposition for nanofilms embedded with different NP sizes does not significantly affect the thicknesses of the NP nanofilms.

5.4.3.3 AFM measurements

Figure 35 contains the thickness data measured using atomic force microscopy for the four-component NP micropatterns fabricated under Conditions I [Figure 35(a)] and II [Figure 35(b)]. The thickness data using AFM measurements are in agreement with the data obtained from the profilometry measurements. Figure 36 contains AFM micrographs of the four-component NP micropatterns fabricated under Condition I [Figure 36(a)] and Condition II [Figure 36(b)]. From the cross-sectional line data in Figure 36(a), it can be seen that the edge of the stripe patterns has a horn-like feature similar to that observed in Figure 30(b), indicating that the lift-off process was not completely done. It also appears that the edge resolution and pattern integrity of the NP patterns in Figure 36(b) is better compared to those in Figure 36(a).



(a)



(b)

Figure 35. Thicknesses data obtained from surface profilometry and AFM measurements for the four-component interdigitated NP micropatterns fabricated under (a) Condition I and (b) Condition II.

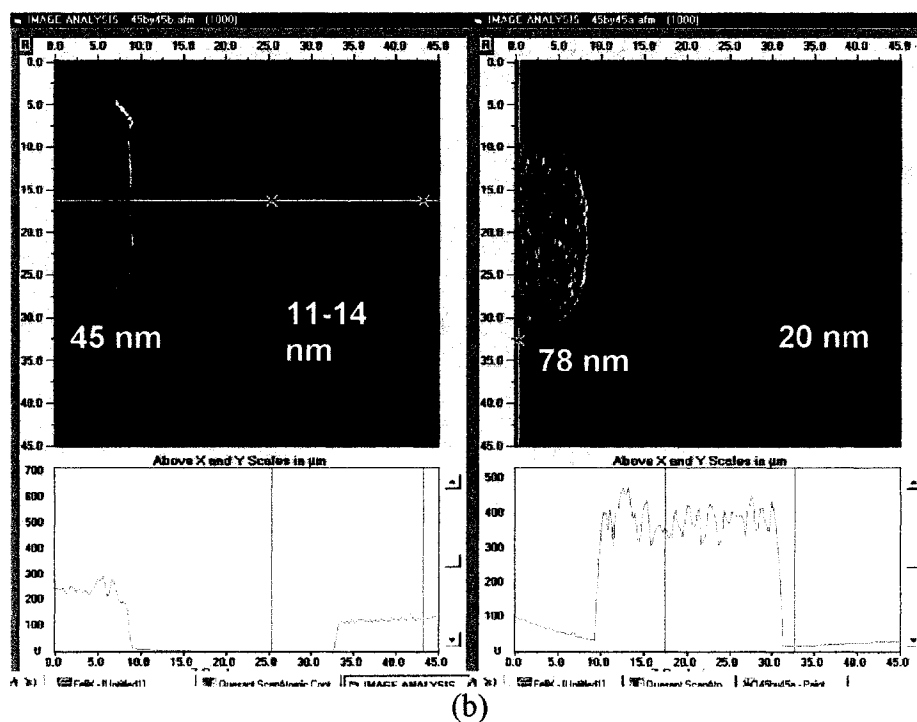
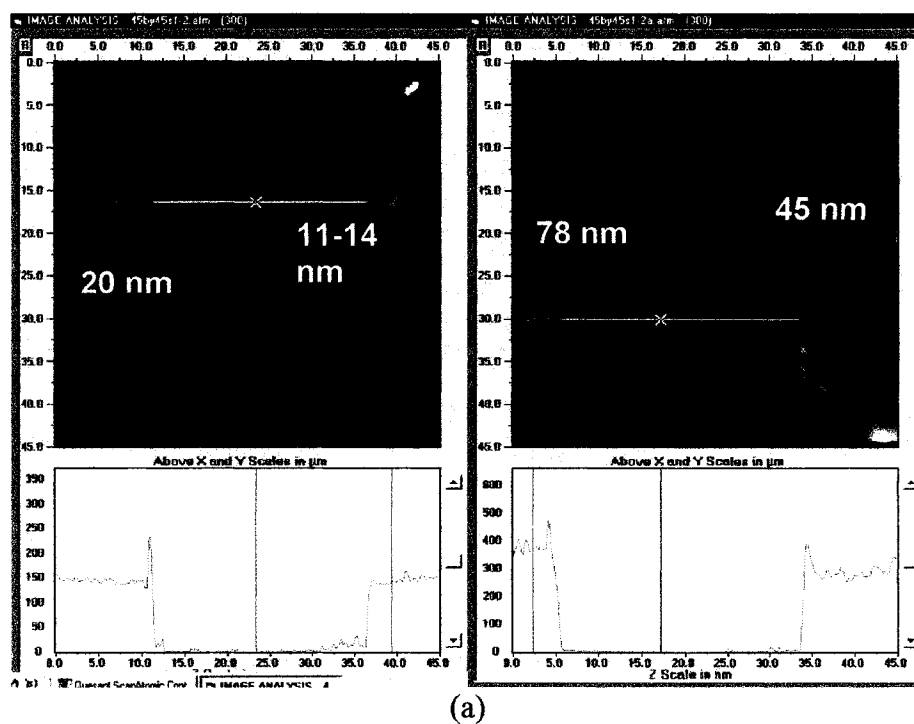


Figure 36. Tiled AFM micrographs of four-component interdigitated NP micropatterns fabricated under (a) Condition I and (b) Condition II.

5.4.3.4 SEM measurements

Figure 37 contains tiled SEM micrographs of the four-component interdigitated NP micropatterns under Condition I [Figure 37(a)] and Condition II [Figure 37(b)]. The images to the right are electron micrographs taken on zoomed regions of the left-hand side images. The particles seen on the background are from dicing of the silicon wafer and not a result of the fabrication process. These electron micrographs indicate the successful use of CSM method to fabricate 3D interdigitated multilayer multicomponent patterns of nanofilms embedded with NPs, with precise spatial arrangements.

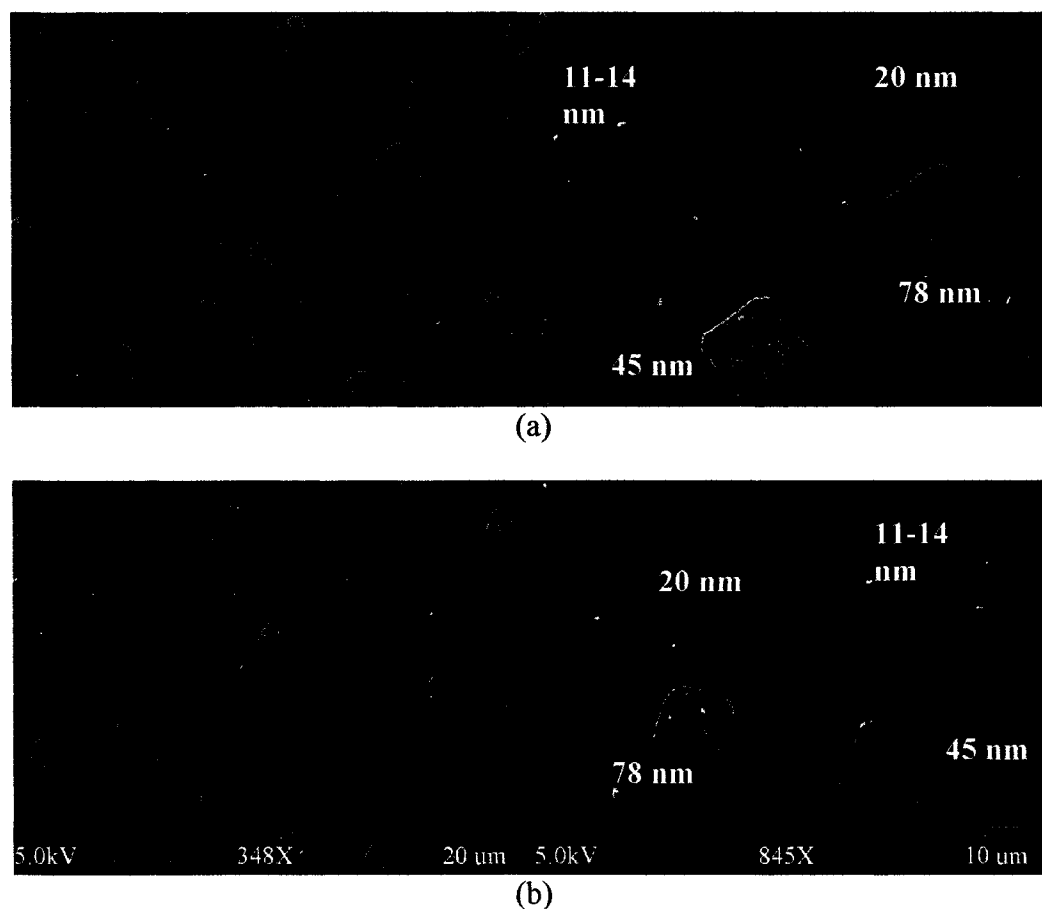


Figure 37. Tiled SEM micrographs of four-component interdigitated NP micropatterns fabricated under (a) Condition I and (b) Condition II.

Figure 38 contains tiled SEM micrographs showing the edges of NP nanofilm patterns of different NP sizes obtained using fabrication Conditions I. These images indicate that the NP patterns possess high degree of line-edge definition, even after multiple lithography and LbL assembly processes.

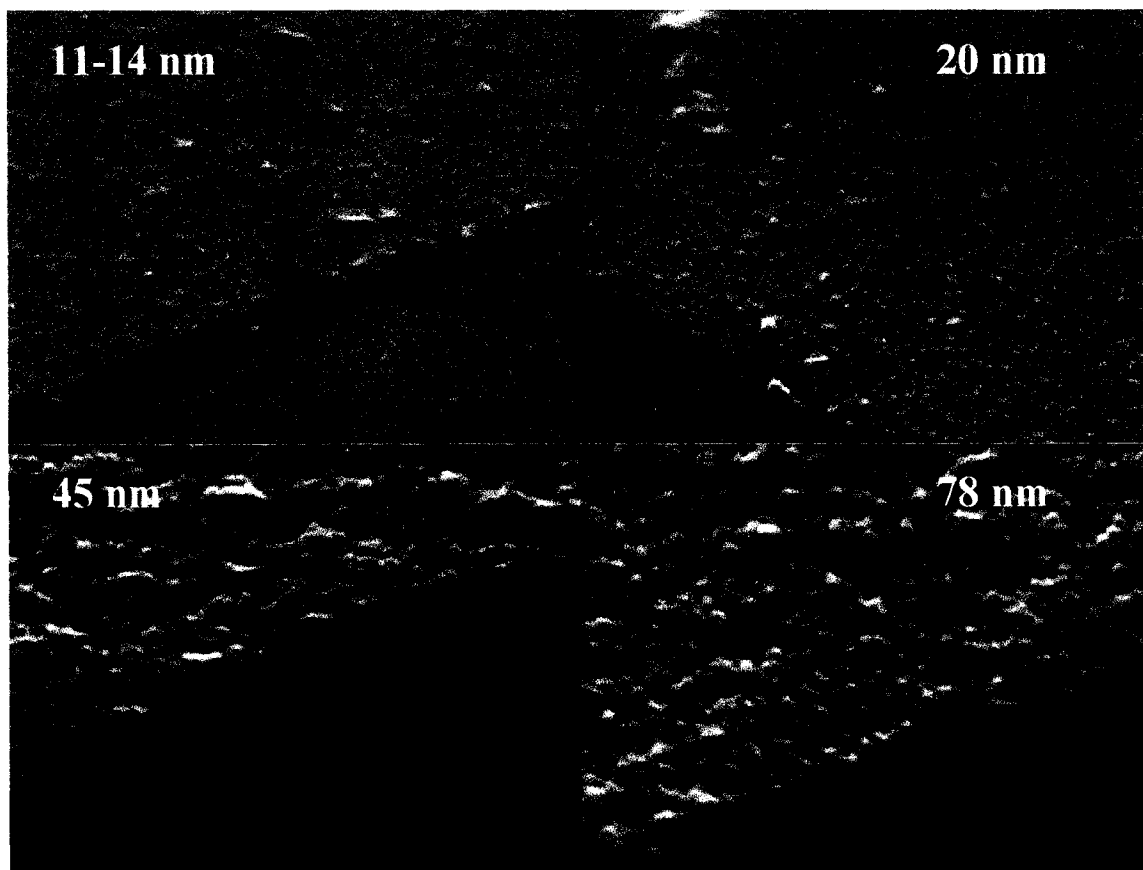


Figure 38. Tiled SEM micrographs of four-component interdigitated NP micropatterns fabricated under Condition I.

5.5 Conclusions

Two- to four-component 3D multilayer heterostructures of colloidal nanoparticles on a single substrate, fabricated using the CSM method, have successfully been demonstrated. The CSM method provides versatility and tunability of micro- and

nanoscale topographies embedded with organic and/or inorganic materials. The fabrication results and metrology results on the multicomponent micropatterns prove the success and usefulness of the CSM method. The ability to construct multicomponent heterostructures with great precision and simplicity overcomes some of the constraints of existing techniques, and the process can be easily integrated into existing automated systems used for lithography and LbL assembly. The metrology results indicate that nanocomposite micropatterns with varying physical and chemical cues could be easily integrated into scaffolds using the current technique. Although not presented in this work, the surfaces of the colloidal nanoparticles could be easily modified with different biologically relevant chemistries using the LbL self-assembly process prior to the deposition of NP nanofilms or the biologically relevant chemistries could be directly used during the LbL deposition process, thereby adding the ability to tune the chemical properties of the 3D micropatterns for use as cell culture scaffolds. The demonstrated examples are highly suitable for a broad array of studies and applications in biology, electronics, photonics, optoelectronics, and chemical and biochemical sensors.

In Chapters 3, 4, and 5, different examples of 3D multicomponent multilayer micropatterns fabricated using methods that combine lithography and LbL assembly processes have been presented. It is important and useful to understand the effect of the processing parameters such as temperature and exposure to chemicals such as resist, acetone, and resist developer used in these fabrication methods on the physical and chemical characteristics of the nanocomposite multilayer films. The investigation into how these process parameters affect the physicochemical properties of the nanofilms is presented in the next chapter.

CHAPTER 6

EFFECT OF FABRICATION PROCESS PARAMETERS ON THE CHARACTERISTICS OF NANOFILMS

6.1 Introduction

In the preceding chapters, different fabrication methods that combine lithography and LbL assembly processes for the construction of 3D multicomponent nanocomposite micropatterns (3D MNMs) of polymers and nanoparticles were presented. Descriptions of the processes and demonstrations of the approach to construction of 3D MNMs were included. However, with any technique, it is important and useful for its broader applicability to understand the effect of the different processing parameters involved in that technique on the resulting product. For example, in a very recent report²⁴² it has been shown that the line-edge definition of patterned multilayer films fabricated using LbL-LO is not affected by the salt concentration (0-1 M range) in the polyelectrolyte solutions, when conventional dip LbL self-assembly is used; whereas, horn-like features at the edges of the patterned multilayer films were observed when spin LbL self-assembly²⁷⁶⁻²⁸² was used. Similarly, in the PSM method involving various process parameters including temperature and exposure to chemicals such as resist, acetone, and resist

developer, the physicochemical properties of the resulting 3D MNMs could depend upon and be affected by these process parameters. As evident from the metrology and cell culture results presented in Chapters 3, 4, and 5, these process parameters did not have any obvious deleterious effects on the desired properties of the fabricated micropatterns. Nevertheless, it is believed that a systematic study of the effects of these process parameters on the physicochemical properties of the nanofilms in the resultant micropatterns would not only aid cell biologists and tissue engineers in adapting this method for their patterning applications but also broaden the applicability of the fabrication methods presented in this research work.

With the goal to understand the effects of the temperature and exposure to chemicals such as resist, acetone, and resist developer (used in the PSM method) on the physicochemical properties of the nanofilms of the resultant micropatterns, non-patterned nanofilms of commonly used polyelectrolytes including PSS, PDDA, PEI, PAH, FITC-PEI, and FITC-PAH were deposited using the LbL assembly process and processed under these different process parameters. Non-patterned nanofilms of a widely studied and well understood enzyme, glucose oxidase (GOx), have also been processed under these different process parameters. The values used in these studies for the different process parameters were chosen from the general range used in the PSM method, as detailed below. The physical characteristics of the nanocomposite films were studied using ellipsometry to obtain thickness information, ultraviolet-visible (UV-Vis) absorption spectroscopy to estimate enzyme activity, and fluorescence microscopy to obtain intensity information and assess uniformity. The chemical characteristics of the

nanocomposite films were studied using attenuated total reflection Fourier-transform infrared (ATR-FTIR) spectroscopy to obtain absorption information.

6.2 Materials

6.2.1 Substrates

Microscope cover glasses ($22 \times 22 \text{ mm}^2$) used as substrates for the fluorescence microscopy studies were purchased from VWR International. Microscope cover glasses ($9 \times 22 \text{ mm}^2$) used as substrates for the ATR-FTIR and UV-Vis studies were purchased from Electron Microscopy Sciences. These substrates were chosen to facilitate their direct use in cuvettes for UV-Vis spectroscopy. Silicon wafers (<100>) purchased from Silicon Inc., were used as the substrates for the ellipsometry studies.

6.2.2 Chemicals

Nano-StripTM was purchased from CYANTEK Corporation. Poly(diallyldimethylammonium chloride) (Mw ~100-200 kDa), poly(sodium 4-styrenesulfonate) (Mw ~1 MDa), poly(ethyleneimine) (Mw ~750 kDa), poly(allylamine hydrochloride) (Mw ~70 kDa), glucose oxidase (Mw ~ 160 kDa), peroxidase (Mw ~44 kDa), *o*-Dianisidine (Mw ~317.2 Da), β -D(+) glucose (Mw ~180.2 Da), sodium acetate (Mw ~136.1 Da), and fluorescein isothiocyanate were purchased from Sigma-Aldrich. Positive photoresist, S1813, and positive resist developer, MF-319, were obtained from Shipley. All chemicals of commercial origin were used as received.

6.2.3 Preparation of Polyelectrolyte and Enzyme Solutions

Solutions of PDDA, PAH, PEI, and PSS with concentration of 2 mg mL^{-1} with 0.5 M KCl and a solution of $500 \text{ } \mu\text{g mL}^{-1}$ for GOx were prepared in Type I DI H₂O and

adjusted to pH 7.4 using HCl and NaOH for use in self-assembly. PAH and PEI were labeled with FITC using standard procedures,²⁵⁹ and separated from dye solution by precipitation with acetone, centrifugation, and resuspension in aqueous solution.

6.3 Methods

6.3.1 Fabrication

Substrates were incubated in Nano-Strip™ at 70 °C for 1 hr to remove organic contaminants and create a uniform negative charge on the substrates, then they were rinsed in DI water and dried using N₂. A precursor layer of PDDA was then deposited on the substrates in all the cases. A basement multilayer of {PSS/PDDA}₃ was not used throughout the LbL assembly processes, except for the enzyme multilayer nanofilms. The substrates were then modified with multilayer architectures of {PSS/PDDA}₃/ {GOx/PEI}₄/GOx and 1-, 3-, and 5-bilayers of {PSS/PDDA}, {PSS/PEI}, {PSS/PAH}, {PSS/FITC-PEI}, and {PSS/FITC-PAH}, using the LbL self-assembly. Also, drying with N₂ was not performed during the LbL assembly to avoid the effect due to inconsistencies in the manual drying process to interfere with the effects of process parameters being studied here.

6.3.2 Characterization

For the ellipsometric measurements, ATR-FTIR measurements, and fluorescence microscopy measurements the same nanofilm coated substrates were used for multiple measurements at different positions on the substrate, as well as for the different values of the process parameters. Multiple measurements were used to reduce the impact of local variations in nanofilm fabrication to interfere with the effects being studied here. For the enzyme activity assays monitored using UV-Vis spectroscopy, a different nanofilm

coated substrate was used for each of the multiple measurements for each value of the process parameter, as well as for each value of the process parameter. This multiple measurement step was done because at the end of each enzyme activity measurement the debris from the assay cocktail was deposited onto the nanofilms. For all the measurements, the nanofilm coated substrates were rinsed with DI water and dried using N₂ after the exposure to acetone, MF319, or S1813. For the temporal stability studies, the nanofilm coated substrates were removed from the DI water solutions and dried using N₂ before making the measurements.

6.3.2.1 Ellipsometry

A spectroscopic ellipsometer (SENTECH, Model-SE 850) was used to measure the thicknesses of the non-patterned multilayer nanofilms. The measurements were performed at an incidence angle of 70° and the 250-850 nm spectral range was used. A spot size of 15 × 5 mm² was used for the ellipsometric measurements. A refractive index of $n_0=1.5$ for a Cauchy layer type was assumed, for all the materials, for thickness calculations using the SPECTRARAY software. The ellipsometric measurements were made at three different positions on the substrates, the average thickness was fitted based on the three measurements using SPECTRARAY, and the mean square error (MSE) for the best fit was obtained. The square-root of this MSE, well known as root mean square error (RMSE) has been used here as the standard deviation.

6.3.2.2 Fluorescence microscopy

Fluorescence microscopy was used for imaging the nanofilms embedded with labeled polyelectrolytes to evaluate the changes in fluorescence intensity quantitatively and to assess the uniformity using an inverted fluorescence microscope (Nikon, Model-

Eclipse TE2000-U) equipped with a high-sensitivity CCD camera (Photometrics, Model-Cool Snap ES). The exposure time used with the 20X objective was 5,000 ms, 1,500 ms, and 1,100 ms for 1-, 3-, and 5-bilayers of {PSS/FITC-PEI}, respectively, and 2,000 ms, 1,000 ms, and 750 ms for 1-, 3-, and 5-bilayers of {PSS/FITC-PAH}, respectively. The measured intensities were normalized using the exposure times for direct comparisons. The image scaling settings used were 0 (low) and 4,095 (high). The value of the image gamma was set to 1.

6.3.2.3 UV-Vis absorbance spectroscopy

The activity of GOx embedded in PEM nanofilms was monitored through a colorimetric assay based on the oxidation of *o*-Dianisidine dihydrochloride through a peroxidase-coupled system using an UV-Vis spectrophotometer (PerkinElmer, Model-Lambda 45 UV/VIS) equipped with a temperature-controlled cuvette holder (Quantum Northwest, Model-TLC 50) and a temperature controller (Quantum Northwest, Model-TC 101). The GOx activity assay comprised 2.4 mL of *o*-Dianisidine solution at pH 5.1, 0.5 ml of β -D(+) glucose solution, and 0.1 mL of peroxidase solution. The $9 \times 22 \text{ mm}^2$ substrates modified with the GOx PEMs were mounted on one of the inner walls of 1 cm path-length quartz cuvettes that do not fall in the path of the light, with the PEMs facing away from the wall of the cuvette. The cocktail solution of *o*-Dianisidine and peroxidase was then poured into the cuvette. While the cocktail solution was continuously stirred with a magnetic bar and a constant temperature of 25 °C, 500 μL of glucose was added to the assay and the absorbance at 500 nm was monitored as a function of time for a total time of 300 s, resulting in a catalytic profile of the GOx embedded in the PEMs. The

results obtained from different experiments were then compared by calculating the slope of the catalytic profiles.

6.3.2.4 Attenuated total reflection-FTIR spectroscopy

Attenuated total reflection mode was used to obtain absorption spectra of the non-patterned nanofilms using a Fourier-transform infrared spectrometer (Thermo Nicolet, Model-Nexus 470) equipped with an ATR accessory (Thermo Nicolet, Model-Smart MIRacle). The pressure clamp was used to obtain repeatable pressure on the sample substrates so that the nanofilm surface conforms to the surface of the ZnSe crystal. All spectra were recorded using 512 scans and a 4 cm^{-1} resolution in the $4,000\text{-}650\text{ cm}^{-1}$ spectral range.

6.3.2.5 Statistical analysis

A student *t*-test was used to assess the statistical significance between the measured physical characteristics of the processed nanofilms and unmodified nanofilms. The tests were performed with a significance level *p* equal to 0.05.

6.4 Results and Discussion

6.4.1 Effect of Processes on Nanofilm Thickness

6.4.1.1 Effect of acetone on nanofilm thickness

Figure 39 contains the thickness data for different nanofilms exposed to acetone obtained from the ellipsometric measurements. Figure 39(a) contains the thickness data for 1-, 3-, and 5-bilayers of PSS/PDDA PEMs. Figure 39(b) contains the thickness data for 1-, 3-, and 5-bilayers of PSS/PEI PEMs. Figure 39(c) contains the thickness data for

1-, 3-, and 5-bilayers of PSS/PAH PEMs. Figure 39(d) contains the thickness data for 1-, 3-, and 5-bilayers of PSS/FITC-PEI PEMs. For the data presented in Figures 39(a)-39(d), the percentage change of nanofilm thicknesses after the maximum exposure time 480 s as compared with the initial condition was highest for the 1-bilayer nanofilms, and decreased with the increase in number of bilayers. For PSS/PDDA and PSS/PAH nanofilms negative percentage changes in nanofilm thicknesses were observed, whereas for the PSS/PEI and PSS/FITC-PEI positive percentage changes in nanofilm thicknesses were observed.

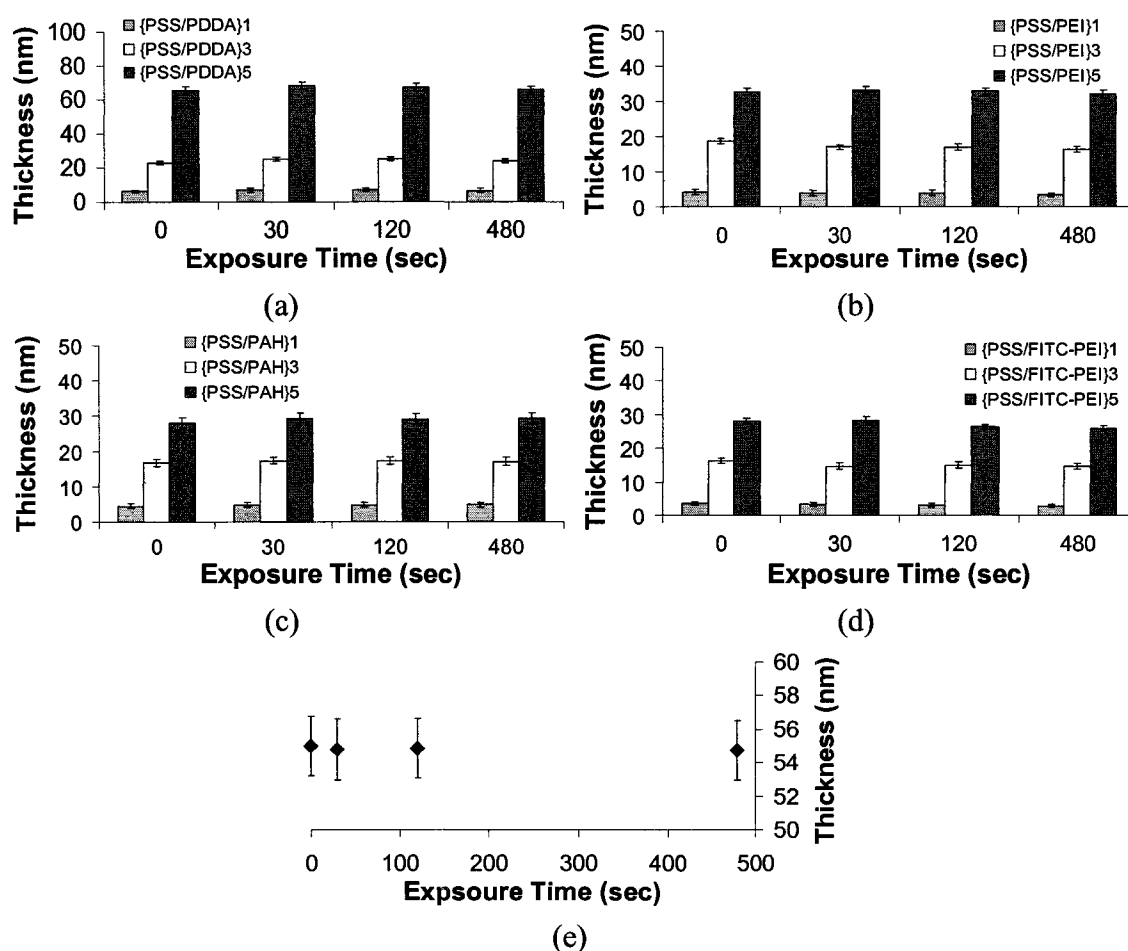


Figure 39. Ellipsometric measurements of nanofilm thickness: Effect of acetone on PEMs of (a) PSS/PDDA, (b) PSS/PEI, (c) PSS/PAH, (d) PSS/FITC-PEI, (e) GOx.

Figure 39(e) contains the thickness data for $\{\text{GOx/PEI}\}_4/\text{GOx}$ PEMs. For the GOx PEMs too a positive percentage change in nanofilm thicknesses was observed. These nanofilms ($p = 0.9141$) have the least value of $\sim 0.45\%$ for the percentage change in thickness. The $\{\text{PSS/FITC-PEI}\}_1$ nanofilms have the highest value of $\sim 18.86\%$ for the percentage change in thickness. However, from t -test it could be stated that acetone does not have significant effect on the thicknesses of the different polyion pairs studied here. These results are in agreement with the observations made in Chapters 3 and 4, where lift-off process step performed in acetone did not significantly affect the expected (estimated from QCM) nanofilm thickness of the micropatterns.

6.4.1.2 Effect of resist developer-MF319 on nanofilm thickness

Figure 40 contains the thickness data for different nanofilms exposed to resist developer-MF319 obtained from the ellipsometric measurements. Figure 40(a), 40(b), 40(c), 40(d) contain the thickness data for 1-, 3-, and 5-bilayer PEMs of PSS/PDDA, PSS/PEI, PSS/PAH, PSS/FITC-PEI, respectively. For the data presented in Figures 40(a) and 40(d), the percentage change of nanofilm thicknesses after the maximum exposure time (30 s) as compared with the initial condition was similar in the case of 1-, 3-, and 5-bilayer nanofilms. For the data presented in Figures 40(b) and 40(c), the percentage change of nanofilm thicknesses was lowest for the 1-bilayer nanofilms, and increased with the increase in number of bilayers. In general, for all the nanofilms a positive percentage change in nanofilm thicknesses was observed.

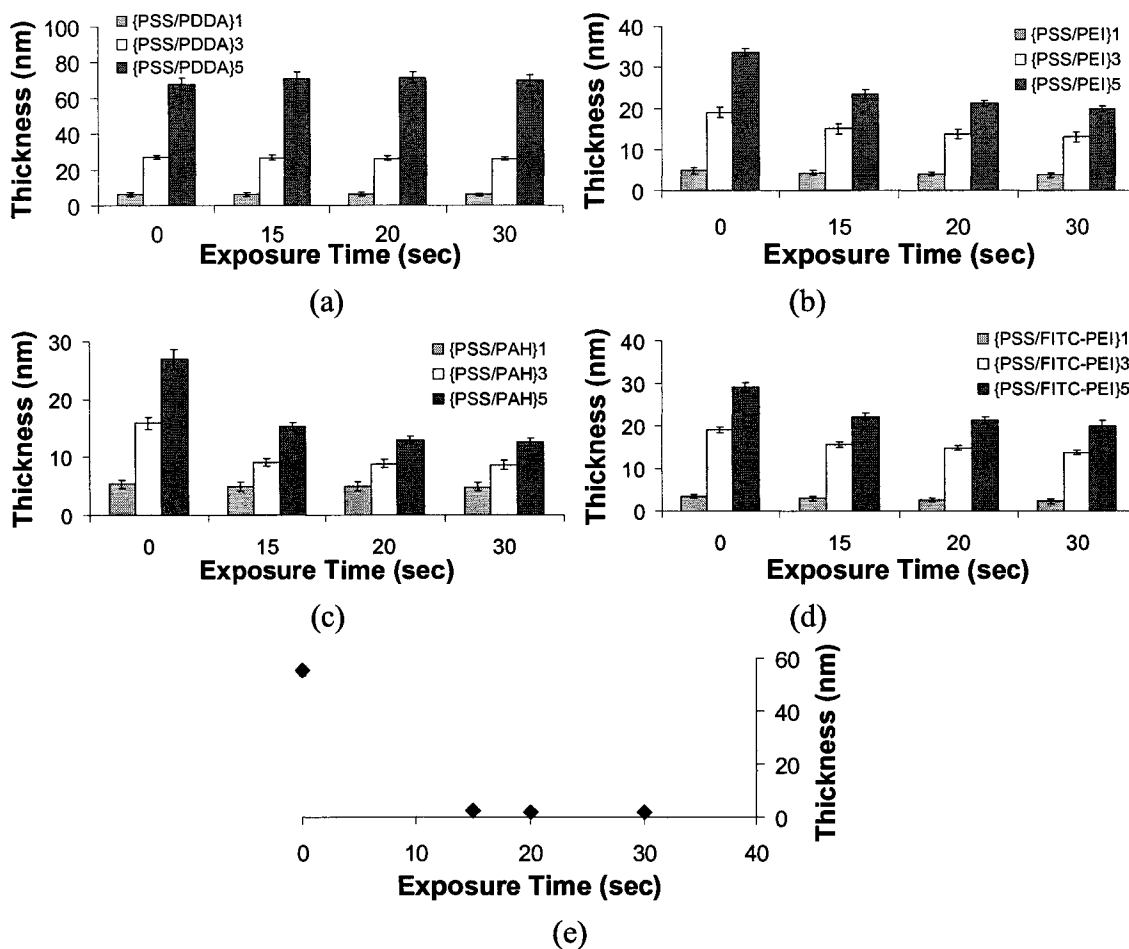


Figure 40. Ellipsometric measurements of nanofilm thickness: Effect of resist developer-MF319 on PEMs of (a) PSS/PDDA, (b) PSS/PEI, (c) PSS/PAH, (d) PSS/FITC-PEI, (e) GOx.

Figure 40(e) contains the thickness data for $\{GOx/PEI\}_4/GOx$ PEMs. For the GOx PEMs too a positive percentage change in nanofilm thicknesses ($p = 0.0005$) was observed, with the highest value of $\sim 97.1\%$ for the percentage change in thickness. The next highest value ($\sim 53.3\%$) of percentage change in thickness is for $\{PSS/PAH\}_5$ nanofilms. The $\{PSS/PDDA\}_1$ nanofilms have the lowest value ($\sim 2.58\%$) of percentage change in thickness, with PSS/PDDA nanofilms, in general, possessing the lowest values. It is clear from the plots and t -test that MF319 affects nanofilms of some polyion pairs significantly, whereas it has no significant effect on nanofilms of some other polyion

pairs. The MF319 solution has a pH 14, and this highly basic pH is believed to be the main reason for the observations made in these studies. The basic nature of MF319 affects the nanofilms (by disintegrating the nanofilms) of weakly charged polyelectrolytes and not those of strongly charged polyelectrolytes. The implication of these observations on the PSM method is that direct exposure of nanofilms of certain polyion pairs might result in deviations from the desired nanofilm properties; such as observed in the case of pattern-on-pattern microstructures discussed in Chapter 4 (Section 4.4.3). However, as evident from the results in Chapters 3 through 5, if the nanofilms are protected by the S1813 coating used for the next lithography steps, then MF319 does not affect the nanofilm properties.

6.4.1.3 Effect of heating time at 115 °C on nanofilm thickness

Figure 41 contains the thickness data for different nanofilms heated at a temperature of 115 °C obtained from the ellipsometric measurements. Figure 41(a), 41(b), 41(c), 41(d) contain the thickness data for 1-, 3-, and 5-bilayer PEMs of PSS/PDDA, PSS/PEI, PSS/PAH, PSS/FITC-PEI, respectively. For the data presented in Figures 41(a)-41(d), the percentage change of nanofilm thicknesses after the maximum heating time (10 min) as compared with the unheated condition was highest for the 1-bilayer nanofilms, and decreased with the increase in number of bilayers. For PSS/PAH and PSS/FITC-PEI nanofilms negative percentage changes in nanofilm thicknesses, and for other nanofilms positive percentage changes were observed. Figure 41(e) contains the thickness data for $\{\text{GOx/PEI}\}_4/\text{GOx}$ PEMs. For the GOx PEMs too a positive percentage change in nanofilm thicknesses was observed.

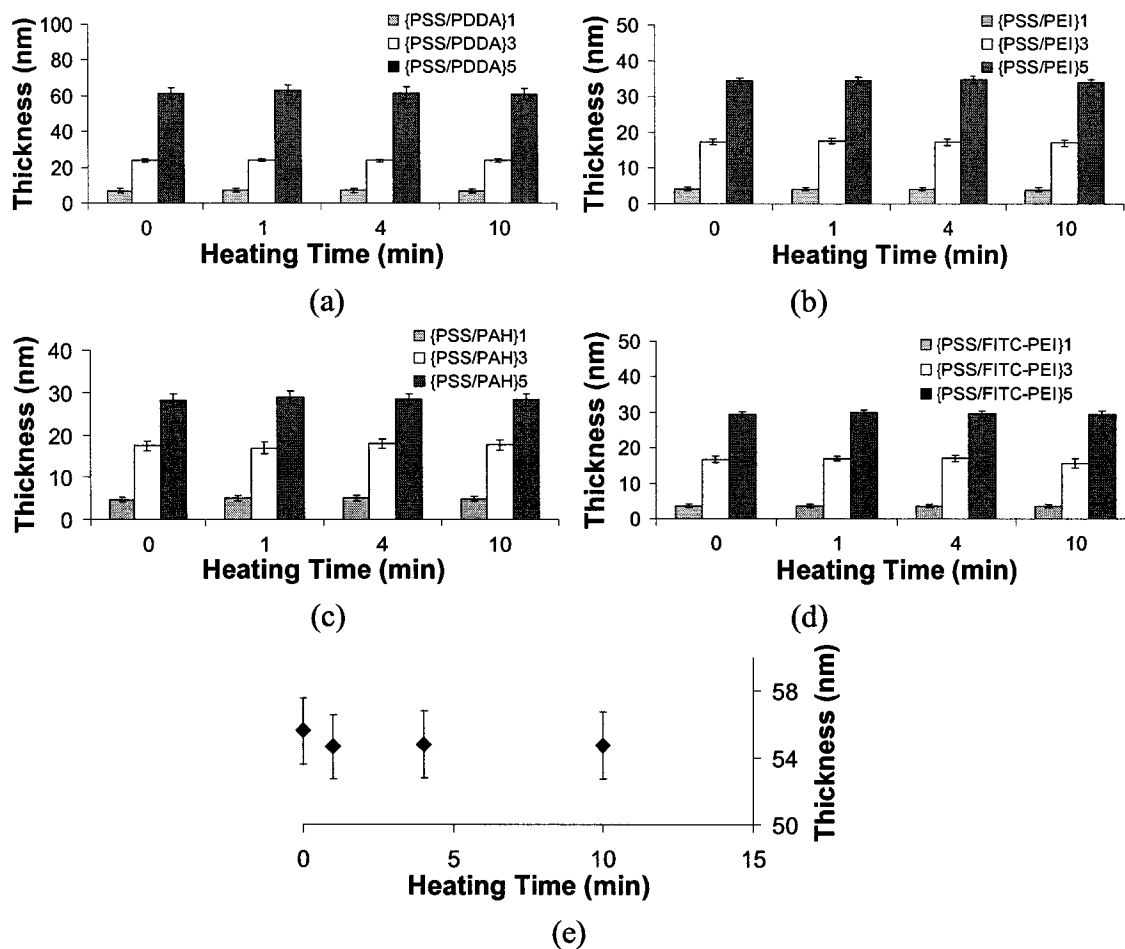


Figure 41. Ellipsometric measurements of nanofilm thickness: Effect of heating time at 115 °C on PEMs of (a) PSS/PDDA, (b) PSS/PEI, (c) PSS/PAH, (d) PSS/FITC-PEI, (e) GOx.

The $\{PSS/PAH\}_1$ nanofilms have the highest value of $\sim 6.05\%$ for the percentage change in thickness, whereas $\{PSS/FITC-PEI\}_5$ nanofilms have the lowest value of 0.10% . However, it is clear from *t*-test that heating at a temperature of 115 °C does not have significant effect on the thicknesses of the different nanofilms presented here.

6.4.1.4 Effect of photoresist-S1813 on nanofilm thickness

Figure 42 contains the thickness data for different nanofilms coated with photoresist-S1813 and removed using acetone for 15 s, and obtained from the

ellipsometric measurements. Figure 42(a), 42(b), 42(c), 42(d) contain the thickness data for 1-, 3-, and 5-bilayer PEMs of PSS/PDDA, PSS/PEI, PSS/PAH, PSS/FITC-PEI, respectively. Similar to the data presented in Figures 39(a)-39(d), the percentage change of nanofilm thicknesses after 1-coating as compared with the initial condition was highest for the 1-bilayer nanofilms, and decreased with the increase in number of bilayers. However, for all nanofilms negative percentage changes in nanofilm thicknesses were observed here.

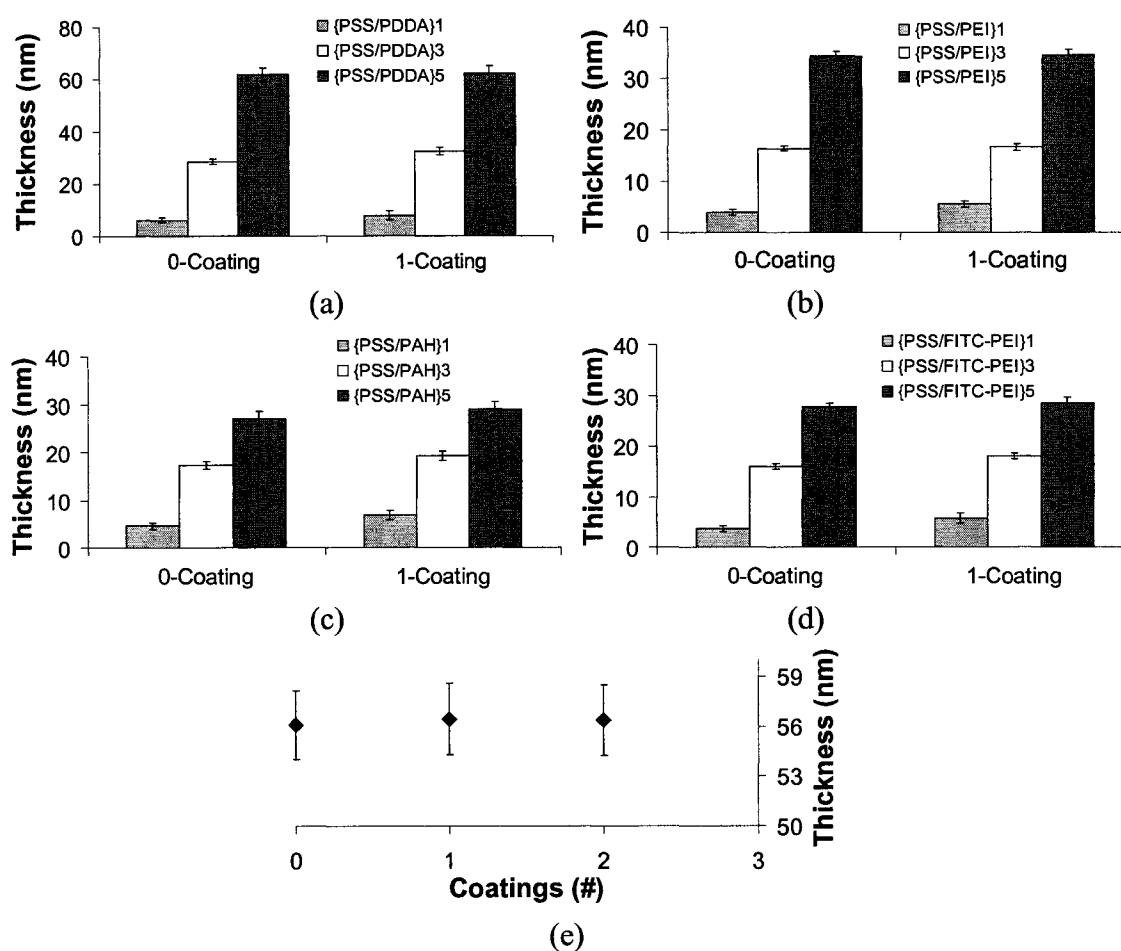


Figure 42. Ellipsometric measurements of nanofilm thickness: Effect of photoresist-S1813 on PEMs of (a) PSS/PDDA, (b) PSS/PEI, (c) PSS/PAH, (d) PSS/FITC-PEI, (e) GOx.

Figure 42(e) contains the thickness data for {GOx/PEI}₄/GOx PEMs. For the GOx PEMs too a negative percentage change in nanofilm thicknesses was observed. These nanofilms have the least value of ~0.46% for the percentage change in thickness. The {PSS/FITC-PEI}₁ nanofilms have the highest value of ~56.79% for the percentage change in thickness. However, it is clear from *t*-test that S1813 coating has no significant effect on the thicknesses of the different nanofilms presented here. This is an expected result, as evident from results shown in Chapters 3 through 5.

In summary, it can be stated that the effect of the different process parameters on the thicknesses of different nanofilms varies for different polyion pairs. One main reason for this behavior could be the charge of the polyions, in general, and the nature of the terminating layer. Strongly charged polyions such as PSS, PDDA, and PEI form highly stable nanofilms, whereas weakly charged polyions such as PAH and PAA are stable in narrow pH ranges. Moreover, it has been shown that multilayer nanofilms ending with a strong polyion are more stable as compared with those ending with a weak polyion.²⁸³ In addition, from all the above results it is clear that the labeling of polyelectrolytes results in lower thicknesses of nanofilms compared with nanofilms of similar unlabeled polyelectrolyte. Labeling of polyelectrolytes with fluorophores reduces the net charge of the material due to reduced ionizable side groups on the molecules. The low standard deviations indicate that the nanofilms are uniform across the substrates.

6.4.2 Effect of Processes on Fluorescence Intensity of Nanofilms

6.4.2.1 Effect of acetone on fluorescence intensity of nanofilms

Figure 43 contains the fluorescence intensity data for different nanofilms exposed to acetone obtained from the quantitative fluorescence microscopy measurements. Figure 43(a) contains the fluorescence intensity data for 1-, 3-, and 5-bilayers of PSS/FITC-PEI PEMs. Figure 43(b) contains the fluorescence intensity data for 1-, 3-, and 5-bilayers of PSS/FITC-PAH PEMs. For the data presented in Figures 43(a) and 43(b), the percentage change of fluorescence intensity of the nanofilms after the maximum exposure time (480 s) as compared with the initial condition was highest for the 1-bilayer nanofilms, and decreased with the increase in number of bilayers. For both nanofilm types, positive percentage changes in fluorescence intensity of the nanofilms were observed. The {PSS/FITC-PEI}₅ nanofilms have the least value of ~11.83% for the percentage change in fluorescence intensity of the nanofilms, whereas the {PSS/FITC-PAH}₁ nanofilms ($p = 0.017$) have the highest value of ~62.09%. It is clear from the plots and *t*-test that acetone does affect the fluorescence intensity of nanofilms of certain polyion pairs.

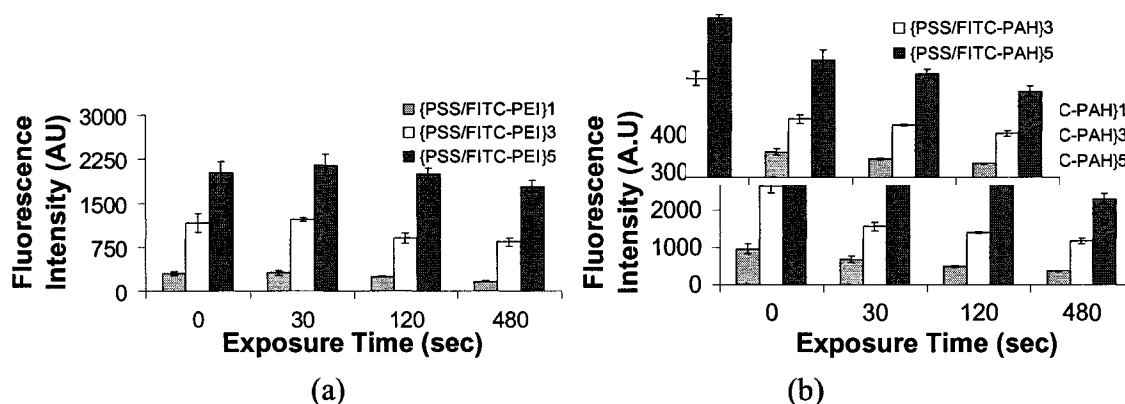


Figure 43. Quantitative measurements of fluorescence intensity of nanofilms: Effect of acetone on PEMs of (a) PSS/FITC-PEI, (b) PSS/FITC-PAH.

6.4.2.2 Effect of resist developer-MF319 on fluorescence intensity of nanofilms

Figure 44 contains the fluorescence intensity data for different nanofilms exposed to resist developer-MF319 obtained from the quantitative fluorescence microscopy measurements. Figure 44(a) and 44(b) contain the fluorescence intensity data for 1-, 3-, and 5-bilayers of PSS/FITC-PEI and PSS/FITC-PAH PEMs, respectively. For the data presented in Figures 44(a) and 44(b), the percentage change of fluorescence intensity of the nanofilms after the maximum exposure time (30 s) as compared with the initial condition was lowest for the 1-bilayer nanofilms, and increased with the increase in number of bilayers. For both nanofilm types positive percentage changes in fluorescence intensity of the nanofilms were observed. The {PSS/FITC-PEI}₁ nanofilms have the least value of ~17.36% for the percentage change in fluorescence intensity of the nanofilms, whereas the {PSS/FITC-PAH}₅ nanofilms ($p = 0.0002$) have the highest value of ~76.63%. It is clear from the plots and t -test that MF319 significantly affects the fluorescence intensity of nanofilms of certain polyion pairs.

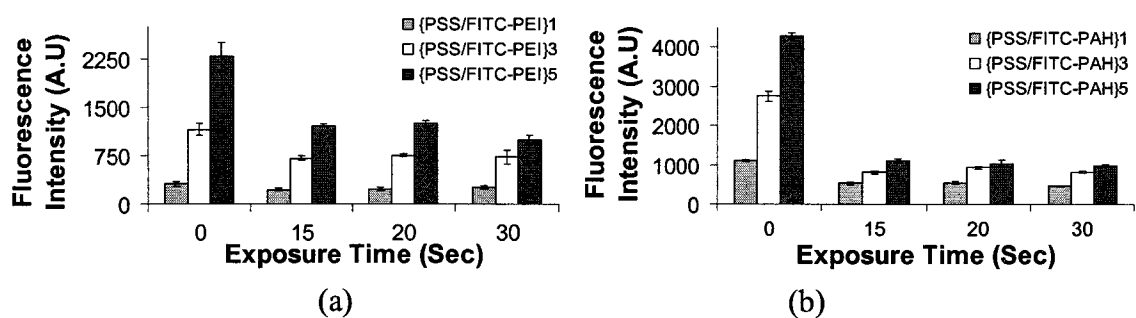


Figure 44. Quantitative measurements of fluorescence intensity of nanofilms: Effect of resist developer-MF319 on PEMs of (a) PSS/FITC-PEI, (b) PSS/FITC-PAH.

6.4.2.3 Effect of heating time at 115 °C on fluorescence intensity of nanofilms

Figure 45 contains the fluorescence intensity data for different nanofilms heated at a temperature of 115 °C obtained from the quantitative fluorescence microscopy measurements. Figure 45(a) and 45(b) contain the fluorescence intensity data for 1-, 3-, and 5-bilayers of PSS/FITC-PEI and PSS/FITC-PAH PEMs, respectively. For the data presented in Figures 45(a) and 45(b), the percentage change of fluorescence intensity of the nanofilms after the maximum heating time (10 min) as compared with the unheated condition was highest for the 1-bilayer nanofilms, and decreased with the increase in number of bilayers. The {PSS/FITC-PAH}₃ nanofilms have the least value of ~3.05% for the percentage change in fluorescence intensity of the nanofilms, whereas the {PSS/FITC-PEI}₁ nanofilms ($p = 0.0238$) have the highest value of ~21.02%. It is clear from the plots and *t*-test that heating at a temperature of 115 °C does not significantly affect the fluorescence intensity of nanofilms presented here.

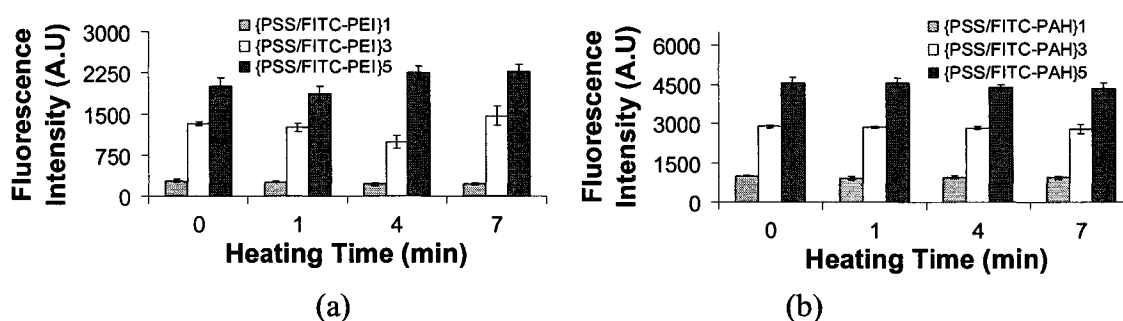


Figure 45. Quantitative measurements of fluorescence intensity of nanofilms: Effect of heating time at 115 °C on PEMs of (a) PSS/FITC-PEI, (b) PSS/FITC-PAH.

6.4.2.4 Effect of photoresist-S1813 on fluorescence intensity of nanofilms

Figure 46 contains the fluorescence intensity data for different nanofilms coated with photoresist-S1813 and removed using acetone for 15 s, and obtained from the quantitative fluorescence microscopy measurements. Figure 46(a) and 46(b) contain the fluorescence intensity data for 1-, 3-, and 5-bilayers of PSS/FITC-PEI and PSS/FITC-PAH PEMs, respectively. For the data presented in Figures 46(a) and 46(b), positive percentage changes in fluorescence intensity of the nanofilms after 1-coating as compared with the initial condition were observed. The $\{\text{PSS/FITC-PEI}\}_1$ nanofilms have the least value of $\sim 4.98\%$ for the percentage change in fluorescence intensity of the nanofilms, whereas the $\{\text{PSS/FITC-PAH}\}_3$ nanofilms ($p = 0.002$) have the highest value of $\sim 58.06\%$. It is clear from the plots and t -test that S1813 coating does affect the fluorescence intensity of nanofilms of certain polyion pairs.

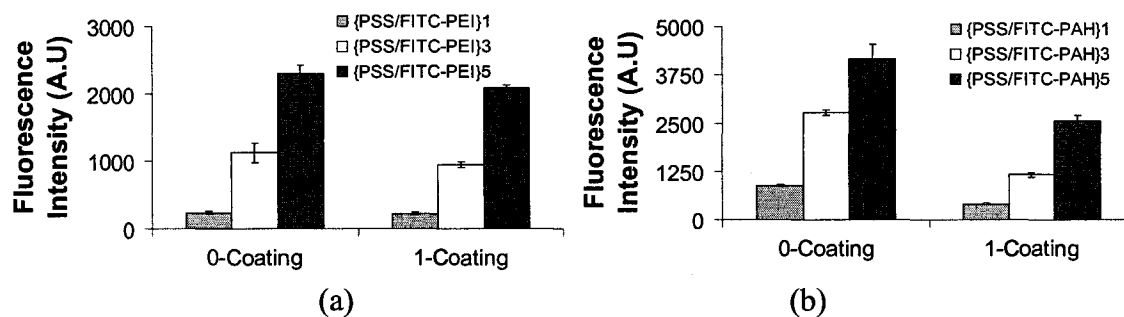


Figure 46. Quantitative measurements of fluorescence intensity of nanofilms: Effect of photoresist-S1813 on PEMs of (a) PSS/FITC-PEI, (b) PSS/FITC-PAH.

In summary, it can be stated that the effect of the different process parameters on the fluorescence intensity of different nanofilms varies for different polyion pairs. As discussed for the nanofilm thickness changes, one main reason for this behavior could be

the charge of the polyions. Labeling of polyelectrolytes with fluorophores further reduces the net charge of the polyion due to reduced charge sites on the polyion. From careful inspection of nanofilm thickness data presented in Figure 39(c), 40(c), 41(c), and 42(c) for PSS/PAH multilayers and the fluorescence intensity data presented in Figure 43(b), 44(b), 45(b), and 46(b) for PSS/PAH multilayers, it appears that the fluorescence intensity changes are due not only to nanofilm loss from the substrate and photobleaching but also to the changes in the local environment of the fluorophore, FITC, caused by the presence of chemicals such as acetone and MF319. Heating of the nanofilms did not cause significant change in the fluorescence intensity, except in the case of {PSS/FITC-PEI}₁. The low standard deviation values indicate that the fluorescence intensity of the nanofilms across the substrates is uniform. Here, FITC was used as model fluorophore due to its wide use in various applications; however, it could be replaced with more stable fluorophores.

6.4.3 Effect of Processes on Activity of Enzyme Nanofilms

Figure 47 contains the activity data for GOx embedded in PEM nanofilms under different processing conditions obtained from UV-Vis spectroscopy measurements. The GOx PEMs possess a multilayer architecture of {PSS/PDDA}₃/GOx/PEI₄/GOx. Figure 47(a), 47 (b), 47(c), 47(d) contain the activity data for GOx PEMs exposed to acetone, exposed to MF319, heated at a temperature of 115 °C, coated with S1813, respectively. The percentage changes in the activity of the GOx PEMs after the final value of a processing condition as compared with the initial condition are found to be ~93.45% for exposure to MF319, ~56.14% for exposure to acetone, ~46.32% for heating at 115 °C, and ~55.48% for coatings of S1813. From the activity data it is evident that the activity of

the enzyme embedded in the PEMs is significantly affected ($p = 0.0175$) by MF319. This decreased activity with exposure to MF319 is attributed to the disintegration of the GOx PEMs (as evident from results in Figure 40(e)) that leads to the quick release of the GOx from the PEMs and eventual denaturation. This hypothesis has been verified by testing the effect of MF319 on GOx solution, where $\sim 98.8\%$ decrease in enzyme activity was observed. In the case of other processing conditions, the GOx PEMs are comparatively intact and the GOx is physically immobile resulting in reduced denaturation. These results are in agreement with the observations made in Chapters 3 and 4, where even after multiple solvent and heating processes, the sPLA₂ enzyme retained its neuronal binding properties.

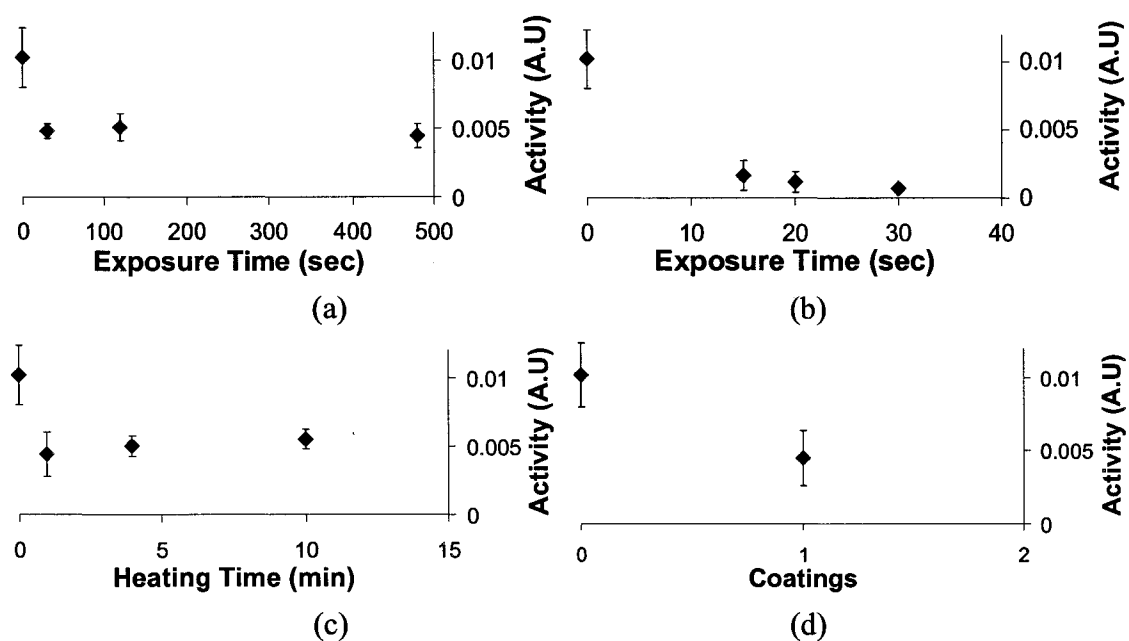


Figure 47. Quantitative measurements of activity of enzyme embedded in PEM nanofilms: Effect of (a) acetone, (b) resist developer-MF319, (c) heating time at 115 °C, (d) photoresist-S1813 on the activity of GOx.

6.4.4 Effect of Processes on Chemical Characteristics of Nanofilms

Substrates coated with 5-bilayer PEMs of PSS/PDDA, PSS/PEI, PSS/PAH, PSS/FITC-PEI were heated at a temperature of 115 °C, exposed to acetone, exposed to MF319, coated with S1813. In all cases, by comparing the ATR-FTIR spectra of the unprocessed nanofilm substrates to the spectra of the processed nanofilm substrates, it is observed that the net absorbance of the nanofilms and the intensities of the different characteristic bands of interest decreased, without introduction of new bands in the spectra of the processed nanofilms. From earlier metrological measurements of these nanofilms, this change in absorbance could mainly be attributed to the loss of the nanofilms. As a typical example, Figure 48 contains the ATR-FTIR spectra of {PSS/PAH}₅ nanofilms before (red spectrum) and after an exposure to MF319 for 30 s (blue spectrum), offset in *y*-axis for clarity. Regions of interest for these nanofilms are the absorption bands due to symmetric and antisymmetric -NH_3^+ deformations and aromatic ring modes, expected between 1,625 and 1,400 cm^{-1} and sulfonate absorbance bands, expected around 1,220, 1,175, 1,033, and 1,005 cm^{-1} (indicated by the arrows in Figure 48). Even though the intensities of the peaks are small for the native nanofilm to start with, it is clear that there is a reduction in the peak intensities after 30 s exposure to MF319. From the results in the preceding sections in the current section, it appears that the various seemingly harsh process parameters used in the PSM method affect the physical properties of the nanofilms of certain polyion pairs and do not show any obvious affects on their chemical characteristics. These changes in physical properties of the nanofilms should be taken into account while engineering 3D MNMs.

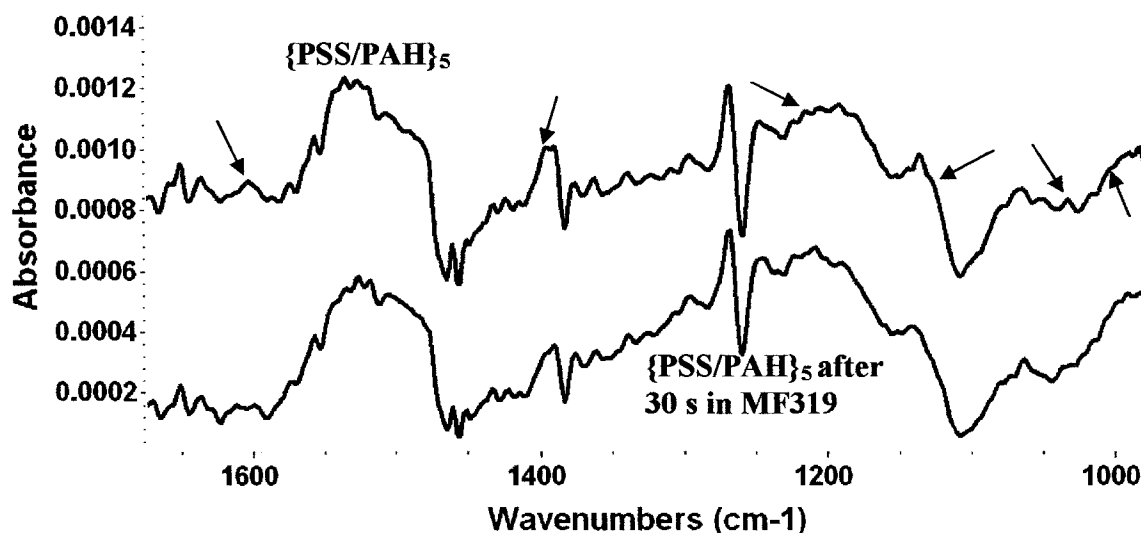


Figure 48. ATR-FTIR spectra of $\{PSS/PAH\}_5$ PEM nanofilms showing the effect of resist developer-MF319 on the characteristic bands of interest (indicated by the arrows).

6.4.5 Temporal Stability of Nanofilm Thickness

Figure 49 contains the thickness data for different nanofilms obtained from ellipsometric measurements at different time intervals over a period of three weeks. Figure 49(a), 49(b), 49(c), 49(d) contain the thickness data obtained at different time intervals for 1-, 3-, and 5-bilayer PEMs of PSS/PDDA, PSS/PEI, PSS/PAH, PSS/FITC-PEI, respectively. Figure 49(e) contains the thickness data obtained at different time intervals for $\{PSS/PDDA\}_3/\{GOx/PEI\}_4/GOx$ PEMs. From Figure 49(a) it is clear that the 5-bilayer PEMs of PSS/PDDA are stable ($p \sim 0.9$) over a period of three weeks. The percentage change in thickness after three weeks as compared with the initial values for these nanofilms is 4.23%, the lowest among the PEMs studied here. Moreover, 1-bilayer PEMs of PSS/PEI and PSS/FITC-PEI are stable over the period of last two weeks. The percentage changes over the period of last two weeks for 1-bilayer PEMs of PSS/PEI and PSS/FITC-PEI are $\sim 11.25\%$ and $\sim 6.63\%$, respectively. The highest percentage changes

over a period of three weeks are shown by 1-bilayer PEMs of PSS/PDDA and PSS/PAH, which are $\sim 611.32\%$ and $\sim 667.19\%$, respectively.

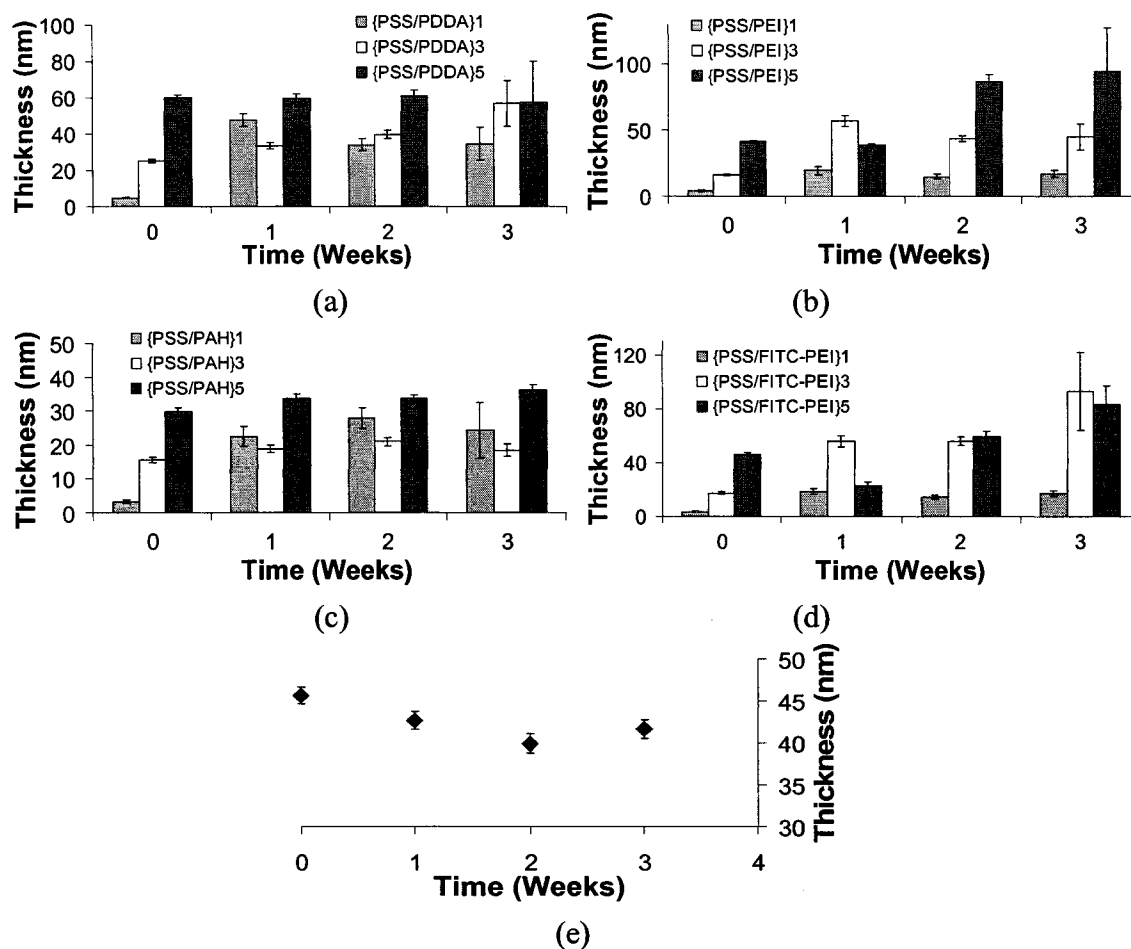


Figure 49. Ellipsometric measurements of nanofilm thickness: Temporal stability of (a) PSS/PDDA, (b) PSS/PEI, (c) PSS/PAH, (d) PSS/FITC-PEI, and (e) GOx PEMs in DI water.

Overall, among all the different nanofilms studied here for the different time intervals, $\{\text{PSS/PDDA}\}_1$ ($p = 0.0021$) have the highest percentage change of $\sim 880.66\%$ in thickness after one week and $\{\text{PSS/PDDA}\}_5$ ($p = 0.9779$) have the lowest percentage change of $\sim 0.12\%$ in thickness after one week. Also, after the first week, positive percentage changes in thickness of $\sim 880.66\%$, $\sim 379.56\%$, $\sim 609.46\%$, $\sim 412.26\%$ are

observed for 1-bilayer PEMs of PSS/PDDA, PSS/PEI, PSS/PAH, PSS/FITC-PEI, respectively. This swelling behavior could be attributed to the presence of salt in PEMs, hydration²⁸⁴ of the PEMs, and pH changes in the DI water in which the nanofilm coated substrates are placed. In general, PEMs have been treated either as densely packed hydrogels whose crosslinking density is controlled by the charge distribution along the chains or as glassy, quasi-frozen state.²⁸⁵ The densely packed hydrogel model could be used here to explain the swelling behavior of the PEMs; with the change in pH of the DI water and in the presence of NaCl salt, the charge distribution changes thereby changing the crosslinking density. Further, it has been shown that different polyion pairs exhibit different swelling behavior.^{284,286} From gross examination of the nanofilm surfaces of these substrates, it was seen that the nanofilm surfaces were rougher at week 1 as compared with at week 0. Also, as indicated by the standard deviations of the thicknesses, the uniformity of the nanofilm surfaces is decreasing over time.

6.4.6 Temporal Stability of Fluorescence Intensity of Nanofilms

Figure 50 contains the fluorescence intensity data for different nanofilms obtained from quantitative fluorescence measurements at different time intervals over a period of two weeks. Figure 50(a) and 50(b) contain the fluorescence intensity data obtained at different time intervals for 1-, 3-, and 5-bilayer PEMs of PSS/FITC-PEI and PSS/FITC-PAH, respectively. From the intensity measurements, it is seen that the percentage change in fluorescence intensity after two weeks as compared with the initial values is least for 1-bilayer PEMs of PSS/FITC-PEI, and increases with the number of bilayers. An opposite trend is observed in the case of PEMs of PSS/FITC-PAH, where the percentage change in fluorescence intensity after two weeks as compared with the initial values is

highest for 1-bilayer PEMs of PSS/FITC-PAH, and decreases with the number of bilayers. Overall, after two weeks, PEMs of $\{\text{PSS}/\text{FITC-PEI}\}_1$ have the lowest percentage change of $\sim 8.76\%$ in intensity and $\{\text{PSS}/\text{FITC-PAH}\}_1$ nanofilms ($p = 0.0054$) have the highest percentage change of $\sim 45.41\%$. As discussed in the preceding sections, this reduction in fluorescence intensity could be attributed to photobleaching, hydration of the PEMs, and denaturation of the fluorophores caused due to pH changes in the DI water in which the nanofilm coated substrates are placed. The low standard deviation values indicate that the fluorescence intensity of the nanofilms across the substrates is uniform even after two weeks immersion in DI water.

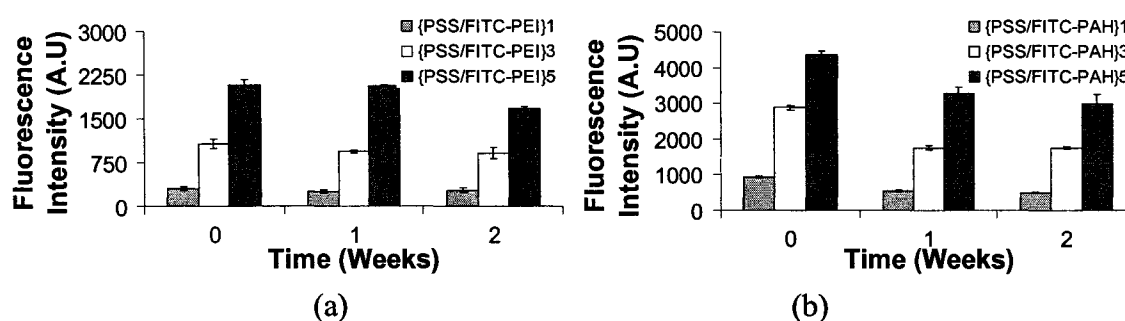


Figure 50. Quantitative measurements of fluorescence intensity of nanofilms: Temporal stability of (a) PSS/FITC-PEI and (b) PSS/FITC-PAH PEMs in DI water.

6.5 Conclusions

The effects of different process parameters involved in the PSM method including temperature and exposure to chemicals such as resist, acetone, and resist developer on the physicochemical properties of the multilayer nanofilms were studied for commonly used polyelectrolytes, including PSS, PDDA, PEI, PAH, FITC-PEI, and FITC-PAH, as well as a widely studied and well understood enzyme, GOx. The results from the ellipsometric, fluorescence microscopy, UV-Vis spectroscopy, and ATR-FTIR spectroscopy

measurements indicate that the physiochemical properties of the multicomponent multilayer micropatterns constructed using the PSM method are highly dependent on the polyion pairs used. Nevertheless, the versatile nature of the LbL assembly process allows the fine tuning of the multilayers. In general, acetone, heating, and S1813 have no significant effects on the nanofilms; whereas, due to its highly basic nature, MF319 does have significant effect on nanofilms of weakly charged polyions such as PAH. However, only the regions of nanofilms that are directly exposed to MF319 are affected, and not those regions that are protected by a photoresist coating. With these limited representative polyions tested here, it is believed that the PSM method will find applications in wide range of applications.

CHAPTER 7

CONCLUSIONS AND FUTURE WORK

7.1 Conclusions

In this dissertation, 3D multicomponent nanocomposite microstructures (3D MNMs) of polymers and colloidal nanoparticles have been constructed and characterized. The work presented here involves development of techniques for the fabrication of 3D MNMs, characterization of the 3D MNMs, applications of 3D MNMs, and evaluation of the process parameters involved in the developed techniques. These results clearly demonstrate the feasibility of the polymer 3D MNMs for biotechnological applications; specifically, they have potential as tailored surfaces for direct comparison of cell-material interactions on a single substrate, and for co-culture systems. In reality, the approach described here may enable study of and control over cell-biomaterial and cell-cell interactions in a whole new fashion. The techniques developed in this work represent a major advancement of nanoscale engineering through the integration of nanoscale LbL self-assembly and microscale photolithographic patterning for constructing 3D MNMs with varying physical and chemical properties in precise spatial arrangements. These techniques are analogous to surface micromachining, except that the deposition materials are polymers, biological materials, and colloidal nanoparticles that are used to produce 3D MNMs. The ability to finely tune the physical and chemical properties of the 3D

MNMs has also been demonstrated, and the resulting 3D MNMs have shown to influence the cell behavior. A major finding of this work, related to the applicability of the developed techniques, is that most of the seemingly harsh processes involved in constructing the 3D MNMs have minimal or no deleterious effects on the biological models used here. The exception is the resist developer (MF319) which, due to its highly basic nature, results in disintegration of nanofilms exposed to it directly. Nevertheless, the methods developed here are not limited by the photoresists and resist developers used here; biocompatible photoresists and aqueous-based developers could potentially be used. This work was pursued towards the development of organic and inorganic nanofilm scaffolds, which can eventually be combined to achieve functionality desired for specific applications.

The implications of this research work extend beyond the application examples studied here. In other biotechnological areas, the 3D MNMs could play an important role in stem cell research, as a tool to understand cues for proliferation, migration, and differentiation under different physicochemical conditions. Also, defined spatial arrangements of anchorage-dependent cells could create a high level of complexity in co-cultures and could be used as a tool for analyzing stem cell behavior in the presence of differentiated cells.^{146,162,164} Time-varying signals could also be easily presented to the cells by integrating biodegradable materials into the multilayer assembly process,¹⁰⁴⁻¹⁰⁷ thereby dynamically influencing the cell behavior. It is anticipated that the 3D MNMs developed in this work will provide general platforms for studying biological processes, which will not only impact stem cell research in general but also provide useful information in support of biomedical device development, and tissue engineering.

Although the intended purpose for developing 3D MNMs is to produce novel bioactive systems, their applicability is more general and may find use in a broad range of applications including electronics, photonics, optoelectronics, and chemical and biochemical sensors.

The novel contributions of the author to the field of science and engineering include the development of platform technique for constructing two-component polymer 3D MNMs on each half of a substrate; development of platform technique for constructing multicomponent microstructures of multilayer nanocomposite polymer and colloid films on a single substrate; illustrations of applications of these techniques to cell-related studies; and detailed analysis of the processes involved in the developed techniques.

7.2 Future Work

7.2.1 Dynamic Micropatterns of Biodegradable Nanofilms

The work presented in this dissertation focused on the precise spatial arrangement of physical and chemical cues that could be presented as the microenvironment for cells. However, the *in vivo* ECM environment is not static, it is dynamic. The *in vivo* environment of cells provides not only structural support and specific chemical properties for static interactions, but also provides temporally-varying signals that shape the formation and behavior of cells. Therefore, it would be appropriate to incorporate dynamic temporal nature in the multicomponent multilayer micropatterns by integrating biodegradable/decomposable materials and active/responsive biomaterials into the

multilayer assembly process, thereby dynamically influencing the cell behavior. This dynamic aspect would be highly useful in the current stem cell studies.

7.2.2 Co-culture Systems for Stem Cell Research

In Chapter 4, preliminary results on co-culture systems using the PSM method have been presented. However, as shown in the results in Chapter 4 and 5, the current method could accommodate more than two-materials and should be used to create a high level of complexity in co-culture systems. Studies of cell-cell communication and engineering of functional tissues are two areas that benefit from co-culture of multiple cell types. Such co-cultures may also prove a useful tool for analyzing stem cell behavior under various bio-physicochemical conditions.

REFERENCES

- ¹ <http://www.nano.gov/html/facts/whatIsNano.html>.
- ² A. Magnani, A. Priamo, D. Pasqui, and R. Barbucci, "Cell behaviour on chemically microstructured surfaces," *Materials Science and Engineering C*, vol. 23, pp. 315, 2003.
- ³ R. S. Kane, S. Takayama, E. Ostuni, D. E. Ingber, and G. M. Whitesides, "Patterning proteins and cells using soft lithography," *Biomaterials*, vol. 20, pp. 2363, 1999.
- ⁴ N. M. Dowell-Mesfin, M. A. Abdul-Karim, A. M. P. Turner, S. Schanz, H. G. Craighead, B. Roysam, J. N. Turner, and W. Shain, "Topographically modified surfaces affect orientation and growth of hippocampal neurons," *Journal of Neural Engineering*, vol. 1, pp. 78, 2004.
- ⁵ G. Szebenyi, E. W. Dent, J. L. Callaway, C. Seys, H. Lueth, and K. Kalil, "Fibroblast Growth Factor-2 Promotes Axon Branching of Cortical Neurons by Influencing Morphology and Behavior of the Primary Growth Cone," *J. Neurosci.*, vol. 21, pp. 3932-3941, 2001.
- ⁶ L. Decker, W. Baron, and C. Ffrench-Constant, "Lipid rafts: microenvironments for integrin-growth factor interactions in neural development," *Biochem Soc Trans*, vol. 32, pp. 426-30, 2004.
- ⁷ S. Svedhem, D. Dahlborg, J. Ekeröth, J. Kelly, F. Hook, and J. Gold, "In Situ Peptide-Modified Supported Lipid Bilayers for Controlled Cell Attachment," *Langmuir*, vol. 19, pp. 6730-6736, 2003.
- ⁸ L. Richert, P. Lavalle, D. Vautier, B. Senger, J. F. Stoltz, P. Schaaf, J. C. Voegel, and C. Picart, "Cell Interactions with Polyelectrolyte Multilayer Films," *Biomacromolecules*, vol. 3, pp. 1170-1178, 2002.
- ⁹ B. D. Boyan, S. Lossdorfer, L. Wang, G. Zhao, C. H. Lohmann, D. L. Cochran, and Z. Schwartz, "Osteoblasts generate an osteogenic microenvironment when grown on surfaces with rough microtopographies," *Eur Cell Mater*, vol. 6, pp. 22-7, 2003.

- ¹⁰ J. L. Tan, J. Tien, D. M. Pirone, D. S. Gray, K. Bhadriraju, and C. S. Chen, "From the Cover: Cells lying on a bed of microneedles: An approach to isolate mechanical force," *PNAS*, vol. 100, pp. 1484-1489, 2003.
- ¹¹ K. K. Parker, A. L. Brock, C. Brangwynne, R. J. Mannix, N. Wang, E. Ostuni, N. A. Geisse, J. C. Adams, G. M. Whitesides, and D. E. Ingber, "Directional control of lamellipodia extension by constraining cell shape and orienting cell tractional forces," *FASEB J*, vol. 16, pp. 1195-1204, 2002.
- ¹² A. Brock, E. Chang, C.-C. Ho, P. LeDuc, X. Jiang, G. M. Whitesides, and D. E. Ingber, "Geometric determinants of directional cell motility revealed using microcontact printing," *Langmuir*, vol. 19, pp. 1611, 2003.
- ¹³ C. G. Galbraith, K. M. Yamada, and M. P. Sheetz, "The relationship between force and focal complex development," *J. Cell Biol.*, vol. 159, pp. 695-705, 2002.
- ¹⁴ N. Q. Balaban, U. S. Schwarz, D. Riveline, P. Goichberg, G. Tzur, I. Sabanay, D. Mahalu, S. Safran, A. Bershadsky, L. Addadi, and B. Geiger, "Force and focal adhesion assembly: a close relationship studied using elastic micropatterned substrates," *Nat Cell Biol*, vol. 3, pp. 466-72, 2001.
- ¹⁵ D. E. Discher, P. Janmey, and Y.-l. Wang, "Tissue Cells Feel and Respond to the Stiffness of Their Substrate," *Science*, vol. 310, pp. 1139-1143, 2005.
- ¹⁶ A. J. Engler, M. A. Griffin, S. Sen, C. G. Bonnemann, H. L. Sweeney, and D. E. Discher, "Myotubes differentiate optimally on substrates with tissue-like stiffness: pathological implications for soft or stiff microenvironments," *J. Cell Biol.*, vol. 166, pp. 877-887, 2004.
- ¹⁷ P. D. Arora, N. Narani, and C. A. G. McCulloch, "The Compliance of Collagen Gels Regulates Transforming Growth Factor- β Induction of α -Smooth Muscle Actin in Fibroblasts," *Am. J. Pathol.*, vol. 154, pp. 871-882, 1999.
- ¹⁸ T. Yeung, P. C. Georges, L. A. Flanagan, B. Marg, M. Ortiz, M. Funaki, N. Zahir, W. Ming, V. Weaver, and P. A. Janmey, "Effects of substrate stiffness on cell morphology, cytoskeletal structure, and adhesion," *Cell Motility and the Cytoskeleton*, vol. 60, pp. 24-34, 2005.
- ¹⁹ E. Brynda, J. Pachernik, M. Houska, Z. Pientka, and P. Dvorak, "Surface immobilized protein multilayers for cell seeding," *Langmuir*, vol. 21, pp. 7877-83, 2005.
- ²⁰ T. Wang, G. Dang, Z. Guo, and M. Yang, "Evaluation of autologous bone marrow mesenchymal stem cell-calcium phosphate ceramic composite for lumbar fusion in rhesus monkey interbody fusion model," *Tissue Eng*, vol. 11, pp. 1159-67, 2005.

- 21 T. Yamasaki, M. Deie, R. Shinomiya, Y. Izuta, Y. Yasunaga, S. Yanada, P. Sharman, and M. Ochi, "Meniscal regeneration using tissue engineering with a scaffold derived from a rat meniscus and mesenchymal stromal cells derived from rat bone marrow," *J Biomed Mater Res A*, vol. 75, pp. 23-30, 2005.
- 22 Y. Takahashi, M. Yamamoto, and Y. Tabata, "Osteogenic differentiation of mesenchymal stem cells in biodegradable sponges composed of gelatin and beta-tricalcium phosphate," *Biomaterials*, vol. 26, pp. 3587-96, 2005.
- 23 F. W. H. Sutherland, T. E. Perry, Y. Yu, M. C. Sherwood, E. Rabkin, Y. Masuda, G. A. Garcia, D. L. McLellan, G. C. Engelmayr, Jr., M. S. Sacks, F. J. Schoen, and J. E. Mayer, Jr., "From Stem Cells to Viable Autologous Semilunar Heart Valve," *Circulation*, vol. 111, pp. 2783-2791, 2005.
- 24 H. Huang, Y. Nakayama, K. Qin, K. Yamamoto, J. Ando, J. Yamashita, H. Itoh, K. Kanda, H. Yaku, Y. Okamoto, and Y. Nemoto, "Differentiation from embryonic stem cells to vascular wall cells under in vitro pulsatile flow loading," *J Artif Organs*, vol. 8, pp. 110-8, 2005.
- 25 J. D. Mendelsohn, S. Y. Yang, J. A. Hiller, A. I. Hochbaum, and M. F. Rubner, "Rational design of cytophilic and cytophobic polyelectrolyte multilayer thin films," *Biomacromolecules*, vol. 4, pp. 96, 2003.
- 26 T. Pompe, S. Zschoche, N. Herold, K. Salchert, M. F. Gouzy, C. Sperling, and C. Werner, "Maleic Anhydride Copolymers-A Versatile Platform for Molecular Biosurface Engineering," *Biomacromolecules*, vol. 4, pp. 1072-1079, 2003.
- 27 H. Kim, J. Doh, D. J. Irvine, R. E. Cohen, and P. T. Hammond, "Large area two-dimensional B cell arrays for sensing and cell-sorting applications," *Biomacromolecules*, vol. 5, pp. 822, 2004.
- 28 D. R. Marshak, R. L. Gardner, and D. Gottlieb, *Stem Cell Biology*. Cold Spring Harbor, New York: Cold Spring Harbor Laboratory, 2001.
- 29 C. S. Chen, M. Mrksich, S. Huang, G. M. Whitesides, and D. E. Ingber, "Geometric Control of Cell Life and Death," *Science*, vol. 276, pp. 1425-1428, 1997.
- 30 G. E. Rutkowski, C. A. Miller, S. Jeftinija, and S. K. Mallapragada, "Synergistic effects of micropatterned biodegradable conduits and Schwann cells on sciatic nerve regeneration," *J Neural Eng*, vol. 1, pp. 151-7, 2004.
- 31 R. G. Nuzzo and D. L. Allara, "Adsorption of bifunctional organic disulfides on gold surfaces," *J. Am. Chem. Soc.*, vol. 105, pp. 4481-4483, 1983.
- 32 Y. Xia and G. M. Whitesides, "Soft Lithography," *Annual Review of Materials Science*, vol. 28, pp. 153-184, 1998.

- ³³ N. S. Sampson, M. Mrksich, and C. R. Bertozzi, "Surface molecular recognition," *PNAS*, vol. 98, pp. 12870-12871, 2001.
- ³⁴ D. H. Lee, D. Kim, T. Oh, and K. Cho, "Phase state effect on adhesion behavior of self-assembled monolayers," *Langmuir*, vol. 20, pp. 8124-30, 2004.
- ³⁵ M. Mrksich, "A surface chemistry approach to studying cell adhesion," *Chem. Soc. Rev.*, vol. 4, pp. 267-273, 2000.
- ³⁶ M. Kato and M. Mrksich, "Rewiring cell adhesion," *Journal of the American Chemical Society*, vol. 126, pp. 6504, 2004.
- ³⁷ M. Mrksich, "Tailored substrates for studies of attached cell culture," *Cell Mol Life Sci*, vol. 54, pp. 653-62, 1998.
- ³⁸ Y.-Y. Luk, M. Kato, and M. Mrksich, "Self-assembled monolayers of alkanethiolates presenting mannitol groups are inert to protein adsorption and cell attachment," *Langmuir*, vol. 16, pp. 9604, 2000.
- ³⁹ J. Tien, Y. Xia, and G. M. Whitesides, "Thin Films," pp. 227-253, 1998.
- ⁴⁰ J. Tien, C. M. Nelson, and C. S. Chen, "From the Cover: Fabrication of aligned microstructures with a single elastomeric stamp," *PNAS*, vol. 99, pp. 1758-1762, 2002.
- ⁴¹ J. L. Tan, J. Tien, and C. S. Chen, "Microcontact printing of proteins on mixed self-assembled monolayers," *Langmuir*, vol. 18, pp. 519, 2002.
- ⁴² C. Roberts, C. S. Chen, M. Mrksich, V. Martichonok, D. E. Ingber, and G. M. Whitesides, "Using mixed self-assembled monolayers presenting RGD and (EG)₃OH groups to characterize long-term attachment of bovine capillary endothelial cells to surfaces," *Journal of the American Chemical Society*, vol. 120, pp. 6548, 1998.
- ⁴³ L. Yan, X.-M. Zhao, and G. M. Whitesides, "Patterning a preformed, reactive SAM using microcontact printing," *Journal of the American Chemical Society*, vol. 120, pp. 6179, 1998.
- ⁴⁴ M. N. Yousaf and M. Mrksich, "Diels-Alder Reaction for the Selective Immobilization of Protein to Electroactive Self-Assembled Monolayers," *J. Am. Chem. Soc.*, vol. 121, pp. 4286-4287, 1999.
- ⁴⁵ W. S. Dillmore, M. N. Yousaf, and M. Mrksich, "A photochemical method for patterning the immobilization of ligands and cells to self-assembled monolayers," *Langmuir*, vol. 20, pp. 7223, 2004.

- ⁴⁶ N. Li, A. Tourovskaia, and A. Folch, "Biology on a chip: microfabrication for studying the behavior of cultured cells," *Crit Rev Biomed Eng*, vol. 31, pp. 423-88, 2003.
- ⁴⁷ E. Ostuni, B. A. Grzybowski, M. Mrksich, C. S. Roberts, and G. M. Whitesides, "Adsorption of proteins to hydrophobic sites on mixed self-assembled monolayers," *Langmuir*, vol. 19, pp. 1861, 2003.
- ⁴⁸ D. Amber, K. R. Aithal, J. Roldan, D. Kuila, and D. K. Mills, "Growth and functionality of cells grown on self assembled monolayer," *J. In-Vitro Biol.*, vol. 40, pp. 200, 2004.
- ⁴⁹ K. R. Aithal, A. Doss, D. P. Kumaraswamy, D. K. Mills, and D. Kuila, "Growth and functionality of cells cultured on self assembled monolayers patterned on conducting and semi-conducting substrates," presented at Biomaterials in regenerative medicine: The advent of combination products, Philadelphia, 2004.
- ⁵⁰ S. Lodha and D. B. Janes, "Enhanced current densities in Au/molecule/GaAs devices," *Applied Physics Letters*, vol. 85, pp. 2809, 2004.
- ⁵¹ M. Mrksich, "What can surface chemistry do for cell biology?" *Curr Opin Chem Biol*, vol. 6, pp. 794-7, 2002.
- ⁵² M. N. Yousaf, B. T. Houseman, and M. Mrksich, "Using electroactive substrates to pattern the attachment of two different cell populations," *PNAS*, vol. 98, pp. 5992-5996, 2001.
- ⁵³ W.-S. Yeo and M. Mrksich, "Electroactive substrates that reveal aldehyde groups for bio-immobilization," *Advanced Materials*, vol. 16, pp. 1352, 2004.
- ⁵⁴ C. D. Hodneland and M. Mrksich, "Design of self-assembled monolayers that release attached groups using applied electrical potentials," *Langmuir*, vol. 13, pp. 6001, 1997.
- ⁵⁵ C. D. Hodneland and M. Mrksich, "Biomolecular surfaces that release ligands under electrochemical control," *Journal of the American Chemical Society*, vol. 122, pp. 4235, 2000.
- ⁵⁶ X. Jiang, R. Ferrigno, M. Mrksich, and G. M. Whitesides, "Electrochemical desorption of self-assembled monolayers noninvasively releases patterned cells from geometrical confinements," *Journal of the American Chemical Society*, vol. 125, pp. 2366, 2003.
- ⁵⁷ W. S. Yeo, C. D. Hodneland, and M. Mrksich, "Electroactive monolayer substrates that selectively release adherent cells," *ChemBiochem*, vol. 2, pp. 590-3, 2001.

- ⁵⁸ W.-S. Yeo, M. N. Yousaf, and M. Mrksich, "Dynamic Interfaces between Cells and Surfaces: Electroactive Substrates that Sequentially Release and Attach Cells," *Journal of the American Chemical Society*, vol. 125, pp. 14994, 2003.
- ⁵⁹ G. Decher and J. D. Hong, "Buildup of ultrathin multilayer films by a self-assembly process, 1. Consecutive adsorption of anionic and cationic bipolar amphiphiles on charged surfaces," *European Conference on Organized Organic Thin Films*, pp. 321, 1991.
- ⁶⁰ G. Decher and J. D. Hong, "Buildup of ultrathin multilayer films by a self-assembly process. II. Consecutive adsorption of anionic and cationic bipolar amphiphiles and polyelectrolytes on charged surfaces," *Berichte der Bunsengesellschaft fuer Physikalische Chemie*, vol. 95, pp. 1430, 1991.
- ⁶¹ S. Y. Yang, J. D. Mendelsohn, and M. F. Rubner, "New class of ultrathin, highly cell-adhesion-resistant polyelectrolyte multilayers with micropatterning capabilities," *Biomacromolecules*, vol. 4, pp. 987, 2003.
- ⁶² T. Serizawa, Y. Arikawa, K.-I. Hamada, H. Yamashita, T. Fujiwara, Y. Kimura, and M. Akashi, "Alkaline hydrolysis of enantiomeric poly(lactide)s stereocomplex deposited on solid substrates," *Macromolecules*, vol. 36, pp. 1762, 2003.
- ⁶³ V. Kozlovskaya, S. Ok, A. Sousa, M. Libera, and S. A. Sukhishvili, "Hydrogen-bonded polymer capsules formed by layer-by-layer self-assembly," *Macromolecules*, vol. 36, pp. 8590, 2003.
- ⁶⁴ J.-i. Anzai, Y. Kobayashi, N. Nakamura, M. Nishimura, and T. Hoshi, "Layer-by-layer construction of multilayer thin films composed of avidin and biotin-labeled poly(amine)s," *Langmuir*, vol. 15, pp. 221, 1999.
- ⁶⁵ D. Vautier, V. Karsten, C. Egles, J. Chluba, P. Schaaf, J. C. Voegel, and J. Ogier, "Polyelectrolyte multilayer films modulate cytoskeletal organization in chondrosarcoma cells," *J Biomater Sci Polym Ed*, vol. 13, pp. 713-32, 2002.
- ⁶⁶ M. Fang, P. S. Grant, M. J. McShane, G. B. Sukhorukov, V. O. Golub, and Y. M. Lvov, "Magnetic bio/nanoreactor with multilayer shells of glucose oxidase and inorganic nanoparticles," *Langmuir*, vol. 18, pp. 6338, 2002.
- ⁶⁷ J. Chluba, J. C. Voegel, G. Decher, P. Erbacher, P. Schaaf, and J. Ogier, "Peptide Hormone Covalently Bound to Polyelectrolytes and Embedded into Multilayer Architectures Conserving Full Biological Activity," *Biomacromolecules*, vol. 2, pp. 800-805, 2001.
- ⁶⁸ L. Szyk, P. Schwinte, J. C. Voegel, P. Schaaf, and B. Tinland, "Dynamical behavior of human serum albumin adsorbed on or embedded in polyelectrolyte multilayers," *Journal of Physical Chemistry B*, vol. 106, pp. 6049, 2002.

- ⁶⁹ L. Szyk, P. Schaaf, C. Gergely, J. C. Voegel, and B. Tinland, "Lateral mobility of proteins adsorbed on or embedded in polyelectrolyte multilayers," *Langmuir*, vol. 17, pp. 6248, 2001.
- ⁷⁰ M. Michel, A. Izquierdo, G. Decher, J. C. Voegel, P. Schaaf, and V. Ball, "Layer by Layer Self-Assembled Polyelectrolyte Multilayers with Embedded Phospholipid Vesicles Obtained by Spraying: Integrity of the Vesicles," *Langmuir*, vol. 21, pp. 7854-7859, 2005.
- ⁷¹ M. Michel, D. Vautier, J.-C. Voegel, P. Schaaf, and V. Ball, "Layer by layer self-assembled polyelectrolyte multilayers with embedded phospholipid vesicles," *Langmuir*, vol. 20, pp. 4835, 2004.
- ⁷² P. Schwinte, V. Ball, B. Szalontai, Y. Haikel, J. C. Voegel, and P. Schaaf, "Secondary Structure of Proteins Adsorbed onto or Embedded in Polyelectrolyte Multilayers," *Biomacromolecules*, vol. 3, pp. 1135-1143, 2002.
- ⁷³ N. Jessel, F. Atalar, P. Lavalle, J. Mutterer, G. Decher, P. Schaaf, J.-C. Voegel, and J. Ogier, "Bioactive coatings based on a polyelectrolyte multilayer architecture functionalized by embedded proteins," *Advanced Materials*, vol. 15, pp. 692, 2003.
- ⁷⁴ B. Thierry, F. M. Winnik, Y. Merhi, J. Silver, and M. Tabrizian, "Bioactive coatings of endovascular stents based on polyelectrolyte multilayers," *Biomacromolecules*, vol. 4, pp. 1564, 2003.
- ⁷⁵ H. Zhu, J. Ji, and J. Shen, "Construction of multilayer coating onto poly-(DL-lactide) to promote cytocompatibility," *Biomaterials*, vol. 25, pp. 109, 2004.
- ⁷⁶ P. S. Grant and M. J. McShane, "Development of multilayer fluorescent thin film chemical sensors using electrostatic self-assembly," *IEEE Sensors Journal*, vol. 3, pp. 139, 2003.
- ⁷⁷ J. Lukkari, M. Salomaki, A. Viinikanoja, T. Aaritalo, J. Paukkunen, N. Kocharova, and J. Kankare, "Polyelectrolyte multilayers prepared from water-soluble poly(alkoxythiophene) derivatives," *Journal of the American Chemical Society*, vol. 123, pp. 6083, 2001.
- ⁷⁸ R. Nagarajan, W. Liu, J. Kumar, S. K. Tripathy, F. F. Bruno, and L. A. Samuelson, "Manipulating DNA Conformation Using Intertwined Conducting Polymer Chains," *Macromolecules*, vol. 34, pp. 3921-3927, 2001.
- ⁷⁹ D. Yoo, S. S. Shiratori, and M. F. Rubner, "Controlling bilayer composition and surface wettability of sequentially adsorbed multilayers of weak polyelectrolytes," *Macromolecules*, vol. 31, pp. 4309, 1998.

- ⁸⁰ S. S. Shiratori and M. F. Rubner, "pH-dependent thickness behavior of sequentially adsorbed layers of weak polyelectrolytes," *Macromolecules*, vol. 33, pp. 4213, 2000.
- ⁸¹ N. G. Hoogeveen, M. A. Cohen Stuart, G. J. Fler, and M. R. Bohmer, "Formation and Stability of Multilayers of Polyelectrolytes," *Langmuir*, vol. 12, pp. 3675-3681, 1996.
- ⁸² L. Kolarik, D. N. Furlong, H. Joy, C. Struijk, and R. Rowe, "Building Assemblies from High Molecular Weight Polyelectrolytes," *Langmuir*, vol. 15, pp. 8265-8275, 1999.
- ⁸³ R. Steitz, W. Jaeger, and R. v. Klitzing, "Influence of Charge Density and Ionic Strength on the Multilayer Formation of Strong Polyelectrolytes," *Langmuir*, vol. 17, pp. 4471-4474, 2001.
- ⁸⁴ K. Glinel, A. Moussa, A. M. Jonas, and A. Laschewsky, "Influence of Polyelectrolyte Charge Density on the Formation of Multilayers of Strong Polyelectrolytes at Low Ionic Strength," *Langmuir*, vol. 18, pp. 1408-1412, 2002.
- ⁸⁵ B. Schoeler, G. Kumaraswamy, and F. Caruso, "Investigation of the influence of polyelectrolyte charge density on the growth of multilayer thin films prepared by the layer-by-layer technique," *Macromolecules*, vol. 35, pp. 889, 2002.
- ⁸⁶ G. Decher, J. D. Hong, and J. Schmitt, "Buildup of ultrathin multilayer films by a self-assembly process: III. Consecutively alternating adsorption of anionic and cationic polyelectrolytes on charged surfaces," *Thin Solid Films*, vol. 210-211, pp. 831, 1992.
- ⁸⁷ M. Losche, J. Schmitt, G. Decher, W. G. Bouwman, and K. Kjaer, "Detailed Structure of Molecularly Thin Polyelectrolyte Multilayer Films on Solid Substrates as Revealed by Neutron Reflectometry," *Macromolecules*, vol. 31, pp. 8893-8906, 1998.
- ⁸⁸ S. T. Dubas and J. B. Schlenoff, "Factors Controlling the Growth of Polyelectrolyte Multilayers," *Macromolecules*, vol. 32, pp. 8153-8160, 1999.
- ⁸⁹ G. Ladam, P. Schaad, J. C. Voegel, P. Schaaf, G. Decher, and F. Cuisinier, "In situ determination of the structural properties of initially deposited polyelectrolyte multilayers," *Langmuir*, vol. 16, pp. 1249, 2000.
- ⁹⁰ J. Ruths, F. Essler, G. Decher, and H. Riegler, "Polyelectrolytes I: Polyanion/Polycation Multilayers at the Air/Monolayer/Water Interface as Elements for Quantitative Polymer Adsorption Studies and Preparation of Hetero-superlattices on Solid Surfaces," *Langmuir*, vol. 16, pp. 8871-8878, 2000.

- ⁹¹ M. Li, D. K. Mills, T. Cui, and M. J. McShane, "Cellular response to gelatin- and fibronectin-coated multilayer polyelectrolyte nanofilms," *IEEE Transactions on Nanobioscience*, vol. 4, pp. 170, 2005.
- ⁹² H. Ai, H. Meng, I. Ichinose, S. A. Jones, D. K. Mills, Y. M. Lvov, and X. Qiao, "Biocompatibility of layer-by-layer self-assembled nanofilm on silicone rubber for neurons," *J Neurosci Methods*, vol. 128, pp. 1-8, 2003.
- ⁹³ C. Vodouhe, M. Schmittbuhl, F. Boulmedais, D. Bagnard, D. Vautier, P. Schaaf, C. Egles, J.-C. Voegel, and J. Ogier, "Effect of functionalization of multilayered polyelectrolyte films on motoneuron growth," *Biomaterials*, vol. 26, pp. 545, 2005.
- ⁹⁴ N. B. Jessel, P. Schwinte, R. Donohue, P. Lavallo, F. Boulmedais, R. Darcy, B. Szalontai, J.-C. Voegel, and J. Ogier, "Pyridylamino- β -cyclodextrin as a molecular chaperone for lipopolysaccharide embedded in a multilayered polyelectrolyte architecture," *Advanced Functional Materials*, vol. 14, pp. 963, 2004.
- ⁹⁵ D. R. Reyes, E. M. Perruccio, S. P. Becerra, L. E. Locascio, and M. Gaitan, "Micropatterning neuronal cells on polyelectrolyte multilayers," *Langmuir*, vol. 20, pp. 8805, 2004.
- ⁹⁶ L. Richert, A. J. Engler, D. E. Discher, and C. Picart, "Elasticity of native and cross-linked polyelectrolyte multilayer films," *Biomacromolecules*, vol. 5, pp. 1908, 2004.
- ⁹⁷ A. J. Nolte, M. F. Rubner, and R. E. Cohen, "Determining the Young's Modulus of Polyelectrolyte Multilayer Films via Stress-Induced Mechanical Buckling Instabilities," *Macromolecules*, vol. 38, pp. 5367-5370, 2005.
- ⁹⁸ S. Chinnayelka, H. Zhu, and M. McShane, "Fabrication of Hybrid Organo/Inorgano Polyelectrolyte Microcapsules and their Application in Biomaterial Encapsulation," *Adv. Mater.*, (Submitted).
- ⁹⁹ A. Schneider, G. Francius, R. Obeid, P. Schwinte, J. Hemmerle, B. Frisch, P. Schaaf, J.-C. Voegel, B. Senger, and C. Picart, "Polyelectrolyte multilayers with a tunable young's modulus: Influence of film stiffness on cell adhesion," *Langmuir*, vol. 22, pp. 1193, 2006.
- ¹⁰⁰ Z. Lu, M. D. Prouty, Z. Guo, V. O. Golub, C. S. S. R. Kumar, and Y. M. Lvov, "Magnetic Switch of Permeability for Polyelectrolyte Microcapsules Embedded with Co@Au Nanoparticles," *Langmuir*, vol. 21, pp. 2042-2050, 2005.
- ¹⁰¹ A. A. Antipov, G. B. Sukhorukov, S. Leporatti, I. L. Radtchenko, E. Donath, and H. Mohwald, "Polyelectrolyte multilayer capsule permeability control," *Colloids and Surfaces A: Physicochemical and Engineering Aspects*, vol. 198-200, pp. 535, 2002.

- ¹⁰² M. Muller, B. Kessler, H. J. Adler, and K. Lunkwitz, "Reversible switching of protein uptake and release at polyelectrolyte multilayers detected by ATR-FTIR spectroscopy," *Macromolecular Symposia*, vol. 210, pp. 157, 2004.
- ¹⁰³ E. Kharlampieva and S. A. Sukhishvili, "Release of a dye from hydrogen-bonded and electrostatically assembled polymer films triggered by adsorption of a polyelectrolyte," *Langmuir*, vol. 20, pp. 9677, 2004.
- ¹⁰⁴ J. Zhang, L. S. Chua, and D. M. Lynn, "Multilayered thin films that sustain the release of functional DNA under physiological conditions," *Langmuir*, vol. 20, pp. 8015, 2004.
- ¹⁰⁵ C. Schuler and F. Caruso, "Decomposable Hollow Biopolymer-Based Capsules," *Biomacromolecules*, vol. 2, pp. 921-926, 2001.
- ¹⁰⁶ S. T. Dubas and J. B. Schlenoff, "Polyelectrolyte Multilayers Containing a Weak Polyacid: Construction and Deconstruction," *Macromolecules*, vol. 34, pp. 3736-3740, 2001.
- ¹⁰⁷ E. Vazquez, D. M. Dewitt, P. T. Hammond, and D. M. Lynn, "Construction of hydrolytically-degradable thin films via layer-by-layer deposition of degradable polyelectrolytes," *Journal of the American Chemical Society*, vol. 124, pp. 13992, 2002.
- ¹⁰⁸ C. M. Nelson, S. Raghavan, J. L. Tan, and C. S. Chen, "Degradation of Micropatterned Surfaces by Cell-Dependent and -Independent Processes," *Langmuir*, vol. 19, pp. 1493-1499, 2003.
- ¹⁰⁹ N. A. Kotov, I. Dekany, and J. H. Fendler, "Layer-by-layer self-assembly of polyelectrolyte-semiconductor nanoparticle composite films," *Journal of Physical Chemistry*, vol. 99, pp. 13065, 1995.
- ¹¹⁰ J. Kerimo, D. M. Adams, P. F. Barbara, D. M. Kaschak, and T. E. Mallouk, "NSOM investigations of the spectroscopy and morphology of self-assembled multilayered thin films," *Journal of Physical Chemistry B*, vol. 102, pp. 9451, 1998.
- ¹¹¹ J. W. Ostrander, A. A. Mamedov, and N. A. Kotov, "Two Modes of Linear Layer-by-Layer Growth of Nanoparticle-Polyelectrolyte Multilayers and Different Interactions in the Layer-by-layer Deposition," *J. Am. Chem. Soc.*, vol. 123, pp. 1101-1110, 2001.
- ¹¹² N. A. Kotov, "Ordered layered assemblies of nanoparticles," *MRS Bulletin*, vol. 26, pp. 992, 2001.

- ¹¹³ G. B. Sukhorukov, E. Donath, S. Davis, H. Lichtenfeld, F. Caruso, V. I. Popov, and H. Möhwald, "Stepwise polyelectrolyte assembly on particle surfaces: a novel approach to colloid design," *Polymers for Advanced Technologies*, vol. 9, pp. 759-767, 1998.
- ¹¹⁴ F. Caruso, R. A. Caruso, and H. Mohwald, "Nanoengineering of inorganic and hybrid hollow spheres by colloidal templating," *Science*, vol. 282, pp. 1111, 1998.
- ¹¹⁵ Y. M. Lvov, R. R. Price, J. V. Selinger, A. Singh, M. S. Spector, and J. M. Schnur, "Imaging nanoscale patterns on biologically derived microstructures," *Langmuir*, vol. 16, pp. 5932, 2000.
- ¹¹⁶ A. Jaiswal, J. Colins, B. Agricole, P. Delhaes, and S. Ravaine, "Layer-by-layer self-assembly of Prussian blue colloids," *Journal of Colloid and Interface Science*, vol. 261, pp. 330, 2003.
- ¹¹⁷ V. V. Klechkovskaya, L. V. Nikitin, N. D. Stepina, and I. S. Zhanaveskina, "Self-assembly of magnetic multilayer polymer films on the base of polyelectrolytes and magnetic suspensions," Moscow, Russian Federation, 2003.
- ¹¹⁸ H. S. Kim, B. H. Sohn, W. Lee, J. K. Lee, S. J. Choi, and S. J. Kwon, "Multifunctional layer-by-layer self-assembly of conducting polymers and magnetic nanoparticles," *Thin Solid Films*, vol. 419, pp. 173, 2002.
- ¹¹⁹ F. Hua, Y. Lvov, and T. Cui, "Spatial patterning of colloidal nanoparticle-based thin film by a combinative technique of layer-by-layer self-assembly and lithography," *J Nanosci Nanotechnol*, vol. 2, pp. 357-61, 2002.
- ¹²⁰ H. F. Hamann, S. I. Woods, and S. Sun, "Direct Thermal Patterning of Self-Assembled Nanoparticles," *Nano Lett.*, vol. 3, pp. 1643-1645, 2003.
- ¹²¹ S. Magdassi and M. B. Moshe, "Patterning of organic nanoparticles by ink-jet printing of microemulsions," *Langmuir*, vol. 19, pp. 939, 2003.
- ¹²² F. Hua, T. Cui, and Y. Lvov, "Lithographic approach to pattern self-assembled nanoparticle multilayers," *Langmuir*, vol. 18, pp. 6712, 2002.
- ¹²³ F. Hua, J. Shi, Y. Lvov, and T. Cui, "Patterning of Layer-by-Layer Self-Assembled Multiple Types of Nanoparticle Thin Films by Lithographic Technique," *Nano Lett.*, vol. 2, pp. 1219-1222, 2002.
- ¹²⁴ D. Xia and S. R. J. Brueck, "A Facile Approach to Directed Assembly of Patterns of Nanoparticles Using Interference Lithography and Spin Coating," *Nano Lett.*, vol. 4, pp. 1295-1299, 2004.
- ¹²⁵ V. Santhanam and R. P. Andres, "Microcontact Printing of Uniform Nanoparticle Arrays," *Nano Lett.*, vol. 4, pp. 41-44, 2004.

- ¹²⁶ D. S. Kommireddy, A. A. Patel, T. G. Shutava, D. K. Mills, and Y. M. Lvov, "Layer-by-Layer assembly of TiO₂ nanoparticles for stable hydrophilic biocompatible coatings," *J Nanosci Nanotechnol*, vol. 5, pp. 1081-7, 2005.
- ¹²⁷ D. S. Kommireddy, I. Ichinose, Y. M. Lvov, and D. K. Mills, " Nanoparticle Multilayers: Surface Modification for Cell Attachment and Growth," *Journal of Biomedical Nanotechnology*, vol. 1, pp. 286-290, 2005.
- ¹²⁸ T. J. Webster and J. U. Ejiolor, "Increased osteoblast adhesion on nanophase metals: Ti, Ti6Al4V, and CoCrMo," *Biomaterials*, vol. 25, pp. 4731, 2004.
- ¹²⁹ S. Svedhem, D. Dahlborg, J. Ekeröth, J. Kelly, F. Hook, and J. Gold, "In situ peptide-modified supported lipid bilayers for controlled cell attachment," *Langmuir*, vol. 19, pp. 6730, 2003.
- ¹³⁰ E. Ostuni, C. S. Chen, D. E. Ingber, and G. M. Whitesides, "Selective deposition of proteins and cells in arrays of microwells," *Langmuir*, vol. 17, pp. 2828, 2001.
- ¹³¹ H. D. Inerowicz, S. Howell, F. E. Regnier, and R. Reifenger, "Multiprotein immunoassay arrays fabricated by microcontact printing," *Langmuir*, vol. 18, pp. 5263, 2002.
- ¹³² J. P. Renault, A. Bernard, D. Juncker, B. Michel, H. R. Bosshard, and E. Delamarche, "Fabricating microarrays of functional proteins using affinity contact printing," *Angewandte Chemie - International Edition*, vol. 41, pp. 2320, 2002.
- ¹³³ D. T. Chiu, N. L. Jeon, S. Huang, R. S. Kane, C. J. Wargo, I. S. Choi, D. E. Ingber, and G. M. Whitesides, "Patterned deposition of cells and proteins onto surfaces by using three-dimensional microfluidic systems," *PNAS*, vol. 97, pp. 2408-2413, 2000.
- ¹³⁴ A. Bernard, B. Michel, and E. Delamarche, "Micromosaic immunoassays," *Anal Chem*, vol. 73, pp. 8-12, 2001.
- ¹³⁵ S. K. Bhatia, J. J. Hickman, and F. S. Ligler, "New approach to producing patterned biomolecular assemblies," *Journal of the American Chemical Society*, vol. 114, pp. 4432, 1992.
- ¹³⁶ K. E. Healy, B. Lom, and P. E. Hockberger, "Spatial distribution of mammalian cells dictated by material surface chemistry," *Biotechnology and Bioengineering*, vol. 43, pp. 792, 1994.
- ¹³⁷ C. S. Chen, J. L. Alonso, E. Ostuni, G. M. Whitesides, and D. E. Ingber, "Cell shape provides global control of focal adhesion assembly," *Biochem Biophys Res Commun*, vol. 307, pp. 355-61, 2003.

- ¹³⁸ M. S. Ravenscroft, K. E. Bateman, K. M. Shaffer, H. M. Schessler, D. R. Jung, T. W. Schneider, C. B. Montgomery, T. L. Custer, A. E. Schaffner, Q. Y. Liu, Y. X. Li, J. L. Barker, and J. J. Hickman, "Developmental neurobiology implications from fabrication and analysis of hippocampal neuronal networks on patterned silane-modified surfaces," *Journal of the American Chemical Society*, vol. 120, pp. 12169, 1998.
- ¹³⁹ A. Curtis and C. Wilkinson, "Topographical control of cells," *Biomaterials*, vol. 18, pp. 1573, 1997.
- ¹⁴⁰ M. Matsuzawa, P. Liesi, and W. Knoll, "Chemically modifying glass surfaces to study substratum-guided neurite outgrowth in culture," *J Neurosci Methods*, vol. 69, pp. 189-96, 1996.
- ¹⁴¹ J. M. Corey, B. C. Wheeler, and G. J. Brewer, "Selective silane removal: A technique for micropatterning of neurons in culture," Montreal, Can, 1995.
- ¹⁴² A. Tourovskaia, T. Barber, B. T. Wickes, D. Hirdes, B. Grin, D. G. Castner, K. E. Healy, and A. Folch, "Micropatterns of chemisorbed cell adhesion-repellent films using oxygen plasma etching and elastomeric masks," *Langmuir*, vol. 19, pp. 4754, 2003.
- ¹⁴³ I. H. Yang, C. C. Co, and C.-C. Ho, "Spatially controlled co-culture of neurons and glial cells," *Journal of Biomedical Materials Research - Part A*, vol. 75, pp. 976, 2005.
- ¹⁴⁴ S. N. Bhatia, U. J. Balis, M. L. Yarmush, and M. Toner, "Microfabrication of hepatocyte/fibroblast co-cultures: role of homotypic cell interactions," *Biotechnology Progress*, vol. 14, pp. 378, 1998.
- ¹⁴⁵ A. Khademhosseini, K. Y. Suh, J. M. Yang, G. Eng, J. Yeh, S. Levenberg, and R. Langer, "Layer-by-layer deposition of hyaluronic acid and poly-L-lysine for patterned cell co-cultures," *Biomaterials*, vol. 25, pp. 3583, 2004.
- ¹⁴⁶ J. Fukuda, A. Khademhosseini, J. Yeh, G. Eng, J. Cheng, O. C. Farokhzad, and R. Langer, "Micropatterned cell co-cultures using layer-by-layer deposition of extracellular matrix components," *Biomaterials*, vol. 27, pp. 1479, 2006.
- ¹⁴⁷ E. Takai, E. G. Lima, H. H. Lu, G. A. Ateshian, X. E. Guo, and C. T. Hung, "Natural Trabecular Bone as a Mineralized Substrate for osteochondral Tissue Engineered Hydrogel Constructs," *Trans. Orthop. Res. Soc.*, vol. 49, 2003.
- ¹⁴⁸ H. H. Lu, S. B. Nicoll, and J. Jiang, "Effects of osteoblast and chondrocyte co-culture on chondrogenic and osteoblastic phenotype in vitro," *Trans. Orthop. Res. Soc.*, vol. 49, 2003.

- ¹⁴⁹ P. D'Andrea, A. Calabrese, and M. Grandolfo, "Intercellular calcium signalling between chondrocytes and synovial cells in co-culture," *Biochem J*, vol. 329 (Pt 3), pp. 681-7, 1998.
- ¹⁵⁰ S. N. Bhatia, M. L. Yarmush, and M. Toner, "Controlling cell interactions by micropatterning in co-cultures: hepatocytes and 3T3 fibroblasts," *J Biomed Mater Res*, vol. 34, pp. 189-99, 1997.
- ¹⁵¹ S. N. Bhatia, U. J. Balis, M. L. Yarmush, and M. Toner, "Effect of cell-cell interactions in preservation of cellular phenotype: cocultivation of hepatocytes and nonparenchymal cells," *FASEB J*, vol. 13, pp. 1883-1900, 1999.
- ¹⁵² E. E. Hui and S. N. Bhatia, "Modulation of cell-cell contact at the microscale," presented at From the Nano- to the Micro- Scale in BME BioMEMS, BMES, 2004.
- ¹⁵³ T. C. Holmes, "Novel peptide-based biomaterial scaffolds for tissue engineering," *Trends in Biotechnology*, vol. 20, pp. 16, 2002.
- ¹⁵⁴ F. Yang, R. Murugan, S. Ramakrishna, X. Wang, Y. X. Ma, and S. Wang, "Fabrication of nano-structured porous PLLA scaffold intended for nerve tissue engineering," *Biomaterials*, vol. 25, pp. 1891, 2004.
- ¹⁵⁵ G. A. Silva, C. Czeisler, K. L. Niece, E. Beniash, D. A. Harrington, J. A. Kessler, and S. I. Stupp, "Selective Differentiation of Neural Progenitor Cells by High-Epitope Density Nanofibers," *Science*, vol. 303, pp. 1352, 2004.
- ¹⁵⁶ A. Khademhosseini, J. Yeh, S. Jon, G. Eng, K. Y. Suh, J. A. Burdick, and R. Langer, "Molded polyethylene glycol microstructures for capturing cells within microfluidic channels," *Lab Chip*, vol. 4, pp. 425-30, 2004.
- ¹⁵⁷ S. M. O'Connor, J. D. Andreadis, K. M. Shaffer, W. Ma, J. J. Pancrazio, and D. A. Stenger, "Immobilization of neural cells in three-dimensional matrices for biosensor applications," *Biosens Bioelectron*, vol. 14, pp. 871-81, 2000.
- ¹⁵⁸ L. C. Gerstenfeld, J. Cruceta, C. M. Shea, K. Sampath, G. L. Barnes, and T. A. Einhorn, "Chondrocytes Provide Morphogenic Signals That Selectively Induce Osteogenic Differentiation of Mesenchymal Stem Cells," *Journal of Bone and Mineral Research*, vol. 17, pp. 221-230, 2002.
- ¹⁵⁹ H.-Q. Xian, E. McNichols, A. St. Clair, and D. I. Gottlieb, "A Subset of ES-Cell-Derived Neural Cells Marked by Gene Targeting," *Stem Cells*, vol. 21, pp. 41-49, 2003.
- ¹⁶⁰ M. Horiuchi and Y. Tomooka, "An attempt to generate neurons from an astrocyte progenitor cell line FBD-104," *Neurosci Res*, vol. 53, pp. 104-15, 2005.

- ¹⁶¹ T. H. Young and C. H. Hung, "Behavior of embryonic rat cerebral cortical stem cells on the PVA and EVAL substrates," *Biomaterials*, vol. 26, pp. 4291-9, 2005.
- ¹⁶² A. Khademhosseini and P. W. Zandstra, "Engineering the in vitro cellular microenvironment for the control and manipulation of adult stem cell responses," in *Adult Stem Cells*. Totowa, NJ: The Humana Press Inc., 2004, pp. 289-314.
- ¹⁶³ J. B. Recknor, J. C. Recknor, D. S. Sakaguchi, and S. K. Mallapragada, "Oriented astroglial cell growth on micropatterned polystyrene substrates," *Biomaterials*, vol. 25, pp. 2753, 2004.
- ¹⁶⁴ X. Jiang, H. Zheng, S. Gourdin, and P. T. Hammond, "Polymer-on-polymer stamping: Universal approaches to chemically patterned surfaces," *Langmuir*, vol. 18, pp. 2607, 2002.
- ¹⁶⁵ X. P. Jiang, S. L. Clark, and P. T. Hammond, "Side-by-side directed multilayer patterning using surface templates," *Advanced Materials*, vol. 13, pp. 1669, 2001.
- ¹⁶⁶ A. Kumar, N. L. Abbott, H. A. Biebuyck, E. Kim, and G. M. Whitesides, "Patterned Self-Assembled Monolayers and Meso-Scale Phenomena," *Acc. Chem. Res.*, vol. 28, pp. 219-226, 1995.
- ¹⁶⁷ D. Lehnert, B. Wehrle-Haller, C. David, U. Weiland, C. Ballestrem, B. A. Imhof, and M. Bastmeyer, "Cell behaviour on micropatterned substrata: limits of extracellular matrix geometry for spreading and adhesion," *J Cell Sci*, vol. 117, pp. 41-52, 2004.
- ¹⁶⁸ R. Singhvi, A. Kumar, G. P. Lopez, G. N. Stephanopoulos, D. I. Wang, G. M. Whitesides, and D. E. Ingber, "Engineering cell shape and function," *Science*, vol. 264, pp. 696-8, 1994.
- ¹⁶⁹ T. C. McDevitt, K. A. Woodhouse, S. D. Hauschka, C. E. Murry, and P. S. Stayton, "Spatially organized layers of cardiomyocytes on biodegradable polyurethane films for myocardial repair," *Journal of Biomedical Materials Research - Part A*, vol. 66, pp. 586, 2003.
- ¹⁷⁰ D. W. Branch, J. M. Corey, J. A. Weyhenmeyer, G. J. Brewer, and B. C. Wheeler, "Microstamp patterns of biomolecules for high-resolution neuronal networks," *Med Biol Eng Comput*, vol. 36, pp. 135-41, 1998.
- ¹⁷¹ C. D. James, R. Davis, M. Meyer, A. Turner, S. Turner, G. Withers, L. Kam, G. Banker, H. Craighead, M. Isaacson, J. Turner, and W. Shain, "Aligned microcontact printing of micrometer-scale poly-L-lysine structures for controlled growth of cultured neurons on planar microelectrode arrays," *IEEE Transactions on Biomedical Engineering*, vol. 47, pp. 17, 2000.
- ¹⁷² Y. Xia and G. M. Whitesides, "Soft lithography," vol. 28, *Annual Review of Materials Science*: Annual Reviews Inc, Palo Alto, CA, USA, 1998, pp. 153.

- ¹⁷³ J. C. McDonald, M. L. Chabinyk, S. J. Metallo, J. R. Anderson, A. D. Stroock, and G. M. Whitesides, "Prototyping of microfluidic devices in poly(dimethylsiloxane) using solid-object printing," *Analytical Chemistry*, vol. 74, pp. 1537, 2002.
- ¹⁷⁴ J. C. McDonald and G. M. Whitesides, "Poly(dimethylsiloxane) as a Material for Fabricating Microfluidic Devices," *Acc. Chem. Res.*, vol. 35, pp. 491-499, 2002.
- ¹⁷⁵ E. Ostuni, R. Kane, C. S. Chen, D. E. Ingber, and G. M. Whitesides, "Patterning mammalian cells using elastomeric membranes," *Langmuir*, vol. 16, pp. 7811, 2000.
- ¹⁷⁶ A. Folch and M. Toner, "Cellular micropatterns on biocompatible materials," *Biotechnology Progress*, vol. 14, pp. 388, 1998.
- ¹⁷⁷ H. Jang, S. Kim, and K. Char, "Multilayer line micropatterning using convective self-assembly in microfluidic channels," *Langmuir*, vol. 19, pp. 3094, 2003.
- ¹⁷⁸ H. Zheng, I. Lee, M. F. Rubner, and P. T. Hammond, "Two component particle arrays on patterned polyelectrolyte multilayer templates," *Advanced Materials*, vol. 14, pp. 569, 2002.
- ¹⁷⁹ J. Park and P. T. Hammond, "Multilayer Transfer Printing for Polyelectrolyte Multilayer Patterning: Direct Transfer of Layer-by-Layer Assembled Micropatterned Thin Films," *Advanced Materials*, vol. 16, pp. 520, 2004.
- ¹⁸⁰ J. Park, L. D. Fouché, and P. T. Hammond, "Multicomponent Patterning of Layer-by-Layer Assembled Polyelectrolyte/Nanoparticle Composite Thin Films with Controlled Alignment," *Advanced Materials*, vol. 17, pp. 2575-2579, 2005.
- ¹⁸¹ C.-S. Lee, S.-H. Lee, S.-S. Park, Y.-K. Kim, and B.-G. Kim, "Protein patterning on silicon-based surface using background hydrophobic thin film," *Biosensors and Bioelectronics*, vol. 18, pp. 437, 2003.
- ¹⁸² H. Sorribas, C. Padeste, and L. Tiefenauer, "Photolithographic generation of protein micropatterns for neuron culture applications," *Biomaterials*, vol. 23, pp. 893, 2002.
- ¹⁸³ A. S. Blawas and W. M. Reichert, "Protein patterning," *Biomaterials*, vol. 19, pp. 595, 1998.
- ¹⁸⁴ Y. Ito, "Surface micropatterning to regulate cell functions," *Biomaterials*, vol. 20, pp. 2333, 1999.
- ¹⁸⁵ J. F. Mooney, A. J. Hunt, J. R. McIntosh, C. A. Liberko, D. M. Walba, and C. T. Rogers, "Patterning of functional antibodies and other proteins by photolithography of silane monolayers," *PNAS*, vol. 93, pp. 12287-12291, 1996.

- ¹⁸⁶ A. Douvas, P. Argitis, C. D. Diakoumakos, K. Misiakos, D. Dimotikali, and S. E. Kakabakos, "Photolithographic patterning of proteins with photoresists processable under biocompatible conditions," *Journal of Vacuum Science and Technology B: Microelectronics and Nanometer Structures*, vol. 19, pp. 2820, 2001.
- ¹⁸⁷ P. Argitis, A. Douvas, K. Misiakos, and S. E. Kakabakos, "Patterning of Biomolecules with a New Photolithographic Methodology," *BJ Forum on Nanosized Technology*, pp. 245-250, 2002.
- ¹⁸⁸ A. Douvas, P. Argitis, K. Misiakos, D. Dimotikali, P. S. Petrou, and S. E. Kakabakos, "Biocompatible photolithographic process for the patterning of biomolecules," *Biosens Bioelectron*, vol. 17, pp. 269-78, 2002.
- ¹⁸⁹ J. M. Havard, N. Vladimirov, J. M. J. Frechet, S. Yamada, C. G. Willson, and J. D. Byers, "Photoresists with Reduced Environmental Impact: Water-Soluble Resists Based on Photo-Cross-Linking of a Sugar-Containing Polymethacrylate," *Macromolecules*, vol. 32, pp. 86-94, 1999.
- ¹⁹⁰ C. D. Diakoumakos, A. Douvas, I. Raptis, S. Kakabakos, D. Dimotikalli, G. Terzoudi, and P. Argitis, "Dilute aqueous base developable resists for environmentally friendly and biocompatible processes," *Microelectronic Engineering*, vol. 61-62, pp. 819, 2002.
- ¹⁹¹ M. Li, K. K. Kondabatni, T. Cui, and M. J. McShane, "Fabrication of 3-D Gelatin-Patterned Glass Substrates with Layer-by-Layer and Lift-Off (LbL-LO) Technology," *IEEE Transactions on Nanotechnology*, vol. 3, pp. 115, 2004.
- ¹⁹² J. S. Mohammed, M. A. DeCoster, and M. J. McShane, "Micropatterning of nanoengineered surfaces to study neuronal cell attachment in vitro," *Biomacromolecules*, vol. 5, pp. 1745, 2004.
- ¹⁹³ M. Schena, D. Shalon, R. W. Davis, and P. O. Brown, "Quantitative Monitoring of Gene Expression Patterns with a Complementary DNA Microarray," *Science*, vol. 270, pp. 467-470, 1995.
- ¹⁹⁴ F. Turcu, K. Tratsk-Nitz, S. Thanos, W. Schuhmann, and P. Heiduschka, "Ink-jet printing for micropattern generation of laminin for neuronal adhesion," *Journal of Neuroscience Methods*, vol. 131, pp. 141, 2003.
- ¹⁹⁵ G. P. Lopez, H. A. Biebuyck, R. Harter, A. Kumar, and G. M. Whitesides, "Fabrication and imaging of two-dimensional patterns of proteins adsorbed on self-assembled monolayers by scanning electron microscopy," *J. Am. Chem. Soc.*, vol. 115, pp. 10774-10781, 1993.

- ¹⁹⁶ L. M. Tender, R. L. Worley, H. Fan, and G. P. Lopez, "Electrochemical Patterning of Self-Assembled Monolayers onto Microscopic Arrays of Gold Electrodes Fabricated by Laser Ablation," *Langmuir*, vol. 12, pp. 5515-5518, 1996.
- ¹⁹⁷ R. D. Piner, J. Zhu, F. Xu, S. Hong, and C. A. Mirkin, "'Dip-Pen" Nanolithography," *Science*, vol. 283, pp. 661-663, 1999.
- ¹⁹⁸ K.-B. Lee, J.-H. Lim, and C. A. Mirkin, "Protein nanostructures formed via direct-write dip-pen nanolithography," *Journal of the American Chemical Society*, vol. 125, pp. 5588, 2003.
- ¹⁹⁹ L. Fu, X. Liu, Y. Zhang, V. P. Dravid, and C. A. Mirkin, "Nanopatterning of "Hard" Magnetic Nanostructures via Dip-Pen Nanolithography and a Sol-Based Ink," *Nano Lett.*, vol. 3, pp. 757-760, 2003.
- ²⁰⁰ S. Rozhok, R. Piner, and C. A. Mirkin, "Dip-pen nanolithography: What controls ink transport?" *Journal of Physical Chemistry B*, vol. 107, pp. 751, 2003.
- ²⁰¹ D. Nyamjav and A. Ivanisevic, "Properties of polyelectrolyte templates generated by dip-pen nanolithography and microcontact printing," *Chemistry of Materials*, vol. 16, pp. 5216, 2004.
- ²⁰² J. H. Lim, D. S. Ginger, K. B. Lee, J. Heo, J. M. Nam, and C. A. Mirkin, "Direct-write dip-pen nanolithography of proteins on modified silicon oxide surfaces," *Angew Chem Int Ed Engl*, vol. 42, pp. 2309-12, 2003.
- ²⁰³ L. M. Demers, D. S. Ginger, S. J. Park, Z. Li, S. W. Chung, and C. A. Mirkin, "Direct Patterning of Modified Oligonucleotides on Metals and Insulators by Dip-Pen Nanolithography," *Science*, vol. 296, pp. 1836-1838, 2002.
- ²⁰⁴ K.-B. Lee, S.-J. Park, C. A. Mirkin, J. C. Smith, and M. Mrksich, "Protein Nanoarrays Generated By Dip-Pen Nanolithography," *Science*, vol. 295, pp. 1702-1705, 2002.
- ²⁰⁵ A. Bernard, J. P. Renault, B. Michel, H. R. Bosshard, and E. Delamarche, "Microcontact Printing of Proteins," *Advanced Materials*, vol. 12, pp. 1067-1070, 2000.
- ²⁰⁶ A. Papra, A. Bernard, D. Juncker, N. B. Larsen, B. Michel, and E. Delamarche, "Microfluidic networks made of poly(dimethylsiloxane), Si, and Au coated with polyethylene glycol for patterning proteins onto surfaces," *Langmuir*, vol. 17, pp. 4090, 2001.
- ²⁰⁷ R. Fernandes, H. Yi, L. Q. Wu, G. W. Rubloff, R. Ghodssi, W. E. Bentley, and G. F. Payne, "Thermo-Biolithography: A Technique for Patterning Nucleic Acids and Proteins," *Langmuir*, vol. 20, pp. 906-913, 2004.

- ²⁰⁸ S. A. Sundberg, R. W. Barrett, M. Pirrung, A. L. Lu, B. Kiangsoontra, and C. P. Holmes, "Spatially-Addressable Immobilization of Macromolecules on Solid Supports," *J. Am. Chem. Soc.*, vol. 117, pp. 12050-12057, 1995.
- ²⁰⁹ M. A. Holden and P. S. Cremer, "Light Activated Patterning of Dye-Labeled Molecules on Surfaces," *J. Am. Chem. Soc.*, vol. 125, pp. 8074-8075, 2003.
- ²¹⁰ A. S. Blawas, T. F. Oliver, M. C. Pirrung, and W. M. Reichert, "Step-and-Repeat Photopatterning of Protein Features Using Caged-Biotin-BSA: Characterization and Resolution," *Langmuir*, vol. 14, pp. 4243-4250, 1998.
- ²¹¹ H. M. J. M. C. David John Pritchard, "Micron-Scale Patterning of Biological Molecules," *Angewandte Chemie International Edition in English*, vol. 34, pp. 91-93, 1995.
- ²¹² C. S. Chen, M. Mrksich, S. Huang, G. M. Whitesides, and D. E. Ingber, "Micropatterned surfaces for control of cell shape, position, and function," *Biotechnology Progress*, vol. 14, pp. 356, 1998.
- ²¹³ M. Mrksich and G. M. Whitesides, "Patterning self-assembled monolayers using microcontact printing: a new technology for biosensors?" *Trends in Biotechnology*, vol. 13, pp. 228, 1995.
- ²¹⁴ J. L. Wilbur, A. Kumar, H. A. Biebuyck, E. Kim, and G. M. Whitesides, "Microcontact printing of self-assembled monolayers: applications in microfabrication," *Nanotechnology*, vol. 7, pp. 452, 1996.
- ²¹⁵ T. K. Whidden, D. K. Ferry, M. N. Kozicki, E. Kim, A. Kumar, J. Wilbur, and G. M. Whitesides, "Pattern transfer to silicon by microcontact printing and RIE," *Nanotechnology*, vol. 7, pp. 447, 1996.
- ²¹⁶ J. A. Rogers, R. J. Jackman, and G. M. Whitesides, "Microcontact printing and electroplating on curved substrates: Production of free-standing three-dimensional metallic microstructures," *Advanced Materials*, vol. 9, pp. 475, 1997.
- ²¹⁷ B. D. Gates, Q. Xu, M. Stewart, D. Ryan, C. G. Willson, and G. M. Whitesides, "New approaches to nanofabrication: Molding, printing, and other techniques," *Chemical Reviews*, vol. 105, pp. 1171, 2005.
- ²¹⁸ H. Ai, M. Fang, Y. M. Lvov, D. K. Mills, and S. A. Jones, "Applications of the electrostatic layer-by-layer self-assembly technique in biomedical engineering," Houston, TX, United States, 2002.
- ²¹⁹ N. Patel, R. Padera, G. H. W. Sanders, S. M. Cannizzaro, M. C. Davies, R. Langer, C. J. Roberts, S. J. B. Tendler, P. M. Williams, and K. M. Shakesheff, "Spatially controlled cell engineering on biodegradable polymer surfaces," *FASEB J.*, vol. 12, pp. 1447-1454, 1998.

- ²²⁰ X.-M. Zhao, A. Stoddart, S. P. Smith, E. Kim, Y. Xia, M. Prentiss, and G. M. Whitesides, "Fabrication of single-mode polymeric waveguides using micromolding in capillaries," *Advanced Materials*, vol. 8, pp. 420-424, 1996.
- ²²¹ R. J. Jackman, D. C. Duffy, O. Cherniavskaya, and G. M. Whitesides, "Using elastomeric membranes as dry resists and for dry lift-off," *Langmuir*, vol. 15, pp. 2973, 1999.
- ²²² A. Folch, B.-H. Jo, B.-H. Hurtado, D. J. Beebe, O. Hurtado, and M. Toner, "Microfabricated elastomeric stencils for micropatterning cell cultures," *Journal of Biomedical Materials Research*, vol. 52, pp. 346, 2000.
- ²²³ A. Revzin, P. Rajagopalan, A. W. Tilles, F. Berthiaume, M. L. Yarmush, and M. Toner, "Designing a Hepatocellular Microenvironment with Protein Microarraying and Poly(ethylene glycol) Photolithography," *Langmuir*, vol. 20, pp. 2999, 2004.
- ²²⁴ O. Harnack, I. Raible, A. Yasuda, and T. Vossmeier, "Lithographic patterning of nanoparticle films self-assembled from organic solutions by using a water-soluble mask," *Applied Physics Letters*, vol. 86, pp. 034108, 2005.
- ²²⁵ E. Kumacheva, R. K. Golding, M. Allard, and E. H. Sargent, "Colloid crystal growth on mesoscopically patterned surfaces: Effect of confinement," *Advanced Materials*, vol. 14, pp. 221, 2002.
- ²²⁶ F.-K. Liu, P.-W. Huang, Y.-C. Chang, F.-H. Ko, and T.-C. Chu, "Combining optical lithography with rapid microwave heating for the selective growth of Au/Ag bimetallic core/shell structures on patterned silicon wafers," *Langmuir*, vol. 21, pp. 2519, 2005.
- ²²⁷ L. A. Porter, H. C. Choi, J. M. Schmeltzer, A. E. Ribbe, L. C. C. Elliott, and J. M. Buriak, "Electroless Nanoparticle Film Deposition Compatible with Photolithography, Microcontact Printing, and Dip-Pen Nanolithography Patterning Technologies," *Nano Lett.*, vol. 2, pp. 1369-1372, 2002.
- ²²⁸ S. Griffith, M. Mondol, D. S. Kong, and J. M. Jacobson, "Nanostructure fabrication by direct electron-beam writing of nanoparticles," *Journal of Vacuum Science and Technology B: Microelectronics and Nanometer Structures*, vol. 20, pp. 2768, 2002.
- ²²⁹ J. L. Plaza, Y. Chen, S. Jacke, and R. E. Palmer, "Nanoparticle arrays patterned by electron-beam writing: Structure, composition, and electrical properties," *Langmuir*, vol. 21, pp. 1556, 2005.
- ²³⁰ R. Divan, D. C. Mancini, N. Moldovan, L. Assoufid, Y. S. Chu, Q. Ma, and R. A. Rosenberg, "X-ray patterned deposition of gold nanoparticles from solution," presented at Semiconductor Conference, 2003. CAS 2003. International, 2003.

- ²³¹ K. B. Lee, J. H. Lim, and C. A. Mirkin, "Protein nanostructures formed via direct-write dip-pen nanolithography," *J Am Chem Soc*, vol. 125, pp. 5588-9, 2003.
- ²³² H. Wenchuang, G. H. Bernstein, K. Sarveswaran, and M. Lieberman, "Low temperature development of PMMA for sub-10-nm electron beam lithography," presented at Nanotechnology, 2003. IEEE-NANO 2003. 2003 Third IEEE Conference on, 2003.
- ²³³ C. I. Kuo, H. L. Chen, Y. H. Chu, F. K. Liu, F. H. Ko, and T. C. Chu, "Patterning of self-assembled nanoparticles by electron-beam lithography with chemically amplified resists," presented at Microprocesses and Nanotechnology Conference, 2003. Digest of Papers. 2003 International, 2003.
- ²³⁴ K. Murata, "Super-fine ink-jet printing for nanotechnology," presented at MEMS, NANO and Smart Systems, 2003. Proceedings. International Conference on, 2003.
- ²³⁵ W. Voit, W. Zapka, L. Belova, and K. V. Rao, "Application of inkjet technology for the deposition of magnetic nanoparticles to form micron-scale structures," *IEE Proceedings: Science, Measurement and Technology*, vol. 150, pp. 252, 2003.
- ²³⁶ D. Xuan-Ming, S. Hong-Bo, K. Kaneko, A. Nakamura, S. Shoji, and S. Kawata, "Micro/nanofabrication of two and three dimensional structures by two-photon polymerization," presented at Nanotechnology, 2003. IEEE-NANO 2003. 2003 Third IEEE Conference on, 2003.
- ²³⁷ J. Doh and D. J. Irvine, "Photogenerated polyelectrolyte bilayers from an aqueous-processible photoresist for multicomponent protein patterning," *Journal of the American Chemical Society*, vol. 126, pp. 9170, 2004.
- ²³⁸ J. S. Katz, J. Doh, and D. J. Irvine, "Composition-tunable properties of amphiphilic comb copolymers containing protected methacrylic acid groups for multicomponent protein patterning," *Langmuir*, vol. 22, pp. 353, 2006.
- ²³⁹ X. Jiang and P. T. Hammond, "Selective deposition in layer-by-layer assembly: Functional graft copolymers as molecular templates," *Langmuir*, vol. 16, pp. 8501, 2000.
- ²⁴⁰ H. Jang, S. Kim, and K. Char, "Spin-coating self-assembly for micropatterning of ultrathin multilayer films," San Francisco, CA, United States, 2003.
- ²⁴¹ N. Kohli, R. M. Worden, and I. Lee, "Intact transfer of layered, bionanocomposite arrays by microcontact printing," *Chem Commun (Camb)*, pp. 316-8, 2005.
- ²⁴² J. Cho, H. Jang, B. Yeom, H. Kim, R. Kim, S. Kim, K. Char, and F. Caruso, "Modulating the pattern quality of micropatterned multilayer films prepared by layer-by-layer self-assembly," *Langmuir*, vol. 22, pp. 1356, 2006.

- ²⁴³ K. K. Kondabatni, F. Hua, T. Cui, Y. Lvov, and M. J. McShane, "Micro-patterning of nanosensor elements using layer-by-layer self-assembly, avidin-biotin chemistry, and photolithography," Houston, TX, United States, 2002.
- ²⁴⁴ T. Cui, F. Hua, and Y. Lvov, "Lithographic approach to pattern multiple nanoparticle thin films prepared by layer-by-layer self-assembly for microsystems," *Sensors and Actuators, A: Physical*, vol. 114, pp. 501, 2004.
- ²⁴⁵ Y. Masuda, T. Itoh, and K. Koumoto, "Self-assembly patterning of silica colloidal crystals," *Langmuir*, vol. 21, pp. 4478, 2005.
- ²⁴⁶ A. M. Brozell, M. A. Muha, and A. N. Parikh, "Formation of spatially patterned colloidal photonic crystals through the control of capillary forces and template recognition," *Langmuir*, vol. 21, pp. 11588, 2005.
- ²⁴⁷ D. C. Duffy, R. J. Jackman, K. M. Vaeth, K. F. Jensen, and G. M. Whitesides, "Patterning electroluminescent materials with feature sizes as small as 5 μm using elastomeric membranes as masks for dry lift-off," *Advanced Materials*, vol. 11, pp. 546, 1999.
- ²⁴⁸ D. Ryan, B. A. Parviz, V. Linder, V. Semetey, S. K. Sia, J. Su, M. Mrksich, and G. M. Whitesides, "Patterning multiple aligned self-assembled monolayers using light," *Langmuir*, vol. 20, pp. 9080, 2004.
- ²⁴⁹ T. Vossmeier, S. Jia, E. Delonno, M. R. Diehl, S. H. Kim, X. Peng, A. P. Alivisatos, and J. R. Heath, "Combinatorial approaches toward patterning nanocrystals," *Journal of Applied Physics*, vol. 84, pp. 3664, 1998.
- ²⁵⁰ M. Sastry, A. Gole, and S. R. Sainkar, "Formation of patterned, heterocolloidal nanoparticle thin films," *Langmuir*, vol. 16, pp. 3553, 2000.
- ²⁵¹ L. Li and L. Dai, "Template-free electrodeposition of multicomponent metal nanoparticles for region-specific growth of interposed carbon nanotube micropatterns," *Nanotechnology*, vol. 16, pp. 2111, 2005.
- ²⁵² J. ShaikhMohammed, M. A. DeCoster, and M. J. McShane, "Fabrication of Interdigitated Micropatterns of Self-Assembled Polymer Nanofilms Containing Cell-Adhesive Materials," *Langmuir*, vol. 22, pp. 2738-2746, 2006.
- ²⁵³ M. A. DeCoster, "Group III secreted phospholipase A2 causes apoptosis in rat primary cortical neuronal cultures," *Brain Res*, vol. 988, pp. 20-8, 2003.
- ²⁵⁴ T. Yagami, K. Ueda, K. Asakura, Y. Hayasaki-Kajiwara, H. Nakazato, T. Sakaeda, S. Hata, T. Kuroda, N. Takasu, and Y. Hori, "Group IB secretory phospholipase A2 induces neuronal cell death via apoptosis," *J Neurochem*, vol. 81, pp. 449-61, 2002.

- ²⁵⁵ T. Yagami, K. Ueda, K. Asakura, S. Hata, T. Kuroda, T. Sakaeda, N. Takasu, K. Tanaka, T. Gemba, and Y. Hori, "Human Group IIA Secretory Phospholipase A2 Induces Neuronal Cell Death via Apoptosis," *Mol. Pharmacol.*, vol. 61, pp. 114-126, 2002.
- ²⁵⁶ A. Copic, N. Vucemilo, F. Gubensek, and I. Krizaj, "Identification and Purification of a Novel Receptor for Secretory Phospholipase A2 in Porcine Cerebral Cortex," *J. Biol. Chem.*, vol. 274, pp. 26315-26320, 1999.
- ²⁵⁷ G. Lambeau, J. Barhanin, H. Schweitz, J. Qar, and M. Lazdunski, "Identification and properties of very high affinity brain membrane- binding sites for a neurotoxic phospholipase from the taipan venom," *J. Biol. Chem.*, vol. 264, pp. 11503-11510, 1989.
- ²⁵⁸ G. Lambeau, A. Schmid-Alliana, M. Lazdunski, and J. Barhanin, "Identification and purification of a very high affinity binding protein for toxic phospholipases A2 in skeletal muscle," *J. Biol. Chem.*, vol. 265, pp. 9526-9532, 1990.
- ²⁵⁹ Molecular-Probes, "Amine-Reactive Probes."
- ²⁶⁰ G. Sauerbrey, "Verwendung von Schwingquarzen zur Wägung dünner Schichten und zur Mikrowägung," *Zeitschrift für Physik A Hadrons and Nuclei*, vol. 155, pp. 206, 1959.
- ²⁶¹ Y. Lvov, K. Ariga, I. Ichinose, and T. Kunitake, "Assembly of multicomponent protein films by means of electrostatic layer-by-layer adsorption," *Journal of the American Chemical Society*, vol. 117, pp. 6117, 1995.
- ²⁶² F. Caruso, K. Niikura, D. N. Furlong, and Y. Okahata, "1. Ultrathin multilayer polyelectrolyte films on gold: Construction and thickness determination," *Langmuir*, vol. 13, pp. 3422, 1997.
- ²⁶³ M. Li, T. Cui, D. K. Mills, Y. M. Lvov, and M. J. McShane, " Comparison of Selective Attachment and Growth of Smooth Muscle Cells on Gelatin- and Fibronectin-Coated Micropatterns," *J. Nanosci. Nanotech.*, vol. 5, pp. 1809-1815, 2005.
- ²⁶⁴ A. Folch and M. A. Schmidt, "Wafer-level in-registry microstamping," *Journal of Microelectromechanical Systems*, vol. 8, pp. 85, 1999.
- ²⁶⁵ D. S. Sutherland, M. Broberg, H. Nygren, and B. Kasemo, "Influence of Nanoscale Surface Topography and Chemistry on the Functional Behaviour of an Adsorbed Model Macromolecule," *Macromolecular Bioscience*, vol. 1, pp. 270-273, 2001.
- ²⁶⁶ P. Clark, P. Connolly, A. S. Curtis, J. A. Dow, and C. D. Wilkinson, "Cell guidance by ultrafine topography in vitro," *J. Cell Sci.*, vol. 99, pp. 73-77, 1991.

- ²⁶⁷ C. M. Nolan, M. J. Serpe, and L. A. Lyon, "Thermally modulated insulin release from microgel thin films," *Biomacromolecules*, vol. 5, pp. 1940, 2004.
- ²⁶⁸ S. Y. Yang and M. F. Rubner, "Micropatterning of polymer thin films with pH-sensitive and cross-linkable hydrogen-bonded polyelectrolyte multilayers," *Journal of the American Chemical Society*, vol. 124, pp. 2100, 2002.
- ²⁶⁹ D. W. Branch, B. C. Wheeler, G. J. Brewer, and D. E. Leckband, "Long-term maintenance of patterns of hippocampal pyramidal cells on substrates of polyethylene glycol and microstamped polylysine," *IEEE Transactions on Biomedical Engineering*, vol. 47, pp. 290, 2000.
- ²⁷⁰ J. Shaikh Mohammed, M. A. DeCoster, and M. J. McShane, "Nanoengineering of micropatterns to study neuronal cell attachment in vitro," presented at Biomedical Engineering Society 2005 Annual Fall Meeting, Baltimore: Maryland, 2005.
- ²⁷¹ J. U. Ejiofor and T. J. Webster, "Bone cell adhesion on titanium implants with nanoscale surface features," *International Journal of Powder Metallurgy (Princeton, New Jersey)*, vol. 40, pp. 43, 2004.
- ²⁷² M. K. Gheith, V. A. Sinani, J. P. Wicksted, R. L. Matts, and N. A. Kotov, "Single-walled carbon nanotube polyelectrolyte multilayers and freestanding films as a biocompatible platform for neuroprosthetic implants," *Advanced Materials*, vol. 17, pp. 2663, 2005.
- ²⁷³ T. Gabay, E. Jakobs, E. Ben-Jacob, and Y. Hanein, "Engineered self-organization of neural networks using carbon nanotube clusters," *Physica A: Statistical Mechanics and its Applications*, vol. 350, pp. 611, 2005.
- ²⁷⁴ X. Zhang, S. Prasad, S. Niyogi, A. Morgan, M. Ozkan, and C. S. Ozkan, "Guided neurite growth on patterned carbon nanotubes," *Sensors and Actuators, B: Chemical*, vol. 106, pp. 843, 2005.
- ²⁷⁵ F. Caruso and H. Mohwald, "Preparation and characterization of ordered nanoparticle and polymer composite multilayers on colloids," *Langmuir*, vol. 15, pp. 8276, 1999.
- ²⁷⁶ J. Cho, K. Char, J. D. Hong, and K. B. Lee, "Fabrication of Highly Ordered Multilayer Films Using a Spin Self-Assembly Method," *Advanced Materials*, vol. 13, pp. 1076-1078, 2001.
- ²⁷⁷ S.-S. Lee, J.-D. Hong, C. H. Kim, K. Kim, J. P. Koo, and K.-B. Lee, "Layer-by-layer deposited multilayer assemblies of ionene-type polyelectrolytes based on the spin-coating method," *Macromolecules*, vol. 34, pp. 5358, 2001.
- ²⁷⁸ P. A. Chiarelli, M. S. Johal, J. L. Casson, J. B. Roberts, J. M. Robinson, and H. L. Wang, "Controlled Fabrication of Polyelectrolyte Multilayer Thin Films Using Spin-Assembly," *Advanced Materials*, vol. 13, pp. 1167-1171, 2001.

- ²⁷⁹ C. J. Lefaux, J. A. Zimberlin, and P. T. Mather, "Influence of Ionic Strength on Build-up of Multilayer Thin Films Using Spin Self-Assembly," presented at Polymer Preprints, ACS, Division of Polymer Chemistry, 2002.
- ²⁸⁰ S. S. Lee, K. B. Lee, and J. D. Hong, "Evidence for Spin Coating Electrostatic Self-Assembly of Polyelectrolytes," *Langmuir*, vol. 19, pp. 7592-7596, 2003.
- ²⁸¹ M. S. Johal, J. L. Casson, P. A. Chiarelli, D. G. Liu, J. A. Shaw, J. M. Robinson, and H. L. Wang, "Polyelectrolyte Trilayer Combinations Using Spin-Assembly and Ionic Self-Assembly," *Langmuir*, vol. 19, pp. 8876-8881, 2003.
- ²⁸² P. A. Chiarelli, M. S. Johal, D. J. Holmes, J. L. Casson, J. M. Robinson, and H.-L. Wang, "Polyelectrolyte spin-assembly," *Langmuir*, vol. 18, pp. 168, 2002.
- ²⁸³ R. N. Smith, M. McCormick, C. J. Barrett, L. Reven, and H. W. Spiess, "NMR studies of PAH/PSS polyelectrolyte multilayers adsorbed onto silica," *Macromolecules*, vol. 37, pp. 4830, 2004.
- ²⁸⁴ M. Schonhoff, "Layered polyelectrolyte complexes: Physics of formation and molecular properties," *Journal of Physics Condensed Matter*, vol. 15, pp. 1781-1808, 2003.
- ²⁸⁵ M. Schonhoff, "Self-assembled polyelectrolyte multilayers," *Current Opinion in Colloid and Interface Science*, vol. 8, pp. 86, 2003.
- ²⁸⁶ J. B. Schlenoff, "Charge Balance and Transport in Polyelectrolyte Multilayers," in *Multilayer Thin Films*, G. Decher and J. B. Schlenoff, Eds., 2003, pp. 99-132.